TP 13629E

WAKE VORTEX PREDICTION
An Overview

Prepared for
Transportation Development Centre
Transport Canada

by
Wayne Jackson, ed.

March 2001

101-06272/

TP 13629E

WAKE VORTEX PREDICTION
An Overview

by
Wayne Jackson (Editor), Ottawa
and
Metin Yaras, Carleton University
Jim Harvey, Oracle Telecomputing Inc.
Gregoire Winckelmans, Université catholique de Louvain
Gilles Fournier, Environment Canada
Andrei Belotserkovsky, SABIGO Ltd.

March 2001

This report reflects the views of the authors and not necessarily those of the Transportation Development Centre.

Since some of the accepted measures in the industry are imperial, metric measures are not always used in this report.

Un sommaire français se trouve avant la table des matières.

Transport Canada / Transports Canada

PUBLICATION DATA FORM

1 Transport Canada Publication No.	2 Project No.	3 Recipient's Catalogue No.
TP 13629E	9473	

4 Title and Subtitle	5 Publication Date
Wake Vortex Prediction: An Overview	March 2001
	6 Performing Organization Document No.

7 Author(s)	8 Transport Canada File No.
W. Jackson (ed.), M. Yaras, J. Harvey, et al.	ZCD2450-B-251-6

9 Performing Organization Name and Address	10 PWGSC File No.
Wayne Jackson, Consultant 2200 Elder Street Ottawa, Ontario Canada K2B 6N1	XSD-8-00768
	11 PWGSC or Transport Canada Contract No.
	T8200-8-8528

12 Sponsoring Agency Name and Address	13 Type of Publication and Period Covered
Transportation Development Centre (TDC) 800 René Lévesque Blvd. West Suite 600 Montreal, Quebec H3B 1X9	Final
	14 Project Officer
	H. Posluns

15 Supplementary Notes (Funding programs, titles of related publications, etc.)

Co-sponsored by the Program of Energy Research and Development (PERD)

16 Abstract

Aviation authorities have long recognized that reducing wake vortex separations during instrument meteorological conditions could permit the capacity at major airports to be increased by up to 15 percent, and delays on arrival and departure to be significantly reduced. This improved efficiency would be worth billions of dollars in savings worldwide.

The objectives of this research project were to increase the capacity of major airports, while maintaining or improving existing levels of safety, and to continue the evaluation and development of a Vortex Forecast System (VFS), which had been under development for several years in Russia.

Transport Canada formed a team of experts from Canada, Belgium, and Russia. This team has completed seven years of developing VFS, conducting related studies, and co-operating with other researchers in Europe and North America. VFS is now one of the most capable real-time wake vortex prediction systems in the world.

It is recommended that development of VFS be continued. A specific airport should be selected in Canada to provide a focus for Canadian wake vortex research. Canadian stakeholders such as Transport Canada, NAV CANADA, and major airport authorities should continue wake vortex research and continue to co-operate internationally.

17 Key Words	18 Distribution Statement
Wake vortex forecasting, aviation safety, aviation operational efficiency, real-time prediction, meteorological requirements	Limited number of copies available from the Transportation Development Centre E-mail: *tdccdt@tc.gc.ca*

19 Security Classification (of this publication)	20 Security Classification (of this page)	21 Declassification (date)	22 No. of Pages	23 Price
Unclassified	Unclassified	—	xx, 42, apps	Shipping/ Handling

Transports Canada Transport Canada

FORMULE DE DONNÉES POUR PUBLICATION

1. N° de la publication de Transports Canada	2. N° de l'étude	3. N° de catalogue du destinataire
TP 13629E	9473	

4. Titre et sous-titre	5. Date de la publication
Wake Vortex Prediction: An Overview	Mars 2001
	6. N° de document de l'organisme exécutant

7. Auteur(s)	8. N° de dossier - Transports Canada
W. Jackson (éd.), M. Yaras, J. Harvey, et al.	ZCD2450-B-251-6

9. Nom et adresse de l'organisme exécutant	10. N° de dossier - TPSGC
Wayne Jackson, Consultant 2200 Elder Street Ottawa, Ontario Canada K2B 6N1	XSD-8-00768
	11. N° de contrat - TPSGC ou Transports Canada
	T8200-8-8528

12. Nom et adresse de l'organisme parrain	13. Genre de publication et période visée
Centre de développement des transports (CDT) 800, boul. René-Lévesque Ouest Bureau 600 Montréal (Québec) H3B 1X9	Final
	14. Agent de projet
	H. Posluns

15. Remarques additionnelles (programmes de financement, titres de publications connexes, etc.)

Coparrainée par le Programme de recherche et développement énergétiques (PRDE)

16. Résumé

Les autorités de l'aviation savent depuis longtemps que la réduction des minimums d'espacement de turbulence de sillage, dans des conditions météorologiques de vol aux instruments, permettrait d'accroître jusqu'à 15 p. cent la capacité des grands aéroports, et de réduire de façon importante les temps d'attente au décollage et à l'atterrissage. De plus, ce gain de productivité engendrerait des milliards de dollars d'économies à l'échelle de la planète.

Cette recherche avait pour objectifs d'accroître la capacité des grands aéroports, tout en maintenant ou en améliorant les niveaux actuels de sécurité, et de poursuivre l'évaluation et le développement d'un Système de prévision des sillages tourbillonnaires (SPST) mis au point par des scientifiques russes.

Transports Canada a réuni une équipe d'experts canadiens, belges et russes. Pendant sept ans, cette équipe a travaillé au développement du SPST, a mené des études connexes et a collaboré aux travaux d'autres chercheurs en Europe et en Amérique du Nord. Si bien que le SPST figure maintenant parmi les systèmes de prévision des sillages tourbillonnaires en temps réel les plus puissants du monde.

Il est recommandé de poursuivre le perfectionnement du SPST et, à cette fin, de désigner un aéroport canadien qui servirait de point de convergence de la recherche sur les sillages tourbillonnaires au pays. Dans cette perspective, les groupes canadiens intéressés, comme Transports Canada, NAV Canada et les administrations des grands aéroports, devraient continuer d'appuyer la recherche sur les sillages tourbillonnaires et de coopérer aux travaux menés à l'échelle internationale.

17. Mots clés	18. Diffusion
Prévision des sillages tourbillonnaires, sécurité aérienne, efficacité des opérations aériennes, prévision en temps réel, besoins de données météorologiques	Le Centre de développement des transports dispose d'un nombre limité d'exemplaires. Courriel : *tdccdt@tc.gc.ca*

19. Classification de sécurité (de cette publication)	20. Classification de sécurité (de cette page)	21. Déclassification (date)	22. Nombre de pages	23. Prix
Non classifiée	Non classifiée	—	xx, 42, ann.	Port et manutention

ACKNOWLEDGEMENTS

The authors wish to acknowledge the great contribution of Howard Posluns of the Transportation Development Centre, Transport Canada, and Syd Rennick of Air Navigation System Services and Airspace, Safety and Security, Transport Canada, who provided the overall direction and leadership for the project.

The authors wish to acknowledge the contribution of the following individuals and organizations to this research. In some cases where several individuals from one organization contributed, we name only the main point of contact for the project.

Peter Bartello, Environment Canada
Alexander Belotserkovsky, SABIGO Ltd.
Richard Boudreault, Centre technologique en aerospatiale
Kirk Clawson, US National Oceanic and Atmospheric Administration
Jim Crites, Dallas-Fort Worth International Airport
Tim Dasey, MIT Lincoln Laboratory
Don Delisi, NorthWest Research Associates
Al Drummond, National Research Council of Canada
Irena Fedyushina, Translator
John Fottit, NAV CANADA
George Greene, US Federal Aviation Administration
W.G. (Fred) Habashi, McGill University
Jim Hallock, US Volpe National Transportation Systems Center
Dave Hinton, NASA Langley Research Center
Tom Jacky, US National Transportation Safety Board
Andrew Lyons, MacDonald Dettwiler and Associates
Fotis Mavriplis, Bombardier Inc.
Aston McLaughlin, US Federal Aviation Administration
Miroslav Mokry, National Research Council of Canada
Mario Ouellet, Environment Canada
Fred Proctor, NASA Langley Research Center
Bob Robbins, NorthWest Research Associates
Vernon Rossow, NASA Ames Research Center
Karl Snider, MacDonald Dettwiler and Associates
Ed Spitzer, US Volpe National Transportation Systems Center
Alexander Toutov, Oracle Telecomputing Inc.
Other organizations in the United Kingdom, the United States, Germany, and France

Tribute to Professor Sergei Mikhailovich Belotserkovsky (April 1920 - August 2000)

The Wake Vortex Project Team was deeply saddened at the passing of team member Sergei Belotserkovsky in Moscow in the summer of the year 2000. Sergei came to Montreal in 1993 at the age of 73 to discuss this joint research project, which has extended over seven years. He will always be remembered for signing off each team conference call with "Be happy".

The authors dedicate this report to this most honoured and respected friend.

Sergei Belotserkovsky was born in the ancient town of Livny in the Orel region of Russia. His parents were both instructors at a teachers college for over 50 years, and taught him to appreciate the value of education. In 1937, he entered the Mechanical-Mathematical Faculty of Moscow University. At the beginning of the Patriotic War of 1941 to 1945, he was sent to the front, but after several months was transferred with other university students to a military academy to train as an aviation engineer.

Sergei Belotserkovsky worked as a technician on attack aircraft for six months, then completed his studies at the military academy and graduated from Moscow University, whereupon he was appointed to the staff of the chair headed by the aviation designer Ilyushin. He defended his candidate's thesis in 1948 and his doctoral thesis in 1955. At that time he was associated with the Air Force Academy and the Central Aerohydrodynamics Institute. For the 20 years from 1965 until retiring in 1985, besides lecturing, he was the head of the scientific and educational sections at the Air Force Academy, serving as its Deputy Chief.

He married his school friend Ekaterina Udovydchenko on 5 September 1941, and they had two sons – Andrei, born in 1945, and Alexander, born in 1948.

The combination of university and military education helped Dr. Belotserkovsky to combine the fundamental scientific and practical aspects in his research. Engineering and scientific training of the first cosmonauts headed by Yuri Gagarin occupied a special place in his work. The cosmonauts wrote, "Professor Belotserkovsky worked with us for many years. We, and especially Nikolaev, Leonov, and Volynov, who defended their theses under his leadership, really consider him our teacher. But Gagarin was the most intimate and dear disciple". The space designer Korolev predicted a brilliant scientific future for Gagarin. According to the wishes of Korolev and Gagarin, Belotserkovsky assisted in planning for that, but Gagarin's tragic death prevented the accomplishment.

A debt of honour prompted the teacher to a new mission: to keep for history the bright image of the first cosmonaut. In 1968 Belotserkovsky served on the State Board investigating Gagarin's death. Three books were published: *Gagarin's Diploma* in 1986, *Death of Gagarin* in 1992, and *Computers in Science, Aviation, Life* in 1993.

Professor Belotserkovsky began to construct the method of discrete vortices in the 1940s. In 1959 he published the reference book *Atlas of Unsteady Characteristics for Wings with Various Planeforms*, and later a book with calculation data for profile lattices. For decades, the books were widely used in practice. Between 1950 and 1958, he was the author of ideas for utilizing folding lattice wings in rocket engineering, as described in books such as *Problems of Aerodynamics, Construction Strength and Production Technology of Lattice*

Wings, published jointly in 1965. The new approaches demanded practical action, especially training of specialists in mechanics, mathematics, automation, radio equipment, and computers, so in 1959 he set up a scientific seminar, which has functioned up to the present, holding 350 sessions with 920 lectures in all and attracting some 30,000 participants.

Protracted collaboration with many general designers had a profound impact on Sergei Belotserkovsky's work. He developed and researched many methods in this field. The results of his research have been presented in more than 26 books.

Professor Belotserkovsky founded the Scientific-Industrial Centre SABIGO jointly with his followers, and became its President. During his career he was decorated with the Order of the Red Banner of Labour, two military medals, and several dozen other medals. He has also been the recipient of numerous prizes. He was awarded the Zhukovsky Prize in 1967, the State Prize of the USSR in 1975 and again in 1981, and the Prize of the Council of Ministers of the USSR, also in 1981. In 1995 he received the title of Honoured Scientist of Russia.

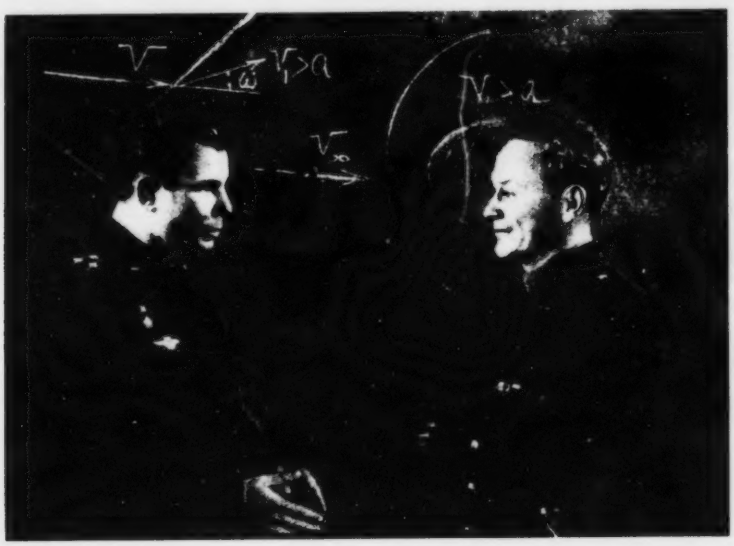

Yuri Gagarin and Sergei Belotserkovsky 1965

EXECUTIVE SUMMARY

The objectives of the Transport Canada Wake Vortex Prediction Project, which was conducted during the years 1993 to 2000, were to increase the capacity of major airports, while maintaining or improving existing levels of safety, and to continue the evaluation and development of the Vortex Forecast System (VFS).

The Transport Canada Wake Vortex Project Team (WVPT) included representatives from Transport Canada, Environment Canada, Oracle Telecomputing Inc. (OTI), Carleton University, Université catholique de Louvain in Belgium, and SABIGO Ltd. of Moscow.

This research was conducted in co-operation with other research organizations in Canada, the United States, the United Kingdom, France, and Germany. In particular, Transport Canada signed an agreement with the US National Aeronautics and Space Agency (NASA) Langley Research Center (LaRC) to conduct a number of co-operative activities.

Aviation authorities have long recognized that safely reducing wake vortex induced separations during instrument meteorological conditions could permit the capacity at major airports to be increased by up to 15 percent, and delays on arrival and departure to be significantly reduced. This improved efficiency would be worth billions of dollars in savings to airlines, airports, and the travelling public.

VFS uses real-time information about the environment and the aircraft, predicted meteorological conditions, and accurate real-time modelling of vortex transport and decay to predict conditions under which the separation may be safely reduced below the current wake vortex standards.

The basic concepts and approaches for VFS were developed by SABIGO starting in the 1970s. VFS was further developed by the WVPT. The principal components of VFS are the Near Wake, Far Wake, and Danger Area Models. The Near Wake Database (NWDB) is calculated offline for each aircraft type based on the information available on the aircraft geometry. The far wake evolution is calculated in real time. The far wake calculation may start from the NWDB, or alternately from a universal near wake profile. The far wake calculations are based on the 2-D cross-plane method of discrete vortices equations describing the vortex motion in incompressible flows. The Far Wake Model includes:

- in ground and near ground effects;
- non-uniform wind shear effects;
- user selectable eddy dissipation rate and turbulent kinetic energy decay modelling;
- supplemental small effective viscosity coefficient; and
- the calculation of time-to-demise.

The Danger Area Model is based on SABIGO's approach to the evaluation of aerodynamic forces and moments acting on aircraft moving in inhomogeneous unsteady

airflow. The calculation is based on a simplified aircraft flight dynamics model plus the aircraft longitudinal inertial moment. The VFS danger area criterion is based on the induced rolling moment. VFS also calculates the maximum rolling moment, which does not cause the roll to exceed the maximum acceptable value.

For operational use, VFS must be interfaced to a number of other systems. For this project, Transport Canada arranged for access to some of these systems through an agreement with NASA LaRC. OTI worked with NASA LaRC to implement these interfaces. VFS requires as input the wind and ambient turbulence, and their predictions for 30 to 60 minutes or more. Vertical profiles for wind and ambient turbulence are provided to VFS as input data.

To best utilize the variable separations, VFS must be interfaced to a suitable air traffic control automation system. OTI's extensive experience with the Center-TRACON Automation System (CTAS) enabled them to interface VFS with CTAS. VFS continuously updates the CTAS separation matrix based on VFS predictions. VFS integrated with NASA LaRC's Aircraft VOrtex Spacing System (AVOSS) and CTAS was part of the AVOSS final demonstration at Dallas-Fort Worth International Airport in July 2000.

At the beginning of the project, a scientific/mathematical evaluation of VFS was conducted by an International Scientific Review Committee, which recommended that the evaluation and development of VFS be continued. At the same time, VFS was tested with data collected at Idaho Falls using the tower fly-by technique. The summary results of this test were that after 120 seconds, VFS achieved an accuracy of 120 feet in the lateral position and 50 to 100 feet in the vertical position.

From 1997 to 2000, the predictive capabilities of VFS were evaluated through comparisons with numerical simulations and wake vortex data collected from field trials. The following main conclusions were drawn from these evaluations. In all cases, the accuracy of the VFS predictions was similar to the measurement accuracy of the field data (about 50 to 100 feet).

- In a calm and non-stratified atmosphere, VFS was capable of predicting the vertical descent and lateral convection of the wake vortices.
- The wake motion in uniformly stratified atmosphere was predicted with essentially the same level of accuracy as in non-stratified atmosphere.
- VFS was observed to adequately reproduce the viscous interaction of wake vortices with the ground.

The VFS predictive capabilities were significantly improved during the final year of the project, especially with respect to decay modelling and the effects of non-uniform wind shear. Subsequently, VFS was compared to two other prediction systems by NorthWest Research Associates using a few hundred test cases. The evaluation results were very positive, with VFS comparing favourably to the other two systems. It has been recommended that more evaluations and comparisons be conducted.

The most significant conclusions of this project are:

- Wake vortices constitute one of the main obstacles in the efficiency of airport takeoff and landing operations. Prescribed minimum separation distances, which were established years ago, are in most cases quite conservative.
- Safely reducing separation during instrument meteorological conditions could permit capacity at major airports to be increased by up to 15 percent, and delays on arrival and departure to be significantly reduced. This improved efficiency would be worth billions of dollars in savings to airlines, airports, and the travelling public.
- Major wake vortex research and development projects are continuing in the United States and Europe.
- Several organizations in Canada, the United States, and Europe have expressed an interest in co-operating with Transport Canada and the WVPT in wake vortex research and further development of VFS.
- During the past seven years the WVPT has made significant advancements in the development of VFS and improved understanding of aviation safety and efficiency with respect to wake vortex modelling, real-time prediction, and the meteorological requirements. VFS is now one of the most capable real-time wake vortex prediction systems in the world.
- Since the current separation standards are considered safe, the main objective of this research is increased operational efficiency. Since Transport Canada's primary role is safety regulation, Transport Canada can no longer justify being the sole sponsor of this research in Canada. The funding for this research in Canada was discontinued in April 2000.

The major recommendations resulting from this project are:

- Canadian aviation stakeholders such as Transport Canada, NAV CANADA, and the major airport authorities should continue wake vortex research in Canada.
- A specific airport should be selected in Canada to provide a focus for Canadian wake vortex research.
- Researchers and aviation authorities in Canada should continue to co-operate internationally.
- VFS development and evaluation should be continued.

SOMMAIRE

Le projet de prévision des sillages tourbillonnaires de Transports Canada, qui s'est échelonné de 1993 à 2000, avait pour objectifs d'accroître la capacité des grands aéroports, tout en maintenant ou en améliorant les niveaux de sécurité, et de poursuivre l'évaluation et le perfectionnement du Système de prévision des sillages tourbillonnaires (SPST).

L'équipe de projet des sillages tourbillonnaires (EPST) réunie par Transports Canada se composait de représentants de Transports Canada, d'Environnement Canada, d'Oracle Telecomputing Inc. (OTI), de l'Université Carleton, de l'Université catholique de Louvain, en Belgique, et de SABIGO Ltd., de Moscou.

Cette recherche a été menée conjointement avec d'autres établissements de recherche du Canada, des États-Unis, du Royaume-Uni, de la France et de l'Allemagne. Une entente de coopération a notamment été conclue entre Transports Canada et le Langley Research Center (LaRC) de la National Aeronautics and Space Agency (NASA).

Les autorités de l'aviation savent depuis longtemps qu'en réduisant, sans prendre de risque, les minimums d'espacement de turbulence de sillage, dans des conditions météorologiques de vol aux instruments, on pourrait accroître jusqu'à 15 p. cent la capacité des grands aéroports, et réduire de façon importante les temps d'attente au décollage et à l'atterrissage. De plus, ce gain de productivité engendrerait des milliards de dollars d'économies pour les compagnies aériennes, les aéroports et le public voyageur.

Le SPST utilise les données en temps réel sur l'environnement et l'aéronef, les prévisions météorologiques et une modélisation précise en temps réel de l'évolution et de la dissipation des sillages tourbillonnaires, pour établir les conditions dans lesquelles il est possible de réduire sans risque le minimum d'espacement entre aéronefs, par rapport aux normes en vigueur.

C'est SABIGO qui, dès les années 1970, a établi les principes sous-jacents au SPST, développé ensuite par l'EPST. Les principaux éléments du système sont des modèles de sillage en champ proche, de sillage en champ éloigné et de zones de danger. Une base de données sur les sillages en champ proche (BDSCP) propre à chaque type d'avion est obtenue par des calculs portant sur les données relatives à la géométrie de l'avion. L'évolution des sillages en champ éloigné est calculée en temps réel. Ce calcul, fondé soit sur la BDSCP, soit sur un profil universel des sillages en champ proche, s'appuie sur la méthode bidimensionnelle (dans la couche limite au sol) des équations de tourbillons discrets, qui décrivent le déplacement des tourbillons dans des écoulements incompressibles. Le modèle de sillage en champ éloigné comprend :

- l'effet de sol et l'effet de la proximité du sol;
- les effets du cisaillement non uniforme du vent;

- le taux de dissipation des tourbillons et la dissipation de l'énergie cinétique turbulente, selon le choix de l'utilisateur;
- un faible coefficient de diffusion efficace supplémentaire;
- le calcul du temps de dissipation.

Le modèle des zones de danger découle de la méthode SABIGO d'évaluation des forces et moments aérodynamiques agissant sur l'avion lorsqu'il se déplace dans un écoulement d'air instable et non homogène. Le calcul est fondé sur un modèle simplifié de la dynamique du vol et du moment d'inertie de l'avion dans l'axe longitudinal. Le critère déterminant de la zone de danger, selon le SPST, est le moment de roulis induit. Le système calcule le moment de roulis maximal, c'est-à-dire le moment entraînant un roulis qui demeure en deçà des valeurs maximales permises.

Pour être utilisé en service, le SPST doit être doté d'interfaces avec divers autres systèmes. Pour les besoins du projet, Transports Canada a eu accès à certains de ces systèmes, à la faveur d'une entente avec le LaRC de la NASA. OTI a collaboré avec le LaRC pour la création de ces interfaces. L'utilisateur doit entrer dans le système les données actuelles et les prévisions (pour au moins 30 à 60 minutes), ainsi que les courbes de répartition verticale, relatives au vent et à la turbulence ambiante.

Pour faire varier de façon optimale les distances de séparation, il importe que le SPST soit relié à un système d'automatisation du contrôle de la circulation aérienne. Grâce à sa vaste expérience du Center-TRACON Automation System (CTAS), OTI a été en mesure de réaliser l'interface SPST-CTAS. Le SPST met continuellement à jour la matrice de séparation du CTAS, selon les prévisions du SPST. Le SPST avait été intégré à l'AVOSS (*Aircraft VOrtex Spacing System*) du LaRC et au CTAS pour la démonstration finale du système AVOSS à l'aéroport international Dallas-Fort Worth, en juillet 2000.

Au départ, le projet a consisté en une évaluation scientifique et mathématique du SPST par un comité international d'évaluation scientifique, lequel a recommandé de poursuivre l'évaluation et le développement du système. Parallèlement à ces travaux, le SPST a été évalué à l'aide de données obtenues par mesure lors du passage des appareils près d'une tour instrumentée, à Idaho Falls. Le résultat majeur de cet essai est qu'en 120 secondes, le SPST peut donner la position latérale, à 120 pi près, du tourbillon, et sa position verticale, avec une précision de 50 à 100 pi.

De 1997 à 2000, le projet a consisté à évaluer la capacité prédictive du SPST par rapport à des simulations numériques et des données sur les sillages tourbillonnaires colligées sur le terrain. Ces évaluations ont mené aux grandes conclusions ci-après. Dans tous les cas, le système donnait des prévisions comparables aux mesures faites sur le terrain, à environ 50 à 100 pi près.

- Dans une atmosphère calme et non stratifiée, le SPST a pu prédire la descente verticale et la convection latérale des sillages tourbillonnaires.

- L'évolution du sillage dans une atmosphère uniformément stratifiée était prédite avec la même précision, essentiellement, que dans une atmosphère non stratifiée.
- Le SPST a su reproduire adéquatement l'interaction visqueuse des sillages tourbillonnaires avec le sol.

La capacité prédictive du SPST a été grandement améliorée au cours de la dernière année du projet, notamment en ce qui a trait à la modélisation de la dissipation des sillages et aux effets du cisaillement non uniforme du vent. Par la suite, pour comparaison, NorthWest Research Associates a soumis quelques centaines de cas au SPST et à deux autres systèmes de prévision. Les résultats se sont avérés très positifs, le SPST se comparant favorablement aux deux autres systèmes. Il a été recommandé de poursuivre les évaluations et les comparaisons.

Voici les grandes conclusions tirées de l'ensemble du projet :

- Les sillages tourbillonnaires constituent un des principaux obstacles à la multiplication des opérations de décollage et d'atterrissage. Les distances de séparation prescrites, établies il y a plusieurs années, s'avèrent, dans la plupart des cas, par trop prudentes.
- La diminution des distances de séparation dans des conditions météorologiques de vol aux instruments permettrait d'accroître jusqu'à 15 p. cent la capacité des grands aéroports et de réduire de façon importante l'attente au décollage et à l'atterrissage. Ce gain de productivité représenterait des milliards de dollars d'économies pour les compagnies aériennes, les aéroports et le public voyageur.
- De grands projets de recherche et de développement sur les sillages tourbillonnaires se poursuivent aux États-Unis et en Europe.
- Plusieurs organismes du Canada, des États-Unis et d'Europe se sont dits intéressés à se joindre à Transports Canada et à l'EPST pour poursuivre la recherche sur les sillages tourbillonnaires et le développement du SPST.
- Au cours des sept dernières années, l'EPST a fait de grands pas dans le développement du SPST et a permis une meilleure compréhension des liens entre, d'une part, la sécurité et la productivité des opérations aériennes, et, d'autre part, la modélisation des sillages tourbillonnaires, les prévisions en temps réel et les besoins de données météorologiques. Le SPST figure maintenant parmi les systèmes de prévision des sillages tourbillonnaires en temps réel les plus puissants au monde.
- Comme les normes actuelles touchant les distances de séparation sont jugées sûres, cette recherche vise essentiellement une plus grande efficacité opérationnelle. Comme le rôle premier de Transports Canada est la réglementation sur la sécurité, celui-ci n'a plus de raison d'être l'unique parrain de cette recherche au Canada et a interrompu sa contribution financière en avril 2000.

Voici les principales recommandations formulées au terme du projet :

- Le milieu canadien de l'aviation, soit Transports Canada, NAV Canada et les administrations des grands aéroports, doit prendre le relais de la recherche sur les sillages tourbillonnaires au Canada.
- Un aéroport doit être désigné au Canada en tant que point de convergence de la recherche sur les sillages tourbillonnaires au Canada.
- Les chercheurs et les autorités de l'aviation du Canada doivent continuer de collaborer aux travaux menés à l'échelle internationale.
- L'évaluation et le perfectionnement du SPST doivent se poursuivre.

TABLE OF CONTENTS

1. INTRODUCTION 1
   - 1.1 Project Objectives 1
   - 1.2 Background 1
   - 1.3 Report Organization 2

2. OPERATIONAL REQUIREMENT 3

3. VORTEX FORECAST SYSTEM 7
   - 3.1 VFS Basic Concepts 7
   - 3.2 VFS Structure 7
   - 3.3 Near Wake Model 9
   - 3.4 Far Wake Model 9
   - 3.5 Danger Area Model 11
   - 3.6 Interface with AVOSS and CTAS 11

4. VFS EVALUATION 13
   - 4.1 Scientific Review Committee and Idaho Falls Data 13
   - 4.2 Memphis Data 13
   - 4.3 NWRA Testing 15

5. METEOROLOGICAL CONSIDERATIONS 17
   - 5.1 Europe 17
   - 5.2 United States 17
   - 5.3 Canada 19

6. RELATED STUDIES BY THE WVPT 21
   - 6.1 Estimation of VFS Performance at an Airport 21
   - 6.2 Data Link 21
   - 6.3 Sensitivity Analysis 22
   - 6.4 Hazard Definition 22
   - 6.5 Flight Data Monitoring 22
   - 6.6 Airborne VFS 23
   - 6.7 Investigation of Near Wakes Shortly after Rollup 24
   - 6.8 Detailed Wake Studies 24
   - 6.9 Comparison of EDR and TKE Decay Models 24
   - 6.10 LES Studies 24
   - 6.11 Numerical Simulations 25

7. OTHER WAKE VORTEX RESEARCH 27
   - 7.1 Canada 27
   - 7.2 United States 28
   - 7.3 Europe 29

8. CONCLUSIONS 31

9. RECOMMENDATIONS 35

REFERENCES 37

APPENDICES

A. Biographies of WVPT Members

B. G.S. Winckelmans and H. Jeanmart, *Investigation of near wakes shortly after rollup*, Université catholique de Louvain, Belgium, April 2000.

C. G.S. Winckelmans, *Detailed Description of the Recent VFS Far Wake Improvements*, Université catholique de Louvain, Belgium, November 2000.

D. G.S. Winckelmans and P. Ploumhans, *Modelisation of non-uniform wind shear effects onto aircraft wake dynamics for the operational VFS: testing on Memphis Case 1132 with non-uniform shear in ground proximity*, Université catholique de Louvain, Belgium, March 2000.

E. T.V. Pogrebnaya and S.D. Shipilov, *Study of the Influence of Aircraft Wing Geometry on Near Wake Characteristics*, SABIGO, Russia, March 2000.

F. A.S. Belotserkovsky and N.A. Baranov, *Hazard Definition*, SABIGO, Russia, December 2000.

G. A.S. Belotserkovsky, N.A. Baranov, and N.A. Belotserkovsky, *Preliminary Development of the Airborne Vortex Forecasting System*, SABIGO, Russia, November 2000.

H. G.S. Winckelmans, *Cross-Comparison of the Coefficients in the EDR and TKE Decay Models*, Université catholique de Louvain, Belgium, November 2000.

I. M.I. Yaras, *Numerical Simulations of Aircraft Far Wake Dynamics in Non-uniform Windshear and Ground Proximity*, Carleton University, Canada, February 2000.

LIST OF FIGURES

Figure 1 VFS Functional Data Flow....8
Figure 2 HALS/DTOP....29

LIST OF TABLES

Table 1 Median Values for Indicated Measures of Differences between Predictions and Observations....16
Table 2 90th Percentile Values for Indicated Measures of Differences between Predictions and Observations....16

GLOSSARY

AMDAR	Aircraft Meteorological Data Relay
ATC	Air Traffic Control
AVOSS	Aircraft VOrtex Spacing System
AWAS	AVOSS Winds Analysis System
CFD	Computational Fluid Dynamics
CTAS	Center-TRACON Automation System
DFW	Dallas-Fort Worth International Airport
DLR	German Institut für Physik der Atmosphäre
EDR	Eddy Dissipation Rate
FAA	US Federal Aviation Administration
HALS/DTOP	Frankfurt High Approach Landing System / Dual Threshold Operation
ICAO	International Civil Aviation Organization
ICAST	International Centre for Aerospace Sciences and Technologies
IFALPA	International Federation of Airline Pilots' Associations
ITWS	Integrated Terminal Weather System
LaRC	NASA Langley Research Center
LES	Large Eddy Simulation
LL	MIT Lincoln Laboratory
MDV	Method of Discrete Vortices
MIT	Massachusetts Institute of Technology
NASA	US National Aeronautics and Space Agency
NLR	Netherlands National Aerospace Laboratory
NTSB	US National Transportation Safety Board
NWDB	Near Wake Database
NWRA	NorthWest Research Associates
OTI	Oracle Telecomputing Inc.
PBL	Planetary Boundary Layer
RANS	Reynolds-Averaged Navier-Stokes (equation)
TAPPS	Terminal Area PBL Prediction System
TDC	Transportation Development Centre
TKE	Turbulent Kinetic Energy
UNW	Universal Near Wake
VFS	Vortex Forecast System
WVPT	Transport Canada Wake Vortex Project Team

1. INTRODUCTION

This report describes the results of the Transport Canada Wake Vortex Prediction Project, which was conducted on behalf of the Transportation Development Centre (TDC) and Air Navigation System Services and Airspace, Safety and Security, Transport Canada. This research project began in 1993 and was completed in March 2000.

1.1 Project Objectives

The project objectives were:

- to increase the capacity of major airports, while maintaining or improving existing levels of safety; and
- to continue the evaluation and development of the Vortex Forecast System (VFS), which can predict the transport and decay of aircraft wake vortices.

1.2 Background

Wake vortices constitute one of the main obstacles in the efficiency of airport takeoff and landing operations. Prescribed minimum separation distances, which were established years ago, are in most cases quite conservative. Aviation authorities, scientists, and researchers have for many years been studying techniques and systems, which would enable safe reduction of these separation distances to improve airport capacities.

Transport Canada received a proposal from Professor Sergei M. Belotserkovsky of the Central Aero-Hydrodynamics Institute in Moscow to continue the development of VFS, which could potentially lead to increases in the capacity of major airports, while maintaining or improving existing levels of safety. The International Centre for Aerospace Sciences and Technologies (ICAST) arranged for Professor Belotserkovsky's first visit to Canada. The ICAST report [1] describes the VFS that existed before the beginning of the Transport Canada Wake Vortex Prediction Project.

In 1993, a technical exchange program was started with Professor Belotserkovsky and his company, SABIGO Ltd. of Moscow. At the same time, Dr. Gregoire Winckelmans of Université Catholique de Louvain in Belgium (formerly at Université de Sherbrooke, Quebec, from 1993 to 1995) and Gilles Fournier of Environment Canada joined the Transport Canada Wake Vortex Project Team (WVPT). Oracle Telecomputing Inc. (OTI) and Dr. Metin Yaras of Carleton University joined the WVPT in 1997. Fotis Mavriplis of Canadair\Bombardier Inc., Al Drummond of the National Research Council of Canada, MacDonald Dettwiler and Associates, and Mario Ouellet of Environment Canada were also members of the WVPT in earlier phases of the project.

Recognizing that potential wake vortex encounter is a worldwide problem, this research was conducted in close co-operation with research organizations in the United States, the United Kingdom, France, and Germany. Most significantly, Transport Canada signed an agreement with the US National Aeronautics and Space Agency (NASA) Langley Research Center (LaRC) to conduct a number of co-operative activities.

1.3 Report Organization

Section 2 reviews the operational requirement for VFS. Section 3 provides an overview of VFS, including interfaces to air traffic control systems. Section 4 describes the VFS evaluation. Section 5 discusses the meteorological considerations. Section 6 describes some related studies by the WVPT. Section 7 highlights other wake vortex research in Canada, Europe, and the United States. Sections 8 and 9 provide project conclusions and recommendations, respectively. Section 10 provides brief biographies for the members of WVPT. The appendices contain more detailed reports by members of the WVPT.

2. OPERATIONAL REQUIREMENT

Safely reducing separation during instrument meteorological conditions could permit capacity at major airports to be increased by up to 15 percent, and delays on arrival and departure to be significantly reduced. This improved efficiency would be worth billions of dollars in savings to airlines, airports, and the travelling public.

Research aimed at reducing wake vortex separation has been conducted in Europe and North America for more than 30 years. During that period, there has been a significant increase in the understanding of and the ability to predict wake vortex transport and decay. There has also been an increase in the understanding of how to use wake vortex prediction systems. It is expected that improvements to systems and increases in understanding will continue for many years, which suggests that the operational requirement for wake vortex prediction systems will also continue to evolve.

While there are no specific stated requirements for wake vortex prediction systems in Canada, the subject was discussed at the International Wake Vortex Meeting held in Ottawa in December 1997 [2]. Some relevant extracts from the proceedings of that meeting are included below.

NAV CANADA

> *"The science has to be sound and the regulators must tell us that the system is safe. A business case has to be made for any proposal to develop and implement such a system. Wake vortices are not presently a flight safety problem, but could become one if traffic pressures encourage a reduction in the current separation limits, which are functional and safe but may not be the most efficient. NAV CANADA is very interested in a commercial off-the-shelf solution. If we have to develop a system, we will need to identify partners who will benefit from its installation. We have to convince our clients that it is in their best interest to use the system and we must be able to recover all costs."*

Canadian Airports Council

> *"The Canadian Airports Council has the same concerns as everyone else about reduced separation. With the advent of Open Skies, we are seeing more smaller commuter type aircraft mixing with the larger types. Airports in Canada are not facing capacity problems, except for Vancouver, Toronto and perhaps Dorval. Each airport is a unique environment: traffic demand, local weather, aircraft types, environment, etc. Every airport, therefore, requires to be considered individually when planning to invest in any vortex prediction system."*

Air Canada Pilots Association

> *"Wake turbulence information is important to maintain a safe and efficient operation. We need information in a form that pilots can understand. We need documented scientific data in a form that makes sense to the pilot. We need information that tells us when and where we may encounter wake turbulence, as well as suggested actions to avoid wake encounters and escape manoeuvres to deal with an inadvertent wake encounter. We also need to know how vortices behave at the stratosphere/troposphere boundary. With the use of reduced vertical separation minimum and the implementation of Free Flight the potential for high altitude wake encounters is increasing."*

Canadian Owners and Pilots Association

> *"Our interest is to avoid vortices. Small aircraft are much more vulnerable. We cannot completely avoid the problem because we have to operate in the same airspace as larger aircraft. It must be kept in mind that the knowledge of general aviation pilots is relatively low."*

Transport Canada

> *"It is the pilots who are ultimately responsible for safety. We need a system that meets our requirements. We care more about safety than we do about reducing separation. We don't need a Cadillac system. We need a system that works."*

Further clarification of the requirement for wake vortex prediction systems is provided by the International Federation of Airline Pilots' Associations (IFALPA) Wake Vortex Policy (July 1998):

> *IFALPA supports the efforts to develop strategies and systems that allow a safe reduction of the standard wake turbulence separation minima, provided the following operational requirements are met:*
>
> *1. General*
>
> *1.1 Safety should always be the primary consideration if wake turbulence separation is planned to be reduced in order to increase aerodrome capacity.*
>
> *1.2 The results of all international research (ongoing or completed) should be taken into account when developing any wake vortex advisory/avoidance system. Any safety issue identified should be resolved to the satisfaction of the Federation before any reduction in wake turbulence separation minima can be agreed.*
>
> *1.3 IFALPA supports the 1997 US FAA Flight Standards position that no planned penetration of wake vortices of any intensity is permitted.*

2. Airborne Wake Vortex Detection

2.1 Although it is recognized that ground prediction systems are needed to properly plan and execute Air Traffic Flow Management and Control on the basis of expected separation values to be applied, IFALPA believes there is a need to develop airborne wake vortex detection and indication systems to enable pilots to make credible wake turbulence avoidance decisions.

3. Ground Based Wake Vortex Advisory and Warning Systems

3.1 Where application of reduced wake turbulence separation minima by ATC (Air Traffic Control) is to be based on a predictive system issuing vortex advisory or warning, such a system should be supplemented by a monitoring system able to reliably detect real location, movement, intensity and duration of wake vortices.

3.2 Prediction and monitoring systems should be capable of assessing the entire airspace where reduced wake turbulence separation minima are to be applied. Hence, the airspace should not be limited to short final approach areas, but include the total approach area, in particular from glide slope intercept to landing, and departure areas where applicable.

3. The prediction (sub) system should be capable of determining a vertical profile of air temperature and wind direction and speed for all relevant altitudes in increments of not more than 1000 ft. based on meteorological data derived from suitably located sensors processed in real-time, to allow a prognosis to be developed about the horizontal and vertical displacement, behaviour and persistence of wake vortices.

3. VORTEX FORECAST SYSTEM

3.1 VFS Basic Concepts

VFS basic concepts and approaches were developed by SABIGO starting in the 1970s [1, 3-5]. The approach to aircraft schematization, which is based on the available aircraft information, gives reasonably accurate results for the calculation of integral aerodynamic characteristics (aerodynamic derivatives), aerodynamic loads, and circulations of the attached vortices. The approach to predicting the location and strength of wake vortices is based on the method of discrete vortices (MDV). The approach to calculating danger areas is based on evaluating the aerodynamic forces and moments acting on aircraft moving in inhomogeneous unsteady airflow. These approaches were further developed by the WVPT: SABIGO implemented further improvements to VFS; Gregoire Winckelmans implemented a number of improvements to the Far Wake Model; OTI interfaced VFS to other systems; Gilles Fournier helped to interpret and provide the meteorological data and forecasts; and Metin Yaras conducted evaluations and ran simulations in support of VFS development.

3.2 VFS Structure

The major components of VFS are:

- the Near Wake Model, which produces the Near Wake Database (NWDB) in the offline mode;
- the Far Wake Model, which predicts the vortex location and strength in real time; and
- the Danger Area Model.

VFS requires as input aircraft type, weight, location, speed, and altitude, as well as profiles of wind and turbulence. Furthermore, when using the NWDB, flap deflection and sideslip angles are required. VFS outputs the vortex location and two measures of strength: a value corresponding to the circulation contained in a circle with a radius of half the wing span centred on the vortex centroid, and the sum of the discrete vortex circulations associated with each vortex. VFS also calculates the location of danger areas, which depend on an acceptable definition of danger area, and may depend on the characteristics of the aircraft following behind. VFS functional data flow is shown in Figure 1.

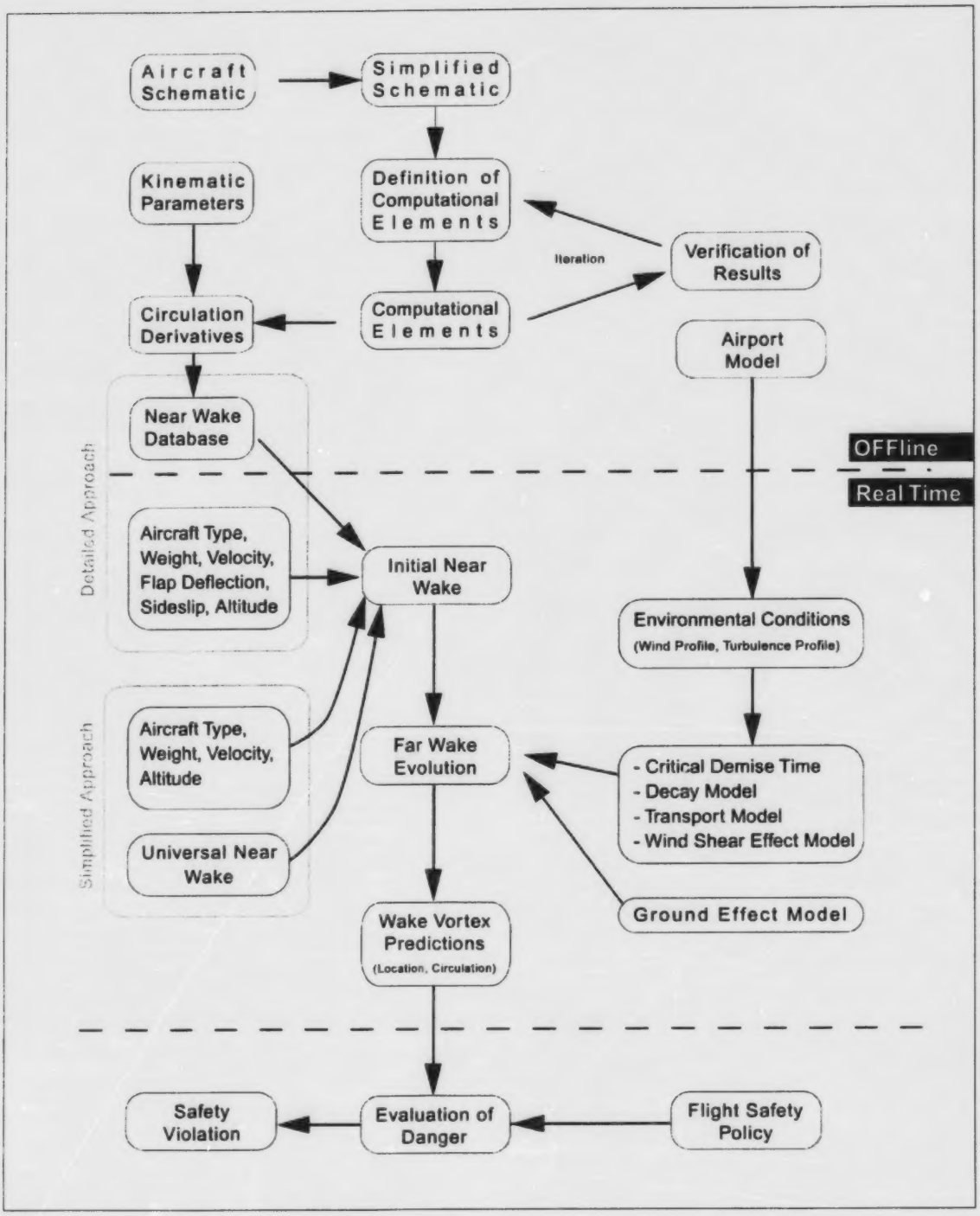

Figure 1: VFS Functional Data Flow

3.3 Near Wake Model

The NWDB is calculated offline for each aircraft type based on the information available on the aircraft geometry [3, 6, 7]. The NWDB contains the circulation derivatives with respect to the main kinematic parameters (aircraft angle of attack, sideslip angle, flap angles, aileron angle, and angular rates), and aerodynamic derivatives of the integral aerodynamic characteristics for several values of aircraft altitude and Mach number.

The NWDB [8-10] has been calculated for a number of aircraft types: B707, B727, B737, B747, B757, B767, B777; A300, A310, A320, A340; DC9, DC10; MD11, MD87, MDXX, LH10, AT72, DH8, and RA46.

3.4 Far Wake Model

The far wake evolution is calculated in real time [4]. Wind and ambient turbulence profiles are provided to VFS from sensors at the airport as a function of altitude and time. To achieve reduced separation on arrival, the wind and turbulence profiles must be predicted for 30 to 60 minutes or more. Such predictions are read as input to VFS.

The far wake calculation may start from the NWDB, or from a Universal Near Wake (UNW) profile as in Proctor et al. [11, 12], but further improved (see Appendix B) and discretized for VFS using discrete vortices.

When the NWDB is used, the angle of attack is evaluated using the condition of correspondence of the aircraft lift to its weight. The calculated value is used in the evaluation of the circulation of the discrete vortices representing the wake shortly after rollup. The aircraft type, weight, speed, and flap angles are required as input.

When the UNW profile is used, the calculated global circulation is used in the evaluation of the circulations of the discrete vortices. The UNW code allows for different levels of spatial resolution, by varying the number of layers used to discretize the port and starboard rollers with the UNW (see Appendix B). The aircraft span, weight, and speed are required as input (see Appendix C), while the aerodynamic characteristics of the aircraft and the flap angle settings are not required.

The far wake calculations are based on 2-D cross-plane MDV equations describing vortex motion in incompressible flows. The Far Wake Model includes:

- in ground and near ground effects;
- non-uniform wind shear effects;
- user selectable eddy dissipation rate (EDR) and turbulent kinetic energy (TKE) decay modelling, with a supplemental small effective viscosity coefficient; and
- the calculation of time-to-demise.

Ground effects are modelled (inviscid for near ground effect, and viscous with production of secondary ground-generated vorticity for in ground effect) on the basis of a ground boundary layer, which leads to the production of secondary discrete vortices at the point of separation of the boundary layers [6, 13-17].

Non-uniform wind shear effects [13] are modelled on the basis of either of two original approaches developed by Winckelmans. One model uses rate of change equations for the discrete vortex circulations (see Appendix D and [18]), while the second and best performing model uses rate of change equations for the discrete vortex positions [18].

The effects of ambient turbulence with length scales that are considerably smaller than the initial spacing of the wake vortex pair are taken into account using either the EDR decay model as in Sarpkaya's model [19], but modified for use within the MDV, or the TKE decay model as in Greene's model [20] using the equations of Donaldson and Bilanin, but modified for use within VFS. Both EDR and TKE models calculate the decay in the discrete vortex circulations. The EDR model uses the universal time-to-demise model and the EDR profile data. The TKE decay model uses the TKE profile. This circulation decay is in addition to the discrete vortex core spreading mechanism, which is implemented through an effective viscosity coefficient [16, 21, 22]. Decay modelling can be of mixed type. The EDR decay model may be used to capture the global circulation decay, and it may be supplemented with a small effective viscosity coefficient to capture the slow core size increase of all discrete vortices.

The Far Wake Model also:

- calculates the time-to-demise (link, burst, etc.) as in Sarpkaya et al. [19] using an accumulated damage model, and a possibly varying EDR profile, which is read as input;
- allows the option to use either least squares polynomial fit or cubic splines fit for calculating the dimensionless profiles for wind, TKE and EDR;
- allows the option to use either the basic Gaussian kernel for the Biot-Savart evaluation, or a fast Biot-Savart kernel to approximate the basic Gaussian kernel (using a high order algebraic kernel), which makes the code about 20 percent faster; and
- allows the total simulated run time to be defined as a variable.

The Far Wake Model outputs the position and circulation of all discrete vortices of the far wake, as well as the positions and global circulation of the port and starboard vortex centroids as a function of time.

3.5 Danger Area Model

Danger areas and safe separations can be calculated offline in advance for many different operational conditions. The output is stored in tables that can be used in real time for the calculation of the required time separations for different leader/follower pairs.

The Danger Area Model is based on SABIGO's approach to the evaluation of aerodynamic forces and moments acting on aircraft moving in inhomogeneous unsteady airflow. The required inputs are the far wake co-ordinates and circulations of the vortices in selected vertical cross sections, and the geometry and aerodynamics of the aircraft following behind. The code calculates the values of the normal and side forces, as well as the values of the pitch, roll, and yaw moments acting on the follower.

Danger area dimensions (and safe separation values) depend on the criterion used for the calculations. Previous SABIGO studies [23] indicate that aircraft encountering wake vortices experience the most violent disturbances because of the induced rolling moment. This would suggest that the induced rolling moment should be used as the criterion for danger areas. However, it is difficult to determine the amount of rolling moment that is dangerous. Another criterion for danger areas is the maximum acceptable roll, which has a clear physical meaning. This criterion, however, requires substantial investigation, models of flight dynamics, and the corresponding initial data (such as the aircraft inertial parameters), which are often not available. VFS uses the criterion based on the induced rolling moment. VFS also calculates the maximum rolling moment, which does not cause the roll to exceed the maximum acceptable value. The calculation is based on a simplified aircraft flight dynamics model plus the aircraft longitudinal inertial moment.

SABIGO has studied the effects of the following factors on the danger area: leader type, follower type, crosswind, ground effect, effective viscosity, and relative path angles between the leader and the follower [7].

3.6 Interface with AVOSS and CTAS

For operational use, VFS needs to be integrated with other systems such as meteorological and vortex sensors, weather prediction systems, and air traffic control systems. For this project, Transport Canada arranged for access to such systems through an agreement with NASA LaRC.

Oracle Telecomputing Inc. (OTI) worked with NASA LaRC to interface VFS with the Aircraft VOrtex Spacing System (AVOSS) developed by NASA LaRC, the weather data network developed for Dallas-Fort Worth International Airport (DFW) by Massachusetts Institute of Technology (MIT) Lincoln Laboratories (LL), and the Terminal Area Planetary Boundary Layer Prediction System developed by North Carolina State University. At NASA's request, OTI implemented the changes to AVOSS and VFS for these interfaces. The integration of VFS with these systems was demonstrated at NASA

LaRC in November 1999. VFS was also adapted to the DFW environment, and was part of the AVOSS final demonstration at DFW in July 2000.

OTI previously site adapted the NASA Center-TRACON Automation System (CTAS) to the Toronto environment. This extensive experience with CTAS made OTI well qualified to interface VFS with CTAS. There is a very close similarity between the output of VFS and the separation matrix used by CTAS. CTAS uses a static separation matrix based on the U.S. Federal Aviation Administration (FAA) wake vortex separation standards. Integrating VFS with CTAS allows the CTAS separation matrix to be continuously updated (every 30 minutes for example) based on VFS predictions. At the request of NASA LaRC, OTI also interfaced AVOSS with CTAS. The integration of VFS and AVOSS with CTAS was done in a way that required only minor change to CTAS, thereby significantly reducing the time and effort that would be required in the future to integrate these systems for operational use. The integration of VFS and AVOSS with CTAS was demonstrated at NASA LaRC in March 1999, and was part of the AVOSS final demonstration at DFW in July 2000.

4. VFS EVALUATION

VFS has been evaluated in many ways including an independent scientific review, sensitivity analysis, developmental testing, and independent comparisons of VFS with field data and other prediction systems. These evaluations, conducted during the various phases of development, have led to a good understanding of the capabilities of VFS, and the various sensors and systems that provide input data to VFS.

Comparison of VFS with the operational requirement has been minimal because the operational requirement for VFS has not been defined in detail. Ultimately, VFS should be evaluated against the cost and the realizable benefits in a particular operational environment. It should be determined what benefits could be achieved at a specific airport. Work with the Vortex Advisory System at Chicago O'Hare [24], the Wake Vortex Warning System at Frankfurt [2 pp 27-32], and AVOSS at DFW [25] are the best examples of this type of evaluation to date.

While VFS was adapted to the DFW environment and was part of the AVOSS final demonstration at DFW in July 2000, there was no attempt to use VFS or to evaluate its accuracy in that operational environment. The evaluations using DFW field data were conducted with recorded data in an offline mode.

VFS predictions were compared to field data from Idaho Falls, Memphis, and DFW. While it is appreciated that this field data is very valuable and may perhaps be the best data available for evaluating wake vortex prediction systems, it must be noted that all such field data has significant uncertainty due to the spatial and temporal variability of the atmosphere, as well as the limitations associated with the field sensors. Care must therefore be taken in assigning the cause of the differences between the predictions and the field data.

4.1 Scientific Review Committee and Idaho Falls Data

Early in the project, a scientific/mathematical evaluation of VFS was conducted by an International Scientific Review Committee, which recommended that evaluation and development of VFS be continued [26]. At the same time VFS was tested with data collected at Idaho Falls using the tower fly-by technique [5, 26, 27, 28]. The summary results of this evaluation were that after 120 seconds, VFS achieved an accuracy of 120 feet in the lateral position and 50 to 100 feet in the vertical position. In addition, Gregoire Winckelmans and Karl Snider conducted a technical review of VFS during a visit to SABIGO in 1995 [3, 4, 29].

4.2 Memphis Data

From 1997 to 2000, a comprehensive evaluation of VFS was conducted by Metin Yaras of Carleton University.

The predictive capabilities of VFS were evaluated through comparisons with aircraft wake data gathered at the Memphis International Airport in 1994-95 [30]. As a result of incomplete similarity between full-scale far wake dynamics and those reproduced in scaled laboratory experiments, full-scale field data was deemed to be more suitable for this evaluation. However, because of spatial and temporal variability of the atmosphere, as well as limitations associated with field sensors, the uncertainty levels in field measurements are typically greater than in well-controlled laboratory experiments. Therefore, particular care was taken in screening the Memphis data to identify the cases to be used in the evaluation of VFS. In addition to the reliability criterion, as much as possible, the test cases were chosen to allow evaluation of VFS with respect to the isolated effects of certain atmospheric conditions and ground proximity. Sixteen cases were selected. Each test case had specified prevailing atmospheric conditions, ground proximity, and aircraft related information. The predictions of VFS were obtained in a test conducted by SABIGO. The following main conclusions were drawn from these evaluations.

1) In a calm and non-stratified atmosphere, VFS was capable of predicting the vertical descent of the wake vortices resulting from mutually induced convection. Lateral convection of the wake by prevailing horizontal winds was also captured accurately. In cases where the prediction accuracy appeared to be relatively poor in these respects, the discrepancy was judged to be related to the potential uncertainty in the lidar measured position of the aircraft.

2) The wake motion in stratified atmosphere was predicted with essentially the same level of accuracy as in non-stratified atmosphere despite the inability of VFS to account for the effects of buoyancy forces or vorticity generation associated with stratification. This result is consistent with the similarity of the wake dynamics for the range of stratification levels encountered during the Memphis field tests [31, 32].

3) Based on two test cases involving non-uniform wind shear, the original VFS was found to be incapable of simulating the interaction between the wake vortices and non-uniform ambient vorticity (i.e., non-uniform wind shear). The capability of modelling non-uniform wind shear effects has since been added to VFS, and has been tested on cases provided by NASA Langley (cases from studies by Proctor et al. [13]), and by NorthWest Research Associates (NWRA) (see section 4.3).

4) As anticipated, VFS failed to reproduce the substantial case-to-case variations in wake vortex trajectories observed under the influence of significant atmospheric turbulence. Due to the stochastic nature of this interaction between the wake and its surroundings, it is unlikely that any prediction algorithm can produce completely reliable results for such conditions. Decay modelling due to turbulence can, however, be improved using the EDR decay model [19]. An EDR decay model has since been added to VFS and included in the test by NWRA (see section 4.3).

5) Finally, VFS was observed to adequately reproduce the viscous interaction of wake vortices with the ground. This was judged on the basis of the timing and extent of the rebound of the wake vortices that result from such an interaction.

4.3 NWRA Testing

During the final year of the project, the Far Wake Model was significantly improved, especially with respect to decay modelling.

After the latest improvements, VFS was evaluated by NASA LaRC as a potential prediction algorithm for AVOSS. As part of this evaluation, VFS was compared to two other prediction systems by NWRA using 211 test cases from Memphis and 191 test cases from DFW. NWRA had also evaluated a previous version of VFS.

Predictions of the latest VFS were evaluated using the same scoring procedures [33] as were used by NWRA for scoring the other two models (referenced herein as Model E and Model T) and the previous version of VFS. The results for Model E, Model T, and the latest VFS are summarized in Tables 1 and 2 below. The definition and derivation of the table entries may be found in [33].

As expected the latest version of VFS had significantly improved performance with respect to the previous version of VFS in predicting circulation values. The lateral position scores for the latest VFS had deteriorated with respect to the previous version of VFS. This was possibly due to the fact that the latest VFS has a shear coefficient that has not been optimized.

A summary of how the results of the latest version of VFS compare with the Model E and Model T results is as follows:

- VFS results for circulation are comparable with the Model E and Model T results; and

- VFS results for vertical position are somewhat worse than the Model E and Model T results, except that VFS median results for Memphis are comparable to the results of the other two models.

It is also noted that the execution speed of the latest VFS is nearly as fast as that of the other two models.

Table 1: Median Values for Indicated Measures of Differences between Predictions and Observations
(Number of cases is shown in parentheses)

Model / Site	RMS $\Delta\Gamma / \Gamma_0$	RMS $\Delta z / b_0$	RMS $\Delta y / b_0$
E / MEM	0.145 (211)	0.415 (211)	0.788 (211)
T / MEM	0.171 (211)	0.431 (211)	0.780 (211)
VFS / MEM	0.163 (211)	0.422 (211)	0.808 (211)
E / DFW	0.156 (191)	0.236 (191)	0.565 (191)
T / DFW	0.168 (191)	0.226 (191)	0.548 (191)
VFS / DFW	0.163 (191)	0.285 (191)	0.625 (191)

Table 2: 90th Percentile Values for Indicated Measures of Differences between Predictions and Observations
(Number of cases is shown in parentheses)

Model / Site	RMS $\Delta\Gamma / \Gamma_0$	RMS $\Delta z / b_0$	RMS $\Delta y / b_0$
E / MEM	0.272 (211)	0.931 (211)	2.300 (211)
T / MEM	0.316 (211)	0.923 (211)	2.214 (211)
VFS / MEM	0.270 (211)	0.947 (211)	2.337 (211)
E / DFW	0.248 (191)	0.500 (191)	1.752 (191)
T / DFW	0.271 (191)	0.487 (191)	1.786 (191)
VFS / DFW	0.253 (191)	0.592 (191)	1.993 (191)

5. METEOROLOGICAL CONSIDERATIONS

To be effective, a wake vortex prediction system requires reliable and accurate input of environmental conditions in the terminal area, and their predictions for 30 to 60 minutes or more. Indeed, atmospheric conditions play a crucial role in airport capacity and the behaviour of wake vortices. For instance, the mean crosswind will induce a lateral displacement of the vortices, while thermal stratification of the Planetary Boundary Layer (PBL), vertical shear of the horizontal wind, and ambient turbulence will all affect the transport and decay of the vortices.

In 1996, SABIGO proposed the use of a wind meter as an input to VFS [34]. The proposed system, which was developed in Russia, can provide wind measurements in three directions with high accuracy and low dynamic errors.

Since the beginning of the project, the WVPT has monitored international developments in weather sensing and nowcasting systems.

5.1 Europe

Some WVPT members attended the WakeNet Workshop at the Institut für Physik der Atmosphäre (DLR) in Oberpfaffenhofen, Germany, in October 1999, where there were a number of presentations on the prediction of far field vortex location and decay. The approaches ranged from simple wind speed persistence forecasting based on statistical wind properties, to terminal weather nowcasting using sophisticated coupling of forecasting tools and the assimilation of measured data, including aircraft data transferred by data link.

CERFACS in France (http://www.cerfacs.fr) has developed and used Large Eddy Simulations (LES) of wake vortices in the atmospheric PBL to study 3D, ground, turbulence, wind, wind shear, and stratification effects. DLR (http://www.pa.op.dlr.de/wirbelschleppe) has also developed and used LES and direct numerical simulations of wake vortices in the convective, stably stratified and sheared atmospheric PBL. It has developed simple models for the real-time prediction of the trajectories and decay of the wake vortices. These have been implemented in the Wake Vortex Warning System at Frankfurt airport. Sensing developments and field studies concentrated on the monitoring of wake vortices, and not on the monitoring of the atmosphere.

5.2 United States

In the United States, NASA Langley and Ames Research Centers have developed technologies to help increase airport capacity levels under instrument meteorological conditions to those achieved under visual conditions. The NASA program (called the Terminal Area Productivity Program) developed AVOSS, which integrates several subsystems. The Weather Subsystem is responsible for providing measurements of wind, temperature, and turbulence levels aloft as well as making short term predictions

(about one hour). This information is used by the AVOSS Predictor Subsystem to predict the time required for the wake vortices of approaching aircraft to move out of the approach corridor or to decay. Variability in the actual and predicted conditions is used to estimate the range of possible wake vortex behaviours, so that a conservative separation value can be applied.

The development of AVOSS included the following activities:

- development of advanced numerical computational models to study the effect of various atmospheric conditions on wake vortex motion and decay;
- development of wake vortex motion and decay prediction algorithms;
- atmospheric PBL modelling to initialize the wake models with realistic turbulent intensities and scale lengths;
- field data collection activities to provide validation data for the numerical models;
- human factors research to provide criteria on the necessary AVOSS update rates and air traffic controller information requirements;
- studies to model the effect of wake vortices on following aircraft when an encounter takes place; and
- wake vortex sensor development.

AVOSS development was co-ordinated closely with the FAA's Integrated Terminal Weather System (ITWS) (http://www.ll.mit.edu/AviationWeather) program for weather support. The atmospheric measurements were used to validate and extend models for predicting wake vortex behaviour. MIT LL and NASA LaRC operated an extensive suite of meteorological sensors, including two sodars, a Doppler profiler, an instrumented 150-foot tower, and shorter towers to estimate the required atmospheric profiles at DFW. This system was integrated with ITWS and included the AVOSS Winds Analysis System (AWAS) to provide a single, consistent view of the winds by considering data from multiple sensors and using data fusion technology developed in the ITWS program. AWAS is an automated algorithm that outputs a vertical profile of horizontal winds specified by a mean and a variance at each output altitude. It is expected that the number and types of sensors for an operational AVOSS system will be reduced from the scientific development test suite deployed at DFW.

In support of the AVOSS demonstration at DFW, North Carolina State University (http://meawx1.nrrc.ncsu.edu) developed the Terminal Area PBL Prediction System (TAPPS), that employs the Mesoscale Atmospheric Simulation System (http://www.meso.com) model to produce mesoscale simulations. A post-processing scheme uses the simulated three-dimensional atmospheric characteristics in the PBL to calculate the turbulence quantities most important to the dissipation of vortices: TKE and EDR. TAPPS was employed to enhance terminal area productivity by providing weather forecasts for AVOSS. The post-processing scheme utilizes experimental data

and similarity theory to determine the turbulence quantities from the simulated horizontal wind field and stability characteristics of the atmosphere.

5.3 Canada

Environment Canada is responsible for meteorological forecasting activities in Canada, including Numerical Weather Prediction. The current regional version of the Canadian Numerical Weather Prediction Model runs at 16 forecast levels and at a 24-km resolution over all of North America. Before the end of 2001, that resolution will be increased to 28 levels and 16 km, then to 10 km by 2004. Appropriate improvements in the parameterization schemes will be included with the increase in resolution. There exists a high resolution version of the model called the High Resolution Model Application Project that is currently running at 10 km on two regions. This will be replaced by 2- to 3-km resolution runs of a non-hydrostatic limited area version of the model that will cover the most populated areas of the country. Other versions of the model will be used for specialized forecasts and it is conceivable that a model similar to TAPPS could be developed to feed VFS. Technical documents on operational forecasting models, the data assimilation system, and the objective analysis may be found at http://www.cmc.ec.gc.ca/cmc/biblios/indexe.html.

Specialized sensing systems similar to the ITWS have not been deployed at Canadian airports; consequently, specialized algorithms similar to the AWAS have not been developed. Canada must therefore look for potential alternatives to these sophisticated systems. The use of an air-ground data link is one good prospect.

Canadian air carriers and other organizations under the lead of Environment Canada are currently developing a national Aircraft Meteorological Data Relay (AMDAR) Program. A wake vortex system would require aircraft to report accurate profiles of temperature, wind, and turbulence in the PBL with a high resolution in time and space near major airports. It is anticipated that in 2001, 15 to 20 Canadian AMDAR-equipped aircraft will service 25 major airports daily. These numbers could increase to 150 aircraft and 70 airports by 2005, and 260 aircraft by 2010. Wind, temperature, pressure, and turbulence (EDR) data will likely be reported on ascent at 10-second intervals for the first 150 seconds, then every 50 seconds until 20 minutes after takeoff. On descent starting at 18,000 feet, observations will be at 20-second intervals until touchdown. It will be possible to select through up-link commands higher reporting frequency at extra communications costs.

From the Canadian AMDAR Program alone, the frequency of reports at the busier Canadian airports, the space resolution of the data, and the accuracy of the data will not be sufficient for wake vortex prediction applications. For example, it has been proposed to RTCA (US Radio Technical Commission for Aeronautics) Subcommittee 169 that minimum operational performance standards for automated meteorological transmission of measurements in the PBL be as follows:

- time resolution to 0.1 second;

- position to within 50 feet, or to Global Positioning System (GPS) resolution;
- temperature resolution to the nearest 0.1°C;
- vertical wind to 0.1 m/s accuracy;
- pressure to 1 hPa accuracy; and
- reporting to at least every 50 feet in altitude.

These types of requirements are achievable if the appropriate resources are provided. However, the aviation community perceives the much higher resolution requirements for wake vortex applications at terminals as specialized supplementary local requirements, not appropriate for AMDAR programs, which are national and global in scope. Therefore, funding and control for these supplementary local requirements should come from the primary users (i.e., airlines, airport authorities, and NAV CANADA), and the data should not be put on the World Meteorological Organization Global Telecommunication System.

6. RELATED STUDIES BY THE WVPT

The WVPT undertook several studies related to wake vortex prediction, some of which are described below.

6.1 Estimation of VFS Performance at an Airport

SABIGO developed a model for evaluating the increase in airport capacity when using VFS. Preliminary results show that this increase could be 15 to 20 percent for busy airports [6, 15].

6.2 Data Link

Data-linked meteorological data and a simple meteorological model may be able to provide accurate short-term (30- to 60-minute) fine resolution Terminal Weather Forecasts required by VFS. OTI and Environment Canada conducted a literature search relative to this possibility. Some of their findings are provided below.

Automatic reporting of meteorology and turbulence data by aircraft is becoming a reality. The US Meteorological Data Communications and Reporting System as well as Automatic Dependent Surveillance are data links providing overlapping service. In the United States, six airlines are currently participating in reporting weather via the Aircraft Communications Addressing and Reporting System. The World Meteorological Organization has set up an AMDAR Panel to globalize this new important source of weather data, which is significantly improving the accuracy of forecasts.

Progress is being made with a new Water Vapour Sensing System for measuring relative humidity aloft. This reading will be added to the meteorological data reported from the aircraft. An accurate relative humidity measurement from the worldwide fleet of aircraft will have a significant impact on the accuracy of 2- to 5-day forecasts, as well as on short-term forecasts (nowcasts).

The Intelligent Weather System's technology was originally developed by the US National Center for Atmospheric Research for monitoring and nowcasting of low-level turbulence at the new Hong Kong airport and for helicopters landing on moving ships (i.e., landing in a turbulent environment), and would be especially suited for the wake vortex requirements. The Intelligent Weather System uses fuzzy logic to diagnose and forecast the best profiles of meteorological parameters from various sources of data, (some overlapping), as opposed to the traditional mathematical and statistical based methods holding large uncertainty bars.

A thesis by B. Hansen outlines a method of retrieving similar temporal cases from a large database to make airport weather predictions more accurate. A fuzzy-logic based methodology for knowledge acquisition, commonly used to build knowledge-based systems, is used to build a case-based reasoning system. Such a system will allow many large unused archives of airport weather observations (ready repositories of

temporal cases) to be tapped for airport weather predictions. This will help to make airport weather predictions more accurate, which will make air travel safer and airlines more profitable. Such a system also offers several advantages compared to statistical prediction, which is currently the most competitive method. Accordingly, a case-based reasoning prediction system was implemented and tested. The system, called WIND-1, was tested with the problem of producing 6-hour predictions of cloud ceiling and visibility at an airport, given a database of 300,000 consecutive hourly airport weather observations (34 years of records). The prediction accuracy of WIND-1 was measured with standard meteorological statistics and compared to a benchmark prediction technique using persistence. In realistic simulations, WIND-1 was shown to be significantly more accurate.

6.3 Sensitivity Analysis

The WVPT recognized the importance of analysing the sensitivity of VFS to errors or perturbations in the input data. SABIGO conducted sensitivity analyses on angle of attack, flap deflection angle, sideslip angle, flight altitude, cross wind, vertical wind, and effective viscosity coefficient (see [15] and Appendix E).

6.4 Hazard Definition

SABIGO conducted a study on the evaluation of danger zones and safe separations, the aim of which was to determine the best criteria to use (rolling moment or maximum allowed angle of roll) and to evaluate the maximum level of the rolling moment, which does not cause the roll of the follower to increase over the acceptable value. SABIGO recommended the use of the admissible rolling moment as a function of aircraft speed and altitude. It also presented an algorithm for the evaluation of danger areas and safe separations (see [6, 23] and Appendix F). C.R. Tatnall published a useful reference on sensor observable wake strength parameters [35].

6.5 Flight Data Monitoring

Data recorded in flight could provide a useful addition to the wake vortex research efforts. For example, it may be possible to detect wake vortex encounters during regular Flight Data Monitoring activities. This quantified encounter information, in conjunction with other information such as the air traffic situation and meteorological conditions, could be very valuable in improving the understanding and real-time prediction of vortex transport and decay.

Wayne Jackson conducted a survey of organizations interested in using Flight Data Monitoring. The results of that survey are included below.

The UK National Air Traffic System runs a wake vortex research program. It keeps a database of wake vortex encounters and also, where possible, obtains traces from flight data recorders. It has completed a preliminary investigation using some 50 wake vortex traces supplied by British Airways. It has also developed some software routines to

automatically detect vortex encounters. Contact Simon Mason at s.mason@rd1-nats.demon.co.uk.

British Airways is interested in the assessment of potential vortex encounters to eliminate these from investigations of aircraft control problems. In the past, it has been necessary to ground aircraft for complex and time consuming system checks because of the difficulty in identifying external influences during upsets. A checking routine for use in specific incidents would therefore be very useful. Additionally, a Flight Data Monitoring event embedded in its routine analysis program would be useful to determine actual encounter frequency. Contact Mike Nebylowitsch at mike.1.nebylowitsch@british-airways.com.

SABIGO has investigated the use of flight recorded data in the study of wake turbulence (as well as atmosphere turbulence) for several years. Recorded flight parameters are analysed on the basis of appropriate mathematical models to reveal the trajectory segments with turbulence or intense wind/vortex effects. Contact Andrei Belotserkovsky at sabigo.smb@g23.relcom.ru.

The US National Transportation Safety Board (NTSB) has about 200 recordings of data and video on wake vortex encounters from flight tests using an instrumented B-737 flying behind a B-727 equipped with smoke generators. Most of the encounters were at separations of about 4 miles. However, some were much closer. The NTSB was only looking at the data in terms of investigating a particular accident. Therefore, very little time was spent in examining the data from a broader wake turbulence point of view. A lot of the data may not have been examined in detail. All of the data is available from the NTSB. Contact Jim Cash at cashj@ntsb.gov.

6.6 Airborne VFS

Ground based wake vortex prediction systems are needed to plan and execute more efficient air traffic flow management and control. There is also a need for airborne wake vortex detection and indication systems to enable pilots to make credible wake turbulence avoidance decisions. SABIGO has studied the possibility of developing an Airborne VFS to display wake vortex danger areas to the pilot (see Appendix G). A demonstration system displays the position of the vortex core and the danger area.

It is anticipated that the Airborne VFS would be derived from the ground based VFS. The Airborne VFS would require input information such as leader type, spacing between leader and follower, phase of flight, wind profile, atmospheric turbulence condition, leader and follower flight paths, and leader flight parameters (including weight).

Further development activities specific to the Airborne VFS would include optimization of pilot display and control, and optimization of the system design for the airborne application.

6.7 Investigation of Near Wakes Shortly after Rollup

Gregoire Winckelmans investigated near wakes shortly after rollup, both numerically and experimentally (see Appendix B). The velocity field induced by the port and starboard vortices was obtained and used as the basis of determining the distribution of circulation within each vortex. The results were compared with the UNW profile proposed by Proctor et al., which serves as the basis in many computational fluid dynamics (CFD) simulations of far wake development. The proposed outer profile was confirmed. The Gaussian profile was also confirmed for the inner profile. It was noted that the profile proposed by Proctor et al. has a significant discontinuity in the first derivative at the location of maximum velocity. A new UNW profile is proposed that is valid for all radii, produces the inner and outer profiles, and transitions smoothly from the inner profile to the outer profile. This new profile was validated with a number of test cases.

6.8 Detailed Wake Studies

In support of VFS development, detailed studies were conducted by Winckelmans et al. from 1996 to 1999, using a high-order version of the MDV. These methods incorporate the redistribution of the vortex particles using high-order schemes, the treatment of viscous diffusion using the exchange of circulations, and the treatment of the no-slip condition at solid boundaries using a boundary element method (to determine the vorticity flux) together with a high-order diffusion method (to distribute this flux to nearby particles). The studies included transport and diffusion of vortex wakes [22], viscous interaction of vortex wakes with the ground [14,17,36], and interaction of vortex wakes with non-uniform wind shear [37]. These studies also served as baseline cases in the development and validation of the simplified models used in VFS (for viscous ground effect, and non-uniform wind shear effect).

6.9 Comparison of EDR and TKE Decay Models

Using the data from Memphis (211 cases) and DFW (191 cases), a study was conducted by Winckelmans et al. to compare the time constant coefficient used by VFS in the EDR and TKE decay models (see Appendix H). These studies helped calibrate the coefficients used in the models.

6.10 LES Studies

Studies of wake vortex decay in a turbulent atmosphere were conducted by Winckelmans et al. using LES [38, 39]. These LES studies were started assuming a wake shortly after rollup (using the UNW profile). Different turbulence levels were studied, ranging from weak to strong turbulence. Different LES models were used with different spatial resolution. These LES studies confirmed that the EDR decay model is better than the TKE decay model. They also helped confirm the coefficient to be used in the EDR decay model in VFS.

6.11 Numerical Simulations

In the evaluations of the original VFS, comparison with field data was limited to motion of the wake vortices. The decay rate was not examined. The primary means of modelling the diffusion of the wake vortices in the original VFS was through an "eddy viscosity" that spreads the core associated with each discrete vortex particle, but does not allow for circulation decay (since it does not allow for viscous interaction of vortices with opposite sense of rotation). With the EDR decay model [19] implemented, VFS now accounts for circulation decay, with the decay being distributed uniformly among the discrete wake vortices, and no account being made for spatial non-uniformity). VFS can now be viewed as a physically more correct, yet still approximate, operational implementation of a "uniform eddy viscosity" model. Typically, very few discrete vortices are utilized by VFS to maintain real-time capability, and this does not allow accurate modelling of the spatial non-uniformity of the eddy viscosity. This, in turn, leads to the question of how realistic it is to assume a constant eddy viscosity throughout the wake-vortex field, and what this constant value should be. To this effect, Metin Yaras performed numerical simulations using a Reynolds-Averaged Navier-Stokes (RANS) solver. The simulation results with fixed eddy viscosity were compared to predictions with a one-equation turbulence model as well as to cross-stream velocity distributions extracted from Memphis field data. Based on these comparisons, use of a constant eddy viscosity in capturing the diffusion of the wake vortices as well as their interaction with variable wind shear and/or the ground was found to be sufficiently accurate in the context of estimating wake vortex trajectories. In the context of these simulations, it was also demonstrated that axial motion within the wake vortices and/or headwind shear has little impact on the wake vortex trajectories in the cross stream plane. This helps justify the use of spatially two-dimensional algorithms such as VFS. A complete report on the RANS simulations is presented in Appendix I.

7. OTHER WAKE VORTEX RESEARCH

In December 1997, Transport Canada hosted an International Wake Vortex Meeting [2]. The principal objectives of this meeting were to promote international co-operation in the development of a real-time wake vortex forecasting system and to discuss improved aviation safety and efficiency in relation to wake vortex modelling, real-time prediction, and meteorological requirements. Experts from Canada, Russia, Belgium, the United States, the United Kingdom, France, and Germany explained their perspectives on the wake vortex issues as well as their proposed solutions. Representatives of airlines, pilots, air navigation service providers, air traffic controllers, airport authorities, governments, and aircraft manufacturers presented their views on the issues.

7.1 Canada

Transport Canada has funded the Wake Vortex Prediction Project since 1993. Prior to that, Transport Canada had co-operated with the United States in several wake vortex research activities through a formal research agreement with the FAA.

The Transport Canada research plans for 1992 included three proposed research activities. One of these studies was a cost-benefit analysis of a wake vortex prediction system at Vancouver. These studies were not completed at that time. The Manager of Airside Operations, Vancouver International Airport Authority, recently indicated to Transport Canada that he is interested in wake vortex prediction technology and its potential implementation at Vancouver.

The National Research Council of Canada has conducted wake vortex research activities over several years. This work includes fundamental studies of wake vortex physics using wind tunnels and modelling. The main focus of these studies was the effect of wake vortices on crop spraying [40]. Since a large portion of the aerial spray is entrained into the trailing vortices, the investigation of the vortex evolution and trajectory is of primary importance. Similar to the vortex forecasting motivated by air traffic safety, attention is paid to the interactions of vortices with the ground boundary layer [41] and atmospheric conditions, such as crosswind. Field experiments supported by numerical modelling were used to explain that a poorer efficiency of the downwind wing atomizers is due to a reduction in the descent speed of the downwind vortex [42]. The underlying phenomenon, known as vortex "bounce", also plays an important role in VFS prediction. More recent explorations, resulting from collaboration with the WVPT and other organizations, involved the experimental investigation of wing tip vortices in a wind tunnel using particle image velocimetry [43] and hot wire anemometry [44], and also the prediction of interactions of aircraft trailing vortices with ambient shear layers [45].

7.2 United States

An annotated bibliography on wake vortices [46] by Hallock is a good reference for wake vortex research and development. To be considered for this bibliography, the publication has to possess a possible implication in the setting of separation standards.

A paper by Hallock [24] summarizes the state of knowledge about aircraft wake vortices in 1990. This paper covers topics such as vortex sensors, current knowledge, gaps in knowledge, vortex avoidance systems, alleviation, and the major issues arising from the evaluation of the Vortex Advisory System at Chicago O'Hare in 1977.

A paper by Rossow [47] provides a comprehensive survey of wake vortex research conducted during the past 30 years. It covers vortex hazard, alleviation, and avoidance methods.

In 1995, the Volpe National Transportation Systems Center published a book and CD [48] meant to enhance wake turbulence training for both pilots and air traffic controllers. This material resulted from a large international effort headed by the US Air Transport Association and Boeing.

The Reduced Spacing Operations element at the NASA LaRC has been developing AVOSS [25] for several years. In July 2000 it demonstrated AVOSS at DFW. The objective of the demonstration was to prove the concept in an operational environment, with all variables present, and provide a system ready for handoff to the FAA and industry for operational development. In conjunction with this demonstration, NASA issued the following press release:

> *"With the support and participation of the FAA, Dallas-Fort Worth International Airport, Air Transport Association, Boeing, Lincoln Laboratory, Transport Canada, and Volpe National Transportation Systems Center, NASA has developed breakthrough technologies for an Aircraft VOrtex Spacing System.*
>
> *"The system provides weather dependent wake vortex spacing criteria for maximizing airport capacity while maintaining safety.*
>
> *"AVOSS will provide air traffic controllers with the first ever accurate and reliable prediction of wake vortex behavior that they can use to safely reduce this spacing.*
>
> *"Using these breakthrough technologies, airports like DFW could reduce takeoff delays as well as increase runway throughput by 10 percent or more during instrument approach conditions."*

The contact at NASA LaRC is Neil O'Connor, c.j.oconnor@larc.nasa.gov (tel.: 757-864-4662). More information can be found on the web site http://avsp.larc.nasa.gov/avoss.

7.3 Europe

To meet future traffic demands, a Capacity Enhancement Program has been agreed between Frankfurt Airport and its partner Deutsche Lufthansa, and Deutsche Flugsicherung (DFS, German Air Navigation Services). This program, known as Stufenplan 2000 was launched in 1995 with a rate of 70 movements per hour. Its declared target is to achieve a level of 80 movements per hour by the year 2000.

The High Approach Landing System / Dual Threshold Operation (HALS/DTOP) is part of Stufenplan 2000. HALS/DTOP is being developed primarily as a capacity enhancing procedure for arriving aircraft. With the help of HALS/DTOP the lateral spacing for approaching aircraft can be reduced from wake vortex separation to radar separation with reduced or equal risk of wake vortex encounter compared to the International Civil Aviation Organization (ICAO) wake vortex separation standard. In effect, the system will not only enhance approach capacity, but also increase the already existing high safety standard of Frankfurt Airport.

To create a second glide slope path located approximately 80 meters above the already existing one, a second, extremely displaced threshold has been implemented on one of the already existing runways. This is illustrated in Figure 2. The second, displaced threshold has been equipped with individual air navigation aids, an approach lighting system (including Precision Approach Path Indicator) and runway markings allowing operations to the lower limits of Category 1 landing conditions. The runway markings and the approach lighting system have been developed in close co-operation with airline pilots and simulations in the Lufthansa flight simulator. The lighting and marking are based on the ICAO Standards but there is a clear discrimination between the new markings/lights and the conventional markings/lights.

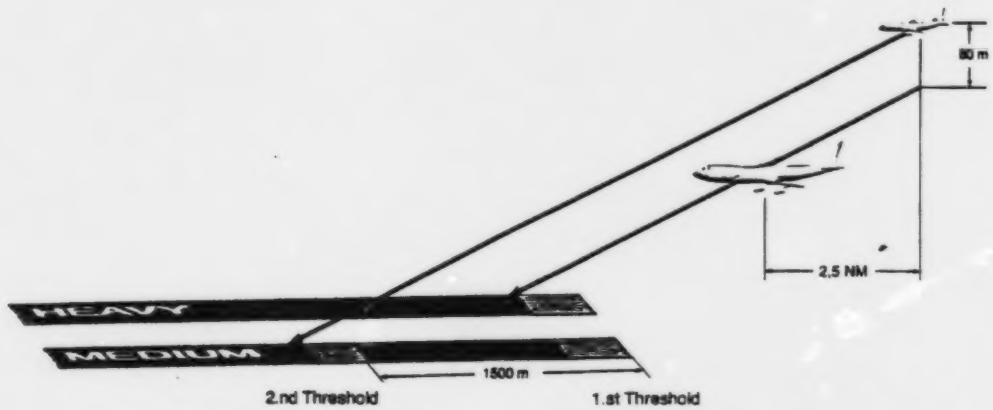

Figure 2: HALS/DTOP

It is very important to recognize the extensive effort made by many organizations in wake vortex research, safety risk assessment, and communication among all parties involved, including future users of HALS/DTOP.

Contact Hartmut Mueller at hartmut.mueller@dfs.de.

Apart from the private and the national research projects, the European Commission has sponsored a number of collaborative wake vortex related research projects.

Wake formation was extensively studied in the Eurowake Project, which was co-ordinated by DASA-Bremen.

- The detection of wake vortices (and other flow disturbances) with on-board forward-looking laser equipment was the objective of the MFLAME Project, which was co-ordinated by Sextant.
- The creation of a wake vortex incident-reporting log was the subject for the ETWIRL Project, which was co-ordinated by RED Scientific.
- Wake vortex evolution and decay in the atmosphere, the prediction of wake vortex-induced aerodynamic forces on an aircraft during wake encounter and the simulation of wake encounters with flight simulators has been the objective of the WAVENC Project [49], which was co-ordinated by the Netherlands National Aerospace Laboratory (NLR).
- In addition, the Commission is sponsoring the Thematic Network WakeNet, which organizes two workshops each year on wake vortex related issues inviting representatives of research institutes, industry, pilot associations, air traffic management, and regulation authorities.

Recently, two new European wake vortex-related collaborative research projects have been initiated (C-Wake and S-Wake). The C-Wake Project considers the wake vortex characterization and control. This project is co-ordinated by DaimlerChrysler Aerospace Airbus and is a follow-up of the previous EUROWAKE Project. S-Wake, is a follow-up of the WAVENC Project. S-Wake is co-ordinated by NLR and addresses the wake vortex safety aspects. Both projects started in January 2000 and have a duration of three years. The co-ordinator is A.C. de Bruin, bruina@nlr.nl (tel.: 0031-527248659). More information is provided at http://www.cerfacs.fr/~wakenet/.

WakeNet has recently published a position paper [50] on aircraft wake vortices, which presents the consolidated view of the WakeNet partners on:

- the nature and characteristics of aircraft wakes; and
- the technical and operational procedures being required to minimize and predict vortex strength and to avoid wake encounters.

This paper addresses the methodological aspects of data evaluation and interpretation, including:

- the description of the wake ages;
- the characterization of wake vortices;
- the correct set-up of field experiments; and
- the correct evaluation of wake data from measurements and simulations.

The paper also includes an inventory of the collective WakeNet state-of-knowledge in the fields of:

- vortex minimization;
- prediction and monitoring of vortex decay;
- vortex detection and warning;
- vortex encounter modelling; and
- wake vortex safety assessment.

The WakeNet paper provides a comprehensive list of questions and required actions to help guide further research activities in each of the above areas.

Other projects are still in the preparation and negotiation phase. For example, I-Wake (an extension of the former MFLAME Project) is intended to study instrumentation systems for on-board wake vortex and other hazards detection, warning, and avoidance.

8. CONCLUSIONS

1) Wake vortices constitute one of the main obstacles in the efficiency of airport takeoff and landing operations. Prescribed minimum separation distances, which were established years ago, are in most cases quite conservative.

2) Safely reducing separation during instrument meteorological conditions could permit capacity at major airports to be increased by up to 15 percent, and delays on arrival and departure to be significantly reduced. This improved efficiency would be worth billions of dollars in savings to airlines, airports, and the travelling public.

3) Authorities in Germany believe that with the help of HALS/DTOP at Frankfurt Airport, the lateral spacing for approaching aircraft can be reduced from wake vortex separation to radar separation while maintaining or reducing the existing level of risk of wake vortex encounters.

4) NASA officials believe that AVOSS will provide air traffic controllers with the first ever accurate and reliable prediction of wake vortex behaviour that can be used to safely reduce vortex spacing. Airports like DFW could reduce takeoff delays as well as increase runway throughput by 10 percent or more during instrument approach conditions.

5) Airports in Canada that are facing capacity problems include Vancouver, Toronto, and possibly Dorval. Each airport is a unique environment (traffic demand, traffic mix, weather, etc.). Every airport therefore requires to be considered individually when planning to invest in a vortex prediction system.

6) The potential benefit of wake vortex prediction systems is clear and increasing with the rising demand for air travel and larger aircraft. The recent decision by Airbus to build larger aircraft will add to the interest in wake vortex research.

7) Aviation authorities, scientists, and researchers in Canada, the U.S., and Europe have for many years been studying techniques and systems that would enable safe reduction of wake vortex separation distances to improve airport capacities. Major wake vortex research and development projects are continuing in the United States and Europe.

8) Several organizations in Canada, the United States, and Europe have expressed an interest in co-operating with Transport Canada and the WVPT in wake vortex research and further development of VFS.

9) Canada could leverage the results of this international effort to the benefit of Canadian aviation. Past agreements with NASA and the FAA would facilitate continued co-operation with the United States. The Canada-European Union Agreement on Co-operation in Science and Technology would be useful for any co-operation with European organizations. The web site found at http://www.cordis.lu/canada/ contains information on the modalities of the

Agreement, the European Union's Fifth Framework R&D Program, the Canadian R&D programs, and funding sources for Canadian participants.

10) During the past seven years the WVPT has made significant advancements in the development of VFS and improved understanding of aviation safety and efficiency with respect to wake vortex modelling, real-time prediction, and the meteorological requirements. VFS is now one of the most capable real-time wake vortex prediction system in the world.

11) The WVPT has seven years experience as a team and strong capabilities in many areas required to develop an operational wake vortex prediction system. WVPT expertise includes:

- computational fluid dynamics;
- method of discrete vortices;
- evaluation methods;
- simulation methods;
- meteorological requirements;
- computers and software;
- operational requirement;
- air traffic control automation; and
- project management.

12) TDC is very experienced and well-positioned to facilitate international co-operation in wake vortex research and development.

13) Since the current separation standards are considered safe, the main objective of this research is increased operational efficiency. Since Transport Canada's primary role is safety regulation, Transport Canada can no longer justify being the sole sponsor of this research in Canada. The funding for this research in Canada was discontinued in April 2000.

14) There is a broad interest and capability in wake vortex prediction in Canada. This is illustrated by the Canadian organizations that participated in the International Meeting held in Ottawa in 1997:

- Aeroports de Montreal
- AeroVations Associates
- Air Canada
- Air Canada Pilots Association
- Air Transport Association Canada
- Canadian Airlines International
- Canadian Forces Directorate of Flight Safety
- Canadian Owners and Pilots Association
- Carleton University
- Environment Canada
- Oracle Telecomputing

- Ottawa-Macdonald-Cartier International Airport
- National Research Council
- NAV CANADA
- Transportation Development Centre
- Transportation Safety Board
- Transport Canada
- University of Ottawa
- Université du Québec à Montréal.

9. RECOMMENDATIONS

1) Canadian aviation stakeholders such as Transport Canada, NAV CANADA, and the major airport authorities should continue wake vortex research in Canada. They should ensure that all interested parties participate, including airlines, pilots' associations, industry, research organizations, universities, the Department of National Defence, the Canadian Owners and Pilots Association, Environment Canada, the National Research Council, and the Transportation Safety Board.

2) A specific airport should be selected in Canada to provide a focus for Canadian wake vortex research.

3) Researchers and aviation authorities in Canada should continue to co-operate internationally.

4) VFS development and evaluation should be continued as follows:

   - There were many significant improvements to VFS during the final year of the project. It would be valuable to conduct further evaluations of these recent changes.
   - VFS should be tested with additional values of the wind shear coefficient.
   - Comparing VFS to other wake vortex prediction systems should be continued.
   - Comparing VFS capabilities to the operational requirements at a specific airport would be most valuable.
   - Further VFS sensitivity analysis would be useful.
   - Further numerical simulation and LES studies would be valuable.
   - A simple stratification model should be added to VFS.
   - The possibility of increasing the accuracy of VFS results through more comprehensive information on the aircraft wing geometry, namely the wing incidence angle and flap geometry, should be investigated.
   - Depending on the interest of the FAA, NASA LaRC, and Canadian stakeholders, the interface of VFS to AVOSS and CTAS is already well developed, and could be further developed and applied to an operational situation. It would be interesting to adapt VFS to other operational environments in Canada and abroad. Depending on the interest in Germany, Frankfurt airport is one possibility.
   - The Airborne VFS should be further developed.

5) Experts in Canada should continue the development of meteorological measuring and prediction systems, and their application to wake vortex prediction. This includes the use of data link. World leading expertise exists in

Canada at the Canadian Meteorological Centre, Environment Canada, Carleton University, Université du Québec à Montréal, and Oracle Telecomputing Inc., to name a few.

6) An internationally accepted definition of vortex strength and hazard should be developed.

7) The possibility of regulators requiring wake vortex data for aircraft certification should be investigated.

8) A wake vortex incident reporting system should be reviewed and possibly implemented in Canada.

REFERENCES

1) W.G. Habashi and F.D. Mavriplis, *Russian Vortex Forecast System and on Visit of Professors S.M. Belotserkovsky and V.Ja. Mitnitsky*, ICAST, Canada, January 1994.

2) H. Posluns, *Proceedings of the International Wake Vortex Meeting, Ottawa, Ontario*, TP 13166, Transportation Development Centre, Canada, December 1997.

3) S.M. Belotserkovsky, *Steady Aerodynamic Characteristics and Free Vortex Circulations for B-767-200 and B-757-200 Aircraft* (called Near Wake report), SABIGO, Russia, November 1994.

4) S.M. Belotserkovsky, *Simulation of Aircraft Wake Vortex Motion* (called Far Wake Report), SABIGO, Russia, January 1995.

5) S.M. Belotserkovsky, *Information Processing Part of the System "Vortex Situation Forecasting at Airports"*, MacDonald Dettwiler and Associates, Canada, March 1995.

6) S.M. Belotserkovsky, *Computer Vortex Forecast System*, TP 13373E, Transportation Development Centre, Canada, March 1999.

7) S.M. Belotserkovsky, *Computer Vortex Forecast System*, SABIGO, Russia, May 1999.

8) S.M. Belotserkovsky, *Typical Data Base of Near Wake and Aerodynamic Derivatives for Boeing 737-300 Aircraft*, SABIGO, Russia, 1996.

9) S.M. Belotserkovsky, *Steady and Unsteady Aerodynamic Characteristics and Free Vortex Circulation Derivatives for B707, B727, B737, B747, B757, B767, B777; A300, A310, A320, A340; DC9, DC10; MD11, MD87, MDXX, LH10, AT72, DH8, and RA46 Aircraft*, SABIGO, Russia, 1996.

10) S.M. Belotserkovsky, *ACE 2.0: Software Package for Automatic Construction of a Computational Scheme and Calculation of Steady and Unsteady Characteristics of an Aircraft and its Near Wake at Subsonic and Supersonic Flight Speeds*, SABIGO, Russia, 1996.

11) J. Han, Y.-L. Lin, S. Pal Arya and F. H. Proctor, *Large eddy simulation of aircraft wake vortices in a homogeneous atmospheric turbulence: vortex decay and descent*, AIAA 99-0756, 37th AIAA Aerospace Sciences Meeting and Exhibit, Reno (Nevada), Jan. 11-14, 1999.

12) S. Shen, F. Ding, J. Han, Y.-L. Lin, S. Pal Arya and F. H. Proctor, *Numerical modeling studies of wake vortices: real case simulations*, AIAA 99-0755, 37th AIAA Aerospace Sciences Meeting and Exhibit, Reno (Nevada), Jan. 11-14, 1999.

13) F.H. Proctor, D.A. Hinton, J. Han, D.G. Schowalter and Y.-L. Lin, *Two dimensional wake vortex simulations in the atmosphere: preliminary sensitivity studies*, AIAA 97-0056, 35th Aerospace Sciences Meeting & Exhibit, Reno (Nevada), Jan. 6-10, 1997.

14) G.S. Winckelmans and P. Ploumhans, *Interaction of aircraft vortex wakes with the ground: MDV sample computations using different approaches*, Université catholique de Louvain, Belgium, February 1997.

15) S.M. Belotserkovsky, *Prediction of Aircraft Wake Vortices During Takeoff and Landing*, SABIGO, Russia, 1997.

16) S.M. Belotserkovsky, *Influence of the Ground Boundary Layer on the Position of Far Wake Vortices*, SABIGO, Russia, 1997.

17) G.S. Winckelmans, *Prediction of Aircraft Wake Vortices During Takeoff and Landing*, Université catholique de Louvain, Belgium, June 1997.

18) G.S. Winckelmans, F. Thirifay and P. Ploumhans, *Effect of non-uniform wind shear onto vortex wakes: parametric models for operational systems and comparison with CFD studies*, Proceedings of Fourth WakeNet Workshop on "Wake Vortex Encounter", Amsterdam, The Netherlands, October 16-17, 2000.

19) T. Sarpkaya, R. E. Robins and D. P. Delisi, *Wake-vortex eddy-dissipation model predictions compared with observations*, AIAA 2000-0625, 38th AIAA Aerospace Sciences Meeting and Exhibit, Reno (Nevada), Jan. 10-13, 2000.

20) G. C. Greene, "An approximate model of vortex decay in the atmosphere", *Journal of Aircraft*, Vol. 23, July 1986, pp. 566-573.

21) S.M. Belotserkovsky, *Investigation on Evaluation of Effective Viscosity Factor* μ^*, SABIGO, Russia, 1996.

22) G.S. Winckelmans, *Review of report by SABIGO "Investigation Evaluation of Effective Viscosity Factor* μ^**"*, GSW Consulting Services, U.S.A., November 1996.

23) S.M. Belotserkovsky, *Calculation of Danger Areas in Aircraft Wake Vortices*, SABIGO, Russia, 1996.

24) J.N. Hallock, *Aircraft Wake Vortices: An Assessment of the Current Situation*, DOT-FAA-RD-90-29, Volpe National Transportation Systems Center, U.S.A., January 1991.

25) D.A. Hinton, al., *Design of an Aircraft Vortex Spacing System for Airport Capacity Improvement*, AIAA 2000-0622, NASA LaRC, U.S.A., January 2000.

26) K. Snider, *Wake Vortex Prediction Study*, TP 12593E, Transportation Development Centre, Canada, December 1995.

27) S.M. Belotserkovsky, Evolution of the VFS: Improvement, Testing, Application Examples, SABIGO, Russia, August 1995.

28) S.M. Belotserkovsky, *Evaluation of Mathematical Models for Boeing 727 and 767 Far Wakes*, SABIGO, Russia, 1996.

29) G.S. Winckelmans and K. Snider, *VFS Evaluation Visit*, MacDonald Dettwiler and Associates, Canada, February 20, 1995.

30) M.I. Yaras, *An Evaluation of the Vortex Forecasting System for Predicting Aircraft Far Wake Trajectories*, Carleton University, Canada, September 1998.

31) M.I. Yaras, "Effects of Atmospheric Conditions and Ground Proximity on the Dynamics of Aircraft Vortices", *Canadian Aeronautics and Space Journal*, Volume 44, Number 2, 1998.

32) M.I. Yaras, *Effects of Atmospheric Conditions and Ground Proximity on the Dynamics of Aircraft Wake Vortices: A Study of the 1994-95 Memphis Field Measurements*, TP 13372E, Transportation Development Centre, Canada, March 1999.

33) R.E. Robins, and D.P. Delisi, *Wake Vortex Algorithm Scoring Results*, Final Report for subcontract 4-82U-7473 with Research Triangle Institute, November 2000.

34) S.M. Belotserkovsky, *Provision of Wind Measurement for Vortex Forecast System*, SABIGO, Russia, 1996.

35) C.R. Tatnall, *An Investigation of Candidate Sensor-Observable Wake Strength Parameters for AVOSS*, NASA/CR-1998-206933, NASA LaRC, U.S.A., March 1998.

36) G.S. Winckelmans and P. Ploumhans, *Prediction of Aircraft Wake Vortices During Takeoff and Landing – Phase 4*, TP 13374E, Transportation Development Centre, Canada, March 1999.

37) G.S. Winckelmans and P. Ploumhans, *Prediction of Aircraft Wake Vortices During Takeoff and Landing*, Université catholique de Louvain, Belgium, July 1999.

38) H. Jeanmart and G. S. Winckelmans, *Large-eddy simulations of aircraft wake vortices in a turbulent atmosphere*, 5th National Congress on Theoretical and Applied Mechanics, Louvain-la-Neuve, Belgium, May 23-24, 2000.

39) H. Jeanmart and G. S. Winckelmans, *LES of aircraft wake vortices in a turbulent atmosphere: tensor-diffusivity mixed modelling versus classical modelling*, EUROMECH Colloquium No. 412 on LES of Complex Transitional and Turbulent Flows, Munich, Germany, Oct. 5 - 6, 2000.

40) R.H. Wickens, "A streamtube concept for lift: with reference to the maximum size and configuration of aerial spray emissions", *Canadian Aeronautics and Space Journal*, Vol. 26, No. 2, 1980, pp. 134-143.

41) R.H. Wickens, "A streamtube concept for lift: with reference to the maximum size and configuration of aerial spray emissions", *Canadian Aeronautics and Space Journal*, Vol. 26, No. 2, 1980, pp. 129-133.

42) R.S. Crabbe, M. McCooeye and R.E. Mickle, "The influence of atmospheric stability on wind drift from ultra-low-volume aerial forest spray applications", *Journal of Applied Meteorology*, Vol.33, 1994, pp. 500-507.

43) A.F.K. Yeung and B.H.K. Lee, "Particle image velocimetry study of wing-tip vortices", *Journal of Aircraft*, Vol. 36, 1999, pp. 482-484.

44) F. de Souza, *Near-field tip vortex measurements in a small wind tunnel using PIV and hot-wire anemometry*, 3rd WakeNet Workshop: "Measurement Techniques for Vortex Wakes", Malvern, U.K., May 2000.

45) M. Mokry, "Numerical simulation of aircraft trailing vortices interacting with ambient shear or the ground", to be published in *Journal of Aircraft*, Vol.38, 2001.

46) J.N. Hallock, *Aircraft Wake Vortices: An Annotated Bibliography*, Volpe National Transportation Systems Center, U.S.A., 2000, http://www.volpe.dot.gov/wv/wv-bib.html.

47) V.J. Rossow, "Lift-generated vortex wakes of subsonic transport aircraft", *Progress in Aerospace Sciences*, Vol. 35, No. 6, 1999.

48) G.C. Hay and R.H. Passman, *Wake Vortex Training Aid*, DOT/FAA/RD-95/6, Volpe National Transportation Systems Center, U.S.A., April 1995.

49) A.C. de Bruin, *WAVENC, Wake Vortex Evolution and Wake Vortex Encounter Publishable Synthesis Report*, NLR-TR-2000-079, Nationaal Lucht- en Ruimtevaartlaboratorium, The Netherlands, 2000.

50) T. Gertz, F Holzäpfel, and D. Darracq, *WakeNet Position Paper on Aircraft Wake Vortices*, European Union, April 2001.

APPENDIX A

Biographies of WVPT Members

SABIGO Ltd. is a Russian company specializing in the development and application of numerical methods in aerodynamics and flight dynamics, as well as their application. The aerodynamic methods are based mostly on the method of discrete vortices (MDV). The first president of SABIGO, Professor Sergei Belotserkovsky was the MDV founder in Russia. The company functions as a part of design/build teams and in privatization projects as technical experts. SABIGO's professional staff includes scientists in different areas of aeronautics and applied mathematics, all trained to provide services individually or as part of a team. The honeycomb wing design, development, promotion, and the most efficient know-how for its production is one example of SABIGO's activities. The scientific works, both fundamental and applied, of SABIGO's personnel (more than 30 monographs and 400 articles) have been published in 11 countries, including the United States, Canada, Germany, France, China, and India. The 24 inventions and 5 patents reflect the company's strongly innovative business philosophy and management style. SABIGO's efforts have been recognized with six scientific prizes. The Transport Canada Wake Vortex Prediction Project was started based on a proposal from SABIGO to undertake a co-operative effort to continue the development, evaluation and application of VFS. SABIGO provided the initial VFS and contributed to many aspects of VFS development and to several related studies. It developed the Near Wake Model and NWDBs for several aircraft types. It provided the general concepts and the early development of the Far Wake Model. It developed the Danger Area Model. Its studies included sensitivity studies, evaluation of benefits at an airport, airborne VFS, 3-D wind sensor, near wake automation, and the effective viscosity coefficient.

Gilles Fournier is a Senior Environmental Monitoring Scientist with the Atmospheric Monitoring and Water Survey Directorate, Meteorological Service of Canada, Environment Canada, where he develops national strategic plans for atmospheric and hydrologic monitoring systems to meet a broad range of departmental and external client needs. He produces information, analyses and advice on national atmospheric and hydrologic monitoring networks, current and future measurement technologies, data processing and analysis technologies, and network topology. Gilles designs, develops and manages the implementation of new networks and systems to meet emerging requirements. Examples are the Canadian Lightning Detection Network implemented in 1997 - 1998, and most recently the implementation of the Canadian AMDAR Program. Gilles has been associated with the WVPT since its inception. His main tasks have been to provide advice on the meteorological aspects of the development of VFS, and to assist in understanding, interpreting and preparing the wake vortex and meteorological data for field trials and other testing.

Gregoire Winckelmans is a Professor at the Université Catholique de Louvain, Belgium. He is most active in fluid dynamics research and related computational methods. His work includes the development of high accuracy vortex methods for the numerical simulation of complex unsteady 3-D flows (including highly separated flows such as bluff body flows), and the development of new models for the LES of turbulent flows (including those at very high Reynolds number, such as aircraft vortex wakes). He has been part of the WVPT from the beginning, providing expertise in MDV and CFD. Initially, Gregoire was involved in the evaluation and validation of VFS developed by SABIGO. For the final two years of the project he made a substantial contribution to the further development and enhancement of VFS. Gregoire implemented VFS models to take into account the viscous ground effect,

the effect of turbulence on vortex decay, and the effect of non-uniform wind shear on vortex trajectories.

Oracle Telecomputing Inc. is a Canadian company specializing in Air Traffic Management (ATM) systems. Its Flight Planning, NOTAM and Weather systems are used in Flight Service Stations and Base Weather Operations across Canada and around the world. Its Radar Processing and Display Systems and Flight Data Management Systems are used in Canada, the United Kingdom, Malaysia and Cuba. OTI has been involved with the Wake Vortex Prediction Project since 1996. It built interfaces to allow VFS to replace the Wake Forecasting module in AVOSS. OTI had previously site adapted CTAS for Toronto. As a result of this experience, OTI was able to modify CTAS to incorporate dynamic separation based on a variable separation matrix derived from wake turbulence forecasts generated by AVOSS and VFS.

Metin Yaras is a faculty member of the Department of Mechanical and Aerospace Engineering at Carleton University. His research efforts focus on fluid dynamics problems with similar emphasis on experimental and numerical techniques. His current projects include the experimental study of the effects of free stream turbulence on an isolated vortex; measurement of the structure of wall-jet vortices; measurement of periodic unsteady flows in three-dimensional diffusing bends of strong curvature; turbulence modelling techniques for three-dimensional separated flows; experimental study of the effects of pressure gradient history, free-stream turbulence and periodic unsteadiness on separation-bubble transition; transition modelling using LES; and numerical modelling of wing flutter. Metin has been working with the WVPT since 1996. His activities have included the evaluation of VFS using field data, and the study of the effects of the atmosphere and the ground on vortex dynamics using simulations with the grid based general Navier-Stokes solver, which he had previously developed. These studies were related to the potential short-term improvements to VFS, and they included validation of the constant effective viscosity approximation through comparisons with higher order effective viscosity models, modelling a stratified atmosphere to look at the effect of stratification on the effective viscosity, and examining how the flow dynamics in the third spatial dimension (i.e., along the vortex axis) affect the wake vortex trajectory and diffusion.

Wayne Jackson is a Research Project Officer working under contract to TDC. He is responsible for managing research and development projects in aviation such as air traffic flow management, aircraft wake turbulence modelling, Cockpit Voice Recorder explosion analysis, Transport Canada Aviation process modelling, flight recorder location study, flight data monitoring, airway design expert system, air traffic conflict resolution, flight recorder configuration standard, corrosion pillowing effect on fuselage lap joints, and Satellite Navigation optimization. This position includes responsibility for co-ordination with industry, pilots, airline managers, engineers, scientists, aviation safety regulators, safety investigators, and managers of the Canadian Air Navigation System. Wayne has been associated with the WVPT since its inception. His responsibilities have included project initiation, project management, engineering support, international co-ordination, contract management, co-ordinating the project review committee, software consulting and document preparation.

APPENDIX B

Investigation of Near Wakes Shortly after Rollup

Grégoire S. Winckelmans* and Hervé Jeanmart†

April 13, 2000

* Professor, Centre for Systems Engineering and Applied Mechanics (CESAME), Mechanical Engineering Department, Université Catholique de Louvain, Louvain-la-Neuve 1348, Belgium. Also: 4318 Lindblade Dr., Los Angeles, CA, USA 90066-6243.

† Assistant and Ph.D. student, Mechanical Engineering Department, Université Catholique de Louvain, Louvain-la-Neuve 1348, Belgium.

Contents

1 The universal near wake 1

2 Simulations of rollup using the method of discrete vortices 4

2.1 Rollup of a near wake from SABIGO 4

2.2 Rollup of a near wake corresponding to elliptical loading 9

3 Experimental investigation of rollup from a rectangular wing in the wind tunnel 12

4 Possibility of using the universal profile as simplified initial condition for the VFS 18

5 Bibliography 20

List of Figures

1 Position of the discrete vortices for MDV-A simulation of the rollup of an B-727 near wake provided by SABIGO: $t = 0$ s (diamonds), 1 s (crosses) and 10 s (squares). Thus, $T = t\,\Gamma_0/b^2 = 0$, 1.98 and 2.64 5

2 Normalized mean azimuthal velocity and circulation profiles at $T = t\,\Gamma_0/b^2 = 1.98$ and 2.64 for MDV-A simulation of the rollup of an B-727 near wake provided by SABIGO 7

3 Normalized mean azimuthal velocity and circulation profiles at $T = t\,\Gamma_0/b^2 = 1.98$ for MDV-A simulation of the rollup of an B-727 near wake provided by SABIGO: comparison with the modified universal profile: $\beta_o = 6$, $\beta_i = 190$, $p = 2$, 3 and 4 8

4 Position of the discrete vortices for MDV-A simulation of the rollup of a near wake corresponding to elliptical loading: $T = 0.1$, 0.5, 1.0, 1.5 and 2.0 9

5 Normalized mean azimuthal velocity and circulation profiles at $T = 2$ for MDV-A simulation of the rollup of a near wake corresponding to elliptical loading. Comparison with the modified universal profile: $\beta_o = 7.5$, $\beta_i = 1400$, $p = 3$ and 4 11

6 Experimental investigation of the rollup of the near wake emanating from a rectangular wing with $A_R = 3.7$. Close view of the wing (top); view of the open test section and of the laser beam for LDV measurements within the rolling wake (bottom) 13

7 Experimental vertical and longitudinal velocity profiles, at $x_c/b = 2$, along a line joining the two vortex centroids for rollup of the near wake produced by a rectangular wing with $A_R = 3.7$ 14

8 Deduced azimuthal velocity profile, at $x_c/b = 2$, for rollup of the near wake produced by a rectangular wing with $A_R = 3.7$ 15

9 Normalized mean azimuthal velocity and circulation profiles at $T \approx 0.30$ for rollup of the near wake produced by a rectangular wing with $A_R = 3.7$. Comparison with the modified universal profile: $\beta_o = 11$, $\beta_i = 800$, $p = 2$, 3 and 4 16

10 Log diagram of the normalized circulation profile at $T \approx 0.30$ for rollup of the near wake produced by a rectangular wing with $A_R = 3.7$. Identification of inner and outer regions of universal profile: $\beta_o \approx 11$, $\beta_i \approx 800$ . . 17

11 Initial position of discrete vortices to use as initial condition for VFS simulations: use of SABIGO's near wake at $T = 0$ (diamonds) or use of the universal near wake at $T = 2$ (crosses) 19

Nomenclature

	Letters	
b	aircraft span	m
b_0	ideal spacing between vortex centoids $= \frac{\pi}{4} b$	m
f	factor for effective spacing between vortex centroids	
h	spatial resolution	m
N	number of vortex particles	
p	parameter in buffer region for the universal near wake profile	
R	effective radius for port and starboard vortices $= \frac{s}{2}$	m
r	radial distance (measured from vortex centroid)	m
s	spacing between port and starboard vortex centroids $= f\, b_0$	m
t	time	s
T	dimensionless time $= \frac{t\Gamma_0}{b^2}$	
x	out of cross-plane coordinate (positive nose to tail)	m
y	cross-plane coordinate (positive port to starboard)	m
z	cross-plane coordinate (positive upward)	m
u, U	velocity component in x-direction	m/s
v	velocity component in y-direction	m/s
w	velocity component in z-direction	m/s
	Greek letters	
β	coefficient in universal near wake	
Γ	circulation	m^2/s
Δ	difference, jump, step	
ν	viscosity	m^2/s
σ	core size of discrete vortex, core size of inner gaussian core	m
ω	wake vorticity	$1/s$
	Subscripts	
c	index for vortex centroids, index for position of maximum velocity	
i, o	indices for inner and outer vortex cores	
p	index for discrete vortex	
port, starb	indices for port and starboard vortices	
0	index for global condition	
θ	index for azimuthal direction	
∞	upstream condition	
	Superscripts	
$*$	effective	

1 The universal near wake

We here consider aircraft vortex wakes shortly after rollup of the near wake. In the approach where the rolled up near wake is "universal", one assumes that the vorticity field created by an aircraft of span b can be approximated by the superposition of two vortices: the port vortex located at $(-y_c, z_c)$ and of circulation $-\Gamma_0$, and the starboard vortex located at (y_c, z_c) and of circulation Γ_0. The spacing between the port and starboard vortex centroids is $2\,y_c = s = f\ b_0$ with $b_0 = \frac{\pi}{4}\,b$ the spacing corresponding to the ideal case with elliptical loading. There is thus some flexibility on spacing through the correction "factor", f. It however must be set as input. It is not expected to vary much from one aircraft to another one. In the ideal case of elliptical loading, one has that $f = 1$. In the real cases, f can be obtained from measurements of aircraft vortex wakes. It is slightly less than unity. Notice that f can also be obtained if one knows the detailed near wake vorticity field, $\omega(y, z)$, before rollup. Indeed, one obtains, by conservation of vertical momentum during rollup, that:

$$\begin{aligned} y_c = \frac{s}{2} \quad &= \quad \frac{\int_{\text{starb}} y\,\omega(y,z)\,dy\,dz}{\int_{\text{starb}} \omega(y,z)\,dy\,dz} = \frac{\int_{\text{starb}} y\,\omega(y,z)\,dy\,dz}{\Gamma_0} \\ \iff \qquad & \Gamma_0\,s = 2\int_{\text{starb}} y\,\omega(y,z)\,dy\,dz = \int y\,\omega(y,z)\,dy\,dz\ , \end{aligned} \tag{1}$$

where "starb" means that the integration is restricted to the starboard half plane. This result is valid for all aircraft wakes. For instance, if one uses SABIGO's near wake represented by discrete vortices of circulation Γ_p, one obtains that:

$$\begin{aligned} y_c = \frac{s}{2} \quad &= \quad \frac{\sum_{p,\text{starb}} y_p\,\Gamma_p}{\sum_{p,\text{starb}} \Gamma_p} = \frac{\sum_{p,\text{starb}} y_p\,\Gamma_p}{\Gamma_0} \\ \iff \qquad & \Gamma_0\,s = 2\sum_{p,\text{starb}} y_p\,\Gamma_p = \sum_{p} y_p\,\Gamma_p\ , \end{aligned} \tag{2}$$

where "starb" means that the sum is restricted to the starboard discrete vortices. Notice that Γ_0 and y_c are already provided by the VFS code when one runs a detailed near wake such as those provided by SABIGO: SABIGO's near wakes could thus also be used to determine both the proper Γ_0 and s (and thus the proper value to use for f).

The aircraft lift is given by:

$$L = \rho U_\infty\,\Gamma_0\,s = \rho U_\infty\,\Gamma_0\,f\,\frac{\pi}{4}b \tag{3}$$

where ρ is the air density and U_∞ is the flight velocity. Thus, the knowledge of the lift, the air density and the flight velocity suffice to determine the product $\Gamma_0\,s$ for all aircraft types, but not each of them separately. If s is also known (i.e., if f is also known), then Γ_0 is determined.

We go back to the universal near wake shortly after rollup. The outer core circulation associated with each vortex is here spread according to the universal profile, i.e., the "best fit" formula of Proctor et al. [7, 9]:

$$\frac{\Gamma(r)}{\Gamma_0} = 1 - \exp\left(-\beta_o\left(\frac{r}{b}\right)^{3/4}\right) = 1 - \exp\left(-\left(\frac{r}{\sigma_o}\right)^{3/4}\right)\ . \tag{4}$$

With $\beta_o \approx 10$, such distributions indeed fit well the 2π-averaged circulation distribution, $\Gamma(r)$, obtained from Lidar measured aircraft wakes shortly after rollup [7, 9]. We will see that this outer formula also fits well our results, both numerical and experimental (although not always with $\beta_o = 10$ as the best choice).

As to the initial wake thickness and diffusion process, it creates a small Gaussian inner core:

$$\frac{\Gamma(r)}{\Gamma_0} = 1 - \exp\left(-\beta_i \left(\frac{r}{b}\right)^2\right) = 1 - \exp\left(-\left(\frac{r}{\sigma_i}\right)^2\right) . \tag{5}$$

The inner gaussian core size is thus $\sigma_i/b = 1/\sqrt{\beta_i}$. For small r/σ_i, one has that:

$$\frac{\Gamma(r)}{\Gamma_0} \approx \left(\frac{r}{\sigma_i}\right)^2 \iff u_\theta(r) \approx \frac{\Gamma_0}{2\pi}\frac{r}{\sigma_i^2} \iff \frac{du_\theta}{dr}(r) \approx \frac{\Gamma_0}{2\pi}\frac{1}{\sigma_i^2} . \tag{6}$$

The velocity is thus linear and its slope can be used to determine σ_i.

Actually, in [7, 9], it is proposed that the inner gaussian core formula should be used for $0 \leq r \leq r_c$ where r_c corresponds to the point of maximum azimuthal velocity: $u_\theta(r) = \Gamma(r)/(2\pi r)$ is maximum at $r = r_c$. Typical values corresponding to real case aircraft wakes shortly after rollup are reported in [7, 9]: $r_c/b = 0.040 - 0.050$. It is also proposed that the gaussian profile should be taken as:

$$\frac{\Gamma(r)}{\Gamma_0} = 1.4 \left(1 - \exp\left(-10 \left(\frac{r_c}{b}\right)^{3/4}\right)\right) \left(1 - \exp\left(-1.2527 \left(\frac{r}{r_c}\right)^2\right)\right) \tag{7}$$

The factor 1.2527 is determined by the continuity with the outer formula at $r = r_c$ and by the factor 1.4 in front:

$$1.4\,(1 - \exp(-1.2527)) = 1 . \tag{8}$$

For small r/r_c, one obtains that:

$$\frac{\Gamma(r)}{\Gamma_0} \approx (1.04 - 1.14) \left(\frac{r}{\sigma_i}\right)^2 \tag{9}$$

where 1.04 corresponds to $r_c/b = 0.040$ and 1.14 to $r_c/b = 0.050$. Thus, we conclude that σ_i and r_c are very close (although not exactly equal): $\sigma_i/r_c = 0.93 - 0.98$.

Notice that a substantial fraction of the total circulation is concentrated within the circle of radius r_c:

$$\frac{\Gamma(r_c)}{\Gamma_0} = 1 - \exp\left(-10 \left(\frac{r_c}{b}\right)^{3/4}\right) = 0.59 - 0.65 \tag{10}$$

where 0.59 corresponds to $r_c/b = 0.040$ and 0.65 to $r_c/b = 0.050$.

As to the factor 1.4 in front, it was determined for best fit with the observed maximum velocity at r_c. This maximum velocity is:

$$\frac{u_\theta\, b}{\Gamma_0}\Big|_{\max} = \frac{u_\theta(r_c)\, b}{\Gamma_0} = \frac{1}{2\pi} \frac{\left(1 - \exp\left(-10 \left(\frac{r_c}{b}\right)^{3/4}\right)\right)}{\frac{r_c}{b}} = 2.08 - 2.35 . \tag{11}$$

where 2.08 corresponds to $r_c/b = 0.050$ and 2.35 to $r_c/b = 0.040$.

The full profile is thus continuous at $r = r_c$ but not differentiable, see, e.g., Fig. 2 in [9]. We here propose a modified universal profile that is a valid fit for all r values, and that goes smoothly from the gaussian inner core to Proctor's universal outer core function:

$$\frac{\Gamma(r)}{\Gamma_0} = 1 - \exp\left(\frac{-\beta_i \left(\frac{r}{b}\right)^2}{\left(1 + \left(\frac{\beta_i}{\beta_o}\left(\frac{r}{b}\right)^{5/4}\right)^p\right)^{1/p}} \right) . \tag{12}$$

Whatever the p value, all such functions have the proper inner and outer limits of Eqs. (4) and (5). The location of the buffer region corresponds to $r \approx r_c$ (i.e., the region with maximum azimuthal velocity) and is obtained from:

$$\frac{\beta_i}{\beta_o}\left(\frac{r_c}{b}\right)^{5/4} \approx 1 \qquad \rightarrow \qquad \frac{r_c}{b} \approx \left(\frac{\beta_o}{\beta_i}\right)^{4/5} . \tag{13}$$

This location is thus independent of the p parameter: it is determined by the ratio β_i/β_o. The p parameter serves only to fine tune the fit in terms of the amplitude for the maximum velocity. A good fit is obtained when using $p \approx 3$. and is relatively insensitive to p in that range, as we shall see: values of $p = 2$ to $p = 4$ are also investigated in what follows.

The typical values of $r_c/b = 0.040 - 0.050$ lead, according to Eq. (13), to $\beta_i/\beta_o = 42 - 56$. With $\beta_o \approx 10$, this gives $\beta_i = 420 - 560$ and thus $\sigma_i/b = 1/\sqrt{\beta_i} \approx 0.042 - 0.049$: this confirms, again, that σ_i is close to r_c, although not exactly equal to r_c.

Actually, if one wishes to simplify things even further, one can postulate that σ_i and r_c are equal. One then obtains a relationship between β_i and β_o:

$$\left(\frac{\beta_o}{\beta_i}\right)^{4/5} \approx \frac{1}{\beta_i^{1/2}} \qquad \rightarrow \beta_i \approx \beta_o^{8/3} . \tag{14}$$

For instance, with $\beta_o = 10$, this gives $\beta_i = 464$. This is not bad: this value is certainly within the bracket mentioned above: $420 - 560$. Of course, this further assumption is not necessary: one can, in general, keep β_i and β_o as separate parameters. The equation (14) is however quite useful.

Finally, we notice that the inner core size, σ_i (and thus r_c), is necessarily not completely universal, since it grows slowly in time. σ_i essentially depends on the initial thickness of the near wake (a Reynolds number effect related to the thickness of the boundary layers at the trailing edge of the wing) and on the effective diffusion during the time of rollup considered (another Reynolds number effect): the effective time is $t \approx x/U_\infty$ where x is the position of the cross-plane considered behind the aircraft. The dimensionless time is defined as: $T = t\,\Gamma_0/b^2$.

We will see that, even at early rollup (e.g., $T \approx 0.3$), the modifed universal profile is already a good approximation of the wake for simple systems such as a wing (no fuselage, no flaps). For more complex systems such as a complete aircraft, the universal profile is found to be a good approximation at later times, say $T \geq 2$ or so.

2 Simulations of rollup using the method of discrete vortices

The VFS is based on the simplified, real-time, method of discrete vortices: MDV-A. MDV-A and MDV-B (for detailed studies, not real-time) methods were presented in [1, 2, 12, 13, 14, 3, 15, 16], including taking into account the effective ν^* diffusion effects and the viscous ground effects (inviscid for "near ground effects", NGE, and viscous for "in ground effects", IGE). In MDV-A, one uses N discrete vortices, each of which carries an amount of circulation, Γ_p, that is spread using a Gaussian core function with core size σ_p: the circulation due to the p discrete vortex within a circle of radius r centered on the discrete vortex is $\Gamma_p(r) = \Gamma_p \left(1 - \exp(-r^2/\sigma_p^2)\right)$ with $\sigma_p^2(t) = \sigma_p^2(0) + 4\nu^* t$ (in the case of constant and uniform effective viscosity, ν^*). Each discrete vortex is convected by the local velocity field: field induced by all other discrete vortices (the so-called Biot-Savart law) plus wind velocity, if any.

In the present investigation, there are no applied cross-wind and no ground proximity effects. We only investigate the early rollup for wakes OGE. As there is no detailed vorticity field reconstruction in MDV-A (and certainly no way to do it properly with so few discrete vortices), the vorticity centroids for the port and starboard vortices are computed from the circulation-weighted averages of the discrete particle positions:

$$
\begin{aligned}
y_{c,\text{port}} &= \frac{\sum_{p,\text{port}} y_p \, \Gamma_p}{\sum_{p,\text{port}} \Gamma_p} \,, \\
z_{c,\text{port}} &= \frac{\sum_{p,\text{port}} z_p \, \Gamma_p}{\sum_{p,\text{port}} \Gamma_p} \,, \\
y_{c,\text{starb}} &= \frac{\sum_{p,\text{starb}} y_p \, \Gamma_p}{\sum_{p,\text{starb}} \Gamma_p} \,, \\
z_{c,\text{starb}} &= \frac{\sum_{p,\text{starb}} z_p \, \Gamma_p}{\sum_{p,\text{starb}} \Gamma_p} \,,
\end{aligned}
\tag{15}
$$

where the sum is done over the discrete vortices that were used for the near wake discretization. This is done by "flagging" them initially: flag = 1 for the starboard discrete vortices and flag = -1 for the port discrete vortices. For SABIGO's near wake in the presence of cross-wind and thus sideslip there is some ambiguity for the discrete vortices that are initially on the vertical tail: they are flagged with flag = 0 and it is considered that they participate at 50% to each centroid computation. Without cross-wind, there is no ambiguity as these discrete vortices have zero circulation.

2.1 Rollup of a near wake from SABIGO

One of the initial condition that was used for the early rollup studies is a near wake provided by SABIGO for Case1132: a B-727 with flap deflection of 20 deg. This corresponds to a near wake discretized using the "aircraft squeleton" with $N = 62$ discrete vortices, see Fig. 1. The span is $b = 32.9$ m. The half-wake circulation, Γ_0, is here obtained as $\Gamma_0 = 286$ m^2/s (which corresponds to the value recommended for Case 1132 [19, 16, 20],

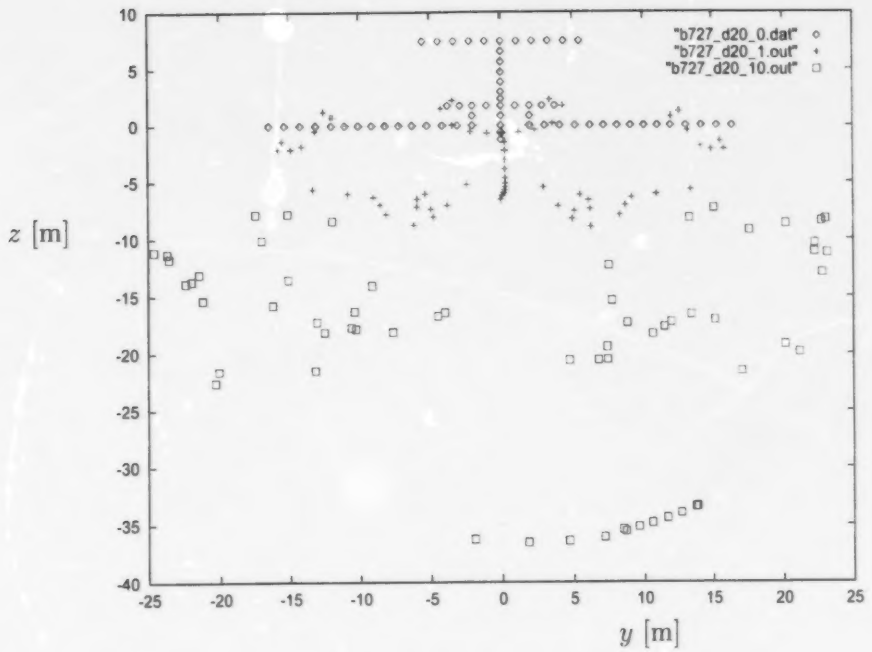

Figure 1: Position of the discrete vortices for MDV-A simulation of the rollup of an B-727 near wake provided by SABIGO: $t = 0$ s (diamonds), 1 s (crosses) and 10 s (squares). Thus, $T = t\,\Gamma_0/b^2 = 0$, 1.98 and 2.64

hence the choice of flap deflection angle to obtain this circulation). This is the average between port and starboard vortex: indeed, the initial near wake provided is not exactly symmetric, as a small sideslip was assumed for Case 1132: we will not worry about that: all results will be averaged over the port and starboard vortex.

This near wake is used as initial condition in a simulation using the MDV-A (as in VFS). The initial core size of each discrete vortex is set to $\sigma_p = 1$ m, hence $\sigma_p/b = 0.030$. The simulation is inviscid (i.e., $\nu^* = 0$: here σ_p is thus constant in time) and goes up to $t = 10$ s. The time integration is done very accurately: use of a fourth order Runge-Kutta scheme and of a small time step: $\Delta t = 0.025$ s. The evolution of the discrete vortices is shown in Fig. 1. It is seen that the coherence of the initial condition is lost quite quickly: the limited number of discrete vortices is not sufficient to truly discretize the near wake finely and thus capture all spatial details of the complex rollup evolution. One can only analyze the results in a statistical sense. This is what we will do next.

Considering a frame of reference centered on one vortex centroid (port or starboard), one can compute the azimuthal velocity, $u_\theta(r, \theta)$, along a circle of radius r centered on the vortex centroid. This can then be 2π-averaged to obtain the mean $u_\theta(r)$ as a function of r in an appropriate statistical sense. The obtained result is here also averaged over the port and starboard vortices (due to the small asymmetry in the provided near wake). The obtained results at $t = 7.5$ s and $t = 10$ s are made dimensionless (using b and Γ_0) and are shown in Fig. 2. The dimensionless time for these profiles is: $T = t\,\Gamma_0/b^2 = 1.98$ and 2.64. The corresponding circulation profiles are easily obtained from the fact that

$u_\theta(r) = \Gamma(r)/(2\pi r)$. They also shown in Fig. 2. It is clear that these mean profiles are similar. We will now see if they can be fitted using the universal profile.

The comparison, at $T = 1.98$, with the modified universal profile, Eq. (12), is shown in Fig 3. The value of $\beta_o \approx 6$ is obtained, both at $T = 1.98$ and $T = 2.64$, for best fit of the outer part of the profiles. This value is lower than $\beta_o \approx 10$ proposed in [7, 9]. The value of β_i is obtained for best fit of the inner part of the profiles. One only needs to examine the slope of u_θ near $r = 0$: for a gaussian profile, this slope must be equal to $\Gamma_0/(2\pi\sigma_i^2)$. This determines σ_i and thus β_i since $\sigma_i/b = 1/\sqrt{\beta_i}$. Here, we obtain $\beta_i \approx 190$ at $T = 1.98$ and $\beta_i \approx 165$ at $T = 2.64$: the effective inner gaussian core is thus spreading slowly: $\sigma_i = 2.38$ m at $t = 7.5$ s (and thus $\sigma_i/b = 0.073$), and $\sigma_i = 2.56$ m at $t = 10$ s (and thus $\sigma_i/b = 0.078$). This small effective spreading is due to the rollup effect only, as the simulation was here inviscid. Moreover, the effective σ_i/b obtained here is too large: aircraft data provide $\sigma_i/b \approx 0.040 - 0.050$. As consequence, the maximum normalized velocity is quite small: here $(u_\theta\, b/\Gamma_0)\Big|_{rmmax} \approx 1.1$ (instead of 2.1 - 2.3 for real aircraft wakes).

Notice that, for MDV simulations, the obtained σ_i is necessarily larger than the core size of each individual discrete vortex (here we used $\sigma_p = 1$ m). Moreover, it is also sensitive to the level of discretisation used (here quite poor as we only had $N = 62$ discrete vortices).

As to the p parameter to join the inner and outer profiles, it is seen that $p = 3$ produces a good fit in the transition region, but that $p = 2$ is also pretty close (although not as good). For the fit at $T = 2.64$, the best result is obtained when $p = 4$ but $p = 3$ is also pretty close. $p = 3$ is thus a good value to use in general. The fit is not that sensitive around that value: no need to argue about the exact p value as long as it is around $p = 3$.

One should not worry too much about not being able to capture the inner gaussian core with the proper core size, and thus the maximum velocity, when using the VFS based on the MDV with a necessarily limited number of discrete vortices. We'll come back to that point when we introduce the possibility of using the universal wake as simplified initial condition for the operational VFS. The maximum normalized velocity, is something difficult to capture when using coarse resolution. We notice that high values of r_c/b (and thus of σ_i/b) were also used in large-eddy simulations (LES) reported in [6]: they used $r_c/b = 0.098$, probably because of the limited resolution they could afford. This is twice larger than for real aircraft wakes shortly after rollup. This also leads to too low a maximum velocity: 1.34 instead of 2.1 - 2.3

As to the outer distribution, the fact that we obtain $\beta_o \approx 6$ instead of $\beta_o \approx 10$ is more worrying. Indeed, aircraft data indicate that the value is $\beta_i \approx 10$ and that it is quite universal [7, 9]. It could be that the level of discretisation of the near wake has an effect of the obtained β_o after rollup. Notice also that Eq. (14)here gives: $6^{8/3} \approx 120$: not far from the observed values $165 - 190$. Is $N = 62$ discrete vortices enough to produce a valid detailed near wake or is it too coarse a discretization? This is a valid question; it would be worth running this rollup study using a more finely discretized near wake.

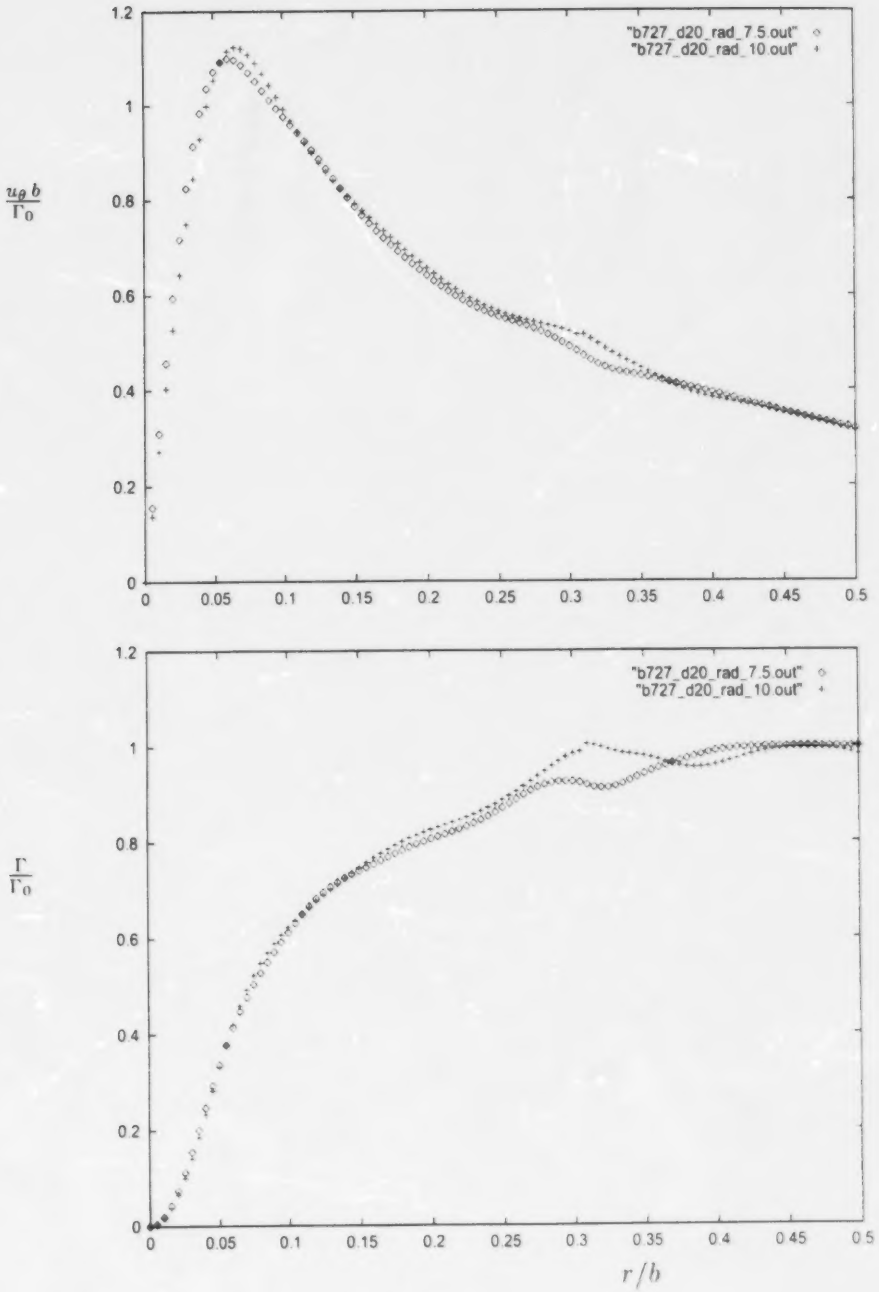

Figure 2: Normalized mean azimuthal velocity and circulation profiles at $T = t\,\Gamma_0/b^2 = 1.98$ and 2.64 for MDV-A simulation of the rollup of an B-727 near wake provided by SABIGO

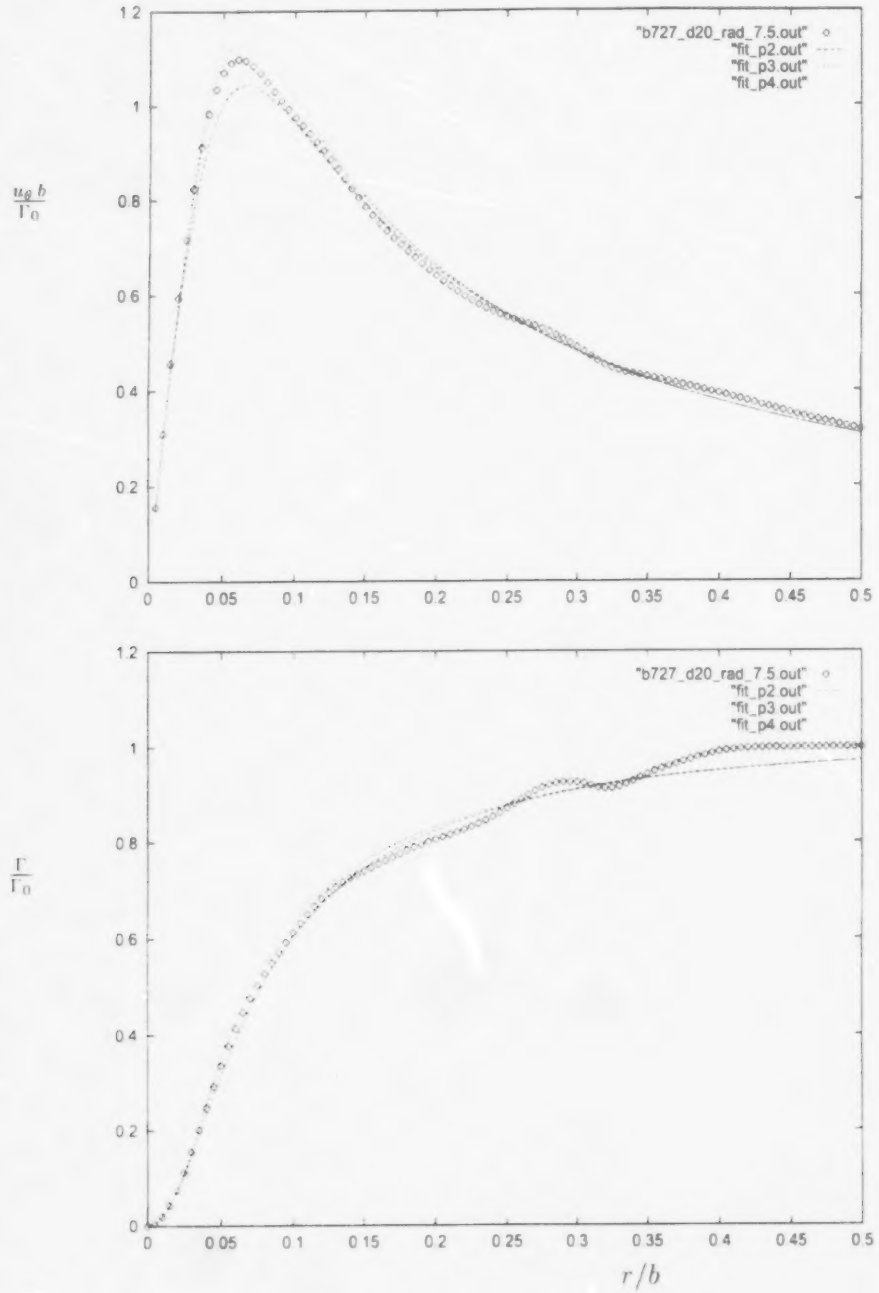

Figure 3: Normalized mean azimuthal velocity and circulation profiles at $T = t\,\Gamma_0/b^2 = 1.98$ for MDV-A simulation of the rollup of an B-727 near wake provided by SABIGO: comparison with the modified universal profile: $\beta_o = 6$, $\beta_i = 190$, $p = 2$, 3 and 4

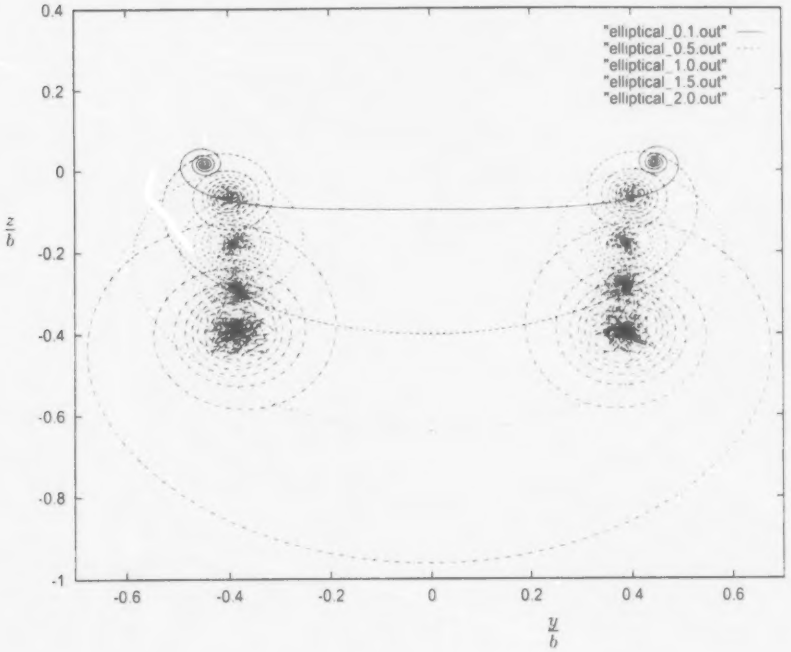

Figure 4: Position of the discrete vortices for MDV-A simulation of the rollup of a near wake corresponding to elliptical loading: $T = 0.1$, 0.5, 1.0, 1.5 and 2.0

2.2 Rollup of a near wake corresponding to elliptical loading

The next initial condition used for early rollup study is a near wake corresponding to the ideal elliptical loading. This corresponds to the ideal wing: wing of elliptical shape, no fuselage, no flaps. The near wake is here discretized very finely: we use $N = 1000$ discrete vortices. The near wake is however much simpler than that of a real aircraft. This is thus fine discretization of a simple near wake. This near wake is used as initial condition in a simulation using the MDV-A (as in VFS). The initial core size of each discrete vortex is set to $\sigma_p/b = 0.01$. The simulation is, again, inviscid (i.e., $\nu^* = 0$, hence σ_p is again constant in time) and proceeds up to $T = 2$. The time integration is also done very accurately: fourth order Runge-Kutta scheme with $\Delta T = 0.001$ The evolution of the discrete vortices is shown in Fig. 4. Here, the coherence is maintained: the vortex sheet rolls up into two well-defined vortices.

The obtained mean azimuthal velocity profile, $u_\theta(r)$, at $T = 2$ is shown in Fig. 5. The corresponding mean circulation profile obtained from $u_\theta(r) = \Gamma(r)/(2\pi r)$ is also shown.

Here also the obtained results can be nicely fitted using the modified universal profile. Examining the slope of u_θ near $r = 0$, we obtain that $\sigma_i/b \approx 0.027$ and thus that $\beta_i \approx 1400$. This gaussian core is thus too thin compared to aircraft data (with $\sigma_i/b \approx 0.04 - 0.05$): this is due to the initial vortex sheet used here being very thin: we used $\sigma_p/b = 0.01$ for the discrete vortices. As they were spaced by $h/b = 0.001$, the near wake was also very finely discretized. It is here confirmed that the obtained σ_i is controlled by the choice of σ_p and that, with very fine discretization in the case of a simple wing, it is

only slightly higher than σ_p.

Notice that, had we run the MDV in the viscous mode, we would have obtained a slightly higher σ_i, as σ_p would then have grown a little in time according to $\sigma_p(t) = \sigma_p(0) + 4\nu^* t$.

As to the outer profile, it is here well fitted when using $\beta_o = 7.5$. Again, the value obtained here is less than the proposed value of $\beta_o = 10$. Concerning the p parameter for the best level of the maximum velocity in the buffer region, it is seen that $p = 3$ is a good choice, and that $p = 4$ is also fine, see Fig. 5. It is thus concluded that the modified universal profile here also provides a very good fit for all values of r.

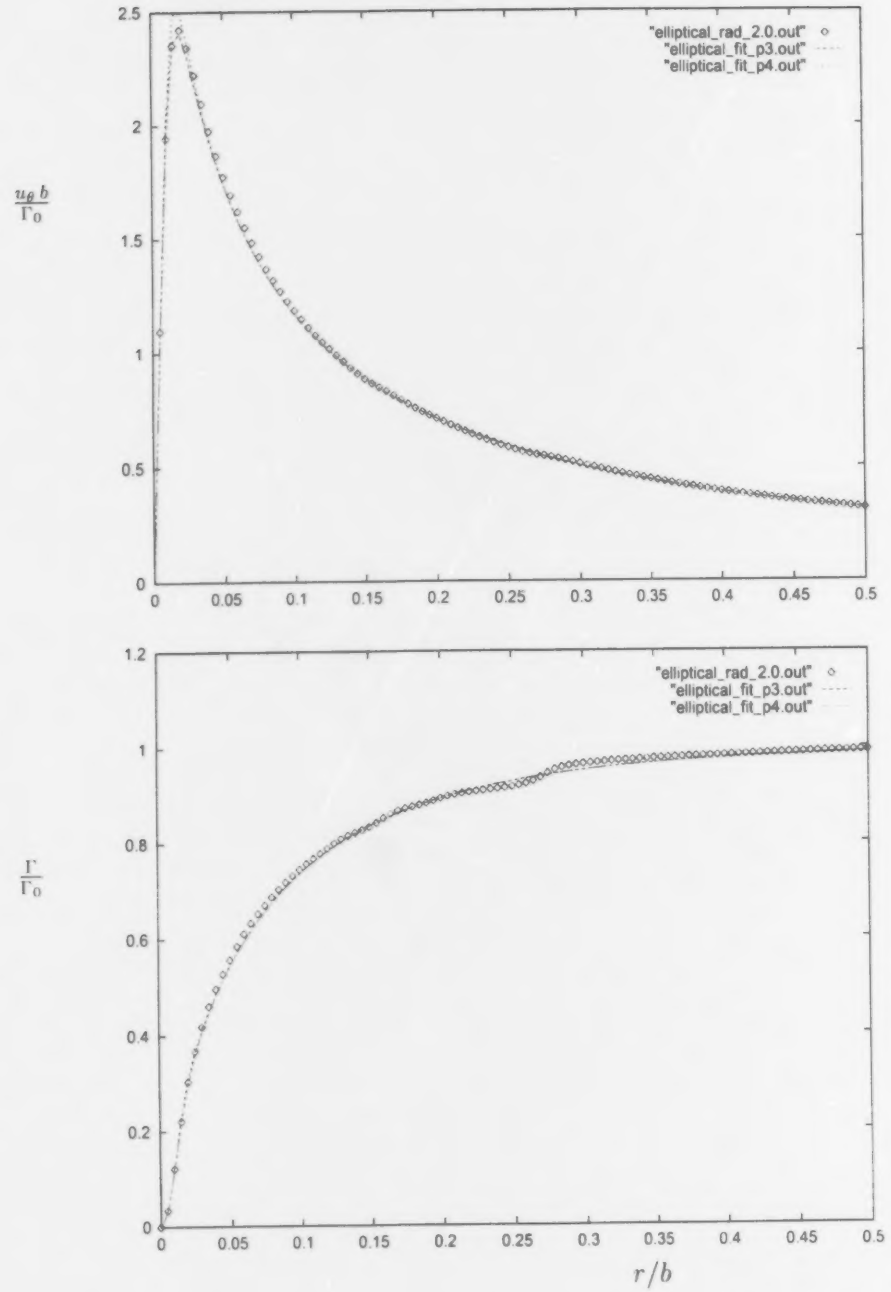

Figure 5: Normalized mean azimuthal velocity and circulation profiles at $T = 2$ for MDV-A simulation of the rollup of a near wake corresponding to elliptical loading. Comparison with the modified universal profile: $\beta_o = 7.5$, $\beta_i = 1400$, $p = 3$ and 4

3 Experimental investigation of rollup from a rectangular wing in the wind tunnel

The possible universality of the circulation profile shortly after rollup is of sufficient interest that it was decided to investigate it experimentally, in our wind tunnel, using a rectangular wing, see Fig 6. This work was conducted by H. Jeanmart, out of this contract, but is nevertheless reported in view of its obvious interest in the present investigation.

The experimental setup is shown in Fig. 6. The wing has a span $b = 0.37$ m and a chord $c = 0.10$ m. This is thus a wing of small aspect ratio: $A_R = b/c = 3.7$. The upstream velocity is $U_\infty = 25.9$ m/s. Two component Laser Doppler Velocimetry (LDV) is used. The measurement is done at a distance $x_c = 2\,b = 0.74$ m from the trailing edge of the wing. The velocity measurements are made along a line passing through the port and starboard vortex centroids. The position of the centroids, $(x_c, -y_c, z_c)$ and (x_c, y_c, z_c) is easily identified, first visually (using smoke visualisation), then fine tuning using the LDV system itself.

We thus measure the vertical, w, and longitudinal, u, velocity components along the line, (x_c, y, z_c). The measured velocity profiles are shown in Fig. 7. In term of effective rolling up time, we have that $t \approx x_c/U_\infty = 0.0286$ s.

From the measured w profile, one can isolate the contribution due to each vortex. The obtained profile is then a good representation of $u_\theta(r)$ and is shown in Fig. 8.

One can then determine the global circulation, Γ_0, of each vortex. We here obtained $\Gamma_0 \approx 1.45\text{m}^2/\text{s}$. The dimensionless time for the rolled up wake is thus also obtained:

$$T = \frac{t\,\Gamma_0}{b^2} \approx \frac{x_c}{b}\,\frac{\Gamma_0}{U_\infty\,b} = 0.30\,. \tag{16}$$

The cross-plane investigated is thus representative of the early stages of rollup. The normalized velocity and circulation profiles can now be produced and are shown in Fig. 9. Also shown is the fit obtained when using the modified universal profile. The parameters were here obtained by examining the circulation profile in a log diagram, see Fig. 10. For each region (inner or outer), one obtains that

$$\log\left(-\log\left(1-\Gamma(r)/\Gamma_0\right)\right) = \log(\beta) + n\,\log(r/b) \tag{17}$$

is indeed a good fit. For the inner Gaussian region (thus $n = 2$), we here obtain that $\beta_i \approx 800$, and thus that $\sigma_i/b \approx 0.035$. The inner core is thus slightly smaller than the value $\sigma_i/b = 0.040 - 0.050$ but not much smaller. The maximum normalized velocity is about right: $(u_\theta\,b/\Gamma_0)\big|_{\text{max}} \approx 2.2$. Recall also that this is early time in the rollup: T is only equal to 0.30. At later times, the inner core would be fater. For the outer region, we confirm that, even for such early time, the outer universal profile is found to be a good fit to the data and that $n = 0.75$ is the correct value for the exponent. We also obtain that $\beta_o \approx 11$: close to the proposed value of $\beta_o \approx 10$. This experiment on a rectangular wing (admitedly of small aspect ratio: $A_R = 3.7$ only) confirms that, even at early times within the rollup process, the universal circulation profile can be used as a good approximation of the exact profile.

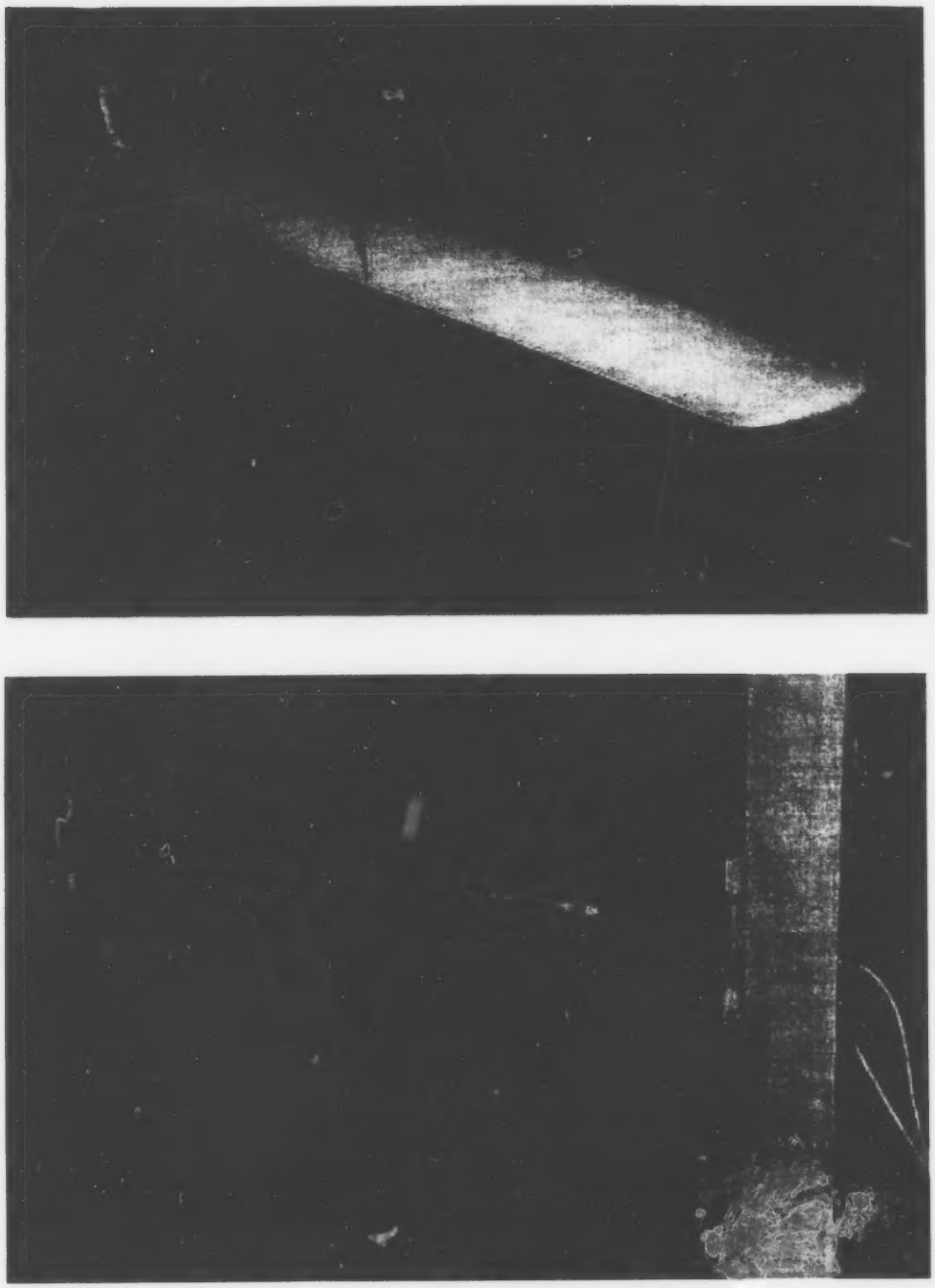

Figure 6: Experimental investigation of the rollup of the near wake emanating from a rectangular wing with $A_R = 3.7$. Close view of the wing (top); view of the open test section and of the laser beam for LDV measurements within the rolling wake (bottom)

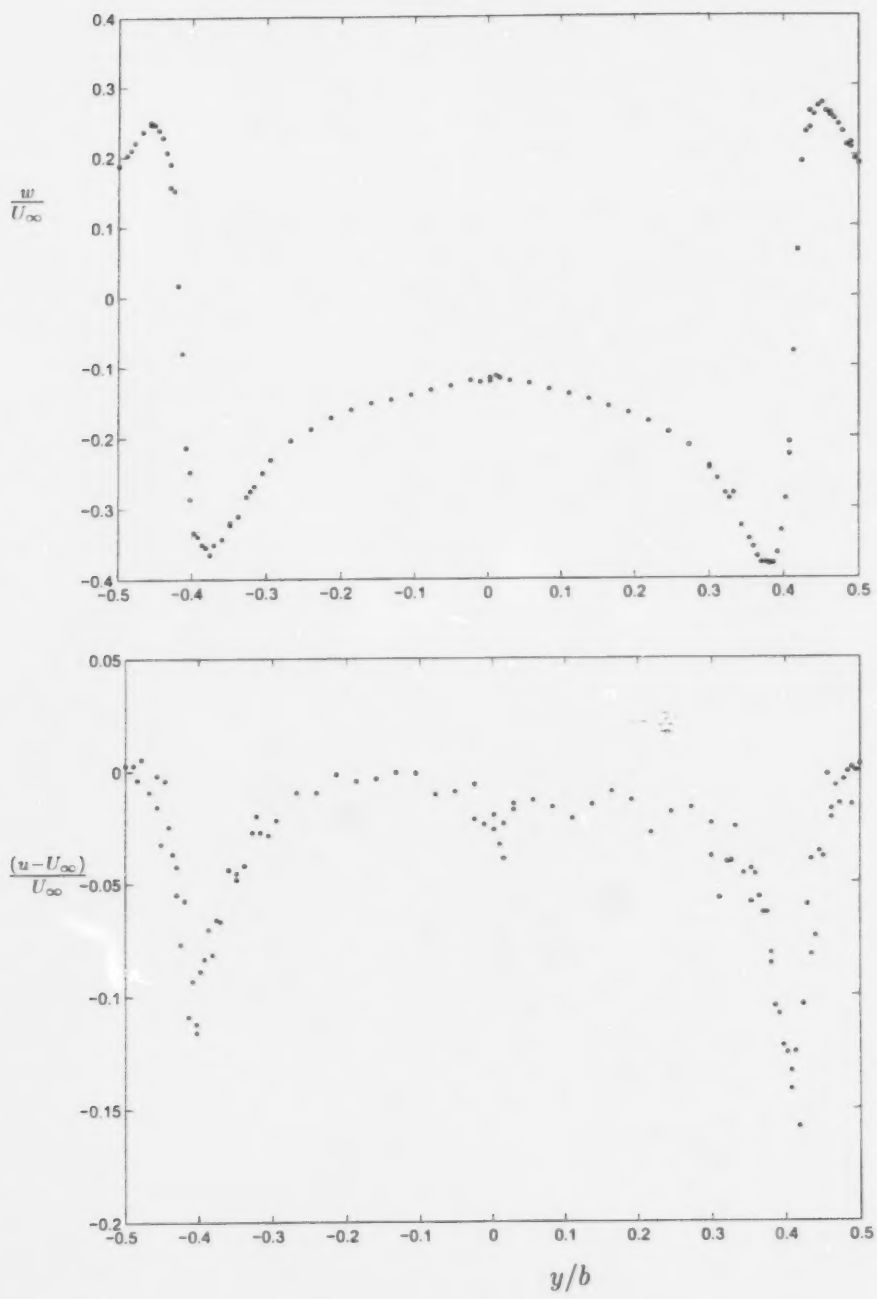

Figure 7: Experimental vertical and longitudinal velocity profiles, at $x_c/b = 2$, along a line joining the two vortex centroids for rollup of the near wake produced by a rectangular wing with $A_R = 3.7$

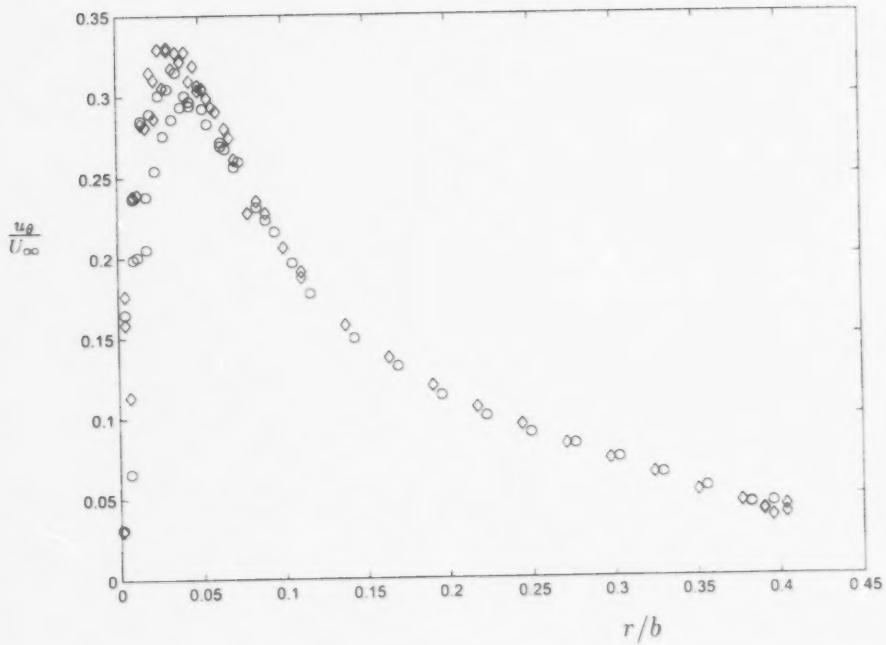

Figure 8: Deduced azimuthal velocity profile, at $x_c/b = 2$, for rollup of the near wake produced by a rectangular wing with $A_R = 3.7$

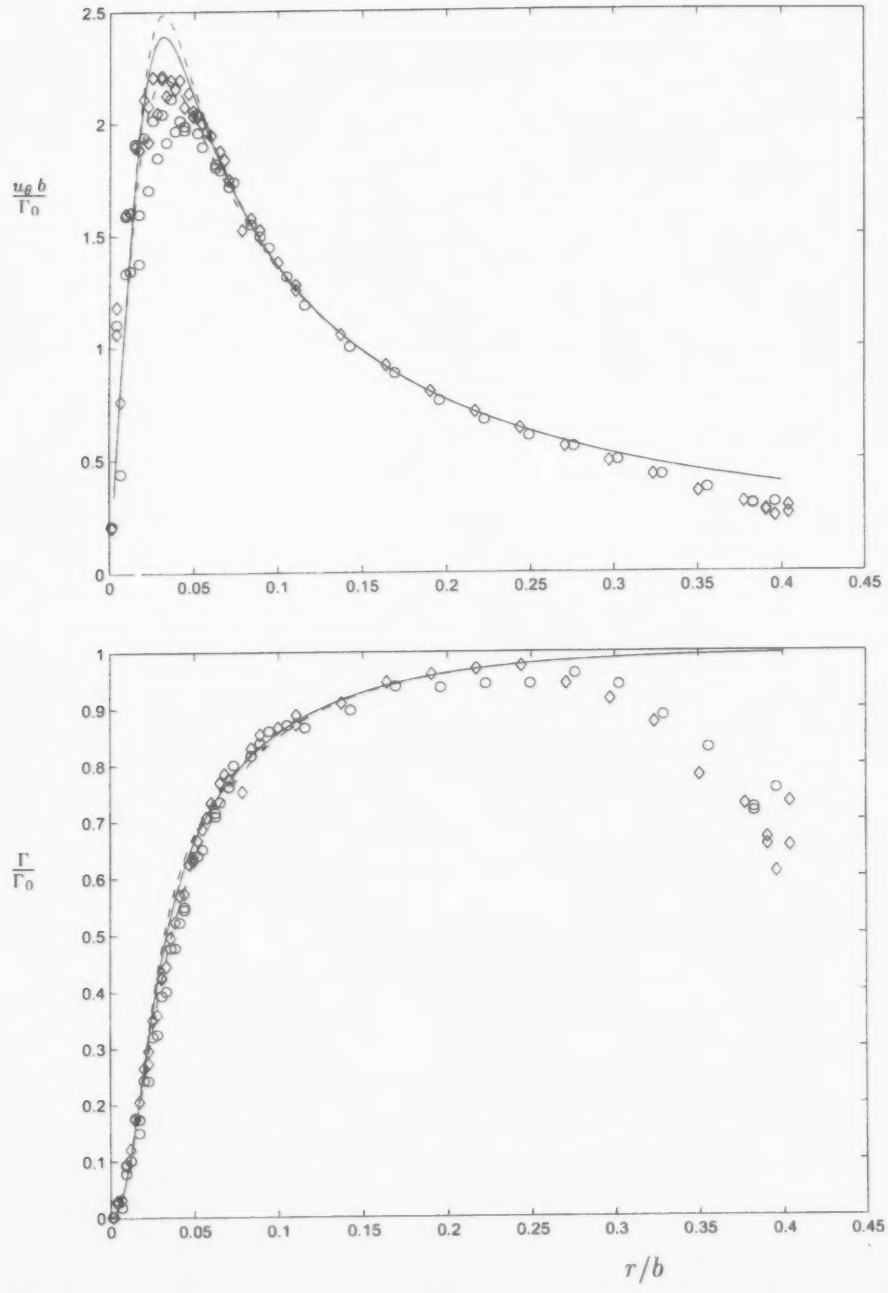

Figure 9: Normalized mean azimuthal velocity and circulation profiles at $T \approx 0.30$ for rollup of the near wake produced by a rectangular wing with $A_R = 3.7$. Comparison with the modified universal profile: $\beta_o = 11$, $\beta_i = 800$, $p = 2$, 3 and 4

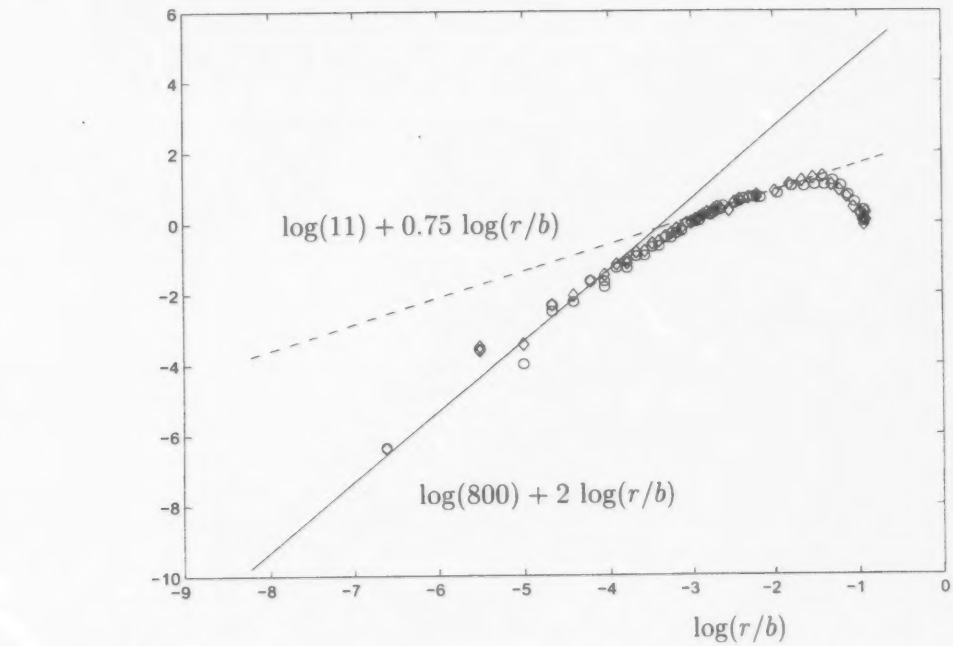

Figure 10: Log diagram of the normalized circulation profile at $T \approx 0.30$ for rollup of the near wake produced by a rectangular wing with $A_R = 3.7$. Identification of inner and outer regions of universal profile: $\beta_o \approx 11$, $\beta_i \approx 800$

4 Possibility of using the universal profile as simplified initial condition for the VFS

The modified universal circulation profile for the wake vorticity after rollup (i.e., for dimensionless times $T \geq 2$) is found to be a realistic approximation of the exact, 2π-averaged, circulation profile as measured form the vortex centroid: this is confirmed by analyses of measured aircraft vortex wakes [7, 9]; this is also confirmed by our rollup analyses, using the MDV, of an aircraft near wake provided by SABIGO and discretized using $N = 62$ discrete vortices (admitedly a fairly coarse discretrization of the detailed near wake). For a simple wing only (no fuselage, no flaps), the modified universal profile already appears to be a good approximation of the exact profile at very early times: as early as $T \approx 0.3$.

The universal profile could be used as initial condition for the VFS in the cases with limited knowledge of the initial detailed vortex wake (i.e., cases with no detailed near wake database available, or cases where the operational information is not sufficient to produce a detailed near wake anyway). Moreover, in view of the necessarily limited number of vortices used to discretize the near wakes anyway, and thus of the fast loss of coherence in the rollup evolution of these near wakes, see Fig. 1, it appears that the universal near wake might be a simple and sufficient initial condition for operational use.

This, of course, requires that Γ_0 and s (or, equivalently f since $s = f\,\frac{\pi}{4}\,b$) be both determined. Recall that the aircraft lif only determine the product $\Gamma_0\,s$. If anything, detailed near wake studies and near wake databases will always be useful as they allow to better predict both Γ_0 and s from the detailed wake before rollup.

In what follows, it is assumed that both Γ_0 and s are known. In the absence of information on f, elliptical loading can be assumed as approximation, i.e., $f \approx 1$. Γ_0 is then also determined.

The vortex centroids are separated by s. The radius of discretization of each vortex is taken as $R = s/2$. Each vortex is discretized using one discrete vortex in the center plus 3 layers of discrete vortices: 8 discrete vortices in the first layer, 16 in the second layer and 24 in the third layer, for a total of 49, see Fig. 11. With the layer discretization that is used, all vortices are discretizing an identical fluid area which is equal to $\pi r_l^2 = \pi R^2/49$ where r_l is the radius for the center vortex, and thus $r_l/R = 1/7$. This also gives: $r_l/b = f\,\frac{\pi}{8}\,r_l/R = 0.056\,f$. r_l/b is thus of the order of r_c/b. The total number of discrete vortices (port + starboard vortices is thus $N = 98$: this number is of the order of what is used in the near wakes used in VFS so far. (One could, of course, increase the resolution by using more layers.)

The amount of circulation to provide to each layer is computed using the outer part of the universal distribution. Indeed, with the fairly crude discretization used here (which has r_l/b slightly higher than 0.050), only the center discrete vortex participates to the inner Gaussian core. Recall that, with $r_c/b = 0.040 - 0.50$, 60 to 65% of Γ_0 is within the circle of radius r_c. The three layers are thus all within the outer region corresponding to Eq. (4). The crude discretization is such that there is no need to use the complete function of Eq. (12): the outer core function of Eq. (4) here suffices. Assuming that $\beta_o = 10$, we obtain, after calculation, that the center discrete vortex carries 68.4% of Γ_0.

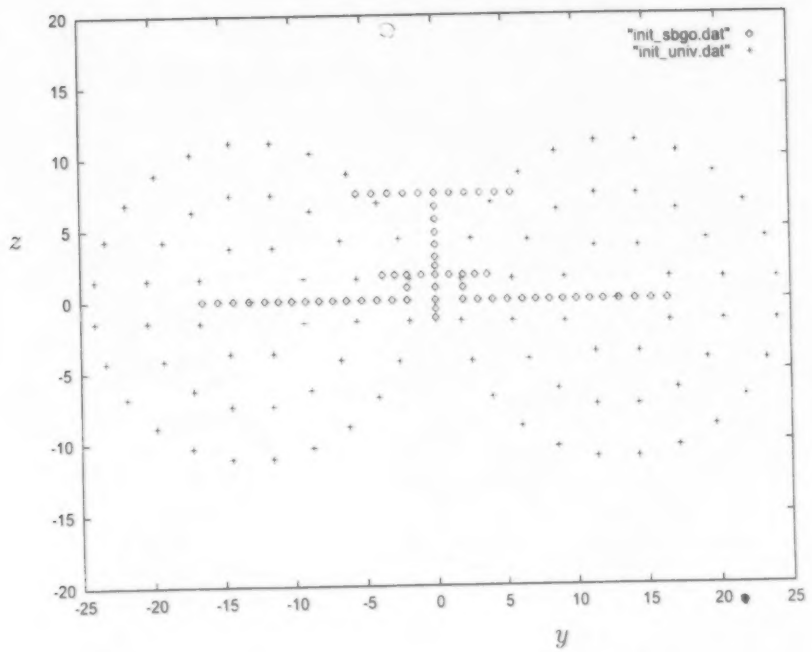

Figure 11: Initial position of discrete vortices to use as initial condition for VFS simulations: use of SABIGO's near wake at $T = 0$ (diamonds) or use of the universal near wake at $T = 2$ (crosses)

that the first layer carries 24.3%, that the second layer carries 5.1% and that the third layer carries the remaining 2.2%. The amount of circulation to provide to each discrete vortex is thus determined. Such initial conditions were already used, with good success, in VFS studies reported in [17].

5 Bibliography

References

[1] S. M. Belotserkovsky et al., *Development and adaptation of VFS for field tests: II. Evaluation of mathematical models for Boeing 727 and 767 far wakes*, SABIGO, Moscow, Russia, 1996.

[2] S. M. Belotserkovsky et al., *Development and adaptation of VFS for field tests: III. Investigation on evaluation of effective viscosity factor ν^**, SABIGO, Moscow, Russia, May 1996.

[3] S. M. Belotserkovsky et al., *Influence of the ground boundary layer on the position of far wake vortices*, Science-Engineering Center SABIGO Ltd., Moscow, Russia, Sept. 1997.

[4] S. M. Belotserkovsky et al., *Computer Vortex Forecast System*, Phase 4 Final Report TP 13373E, Science-Engineering Center SABIGO Ltd., Moscow, Russia, March 1999.

[5] S. M. Belotserkovsky et al., *Computer Vortex Forecast System (VFS)*, Phase 5 Draft Final Report, Science-Engineering Center SABIGO Ltd., Moscow, Russia, May 1999.

[6] J. Han, Y.-L. Lin, S. Pal Arya and F. H. Proctor, Large eddy simulation of aircraft wake vortices in a homogeneous atmospheric turbulence: vortex decay and descent, *37th Aerospace Sciences Meeting & Exhibit*, Jan. 11-14, 1999, Reno NV, paper AIAA 99-0756.

[7] F. H. Proctor, The NASA-Langley wake vortex modelling effort in support of an operational aircraft spacing system, *36th Aerospace Sciences Meeting & Exhibit*, Jan. 12-18, 1998, Reno NV, paper AIAA 98-0589.

[8] F. H. Proctor and J. Han, Numerical study of wake vortex interaction with the ground using the Terminal Area Simulation System, *37th Aerospace Sciences Meeting & Exhibit*, Jan. 11-14, 1999, Reno NV, paper AIAA 99-0754.

[9] S. Shen, F. Ding, J. Han, Y.-L. Lin, S. Pal Arya and F. H. Proctor, Numerical modeling studies of wake vortices: real case simulations, *37th Aerospace Sciences Meeting & Exhibit*, Jan. 11-14, 1999, Reno NV, paper AIAA 99-0755.

[10] R. E. Robins and D. P. Delisi, Further development of a wake vortex predictor algorithm and comparisons to data, *37th Aerospace Sciences Meeting & Exhibit*, Jan. 11-14, 1999, Reno NV, paper AIAA 99-0757.

[11] R. A. Stuever and G. C. Greene, An analysis of relative wake-vortex hazard for typical transport aircraft, *32nd Aerospace Sciences Meeting & Exhibit*, Jan. 10-13, 1994, Reno, NV, paper AIAA 94-0810.

[12] G. S. Winckelmans,*Review of report by SABIGO: "Development and adaptation of VFS for field tests; III. Investigation on evaluation of effective viscosity factor ν^*"*, Mechanical Engineering Department, Université catholique de Louvain, Louvain-la-Neuve, Belgium, November 1996.

[13] G. S. Winckelmans and P. Ploumhans, *Interaction of aircraft vortex wakes with the ground: MDV sample computations using different approaches*, Mechanical Engineering Department, Université catholique de Louvain, Louvain-la-Neuve, Belgium, February 1997.

[14] G. S. Winckelmans, *Prediction of aircraft wake vortices during takeoff and landing - Phase 3*, Final Report, Mechanical Engineering Department, Université catholique de Louvain, Louvain-la-Neuve, Belgium, June 26, 1997.

[15] G. S. Winckelmans and P. Ploumhans, *Prediction of aircraft wake vortices during takeoff and landing - Phase 4*, Final Report TP 13374E, Mechanical Engineering Department, Université catholique de Louvain, Louvain-la-Neuve, Belgium, March 1999.

[16] G. S. Winckelmans and P. Ploumhans, *Prediction of aircraft wake vortices during takeoff and landing - Phase 5*, Draft Final Report, Center for Systems Engineering and Applied Mechanics (CESAME), Mechanical Engineering Department, Université catholique de Louvain, Louvain-la-Neuve, Belgium, July 5, 1999.

[17] G. S. Winckelmans and P. Ploumhans, *Modelisation of non-uniform wind shear effects onto aircraft wake dynamics for the operational VFS: testing on Memphis Case 1132 with non-uniform shear in ground proximity*, Interim Phase 6 Report, Center for Systems Engineering and Applied Mechanics (CESAME), Mechanical Engineering Department, Université catholique de Louvain, Louvain-la-Neuve, Belgium, March 23, 2000.

[18] M. I. Yaras, *An evaluation of the Vortex Forecasting System for predicting aircraft far-wake trajectories*, Final Report TP 13371E, Department of Mechanical and Aerospace Engineering, Carleton University, Ottawa, Canada, March 1999.

[19] M. I. Yaras, *Effects of atmospheric conditions and ground proximity on the dynamics of aircraft wakes vortices: a study of the 1994-95 Memphis field measurements*, Final Report TP 13372E, Department of Mechanical and Aerospace Engineering, Carleton University, Ottawa, Canada, March 1999.

[20] M. I. Yaras, *Numerical simulations of aircraft far-wake dynamics in nonuniform windshear and ground proximity*, Phase 6 Interim Report, Department of Mechanical and Aerospace Engineering, Carleton University, Ottawa, Canada, Feb. 6, 2000.

APPENDIX C

Detailed Description of the Recent VFS Far Wake Improvements

Gregoire S. Winckelmans

November 2000

As mentioned previously, the VFS far wake model has improved significantly compared to the version 2 that was used for scoring by NorthWest Research Associates (NWRA), see [7], especially with respect to decay modeling. As the descent rate directly relates to decay, improved decay modeling also leads to improved descent rate modeling.

The latest version, VFS version 4, includes the implementation of:

1. The evaluation of the time-to-demise (link, burst, etc., as in Sarpkaya et al. [8]) as well as the evaluation of the fraction of time-to-demise attained, $fraction_{demise}$, as time proceeds. The implementation uses an "accumulated damage" model which best uses the possibly varying eddy dissipation (EDR) profile that the vortex wake encounters as it moves downward (EDR profile data are read as input).

Defining $b_0 = (\pi/4)\,b$ (with b the wing span) the ideal spacing (corresponding to elliptical loading) between the port and starboard vortex centroids, and Γ_0 the initial global circulation of the half wake, the ideal descent rate, $V_0 = \Gamma_0/(2\pi\, b_0)$, is used as reference velocity. Dimensionless time is then defined as $T = tV_0/b_0$. The dimensionless time-to-demise, $T_{demise} = t_{demise}V_0/b_0$, is then taken as the universal function of dimensionless EDR, $\eta = (EDR\, b_0)^{1/3}/V_0$. The accumulated damage model is then:

$$fraction_{demise}(T) = \int_0^T \frac{dT}{T_{demise}(\eta(Y_c(T)))},$$

where $Y_c(T)$ is the dimensionless wake height at dimensionless time T: it is taken as the mean between the port and starboard centroid heights. In the case of uniform EDR profile, the accumulated damage model folds back to the classical model for time-to-demise evaluation.

The code outputs $fraction_{demise}(T)$ as time proceeds. Moreover, if it is found to be greater than unity at the end of the simulation, the code also outputs the time at which the wake demise was attained (i.e., when $fraction_{demise}$ passed unity).

2. The EDR decay model (model based on eddy dissipation rate, as in Sarpkaya et al. [8], but modified for the VFS which is based on the method of discrete vortices (MDV)). The EDR model uses the universal time-to-demise model and the EDR profile data.

In lack of EDR profile information, one can instead provide a turbulence length, $L_{turb} = (2\,TKE)^{3/2} / EDR$ and then approximate EDR from TKE data. So far, this option assumes a uniform L_{turb} (no profile); it can be used with uniform or non-uniform TKE profiles.

The EDR decay model is programmed in VFS as a change in each discrete vortex circulation:

$$\frac{d\Gamma_i}{dt} = -C_e \frac{\Gamma_i}{t_{demise}}$$

It is only applied to the discrete vortices belonging to the primary near wake. The eventual secondary vortices (produced when IGE) are not subjected to the decay model (they are however still subjected to the effective diffusion of the discrete core size using a small effective viscosity value: typically 0.03 m^2/s).

3. The TKE decay model (model based on turbulence kinetic energy, as in Greene et al. [1], but modified for the VFS), and which uses the TKE profile (TKE profile data are read as input). The TKE decay model is also programmed as a change in each discrete vortex circulation:

$$\frac{d\Gamma_i}{dt} = -C_Q \left(\frac{q_{rms}}{s_0} \right) \Gamma_i$$

where $q_{rms} = (2\,TKE)^{1/2}$ is the turbulence rms velocity (its dimensionless value is $Q = q_{rms} / V_0$) and s_0 is the initial spacing between the vortex centroids.

Note that the EDR decay model has been shown to be superior to the TKE decay model [8]. It is also better because it is "richer" in modeling: through the universal non-linear function $T_{demise}(\eta)$.

4. The possibility of using, as initial condition, the universal near wake (UNW) shortly after rollup: with circulation profile across each vortex as in Proctor et al. [2, 9], but further improved (see [11]) and discretized for the VFS using the discrete vortices.

This possibility allows to produce a simplified near wake without using the aerodynamic characteristics of the aircraft and without the need for the flap angle setting.

It also allows for a correction factor, f_s, to the ideal spacing corresponding to elliptical loading: the initial spacing between the vortex centroids, s_0, is thus equal to $s_0 = f_s b_0$. Real aircraft wakes have f_s close to unity. Actually, the NWDB developed by SABIGO for many aircraft could also be used to determine the best f_s value to use for each aircraft type. For now, the factor is set to the ideal spacing: $f_s = 1$.

Recalling that the lift of the aircraft is $W = \rho V \Gamma_0 s_0$ (where W is its weight, ρ is the air density and V is the flight speed), one sees that the determination of the proper f_s factor is indeed of significant interest: for the same lift and flight speed, passing from $f_s = 1$ (ideal spacing) to $f_s = 0.9$ would lead to an increase of 10% in the initial wake circulation.

When using the UNW, the code also allows for different levels of spatial resolution. This is accomplished by varying the number of layers, n_c, used to discretize the two rollers (port and starboard vortices) with the universal circulation profile: for instance, setting

$n_c = 2$ produces a total of $N = 50$ discrete vortices (25 for each roller); setting $n_c = 3$ produces a total of $N = 98$ discrete vortices, etc., see [11].

From our testing, it appears that $n_c = 2$ suffices for operational use. The code then runs about 3.2 times faster than when $n_c = 3$ (as the expensive part of the code, the Biot-Savart velocity evaluation, grows like $O(N^2)$). For comparison, SABIGO's NWDB for the B727 uses 62 discrete vortices to discretize the near wake based on the "squeleton" configuration of the aircraft. This is also few vortices for an operational near wake.

Note: there is even the possibility of setting $n_c = 0$: the initial near wake is then made of only 2 discrete vortices (one for each roller); the code then runs very fast.

5. The modelling of non-uniform wind shear effects. It is based on original models developed by Winckelmans et al., that were implemented within the MDV, and also further simplified for operational use within the VFS (see [10,12]). In validation studies [12], the second model (Model 2) proved significantly better than the first one (Model 1): it is the model retained.

6. The use of cubic splines for the operational approximation of all required dimensionless profiles: dimensionless wind, TKE and EDR profiles.

7. The possibility of using a fast Biot-Savart kernel that approximates well the basic Gaussian kernel (using a high order algebraic kernel that is also scaled properly). Everything else being kept equal, this choice makes the code about 20% faster, with essentially identical results on all operational outputs. Interesting timing comparisons are provided below.

8. The possibility of defining the total physical run time as input (i.e., not necessarily run for $t = 120$ s).

9. The VFS now outputs two "measures" of circulation for the port and starboard vortices:

a) what was output previously, and which corresponds to an efficient (yet approximate) estimation of the circulation contained in a circle of radius $s_0 / 2$ centered on each vortex centroid;

b) the sum of the discrete vortex circulations associated to each vortex: port and starboard.

In both cases, the secondary vortices are not counted. b) is a smoother measure than a) when running the VFS using the EDR or TKE decay models; they both however give roughly the same time evolution. a) is to be used when running the VFS as in the previous versions (versions 1 and 2), i.e., using a significant effective viscosity (e.g., 0.1 m^2/s and more) but no EDR or TKE decay model.

The VFS version 4 also preserves all previous capabilities:

1. The use, as initial condition, of the Near Wake Data Base (NWDB) of SABIGO.

2. The decay model based only on the effective turbulent viscosity.

3. The possibility of still using least-squares polynomial fits for all profiles: wind, TKE and EDR profiles.

4. The basic Gaussian kernel for the Biot-Savart evaluation.

Notice that decay modeling can now be of the mixed-type: e.g., use the EDR decay model to capture the global circulation decay, but supplement it with a small effective viscosity (e.g., 0.03 m^2/s) to also capture the slow core size increase of all discrete vortices as time proceeds.

The coefficients of the EDR and TKE decay models were tuned to the VFS, as decay here represents the global half wake circulation, $\Gamma(t)$, and not the circulation averaged from 3 to 10 meters, $\Gamma_{3\to10}(t)$. The confusion must be avoided as the differences are

significant. Even at early times, shortly after rollup, one already has typically: $\Gamma_{3\to 10}/\Gamma = 0.85$: this is indeed significant. In that respect, it is important to keep in mind that the VFS outputs a circulation that represents closely the global half wake circulation, $\Gamma(t)$ (not $\Gamma_{3\to 10}(t)$).

In the previous NWRA scoring, the VFS initial conditions (especially $\Gamma_0 = \Gamma(0)$) were probably not very good for some aircraft types. For example, insufficient information about the geometry of the DC-9 led to significant uncertainty in SABIGO's Near Wake Data Base for this type. The DC-9 was one of the most used in the scoring. The possibility of also using the universal near wake as input now allows to use initial conditions that are consistent with what is used by other modelers (i.e., with less information of the detailed near wake, on the flap setting, etc.), while still being able to use refinement brought by the f_s factor.

It should be also mentioned that, although cubic splines (or least-squares polynomial fits) are used for the case of detailed profiles, all types of data files can exist for the files "udata", "kdata" and "edata" (wind, TKE and EDR data). The special cases of having one point only (uniform profile) or two points only (linear profile) are handled specially. Evaluation for out of range heights (heights below the first data point or above the last data point) are also handled specially without using the cubic splines fit: a simple linear profile is used; it is built using the closest two data points. The approach to the profile approximations is thus quite general.

Some Findings

The use of the simplified universal near wake (UNW) assumption consistently leads to results that are smoother than when using the NWDB. The simulation is less "rugged": the centroid trajectories are smoother, the measure a) for circulation is smoother. This can be attributed to the fact that the operational NWDB have a coarse resolution to discretize the details of the wake prior to rollup (e.g., 62 discrete vortices for a B727 NWDB).

Hence, when those discrete vortices roll up, they do not form very coherent vortex structures for the port and starboard rollers, even at early times. The universal near wake being, by construction, simplified but well-structured leads to simulations that tend to maintain the coherent port and starboard vortex structures.

It was also verified that the model for non-uniform wind shear effects produces smoother circulation variations when the vortex structures are more coherent.

A high resolution SABIGO's detailed near wake (requiring, unfortunately, many more discrete vortices and thus too high a penalty for operational use with the present code that is still $O(N^2)$) could also produce coherent port and starboard vortices, as well as the finer details.

For this approach to be viable operationally, one would then need the fast multipole method in order to make the Biot-Savart evaluation $O(N \log N)$ instead of $O(N^2)$. The fast multipole technology exists within our group. If required, it could be implemented with little effort into the VFS as a self-contained "fast Biot-Savart" module.

Measured Timings

A few timings are provided below (arbitrary units). First a case with initial discrete core size squared (dimensionless) $t_{n0} = 0.001$ and with a time step $\Delta t = 0.20$ s:

	NWDB (*N*=62)	**UNW (*N*=50)**	**UNW (*N*=98)**
basic kernel:	7.9	5.2	17.3
fast kernel:	6.2	4.3	13.7

Moreover, as the universal near wake is less violent an initial condition, and since one then uses a higher initial discrete vortex core size, $t_{n0} = 0.005$, one can also increase the time step to $\Delta t = 0.50$ s and still obtain essentially the same operational results. Actually, even SABIGO's NWDB can be used with $t_{n0} = 0.005$ and $\Delta t = 0.50$ s. The CPU time is,

of course, further reduced. Here are some timings for a case with initial discrete core size squared (dimensionless) $t_{n0} = 0.005$ and time step $\Delta t = 0.50$ s:

	NWDB (*N*=62)	**UNW (*N*=50)**	**UNW (*N*=98)**
basic kernel:	4.2	2.8	8.0
fast kernel:	3.7	2.2	6.2

The conclusion is that the VFS can be quite fast, yet still provide essentially the same operational results.

APPENDIX D

Modelisation of Non-uniform Wind Shear Effects onto Aircraft Wake Dynamics for the Operational VFS: Testing on Memphis Case 1132 with Non-uniform Shear in Ground Proximity

Grégoire S. Winckelmans* and Paul Ploumhans†

March 23, 2000

* Professor, Centre for Systems Engineering and Applied Mechanics (CESAME), Mechanical Engineering Department, Université Catholique de Louvain, Louvain-la-Neuve 1348, Belgium. Also: 4318 Lindblade Dr., Los Angeles, CA, USA 90066-6243.

† Ph.D. student, Mechanical Engineering Department, Université Catholique de Louvain, Louvain-la-Neuve 1348, Belgium.

Contents

1 Simplified modeling of non-uniform wind shear effects **1**

2 Memphis Case 1132 **4**

3 SABIGO's near wake **7**

4 The universal near wake **7**

5 Simulation results **9**

5.1 VFS simulations IGE without wind 10

5.2 VFS simulations IGE with wind but without wind shear effects 12

5.3 VFS simulations IGE with wind and wind shear effects 12

5.4 VFS simulations OGE with wind and wind shear effects 21

6 Conclusions **22**

7 Bibliography **23**

List of Figures

1 Wind profile for Case 1132: time-averaged experimental data (diamonds); profile reconstructed using the polynomial of degree 10 (dash) 5

2 Vorticity profile for Case 1132: profile obtained by using second order finite differences on the experimental data (diamonds); profile obtained by differentiating once the polynomial fit (dash) 6

3 Derivative of vorticity profile for Case 1132: profile obtained by using second order finite differences on the experimental data (diamonds); profile obtained by differentiating twice the polynomial fit (dash) 7

4 Initial position of the discrete vortices for VFS simulations of Case 1132: SABIGO's near wake (diamonds); universal near wake (crosses) 8

5 Vertical and lateral displacements of the centroids for VFS simulations of Case 1132 without wind. Because of symmetry, only the starboard vortex is shown: SABIGO's near wake (solid); universal near wake (dash) 11

6 Vertical and lateral displacements of the centroids for VFS simulations of Case 1132 with wind but without wind shear effects: SABIGO's near wake: port (solid) and starboard (dash); universal near wake: port (short dash) and starboard (dot) 13

7 Vertical and lateral displacements of the centroids for VFS simulations of Case 1132 with wind and modeling of wind shear effects ($\beta^* = 1$): SABIGO's near wake: port (solid) and starboard (dash); universal near wake: port (short dash) and starboard (dot) 14

8 Vertical and lateral displacements of the centroids for VFS simulations of Case 1132 with wind and modeling of wind shear effects ($\beta^* = 2$): SABIGO's near wake: port (solid) and starboard (dash); universal near wake: port (short dash) and starboard (dot) 15

9 Vertical and lateral displacements of the centroids for VFS simulations of Case 1132 with wind and modeling of wind shear effects ($\beta^* = 3$): SABIGO's near wake: port (solid) and starboard (dash); universal near wake: port (short dash) and starboard (dot) 16

10 Vertical and lateral displacements of the centroids for VFS simulations of Case 1132 with wind and modeling of wind shear effects ($\beta^* = 4$): SABIGO's near wake: port (solid) and starboard (dash); universal near wake: port (short dash) and starboard (dot) 17

11 Vertical and lateral displacements of the centroids for experimental database and for VFS simulations of Case 1132 with wind and modeling of wind shear effects universal near wake with $\beta^* = 3$: port (solid) and starboard (dash); universal near wake with $\beta^* = 4$: port (short dash) and starboard (dot) experimental data: port (diamonds) and starboard (crosses) 18

12 Vertical displacement of the centroids for VFS simulations of Case 1132 OGE, with wind and modeling of wind shear effects: universal near wake run at $\beta^* = 0$ (no wind shear effects), 2, 3 and 4 19

Nomenclature

	Letters	
b	aircraft span	m
b_0	ideal spacing between vortices $= \frac{\pi}{4} b$	m
h^2	effective fluid element area	m^2
h	spatial resolution, effective fluid element length	m
N	number of vortex particles	
q	exponent in buffer region in universal near wake profile	
R	effective radius for port and starboard vortices $= \frac{b_0}{2}$	m
Sh	shear parameter $= \frac{dV}{dz} \frac{b^2}{\Gamma_0}$ or $\frac{\Delta V}{\Delta z} \frac{b^2}{\Gamma_0}$	
$\widetilde{Sh}$	'jump' shear parameter $= \frac{\Delta V\, b}{\Gamma_0}$	
t, T	time	s
x	out of cross-plane coordinate (positive nose to tail)	m
y	cross-plane coordinate (positive port to starboard)	m
z	cross-plane coordinate (positive upward)	m
v	Biot-Savart velocity component in y-direction	m/s
V	wind velocity component in y-direction	m/s
w	Biot-Savart velocity component in z-direction	m/s
W	wind velocity component in z-direction	m/s
	Greek letters	
β	coefficient in universal near wake, parameter in wind shear model	
γ	circulation per unit length	m/s
Γ	circulation	m^2/s
Δ	difference, jump, step	
ν	viscosity	m^2/s
σ	core size of Gaussian vortex particle	m
ω	wake vorticity	1/s
Ω	wind vorticity	1/s
	Subscripts	
c	index for vortex centroids	
i, o	indices for inner and outer vortex cores	
p	index for discrete vortex	
s	index for spacing	
fast, slow	indices for fast and slowly varying wind profiles	
port, starb	indices for port and starboard vortices	
low, up	indices for lower and upper parts in non-uniform shear profile	
0	index for initial condition, global condition	
θ	index for azimuthal direction	
	Superscripts	
$*$	effective, dimensionless	

1 Simplified modeling of non-uniform wind shear effects

The wind shear studies conducted, in Phase 5, on the Memphis Cases 1132 and 1196 using the 2-D fine grain lagrangian method of discrete vortices (MDV-B) were detailed studies that are not real-time. So were the 2-D and 3-D detailed studies conducted in Phases 5 and 6, on the same cases, using a fine grain eulerian method based on the time-dependent Reynolds-Averaged Navier-Stokes (RANS) equations [24], with different possibilities for the modeling of the effective turbulent viscosity, ν^*.

For the enhancement of the operational VFS algorithm based on MDV-A [5, 6, 20, 21, 22] or even the AVOSS algorithm [13], one must develop a simplified model for taking into account the effects of non-uniform wind shear onto vortex wakes. Such a model was already proposed in the Phase 5 Final Report [21]. We here consider its implementation into the VFS based on MDV-A and its partial validation.

The background vorticity, Ω, corresponds to regions with variation of the horizontal wind, V, with altitude, z: $\Omega(z) = -\frac{dV}{dz}(z)$. These are thus wind shear regions. The non-uniform wind shear regions are those where Ω varies significantly with z.

Here, Ω represents the background wind vorticity and ω represents the aircraft wake vorticity. In absence of the aircraft, the background vorticity is in equilibrium. Hence, we can write:

$$\frac{\partial \Omega}{\partial t} + V \frac{\partial \Omega}{\partial y} + W \frac{\partial \Omega}{\partial z} \approx 0 \,. \tag{1}$$

This is consistent: if $W = 0$ and $\frac{\partial \Omega}{\partial y} = 0$, then $\frac{\partial \Omega}{\partial t} = 0$ and we recover the case of the usual cross-wind function of z only: $V = V(z)$ and $\Omega = \Omega(z) = -\frac{dV}{dz}(z)$.

In the presence of the aircraft, the sum of the background + wake vorticity is also in equilibrium. Indeed (apart from the creation of vorticity at the ground due to the no-slip condition), the wake vorticity interaction with the background vorticity does not amount to net vorticity production/destruction: the total vorticity, background + wake, is conserved in such non-linear interactions. It can however lead to significant changes in the wake vorticity (and thus in its subsequent behavior), as we shall see. Hence, we can write:

$$\frac{\partial}{\partial t}(\Omega + \omega) + (V + v) \frac{\partial}{\partial y}(\Omega + \omega) + (W + w) \frac{\partial}{\partial z}(\Omega + \omega) \approx 0 \,, \tag{2}$$

where (v, w) is the Biot-Savart velocity due to the wake vorticity. By subtraction of the two equations above, we obtain:

$$\frac{D\omega}{Dt} = \frac{\partial \omega}{\partial t} + (V + v) \frac{\partial \omega}{\partial y} + (W + w) \frac{\partial \omega}{\partial z} = -\left(v \frac{\partial \Omega}{\partial y} + w \frac{\partial \Omega}{\partial z} \right) \,. \tag{3}$$

This simple model thus reduces to a convection equation for the wake vorticity, but with an added source term. Thus, in first approximation, the wake vorticity is convected by the total velocity field (wind velocity + Biot-Savart velocity due to the wake vorticity), and its strength is modified by the source term on the right hand side: the dot product

between the Biot-Savart wake velocity and the wind vorticity gradient. In the case of usual cross-wind such as is assumed into VFS, this model equation further reduces to:

$$\frac{D\omega}{Dt} = -w\,\frac{d\Omega}{dz} = w\,\frac{d^2V}{dz^2}\ . \tag{4}$$

Adding back diffusion effects, we obtain the following model equation:

$$\frac{D\omega}{Dt} = w\,\frac{d^2V}{dz^2} + \nabla\cdot(\nu^*\,\nabla\omega)\ . \tag{5}$$

As such, this equation can now be solved using the MDV. The MDV-A and MDV-B methods were presented in [2, 17, 18, 4, 20, 21], including taking into account the effective ν^* diffusion effects and the viscous ground effects (inviscid for "near ground effects", NGE, and viscous for "in ground effects", IGE). To solve the equation above, it suffices to add, to the previous MDV methods, a source term in the evolution equation for the discrete vortex circulations. For instance, in MDV-B as in [20, 21], the evolution equation becomes:

$$\frac{d\Gamma_p}{dt} = \text{PSE diffusion} + h^2\,w(y_p,z_p)\,\frac{d^2V}{dz^2}(z_p)\ . \tag{6}$$

where h^2 is the fluid area associated to each vortex particle: h is here the true particle "size", i.e., the inter-particle spacing after each particle redistribution step, using the $h\times h$ lattice: very much the same as the grid size in eulerian methods on a $h\times h$ grid.

The obvious advantage of the model equation is that it does not require the particle discretization of the background wind vorticity (as was the case in MDV-B Mode 2 and Mode 3 simulations, see [21]). In that sense, an MDV simulation based on this model will cost little more in terms of CPU than the same simulation without wind shear effects. This is essential for the operational VFS based on MDV-A.

We notice also that the simplified model above could also be used to parametrize the simplest algorithms such as the one used in AVOSS [13], assuming that the port and starboard vortices are treated separately, using a system of two coupled ordinary differential equations.

An important consequence of the simplified model is as follows: when the background vorticity, Ω, is uniform (i.e, when the background wind is linear), the source term vanishes. Thus, according to the model, there is then no influence of the background vorticity on the wake vorticity. This is in accordance with our Phase 5 results [21]: we indeed found out, for both Cases 1132 and 1196, that there is essentially no difference in the wake vortex evolution (trajectories, iso-contours of vorticity) between the Mode 2 and the Mode 3 simulations. As the Mode 2 and Mode 3 simulations only differed by a uniform vorticity component (for the slowly varying part of the wind that was linear), the fact that both simulations provided essentially the same results supports the simplified model proposed above. Discussions with Proctor et al. during the March 99 meeting at Langley also indicated that they do not observe, in their CFD simulations, significant wind shear effects when the bakground vorticity is uniform: it requires significant vertical variations of the background vorticity for significant wind shear effects to show up. This is referred to as "non-uniform wind shear".

The simplified model is designed to handle "spread" non-uniform wind shear, i.e., wind shear for which the background vorticity variations occur over a characteristic height that is of the order of, or larger, than the aircraft span. This is indeed the case observed in the real data (such as Cases 1132 and 1196). The case of "abrupt" wind shear most likely cannot be simplified any further than what was already done: the vortex sheet corresponding to an abrupt velocity jump must be discretized using a layer of discrete vortices (e.g., see simulation in [21] using MDV-B). Notice that this is not proper to the MDV methods: the same goes for other methods, e.g., the method of discrete vortex sheets (MDVS) as in [8]. As abrupt wind shear is not expected to be observed in real atmospheric conditions anyway, this special case remains somewhat academic. Real cases fall into the category of spread wind shear.

Remains to implement the simplified model into the VFS which is based on MDV-A. In MDV-A, there is no clear spatial discretisation of the vorticity "field". One uses N discrete vortices (with N quite small), each of which carries a certain amount of circulation, Γ_p, that is spread using a Gaussian core function with core size σ: the circulation due to the p discrete vortex within a circle of radius r centered on the discrete vortex is $\Gamma_p(r) = \Gamma_p \left(1 - \exp(-r^2/\sigma_p^2)\right)$ with $\sigma_p^2(t) = \sigma_p^2(0) + 4\nu^* t$ (in the case of constant and uniform effective viscosity, ν^*). There is thus not vorticity field reconstruction, as in MDV-B. There is just a limited number of discrete "patches" of vorticity that are each spreading in time at a rate specified by ν^*. It is thus difficult to associate a specific fluid area to each discrete vortex. For instance, the vortex sheet that emanates from the trailing edge of a wing is quite thin (i.e., of the order of twice the boundary layer thickness). It can be discretized using N vortices, but there is no well-defined fluid area to assign to each one. In VFS, the spacing between neighbor vortex is $h_s = b/N$, but that does not define the h^2 fluid area. One could take it as $h^2 = h_s \times h_s$. But one could as well take it as $h^2 = h_s \times h_s/2 = h_s^2/2$ or whatever. To find out the correct "order of magnitude" to assign to each discrete vortex, we decided to consider the vortex wake shortly after rollup. The centroids of the port and starboard vortices are then separated by approximately $b_0 = \frac{\pi}{4} b$ and are here seen as circles of radius approximately equal to $R = \frac{b_0}{2}$. Thus, if a total of N discrete vortices is used to discretize the near wake, the order of magnitude for the fluid area to assign to each one is roughly: $h^2 \approx \frac{\pi R^2}{N/2}$.

The simplified evolution equation for MDV-A is finally taken as:

$$\frac{d\Gamma_p}{dt} = \beta^* h^2 w(y_p, z_p) \frac{d^2V}{dz^2}(z_p) \,. \tag{7}$$

The factor β^* is expected to be $O(1)$ but not necessarily equal to unity. It is here used to:

- possibly correct for the uncertainty of the effective fluid area to assign to each discrete vortex;
- possibly correct for significant production/destruction of vorticity by the source term in the regions where there are no discrete vortices to capture this source term. This correction is thus used for "lumping back", onto the N near wake discrete vortices, the possibly significant effects due to the non-locality of the source term in

the model equation. We indeed need to only capture the significant (and sufficient) non-uniform wind shear effects while limiting ourselves to the N near wake discrete vortices, knowing nevertheless that wind shear effects can have a wider spatial spread than the wake itself, see Eq. 7. Moreover, because of the $O(N^2)$ CPU cost of the present VFS algorithm, we certainly must avoid increasing N excessively for the operational VFS.

- possibly capture additional wind shear effects due to 3-D turbulence interacting with the wind shear profile. This is somewhat in the same spirit as the use of an effective turbulent viscosity, ν^*, to capture additional diffusion effects due to 3-D turbulence. Thus, β^* can also be seen as an effective factor due to turbulence and provide for modeling flexibility in that respect.

The model equation with the β^* factor is the model that was implemented into the VFS based on MDV-A in order to produce the "VFS version 3" released to OTI on February 29, 2000. It is understood that the factor β^* is not yet optimized at this time. We will here show results obtained on the investigation of Memphis Case 1132 with different initial conditions for the near wake (SABIGO's near wake versus universal near wake) and different β^*. Recall that Case 1132 is a case of non-uniform wind shear in ground proximity, hence also with significant ground effects. The ground effects are thus also taken into account, see [17, 18, 4, 19, 20, 5, 21, 6]. The interaction between the wind shear effects and the ground effects is non-linear and can lead to complex physics as in [21, 24].

2 Memphis Case 1132

The simplified wind shear model will here be investigated with respect to Memphis Case 1132. Concerning the aircraft, we have the following [23, 21, 24]: it is a B-727-100 with $b = 32.92$ m, of half-wake circulation, Γ_0, equal to approximately 286 m^2/s and of initial altitude, z_0, equal to approximately 148 m.

The time-averaged experimental cross-wind profile is shown in Fig. 1. Also shown is the profile reconstructed using the polynomial fit of degree 10 (as is produced so far by the VFS code) and applied to the experimental data from $z = 5$ to $z = 200$ m.

The wind can here be decomposed as

$$V(z) = V_{\text{slow}}(z) + V_{\text{fast}}(z) \,. \tag{8}$$

The slowly varying part of the wind is found to be linear in the range of altitudes that are relevant, see Fig. 1 $V_{\text{slow}}(z) = a_1 z + a_0$, and thus $\Omega_{\text{slow}}(z) = -a_1$ is uniform in z. Here, we obtain: $a_1 = 1.25/160 = 0.00781$/s and $a_0 = -1.50$ m/s.

The fast varying part of the wind profile corresponds to a low level "jet", i.e., two "fat" regions of opposite circulation, the sum being zero, see Fig. 2: one region of circulation per unit length $\gamma = -\Delta V_{\text{fast,up}} \approx -2.18$ m/s, of thickness $\Delta z_{\text{fast,up}} \approx 70$ m and centered at $z \approx 90$ m, and an opposite region of circulation $\gamma = -\Delta V_{\text{fast,low}} \approx 2.18$ m/s, of thickness $\Delta z_{\text{fast,up}} \approx 55$ m and centered at $z \approx 22$ m. For the fast varying part of the wind profile,

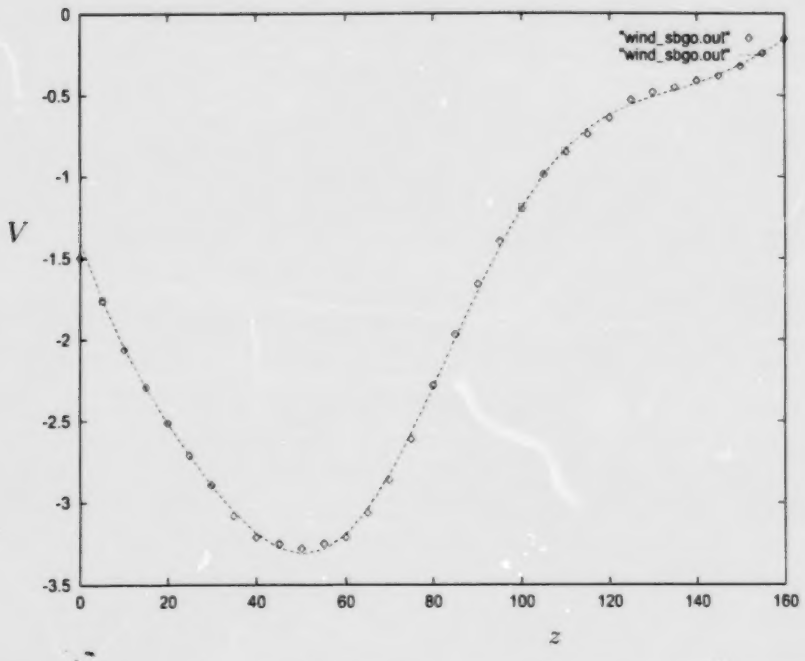

Figure 1: Wind profile for Case 1132: time-averaged experimental data (diamonds); profile reconstructed using the polynomial of degree 10 (dash)

there are two shear parameters: one for the upper part of the profile and one for the lower part. Moreover, there are different possible definition for the shear parameter: Sh which makes use of the difference of velocity and of the difference of height over which this difference of velocity occurs, and $\widetilde{Sh}$, which only uses the difference of velocity (i.e., the jump). Both parameters are relevant: Sh is basically a dimensionless measure of the mean vorticity in the layer (i.e., the mean derivative of the velocity field: $\Delta V/\Delta z$), while $\widetilde{Sh}$ is basically a measure of the total circulation (per unit length) in the layer: no matter how thick the layer, its circulation per unit length is equal to the velocity difference on both sides of the layer. In summary, we here have:

$$
\begin{aligned}
Sh_{\text{slow}} &= -\frac{dV_{\text{slow}}}{dz}\,\frac{b^2}{\Gamma_0} = -\frac{1.25}{160}\,\frac{32.9^2}{286} = -0.030\,, \\
Sh_{\text{fast,up}} &= -\frac{\Delta V_{\text{fast,up}}}{\Delta z_{\text{fast,up}}}\,\frac{b^2}{\Gamma_0} = -\frac{2.18}{70}\,\frac{32.9^2}{286} = -0.12\,, \\
Sh_{\text{fast,low}} &= -\frac{\Delta V_{\text{fast,low}}}{\Delta z_{\text{fast,low}}}\,\frac{b^2}{\Gamma_0} = \frac{2.18}{55}\,\frac{32.9^2}{286} = 0.15\,, \\
\widetilde{Sh}_{\text{fast,up}} &= -\Delta V_{\text{fast,up}}\,\frac{b}{\Gamma_0} = -2.18\,\frac{32.9}{286} = -0.25\,, \\
\widetilde{Sh}_{\text{fast,low}} &= -\Delta V_{\text{fast,low}}\,\frac{b}{\Gamma_0} = 2.18\,\frac{32.9}{286} = 0.25\,.
\end{aligned}
\tag{9}
$$

Notice that we do not incorporate, in the definition of the fast varying wind profile

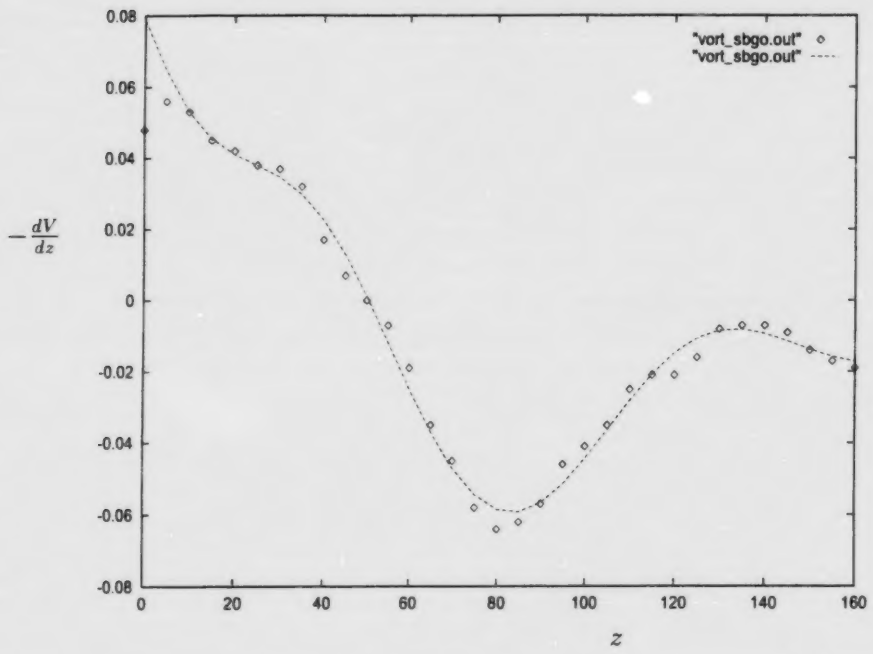

Figure 2: Vorticity profile for Case 1132: profile obtained by using second order finite differences on the experimental data (diamonds); profile obtained by differentiating once the polynomial fit (dash)

and thus of the fast wind shear parameters, the zero velocity condition a the ground. We use the total wind profile as measured up to close to the ground (here $z = 5$ m), and we assume a smooth extrapolation of this profile up to the ground. We then remove, from this profile, the slowly varying part, $V_{\text{slow}} = a_1\, z + a_0$. What is left is the fast varying part of the wind profile, with non-zero value at the ground. The difference between this ground value and the zero value corresponding to the no slip condition is taken care by the small boundary layer near the ground and by the vorticity production at the ground: the viscous ground effect, as was done in [17, 18, 19, 4, 20, 5, 21, 5, 6]. This near ground part is thus considered as part of the viscous ground effect, and not as part of the non-uniform wind shear effects.

Notice that, for Case 1132, it so happens that the fast varying part of the wind profile is zero at the ground. This is so because the slowly varying part of the wind profile is indeed equal to the wind extrapolated to the ground, i.e., to -1.50 m/s, see Figs. 1 and 2. This is not the case in Case 1196.

The vorticity profile, $\Omega(z) = -\frac{dV}{dz}(z) = -a_1 + \Omega_{\text{fast}}(z)$ is shown in Fig. 2: profile obtained by using second order finite differences on the experimental data as well as profiles obtained by differentiating once the polynomial fit. The correspondence between the two profiles is not as good as for the wind profiles, but still quite good.

Finally, the derivative of the vorticity profile, $\frac{d\Omega}{dz}(z) = \frac{d\Omega_{\text{fast}}}{dz}(z) = -\frac{d^2V}{dz^2}(z)$ is shown in Fig. 3: profile obtained by using second order finite differences on the experimental data as well as profiles obtained by differentiating twice the polynomial fit. As expected,

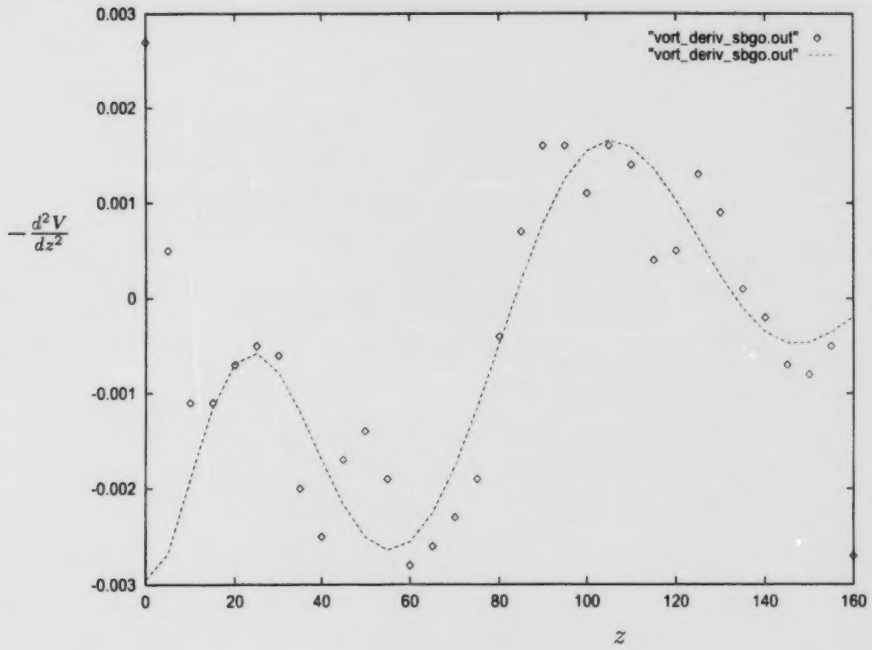

Figure 3: Derivative of vorticity profile for Case 1132: profile obtained by using second order finite differences on the experimental data (diamonds); profile obtained by differentiating twice the polynomial fit (dash)

the correspondence between the two profiles is worse than for the vorticity profiles. Nevertheless, it is not too bad. Recall that it is this profile that acts as part of the forcing term for the simplified wind shear model. We here used the second derivative of the polynomial fit as the forcing term for all simulations on Case 1132.

3 SABIGO's near wake

One of the initial condition that was used for Case 1132 is the near wake provided by SABIGO. This corresponds to a near wake discretized using the "aircraft squeleton" with (only) $N = 62$ discrete vortices, see Fig. 4. Without cross wind, the half-wake circulation, Γ_0, corresponding to this near wake is obtained as $\Gamma_0 = 292.4$ m^2/s. The initial aircraft altitude ($t = 0$) is taken as $z_0 = 148$ m. As there are 62 discrete vortices, we assign to each an approximate fluid area of $h^2 \approx \frac{\pi R^2}{N/2} \approx \frac{2\pi}{N}\left(\frac{\pi b}{8}\right)^2 = 16.9\,\mathrm{m}^2$.

4 The universal near wake

Here, the time $t = 0$ corresponds to the vortex wake shortly after rollup of the near wake. The inital vorticity field is taken as the superposition of two vortices: the port vortex located at $(-y_0, z_0)$ and of circulation $-\Gamma_0$, and the starboard vortex located

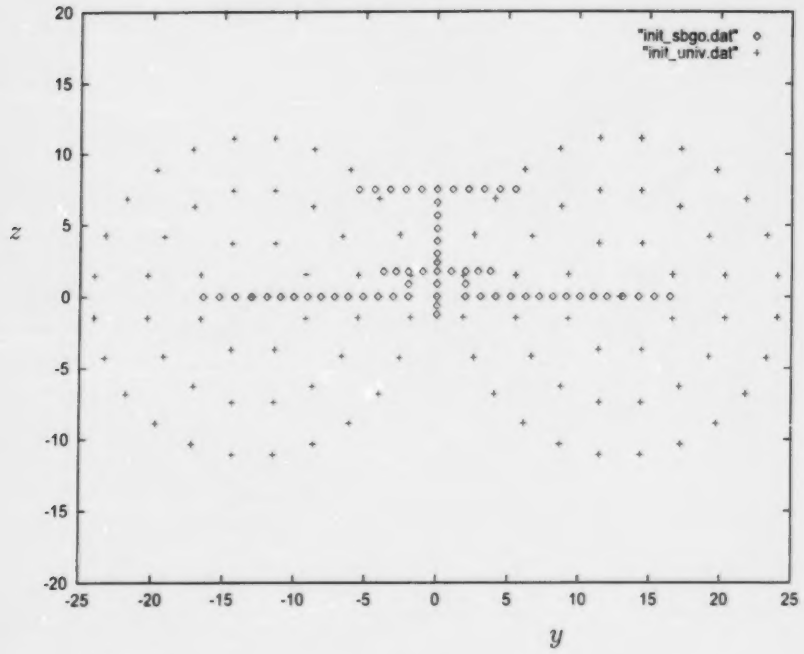

Figure 4: Initial position of the discrete vortices for VFS simulations of Case 1132: SABIGO's near wake (diamonds); universal near wake (crosses)

at (y_0, z_0) and of circulation Γ_0. The numerical values are taken as: $b = 32.92$ m, $\Gamma_0 = 286$ m^2/s (which corresponds to the value recommended for Case 1132 [23, 21, 24]), $y_0 = \frac{b_0}{2} = \frac{\pi}{8} b = 12.93$ m (which corresponds to the value recommended based on elliptical loading [23, 21, 24]) and $z_0 = 148$ m.

The outer core circulation associated with each vortex is here spread according to the universal near wake profile, i.e., the "best fit" formula of [9, 12]:

$$\frac{\Gamma(r)}{\Gamma_0} = 1 - \exp\left(-\beta_o \left(\frac{r}{b}\right)^{3/4}\right) . \tag{10}$$

Such distributions indeed fit well the 2π-averaged circulation distribution, $\Gamma(r)$, obtained from Lidar measured flight data. A typical value is $\beta_o \approx 10$. It can also be shown, using MDV simulations, that such outer-core distributions are indeed obtained as the result of the vortex sheet rollup process (Winckelmans 1999, to be reported in the Phase 6 Final Report). This is also confirmed by wind tunnel measurements of the velocity field, after rollup, of the wake produced by a wing (Winckelmans and Jeanmart, 1999, to be reported in the Phase 6 Final Report). As to the diffusion process, it creates a small Gaussian inner core [9, 12]:

$$\frac{\Gamma(r)}{\Gamma_0} = 1 - \exp\left(-\beta_i \left(\frac{r}{b}\right)^{2}\right) . \tag{11}$$

A typical value for aircraft wakes is $\beta_i \approx 500$. A good fit that is valid for all r and that

goes smoothly from the inner core function to the outer core function is:

$$\frac{\Gamma(r)}{\Gamma_0} = 1 - \exp\left(\frac{-\beta_i\,(r/b)^2}{\left(1 + ((\beta_i/\beta_o)\,(r/b)^{5/4})^q\right)^{1/q}}\right) . \tag{12}$$

All such functions have the proper inner and outer limits of Eqs. (10) and (11). The best fit for the buffer region (i.e., the one that provides the best match in the region with maximum azimuthal velocity, $u_\theta(r) = \Gamma(r)/(2\pi r)$) is obtained when $q = 3 \ldots 4$ (and is quite insensitive to q in that range). This will also be reported in details in the Phase 6 Final Report.

This initial wake vorticity is thus quite realistic. It is essentially the one that was used for the simulations reported in [24]. Here, it is discretized using one discrete vortex in the center plus 3 layers of discrete vortices: 8 vortices in layer 1, 16 in layer 2 and 24 in layer 3, see Fig. 4. The total number of discrete vortices is thus $N = 98$. The radius of discretization is $R = b_0/2 = 12.93$ m. By construction of the layer discretization, the fluid area associated to each vortex is $h^2 = 10.7\,\mathrm{m}^2$. Thus, the corresponding "grid size" is $h = 3.27$ m, quite coarser than for the simulations reported in [24]. The amount of circulation to provide to each layer is computed using the function $\Gamma(r)$. With this fairly crude discretization, only the center vortex is in the inner Gaussian core of Eq. (11): it carries 68.4% of the total circulation, Γ_0: a substantial amount of circulation is thus concentrated in the Gaussian inner core. The layers are all in the outer core region of Eq. (10). Again, the crude discretization is such that there is no need to use the sophisticated function of Eq. (12): the outer core function of Eq. (10) suffices. After calculation of the circulations for the layers, we obtain that layer 1 carries 24.3% of Γ_0, that layer 2 carries 5.1% and that layer 3 carries the remaining 2.2%.

5 Simulation results

The trajectories of the wake centroids are the main diagnotics for all simulations and comparisons. As there is no vorticity field reconstruction in MDV-A (and certainly no way to do it properly with so few discrete vortices), the vorticity centroids for the port and starboard vortices are computed, in VFS, from the circulation-weighted averages of the discrete particle positions:

$$\begin{aligned}
y_{c,\mathrm{port}} &= \frac{\sum_{p,\mathrm{port}} y_p\,\Gamma_p}{\sum_{p,\mathrm{port}} \Gamma_p} , \\
z_{c,\mathrm{port}} &= \frac{\sum_{p,\mathrm{port}} z_p\,\Gamma_p}{\sum_{p,\mathrm{port}} \Gamma_p} , \\
y_{c,\mathrm{starb}} &= \frac{\sum_{p,\mathrm{starb}} y_p\,\Gamma_p}{\sum_{p,\mathrm{starb}} \Gamma_p} , \\
z_{c,\mathrm{starb}} &= \frac{\sum_{p,\mathrm{starb}} z_p\,\Gamma_p}{\sum_{p,\mathrm{starb}} \Gamma_p} ,
\end{aligned} \tag{13}$$

where the sum is done over the discrete vortices that were used for the near wake discretization (i.e., eventual secondary vortices generated at the ground because of viscous

ground effect IGE do not participate to the centroid definitions). This is done by "flagging" them initially: flag = 1 for the starboard discrete vortices and flag = −1 for the port discrete vortices. For the universal wake, the distinction between port and starboard discrete vortices is clear. For SABIGO's near wake, there is some ambiguity for the discrete vortices that are initially on the vertical tail (and that have non-zero Γ_p when there is some sideslip): they are flagged with flag = 0 and it is considered that they participate at 50% to each centroid computation.

It must be clearly stated that vortex centroid positions computed in VFS using the above definitions cannot be compared exactly with the positions of maximum or minimum of vorticity obtained in experimental data and/or in fine grain simulations (such as our MDV-B simulations of [20, 21] or the eulerian simulations of [24]). Comparing centroid positions with max/min vorticity positions is a fair thing to do in most cases, such as OGE and NGE (and is the only thing to do in VFS since one cannot properly reconstruct the vorticity field from so few discrete elements), but, nevertheless, it is not the same thing. Significant differences can be observed between the two definitions for wake IGE. One must keep that in mind when comparing results of VFS simulations to fine grain simulations or to data.

For all simulations, the effective viscosity is set to $\nu^* = 0.1\,\mathrm{m}^2/\mathrm{s}$. The time step is set to $\Delta t = 0.2$ s. Results are presented in dimensionless form using the same convention as in [24]: $b_0 = \frac{\pi}{4} b = 25.86$ m is used as the reference distance and $V_0 = \frac{\Gamma_0}{2\pi b_0}$ is used as the reference velocity ($V_0 = 1.80$ m/s for SABIGO's near wake; $V_0 = 1.76$ m/s for the universal near wake). Dimensionless time is denoted $t^* = t/\frac{b_0}{V_0}$; dimensionless vertical and lateral displacements of the vortex centroids are denoted $z_c^* = z_c/b_0$ and $y_c^* = y_c/b_0$ respectively. As to the dimensionless initial aircraft altitude, it is here equal to $z_0^* = 5.724$.

For the discrete vortices belonging to the near wake, the wind value that is used is the one evaluated at the mean wake height:

$$z_{c,\mathrm{mean}}(t) = \frac{1}{2}\left(z_{c,\mathrm{port}}(t) + z_{c,\mathrm{starb}}(t)\right) . \tag{14}$$

This choice is necessary in order for the VFS algorithm to conserve the wake vertical impulse in cases OGE without wind shear effects:

$$I_z = \int w \, dy \, dz = -\int y \, \omega \, dy \, dz = -\sum_p y_p(t)\,\Gamma_p \tag{15}$$

is conserved in cases OGE (inviscid or viscous) as it should be, see VFS Change Request 9. For the secondary discrete vortices eventually produced at the ground (because of viscous ground effect IGE), the wind value that is used is the one evaluated at the discrete vortex location.

As to the wind shear model, it is applied to each discrete vortex using the wind second derivative evaluated at the discrete vortex location.

5.1 VFS simulations IGE without wind

Simulations are first done in ground effect but without wind. The results are shown in Fig. 5. Initially, we already notice a small difference in the dimensionless descent rates:

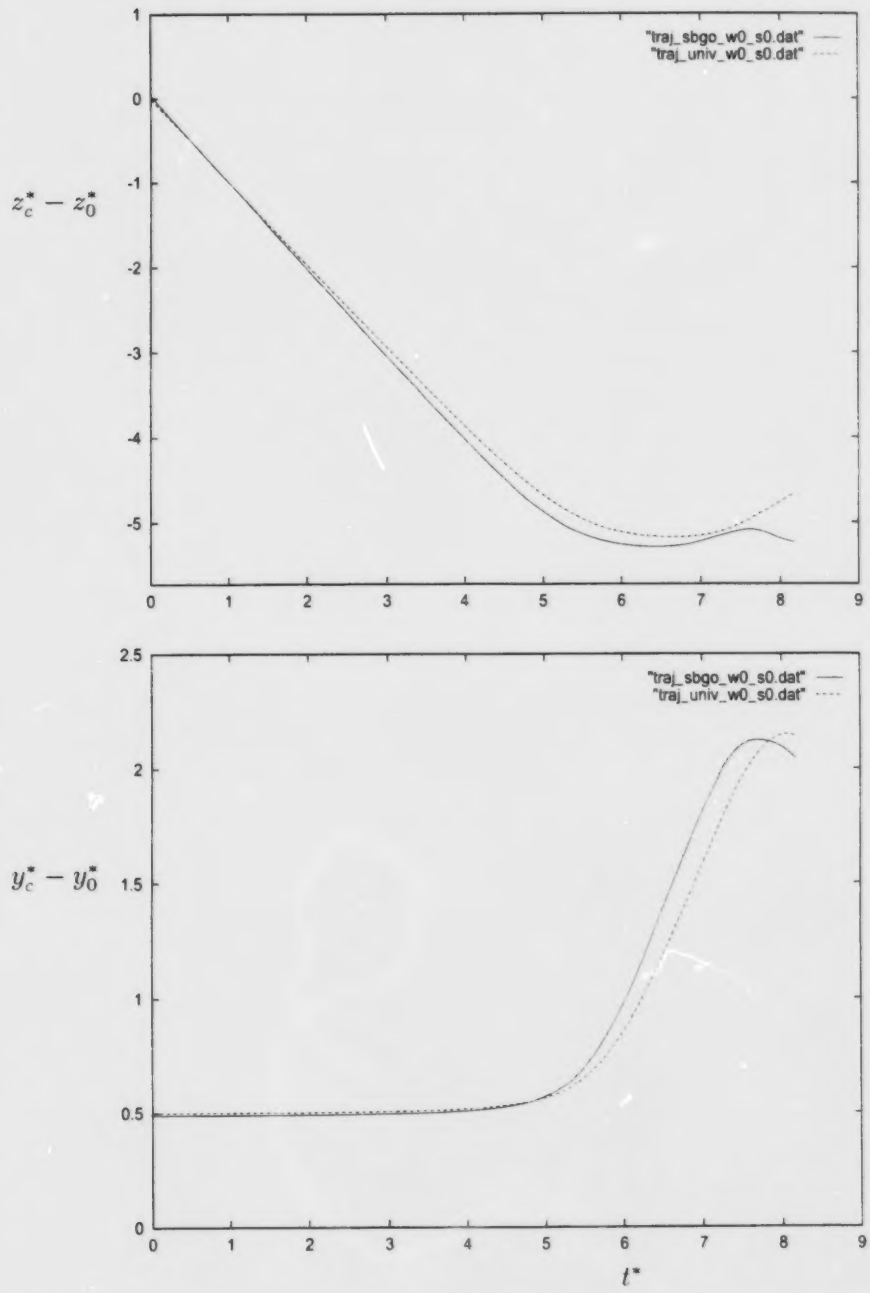

Figure 5: Vertical and lateral displacements of the centroids for VFS simulations of Case 1132 without wind. Because of symmetry, only the starboard vortex is shown: SABIGO's near wake (solid); universal near wake (dash)

this is due to the fact that, after rollup, SABIGO's near wake produces two rollers that are not spaced by exactly $b_0 = \frac{\pi}{4} b = 0.785\, b = 25.86$ m. This is expected as the loading is not elliptical for this wake. In fact, the y_c positions of the vortex centroids are found to be initially at $\pm 0.385\, b$: the spacing between centroids is thus equal initially to $0.770\, b$, i.e., slightly smaller than b_0. The initial dimensionless wake descent rate is thus slightly higher by an amount equal to $0.785/0.770 = 1.02$.

As to the wake evolution, it is as expected: the wake comes first into "inviscid" near ground effect (NGE) and then pursues to "viscous" in ground effect (IGE) with secondary vortices being then produced at the ground. The evolution of both wakes (SABIGO and universal) differ by little: a small rebound is observed in both cases. Apart form the small difference in descent rate and rebound pattern, the present results highly ressemble those presented in Fig. 12 of [24] for the case "without crosswind". This is especially true of the case started from the universal near wake: the vortex centroids here rebound more than for the case started from SABIGO's near wake and match well the vortex trajectories obtained in [24].

5.2 VFS simulations IGE with wind but without wind shear effects

Simulations are done here with ground effect, with wind but without modeling of the wind shear effects. In addition to the Biot-Savart velocity (i.e., the velocity induced by all discrete vortices on all discrete vortices), the discrete vortices are here also convected by the wind profile. The results of the VFS simulations are shown in Fig. 6. Again, the wake evolution is as expected: the wake descends and is convected sideways by the wind profile of Fig. 1. It also comes first into "inviscid" near ground effect (NGE) and then pursues to "viscous" in ground effect (IGE) with secondary vortices being produced at the ground. Again, the evolution of both wakes (SABIGO and universal) differ by little.

5.3 VFS simulations IGE with wind and wind shear effects

Simulations are done next with ground effect, with wind and with modeling of the wind shear effects. Runs are done for different values of β^*: $\beta^* = 1$, 2, 3 and 4. The results are shown in Figs. 7 to 10. Wind shear effects are clearly observed.

Above $z \approx 50$ m (i.e., $z^* \approx 2$), the background non-uniform vorticity is negative, see Fig. 2. The port vortex (of negative vorticity) is enhanced by the background vorticity and the starboard vortex is depleted. This results in tilting of the vortex pair system, the port vortex being brought to a lower z than the starboard vortex. The higher the value for β^*, the more the wind shear effects and the more the tilting.

This tilting effect can be interpreted as significant "rebound of the starboard vortex", something that was already seen in the MDV-B detailed simulations of [21], and that was seen even more in some of the simulations reported in [24]. The simplified wind shear model is thus able to capture this tilting effect.

The vortex wake interaction with the non-uniform wind shear and with the ground is non-linear. Viscous IGE effects are most active when $z^* \leq 2$ or so. Notice that $z^* \approx 2$ here also corresponds to the region of maximum velocity of the near ground jet, see

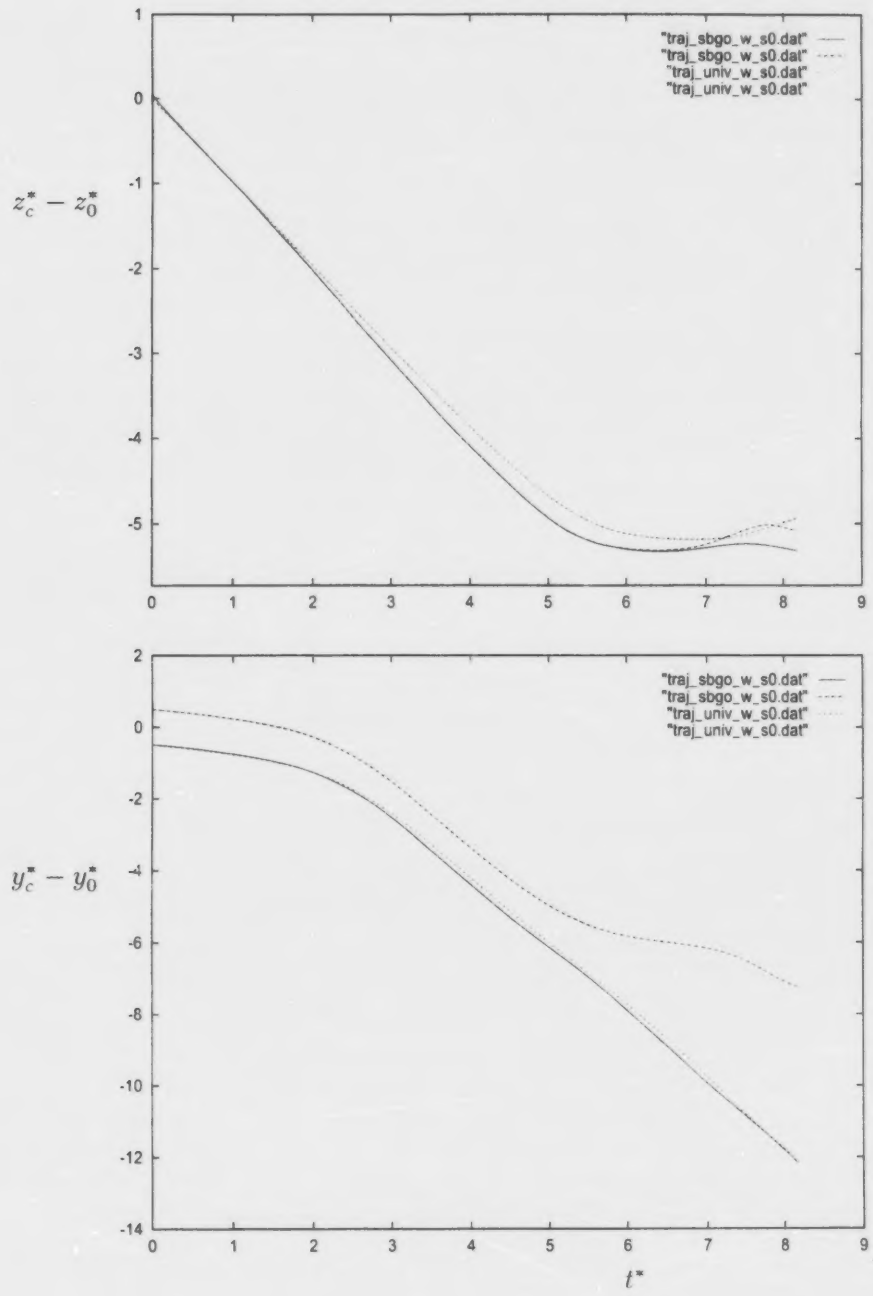

Figure 6: Vertical and lateral displacements of the centroids for VFS simulations of Case 1132 with wind but without wind shear effects: SABIGO's near wake: port (solid) and starboard (dash); universal near wake: port (short dash) and starboard (dot)

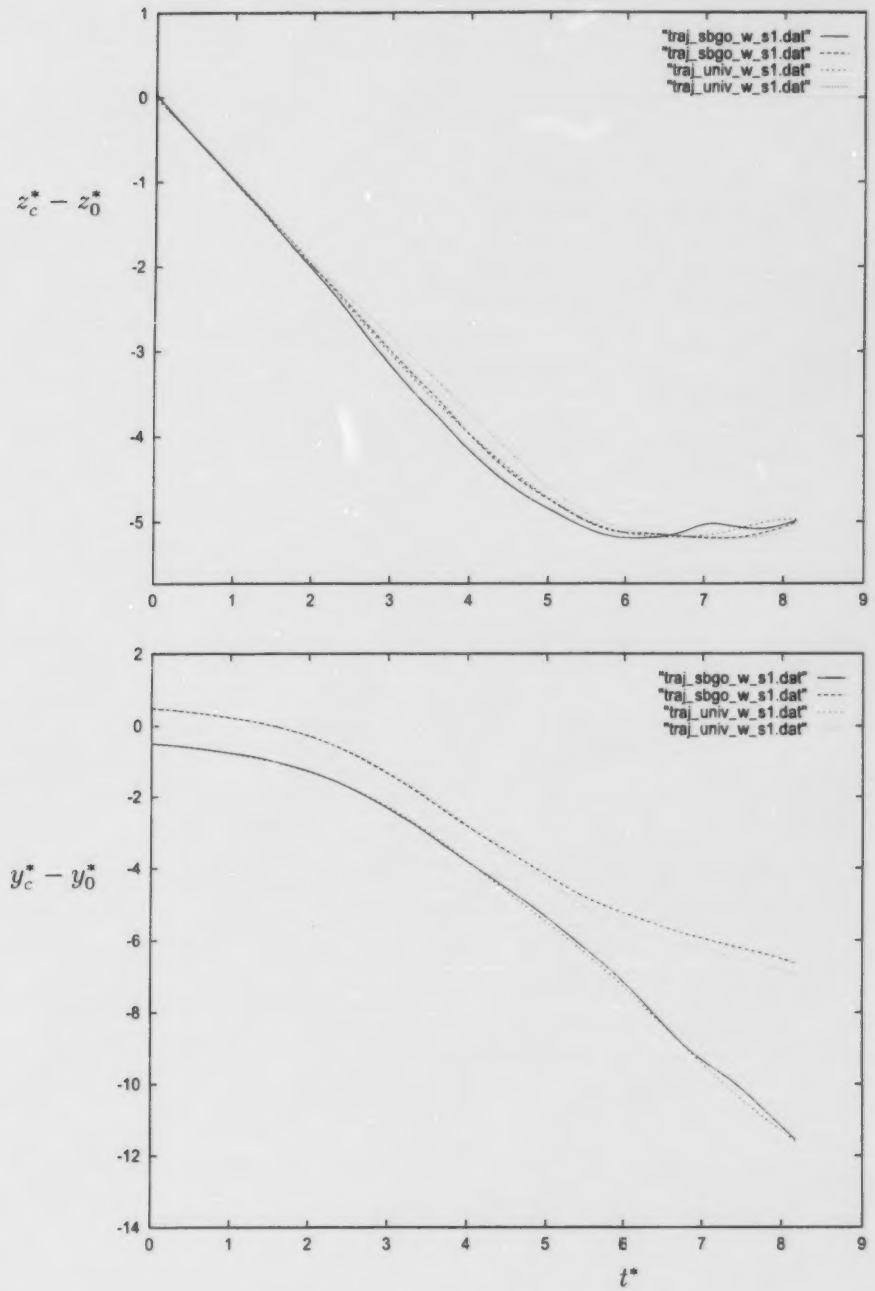

Figure 7: Vertical and lateral displacements of the centroids for VFS simulations of Case 1132 with wind and modeling of wind shear effects ($\beta^* = 1$): SABIGO's near wake: port (solid) and starboard (dash); universal near wake: port (short dash) and starboard (dot)

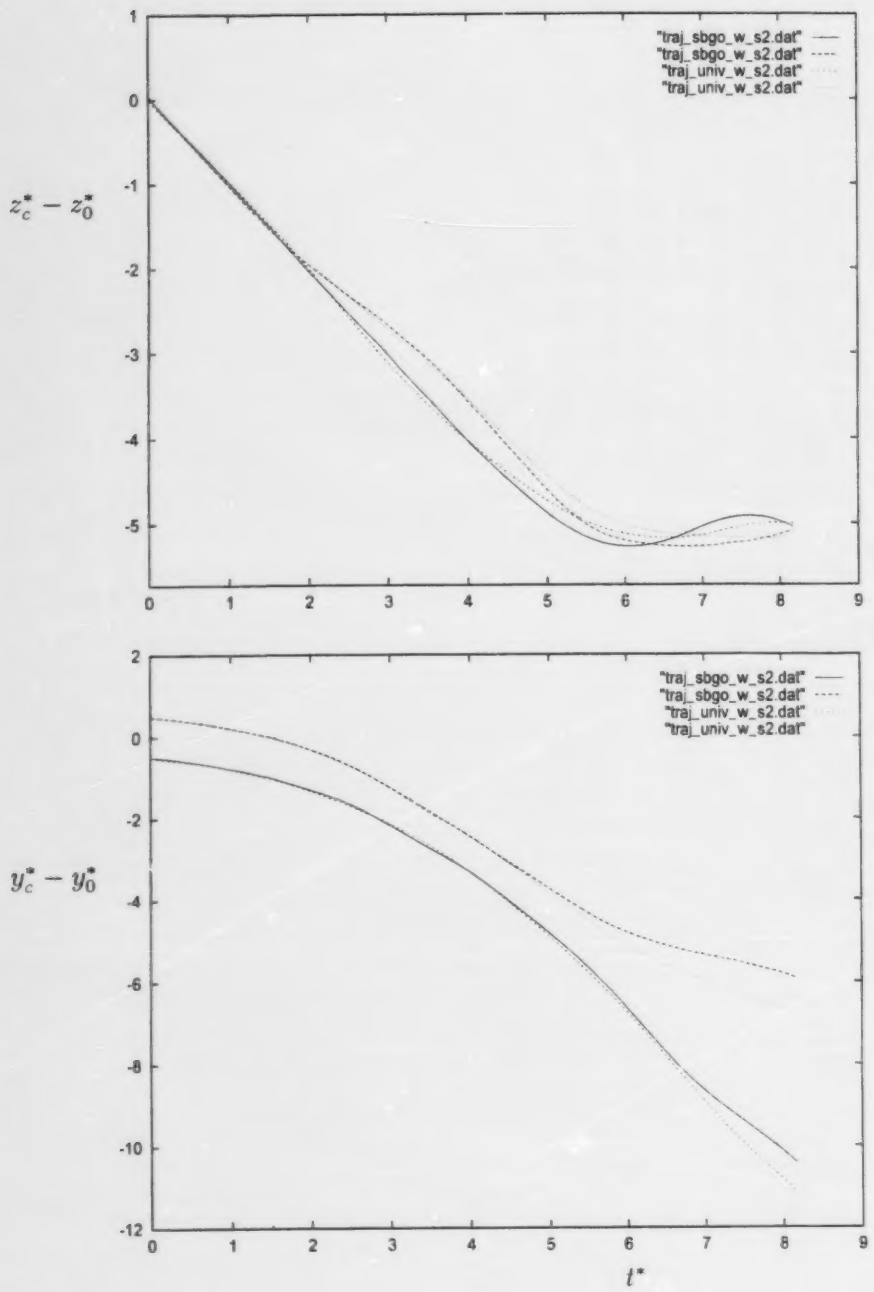

Figure 8: Vertical and lateral displacements of the centroids for VFS simulations of Case 1132 with wind and modeling of wind shear effects ($\beta^* = 2$): SABIGO's near wake: port (solid) and starboard (dash); universal near wake: port (short dash) and starboard (dot)

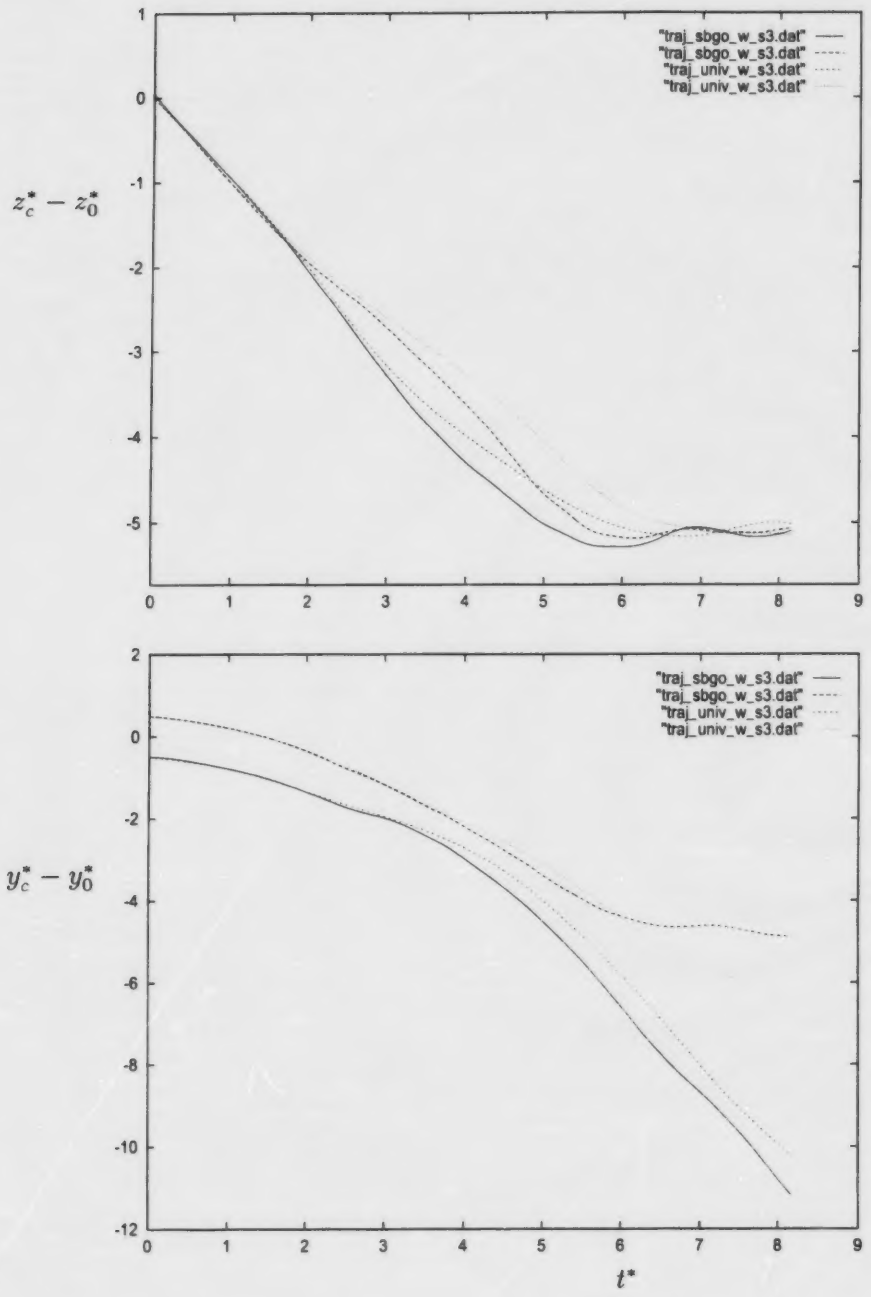

Figure 9: Vertical and lateral displacements of the centroids for VFS simulations of Case 1132 with wind and modeling of wind shear effects ($\beta^* = 3$): SABIGO's near wake: port (solid) and starboard (dash); universal near wake: port (short dash) and starboard (dot)

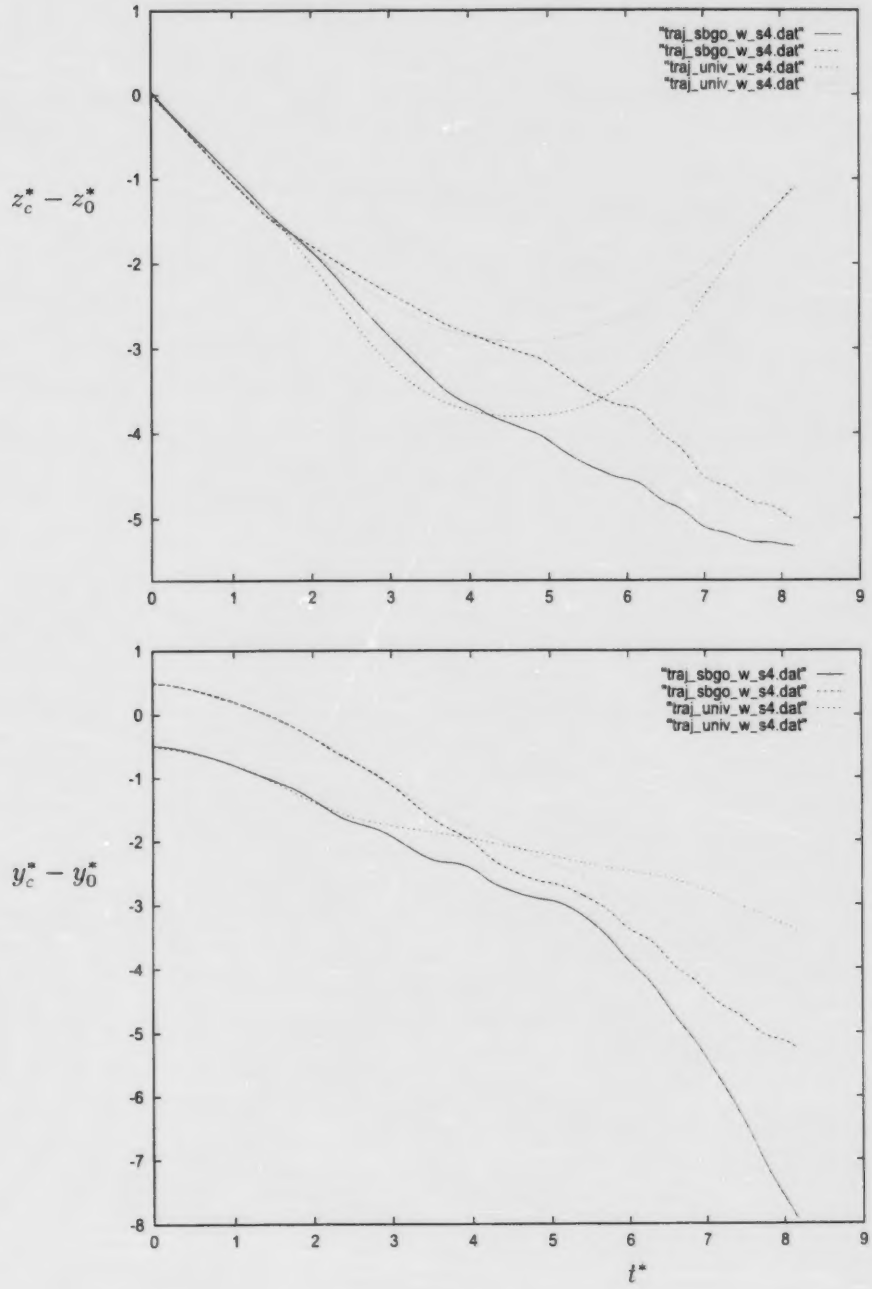

Figure 10: Vertical and lateral displacements of the centroids for VFS simulations of Case 1132 with wind and modeling of wind shear effects ($\beta^* = 4$): SABIGO's near wake: port (solid) and starboard (dash); universal near wake: port (short dash) and starboard (dot)

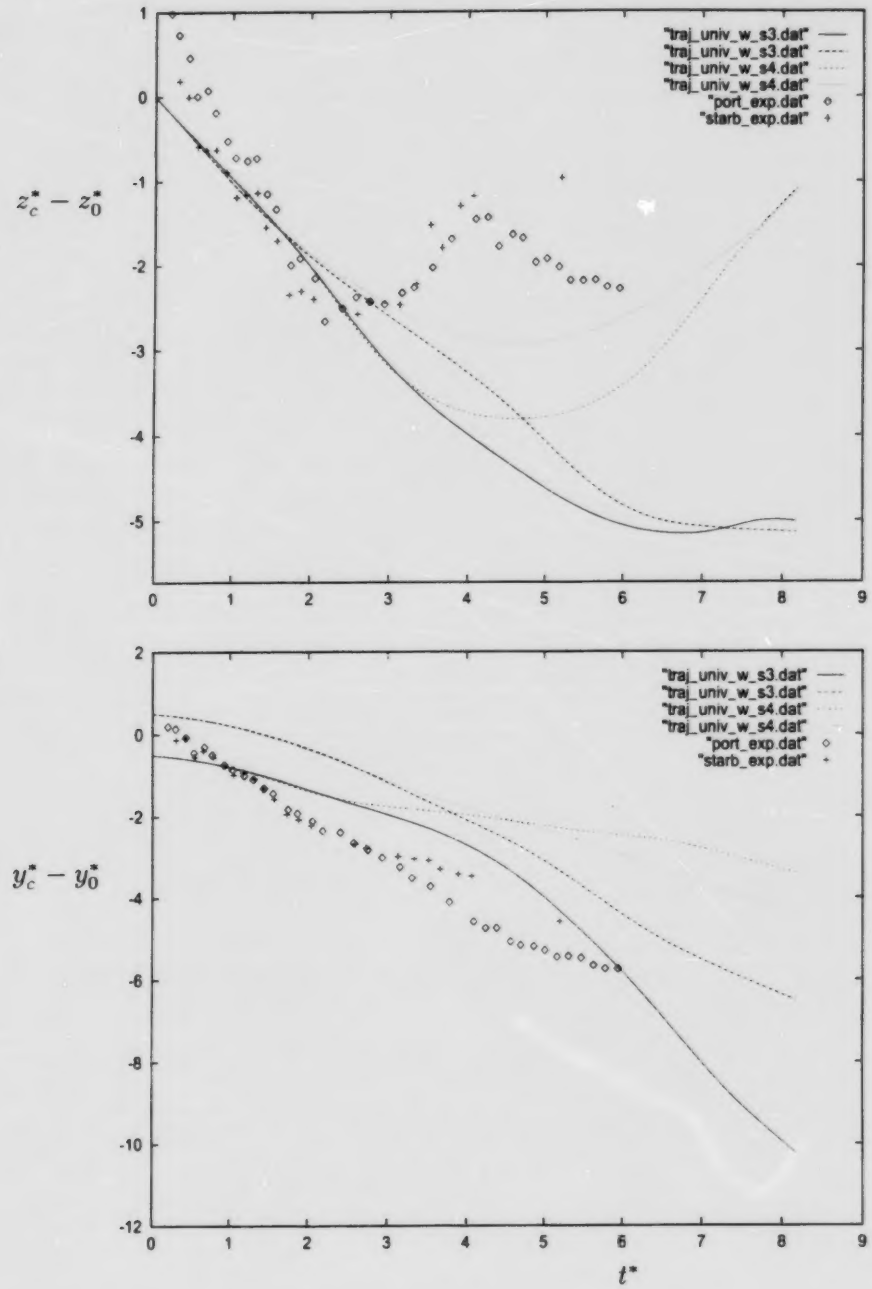

Figure 11: Vertical and lateral displacements of the centroids for experimental database and for VFS simulations of Case 1132 with wind and modeling of wind shear effects universal near wake with $\beta^* = 3$: port (solid) and starboard (dash); universal near wake with $\beta^* = 4$: port (short dash) and starboard (dot) experimental data: port (diamonds) and starboard (crosses)

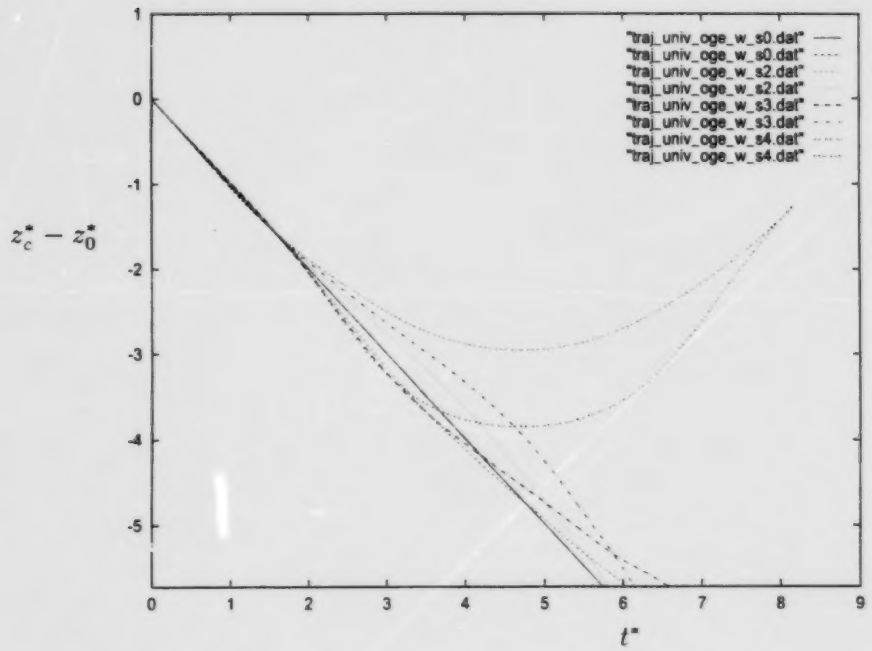

Figure 12: Vertical displacement of the centroids for VFS simulations of Case 1132 OGE, with wind and modeling of wind shear effects: universal near wake run at $\beta^* = 0$ (no wind shear effects), 2, 3 and 4

Fig. 1, and thus to the region when the non-uniform background vorticity changes sign, see Fig. 2. Because of the tilting due to the wind shear effects in the upper part of the jet, the port vortex comes IGE while the starboard vortex is still NGE. Secondary vorticity is thus produced at the ground essentially for the port vortex, leading to a vortex dipole system such as those reported in the ground effect studies of [19, 20] and the wind shear effect + ground effect studies of [21, 24]. This vortex dipole has impulse that tends to bring it back up. This can be sufficient for the port vortex to be seen to "rebound"

For the case with $\beta^* = 1$, the results of both near wakes are still essentially the same, see Fig. 7. Significant differences in the wake centroids trajectories already occur for the case with $\beta^* = 2$, see Fig. 8.

The results obtained using the universal near wake and $\beta^* = 3$ ressemble those presented in Fig. 13 of [24] for the case "with ground". The correspondance is quite good up to the time when the port vortex is again as high as the starboard vortex: $t^* \approx 7$. The subsequent rebound of the port vortex, seen in Fig. 13 of [24], is however not seen in the present VFS simulation. It also wasn't seen in our MDV-B simulations, see Fig. 4 of [21]. Thus, the present VFS results compare well with Fig. 4 of [21] up to $t^* = 8.2$ (i.e., $t = 120$ s), but only well with Fig. 13 of [24] up to $t^* \approx 7$.

Recall that, in VFS based on MDV-A, the viscous ground effect is modeled using a simplified approach which also uses "ad hoc" coefficients. In particular, no-slip is not guaranteed at all points along the ground. The ground effect model only produces very few secondary vortices: only 2 vortices every four time steps or so, and where they are most needed; thus not all along the ground. Such simplified modeling can not be expected to perform as well as detailed simulations (such as MDV-B simulations or eulerian simulations) that respect the no-slip condition at all points along the ground, see [17, 18, 19, 20, 21, 24]. It could thus be that the ground effects in VFS are here too "mild": the ground effect did not create enough of a vortex dipole for the port vortex; thus the port vortex did not rebound significantly.

Part of the differences in rebound of the port vortex could also be due to the assumptions that were made for elaborating the simplified non-uniform wind shear model. The simplified model is only a model: it is not perfect. We notice however that, for simulations without ground, our results compare very well to those of [24] in the case "without ground", see Section 5.4. Finally, part of the differences could also be attributed to the differences between vortex centroids definitions and max/min vorticity centers, see comments in Section 5.

Finally, there is a possibility for the starboard vortex to pass above the port vortex. This remarkable behavior is indeed seen to happen in one simulation: the simulation started from the universal wake and run with $\beta^* = 4$, see Fig. 10. Vortex lateral trajectories do cross at $t^* \approx 4.5$. The subsequent wake behavior is also unexpected: both the port and starboard vortices are seen to rebound. This is thus rebound of the port vortex as well. This simulation, at (probably too) high β^* and thus at (probably too) high wind shear effects, thus produces rebound of both vortices: port and starboard, and up to altitudes comparable to the initial aircraft height. We recall that this was also the case observed in the experimental data: both vortices were seen to rebound, see Fig. 11. Is this behavior due to the wind shear model a possible explanation of what happened in Case 1132? Possibly, but probably not. Indeed, according to the experimental data, the

starboard vortex did not pass above the port vortex, see lateral trajectories in Fig. 11. It would be worth checking that the port and starboard vortex were indeed clearly identified by the Lidar system in Case 1132, i.e., that they indeed did not pass one over the other.

Finally, we notice that the simulations presented in [21] produced some rebound of the port vortex, but not of the starboard vortex. In some cases, the simulations presented in [24] produced significant rebound of the port vortex, but, again, not of the starboard vortex. Rebound of the starboard vortex in Case1132 is thus something difficult to explain. One possibility is that the starboard vortex indeed passes above the port vortex. The issue remains open.

In conlusion, it is seen that the VFS version 3 with simplified non-uniform wind shear modeling can indeed produce significant wind shear effects. One must keep it mind that the non-uniform wind shear sensitivity is controlled by the forcing term in the model: $\beta^* h^2 \frac{d^2V}{dz^2} w$. As there is significant uncertainty on the wind second derivative, $\frac{d^2V}{dz^2}$, see Fig. 3, on the fluid area, h^2, to assign to each discrete vortex in MDV-A, and of the physics of the interaction between turbulence and the mean shear, it follows that non-uniform wind shear effects are difficult to model. The best effective β^* can only be calibrated by validation. Notice that part of the uncertainty on the wind profile is also related to the time-variablity of this profile. Recall that only the time-averaged wind profile is available so far for the operational VFS.

For instance, at $\beta^* = 4$, the differences between SABIGO's near wake and the universal near wake, see Fig. 4, were such that the initial tilting of the vortex pair in the upper part of the jet was stronger for the universal wake than for SABIGO's wake, see Fig. 10. This sufficed for the subsequent behaviors, under the simplified wind shear modeling at such high β^*, to be very different. Recall also the different values of the effective fluid area, h^2, for each near wake: $h^2 = 16.9\,\mathrm{m}^2$ for SABIGO's near wake, versus $h^2 = 10.7\,\mathrm{m}^2$ for the universal near wake. This difference corresponds to the difference in spatial resolution: $N = 62$ discrete vortices versus $N = 98$: $98/62 = 16.9/10.7$. It is thus also difficult to compare thoses cases: they have a different initial configuration, see Fig. 4, but also a different spatial resolution.

5.4 VFS simulations OGE with wind and wind shear effects

Simulations were also done using the wind profile and the modeling of wind shear effects, but by "removing the ground effects" (both inviscid and viscous ground effects). This was done by running the VFS version 3 on the universal near wake using a high initial z_0 and by shifting the wind profile upward by the proper amount. The results obtained for different values of β^* are shown in Fig. 12. It is seen that the results corresponding to the universal near wake run with $\beta^* = 3$ highly ressemble those presented in Fig. 13 of [24] for the case "without ground". This partially comforts us in the ability of the simplified wind shear model to capture the right physics.

Again, the case with $\beta^* = 4$ produces a wind shear effect so strong that the starboad vortex passes over the port vortex. This indicates that $\beta^* = 4$ is probably too high a value to use.

6 Conclusions

Simplified wind shear modeling was developed and was implemented into the VFS code, together with other amendments (other Change Requests) in order to produce the VFS version 3. It uses the second derivative of the wind profile, the approximate effective fluid area assigned to each discrete vortex, and the effective β^* parameter. Part of the effective β^* parameter can be understood as modeling of the turbulent interaction between the vortex wake and the non-uniform wind shear profile. Part can also be understood as a correction of the approximate fluid area associated to each discrete vortex. Finally, part can also be understood as lumping, onto the discrete vortices used to capture the vortex wake, the net wind shear effects from regions that are not covered by the discrete vortices (lumping of non-locality effects).

The new VFS version was tested on Memphis Case 1132, using different near wakes: SABIGO's near wake and the universal near wake. All simulations were done using the same turbulent effective viscosity: $\nu^* = 0.1\,\mathrm{m}^2/\mathrm{s}$. The time-averaged wind profile used was the polynomial fit or degree 10 provided by the VFS code for Case 1132. Thus, the wind shear forcing was obtained from differentiating twice this polynomial and was assumed constant in time. Different values of the effective β^* parameter were investigated: $\beta^* = 1$, 2, 3 and 4.

The VFS obtained vortex centroid trajectories were compared to the vortex trajectories reported in [24] that used fine grain eulerian unsteady RANS simulations started from the universal near wake. The results obtained using the VFS run with $\beta^* \approx 3$ compared well with those reported in [24] using the same near wake: a) case with ground but without wind, b) case with ground, wind and non-uniform wind shear, c) case with wind and non-uniform wind shear but without ground. The vortex trajectories were essentially the same for cases a) and c). They were close for case b), except for too mild a rebound of the port vortex at late times as compared to [24]. Possible causes for the differences in the rebounds were offered. It was also noted that the results for case b) compared well, for all times, with those of the fine grain MDV-B simulations of [21] (where all regions with non-uniform wind vorticity were discretized using discrete vortices: no wind shear modeling used).

At this stage of development and validation, it thus appears that the VFS version 3 is able to capture non-uniform wind shear effects.

A remarkable behavior was also obtained when using the VFS started from the universal near wake and run with $\beta^* = 4$: the starboard vortex passed above the port vortex, leading to rebound of both the port and starboard vortices up to significant altitudes. At this point, however, this behavior cannot be offered as an explanation for what was observed in the real Case 1132 (rebound of both vortices was observed in the data, but, according to the data, it does not appear that the starboard vortex passed above the port vortex). This behavior is probably a peculiar effect produced by the simplified wind shear model at values of β^* that are (too) high. In particular, it was also observed when running the VFS with same wind and β^* but without ground effect.

We believe that further validations of the simplified wind shear model are called for. In that respect, generic cases with non-uniform wind shear (such as generic jet profiles or generic shear layer profiles) should also be investigated, first OGE, then IGE. Comparions

with fine grain lagrangian MDV-B simulations as in [21], fine grain RANS simulations as in [24] or even fine grain Large Eddy Simulations as in [9, 10, 12, 7] would help validate the model and fine tune the effective β^* to use. They would also help fine tune the effective ground effect modeling in VFS.

Notice that one OGE validation of the simplified model was already done here: the case where the (non generic) jet profile of Case1132 was run OGE and compared to the results in [24]: with $\beta^* = 3$, the results on vortex trajectories were indeed very close.

Finally, it appears, from the above discussions and model assumptions, that β^* should also be related to the effective turbulence (i.e. to the effective ν^* viscosity). From the present partial validation of the model and the comparisons with the simulations of [24, 21], we suggest to use, for the time being, the value $\beta^* \approx 3$.

7 Bibliography

References

[1] S. M. Belotserkovsky et al., *Development and adaptation of VFS for field tests: I. Typical data base of near wake and aerodynamic derivatives for Boeing 737-300 aircraft*, SABIGO, 1996.

[2] S. M. Belotserkovsky et al., *Development and adaptation of VFS for field tests: II. Evaluation of mathematical models for Boeing 727 and 767 far wakes*, SABIGO, Moscow, Russia, 1996.

[3] S. M. Belotserkovsky et al., *Development and adaptation of VFS for field tests: III. Investigation on evaluation of effective viscosity factor ν^**, SABIGO, Moscow, Russia, May 1996.

[4] S. M. Belotserkovsky et al., *Influence of the ground boundary layer on the position of far wake vortices*, Science-Engineering Center SABIGO Ltd., Moscow, Russia, Sept. 1997.

[5] S. M. Belotserkovsky et al., *Computer Vortex Forecast System*, Phase 4 Final Report TP 13373E, Science-Engineering Center SABIGO Ltd., Moscow, Russia, March 1999.

[6] S. M. Belotserkovsky et al., *Computer Vortex Forecast System (VFS)*, Phase 5 Draft Final Report, Science-Engineering Center SABIGO Ltd., Moscow, Russia, May 1999.

[7] J. Han, Y.-L. Lin, S. Pal Arya and F. H. Proctor, Large eddy simulation of aircraft wake vortices in a homogeneous atmospheric turbulence: vortex decay and descent, *37th Aerospace Sciences Meeting & Exhibit*, Jan. 11-14, 1999, Reno NV, paper AIAA 99-0756.

[8] M. Mokry, Numerical simulation of aircraft trailing vortices in an interactive graphics environment, *37th Aerospace Sciences Meeting & Exhibit*, Jan. 11-14, 1999, Reno NV, paper AIAA 99-0827.

[9] F. H. Proctor, The NASA-Langley wake vortex modelling effort in support of an operational aircraft spacing system, *36th Aerospace Sciences Meeting & Exhibit*, Jan. 12-18, 1998, Reno NV, paper AIAA 98-0589.

[10] F. H. Proctor and J. Han, Numerical study of wake vortex interaction with the ground using the Terminal Area Simulation System, *37th Aerospace Sciences Meeting & Exhibit*, Jan. 11-14, 1999, Reno NV, paper AIAA 99-0754.

[11] T. Sarpkaya, A new model for vortex decay in the atmosphere, *37th Aerospace Sciences Meeting & Exhibit*, Jan. 11-14, 1999, Reno NV, paper AIAA 99-0761.

[12] S. Shen, F. Ding, J. Han, Y.-L. Lin, S. Pal Arya and F. H. Proctor, Numerical modeling studies of wake vortices: real case simulations, *37th Aerospace Sciences Meeting & Exhibit*, Jan. 11-14, 1999, Reno NV, paper AIAA 99-0755.

[13] R. E. Robins and D. P. Delisi, Further development of a wake vortex predictor algorithm and comparisons to data, *37th Aerospace Sciences Meeting & Exhibit*, Jan. 11-14, 1999, Reno NV, paper AIAA 99-0757.

[14] P. R. Spalart, Airplane trailing vortices, *Annu. Rev. Fluid Mech.* 30: 107–38 (1998)

[15] R. A. Stuever and G. C. Greene, An analysis of relative wake-vortex hazard for typical transport aircraft, *32nd Aerospace Sciences Meeting & Exhibit*, Jan. 10-13, 1994, Reno, NV, paper AIAA 94-0810.

[16] G. S. Winckelmans,*Review of report by SABIGO: "Development and adaptation of VFS for field tests; III. Investigation on evaluation of effective viscosity factor ν^*"*, Mechanical Engineering Department, Université catholique de Louvain, Louvain-la-Neuve, Belgium, November 1996.

[17] G. S. Winckelmans and P. Ploumhans, *Interaction of aircraft vortex wakes with the ground: MDV sample computations using different approaches*, Mechanical Engineering Department, Université catholique de Louvain, Louvain-la-Neuve, Belgium, February 1997.

[18] G. S. Winckelmans, *Prediction of aircraft wake vortices during takeoff and landing - Phase 3*, Final Report, Mechanical Engineering Department, Université catholique de Louvain, Louvain-la-Neuve, Belgium, June 26, 1997.

[19] G. S. Winckelmans and P. Ploumhans, On the efficient simulation of vortex wakes IGE including the viscous interaction with the ground: sample computations using the vortex particle method combined with the boundary element method, Proc. *International Wake Vortex Meeting* organized by Transport Canada and Transportation Development Center, Ottawa, Ontario, Canada, Dec. 2-4, 1997.

[20] G. S. Winckelmans and P. Ploumhans, *Prediction of aircraft wake vortices during takeoff and landing - Phase 4*, Final Report TP 13374E, Mechanical Engineering Department, Université catholique de Louvain, Louvain-la-Neuve, Belgium, March 1999.

[21] G. S. Winckelmans and P. Ploumhans, *Prediction of aircraft wake vortices during takeoff and landing - Phase 5*, Draft Final Report, Center for Systems Engineering and Applied Mechanics (CESAME), Mechanical Engineering Department, Université catholique de Louvain, Louvain-la-Neuve, Belgium, July 5, 1999.

[22] M. I. Yaras, *An evaluation of the Vortex Forecasting System for predicting aircraft far-wake trajectories*, Final Report TP 13371E, Department of Mechanical and Aerospace Engineering, Carleton University, Ottawa, Canada, March 1999.

[23] M. I. Yaras, *Effects of atmospheric conditions and ground proximity on the dynamics of aircraft wakes vortices: a study of the 1994-95 Memphis field measurements*, Final Report TP 13372E, Department of Mechanical and Aerospace Engineering, Carleton University, Ottawa, Canada, March 1999.

[24] M. I. Yaras, *Numerical simulations of aircraft far-wake dynamics in nonuniform windshear and ground proximity*, Phase 6 Interim Report, Department of Mechanical and Aerospace Engineering, Carleton University, Ottawa, Canada, Feb. 6, 2000.

APPENDIX E

Study of the Influence of Aircraft Wing Geometry on Near Wake Characteristics

T.V. Pogrebnaya, S.D. Shipilov (SABIGO)

March 2000

1. Introduction

The present report is dedicated to evaluation of the influence of real flap geometry and the wing incidence angle for modern aircraft types on the near wake parameters. Earlier, SABIGO's calculations were based on aircraft wing geometry corresponding to the aircraft three projections contained in the Jane's reference book. As the wing incidence angle is only several degrees, it cannot be evaluated accurately. As to the flap geometry, for modern aircraft they consist of several segments that are extended considerably when they are down. However, this information is rather difficult to obtain. Therefore, it is interesting to make an estimate of the above-mentioned influence. The most important quantity for near wake is the total circulation of vortices over the wing semispan. Hence, the main object of the present study is to evaluate the effect of the flap geometry and wing incidence angle on this circulation. The calculations are performed for Boeing 737-300. The choice of this aircraft type owes to the fact that we have found the additional information on its geometry [K.G. Udalov, D.S. Komissarov. *Boeing 737*. AVICO Press, Moscow, 1994 (The edition is approved by the Boeing Company)].

2. Main Assumptions

The calculations are based on the method of discrete vortices (the linear theory). Let us consider the aircraft steady flight in ideal medium with the speed U_0 and the angle of attack α. We use the standard coordinate system fixed at the aircraft: the x-axis is aligned with the aircraft longitudinal axis, the y-axis is pointing upwards, and the y-axis is directed to the right.

The dimensionless lift coefficient, c_y, is defined as follows:

$$c_y = \frac{2Y}{\rho U_0^2 S}$$

where Y is the aircraft lift, ρ is the air density, and S is the wing area. The near wake is simulated through free discrete vortices with circulations $\Gamma_i, i = 1,...,n$.

3. Boeing 737-300 Geometry

The aircraft Boeing 737-300 has the wing area S = 105.4 m^2. Three-slotted flaps are partitioned by the engine nacelles into inboard and outboard sections. The maximum flap angle is about 40°. The flap guide rails are designed so that a flap moves rearward almost horizontally. After that it is "broken down" into three segments. The maximum flap extension is 74% of the wing chord.

We have calculated the main aerodynamic parameters and near wake vortex circulations for two flight configurations: the cruise and landing configurations. The calculation scheme for the cruise configuration is presented in Fig. 1a. Here we have three main kinematic parameters: the angle of attack, α; the wing incidence angle, φ; and the flap angle, $\delta_2^{(1)}$. The lift coefficient could be evaluated by means of the corresponding aerodynamic derivatives, $c_y^{\alpha}, c_y^{\varphi}$, and $c_y^{\delta_2^{(1)}}$:

$$c_y = c_y^{\alpha}\alpha + c_y^{\varphi}\varphi + c_y^{\delta_2^{(1)}}\delta_2^{(1)}. \qquad (1)$$

In a similar manner one can evaluate the near wake vortex circulations:

$$\Gamma_i = \Gamma_i^{\alpha}\alpha + \Gamma_i^{\varphi}\varphi + \Gamma_i^{\delta_2^{(1)}}\delta_2^{(1)}, i = 1,...,n. \qquad (2)$$

For this configuration we have calculated $c_y^{\alpha}, c_y^{\varphi}, c_y^{\delta_2^{(1)}}, \Gamma_i^{\alpha}, \Gamma_i^{\varphi}, \Gamma_i^{\delta_2^{(1)}}, i = 1,...,n.$

The calculation scheme for the landing configuration is presented in Figs. 1b and 2. It should be noted that, due to the absence of the full information on the flap geometry, the presented scheme is only an assumption. We have assumed, for example, that each of the flap segments has the same chord. Here we have already five main kinematic parameters: the angle of attack, α; the wing incidence angle, φ; and the flap segment angles, $\delta_2^{(1)}, \delta_2^{(2)}, \delta_2^{(3)}$. The superscripts in brackets correspond to the flap segment numbers in Fig. 1b. Now the lift coefficient and the near wake vortex circulations can be presented as follows:

$$c_y = c_y^{\alpha}\alpha + c_y^{\varphi}\varphi + c_y^{\delta_2^{(1)}}\delta_2^{(1)} + c_y^{\delta_2^{(2)}}\delta_2^{(2)} + c_y^{\delta_2^{(3)}}\delta_2^{(3)}, \qquad (3)$$

$$\Gamma_i = \Gamma_i^{\alpha}\alpha + \Gamma_i^{\varphi}\varphi + \Gamma_i^{\delta_2^{(1)}}\delta_2^{(1)} + \Gamma_i^{\delta_2^{(2)}}\delta_2^{(2)} + \Gamma_i^{\delta_2^{(3)}}\delta_2^{(3)}, i = 1,...,n. \qquad (4)$$

Therefore, for this configuration we have calculated $c_y^{\alpha}, c_y^{\varphi}, c_y^{\delta_2^{(1)}}, c_y^{\delta_2^{(2)}}, c_y^{\delta_2^{(3)}}, \Gamma_i^{\alpha}, \Gamma_i^{\varphi}, \Gamma_i^{\delta_2^{(1)}}, \Gamma_i^{\delta_2^{(2)}}, \Gamma_i^{\delta_2^{(3)}}, i = 1,...,n.$

In the future, when we will have the exact information on the flap geometry, the calculations could be improved through the use of more accurate schemes.

4. Calculation Results

The calculated coefficients of aerodynamic derivatives are presented in Table1.

Table 1. Coefficients of Aerodynamic Derivatives for Boeing 737-300

	Cruise Configuration	Landing Configuration
C_y^{α}	5.801	6.787
C_y^{φ}	3.334	4.122
$C_y^{\delta_2^{(1)}}$	1.363	0.307
$C_y^{\delta_2^{(2)}}$	-	0.558
$C_y^{\delta_2^{(3)}}$	-	1.413

The calculation of the total circulation for the right semiwing was performed as follows. First, we calculate the angle of attack α for the given values of $\varphi, \delta_2^{(1)}, \delta_2^{(2)}, \delta_2^{(3)}$ according to the condition that the aircraft weight equals to the lift:

$$mg = \frac{\rho U_0^2}{2} S c_y$$

where m is the aircraft mass, g is the gravity acceleration. From this relation we have

$$c_y = \frac{2gC_W}{S}$$

where $C_W = \frac{m}{\rho U_0^2}$ is the coefficient of the aircraft mass (according to flight measurements for Boeing 737, it is about 6.7 for landing operations with the speed U_0 = 73 m/s). Then we use (1) and (3) for calculation of the required value of α, as well as (2) and (4) to calculate the circulations of each of the near wake discrete vortices. Finally, the total circulation is the sum of these circulations over the right semiwing. The results are presented in Table 2.

Table 2. Total Circulations for Boeing 737 under Different Flight Conditions

	Cruise Configuration			Landing Configuration		
$\delta_2^{(1)}$	0	0	30	0	0	10
$\delta_2^{(2)}$	-	-	-	0	0	15
$\delta_2^{(3)}$	-	-	-	0	0	30
φ	0	1	1	0	1	1
Γ (m^2/s)	270.5	264.9	205.7	266.8	261.1	219.7

The first column in Table 2 corresponds to the cruise flight mode without account for the wing incidence angle. The second column corresponds to the cruise flight mode with account for the wing incidence angle. The third column corresponds to the landing mode without account for the real flap geometry (i.e. for the aircraft cruise configuration but with the deflected flaps). The forth column corresponds to the landing mode (with extended flaps) without account for the wing incidence angle and with zero flap angles. The fifth column corresponds to the landing mode (with extended flaps) with account for the wing incidence angle and with zero flap angles. The sixth column corresponds to the landing mode with account for the wing incidence angle and with real flap angles corresponding to the position "flaps 30° down".

5. Conclusions

1. The results presented in Table 2 show that the wing incidence angle of 1° reduces the total circulation more than by 2%.
2. The most important is the fact that taking into account of the real flap geometry increases the total circulation approximately by 7%.
3. As the both factors lead to changes in the near wake structure, it is very desirable to consider them for calculation of the VFS Near Wake Database.

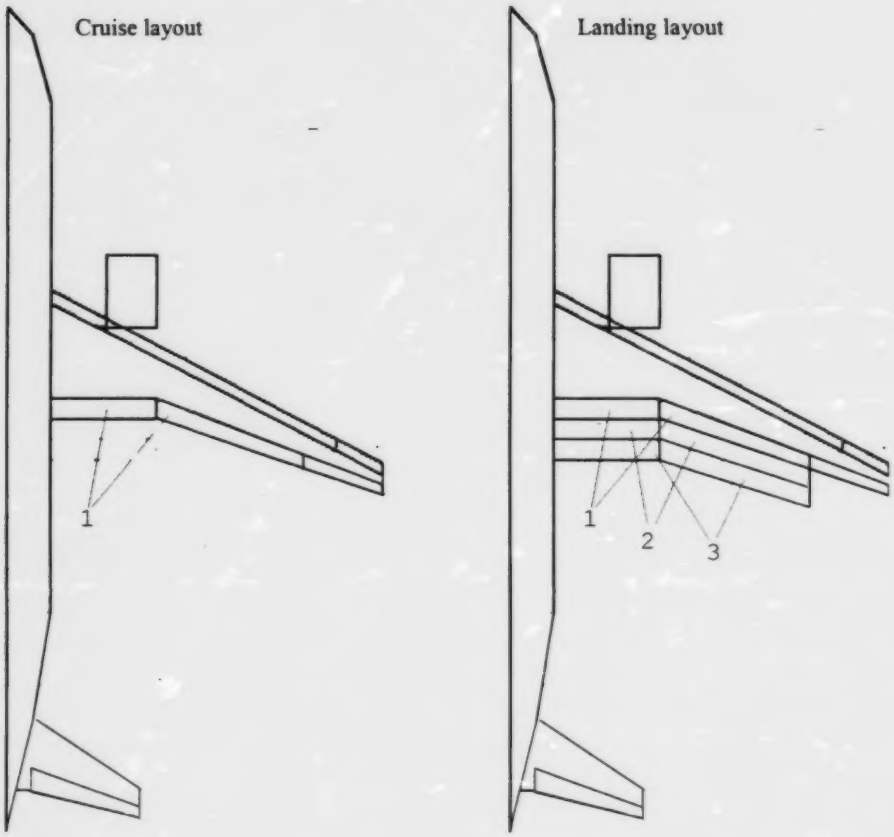

Fig. 1. Calculation schemes for the cruise (a) and landing (b) configurations of Boeing 737-300

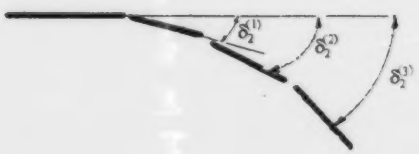

Fig. 2. Calculation scheme for flaps of Boeing 737-300

APPENDIX F

Hazard Definition

SABIGO Ltd.

December 1999

1. Introduction

An aircraft encountering the leader wake vortices experiences the most violent disturbances due to the induced rolling moment. This fact was supported by the previous SABIGO's studies. Therefore, it makes sense to use the induced rolling moment as a criterion for evaluation of danger zones. The problem is what magnitude of the rolling moment is dangerous.

On the other hand, one of the usual conditions for vortex safety is the requirement that aircraft roll, γ, does not exceed some given value, γ_{lim}. This value equals typically to 10°. The criterion in the form of the maximum acceptable roll has clear physical meaning. However, its use for evaluation of danger zones demands large volumes of investigation, as well as invoking flight dynamics models and the corresponding initial data (such as the aircraft inertial parameters) which are known not necessarily.

Hence, in the first stage of the studies SABIGO used the criterion based on the acceptable level of the rolling moment. The decision on the acceptable level of the rolling moment was made by intuition.

To come to an agreement between calculations on the base of the both above criteria, we have performed the proper study. The aim was to evaluate the acceptable level of the rolling moment which effect does not cause the increase of the follower roll over the acceptable value γ_{lim}.

2. Mathematical Model

The study was based on the following simplified flight dynamics model.

Let the follower flies steadily along a rectilinear horizontal line. Then the aircraft is brought instantaneously at the leader wake vortex centroid. As a result, the follower experiences the vortex rolling moment of the constant value. The moment causes the follower rolling motion. It was supposed that the follower stabilization system does not function and only the pilot responds to the aircraft roll. After the given time period (the pilot reaction time), the pilot deflects instantaneously the ailerons through the maximum possible angles to compensate the vortex rolling moment. Clearly, the vortex rolling

moment must not be more than the aileron rolling moment. Otherwise, the aircraft roll will continue.

The model does not account for the aircraft displacement due to the lateral motion. However, the aircraft lateral motion leads to the decrease (in magnitude) of the vortex rolling moment experienced by the follower, as it moves away from the vortex centre. Therefore, the assumption of the constant vortex rolling moment overestimates the vortex effect.

Thus, after the aileron deflection, the aircraft experiences the rolling moment of another constant value.

The presented flight dynamics model ignores the available cross couplings (above all, the aerodynamic ones) between the aircraft roll and yaw channels. However, such simplification is justified as the aircraft lateral motion parameters are small at the initial phase of the aircraft roll motion.

Note that the presented model can easily be extended through inclusion of the aircraft roll stabilization autopilot.

Consider the linearized equation for the aircraft roll:

$$\frac{d^2\gamma}{dt^2} - \frac{\rho VSl^2}{2J} m^{\omega_x} \frac{d\gamma}{dt} - \frac{\rho VSl^2}{2J} m^{\omega_y} \frac{d\psi}{dt} - \frac{\rho V^2 Sl}{J} m^{\beta}\beta = \frac{\rho V^2 Sl}{J}\left(m^{\delta_1}\delta_1 + m^{\delta_2}\delta_2\right).$$

Here γ is the roll; β is the sideslip; ψ is the yaw; δ_1 is the aileron angle; δ_1 is the rudder angle; J is the aircraft longitudinal inertial moment; V is the aircraft speed; S and l are the aircraft reference area and length respectively (usually l is the wingspan); $m^{\omega_x}, m^{\omega_y}$ and m^{β} are the derivatives of the aircraft aerodynamic rolling moment coefficient with respect to the dimensionless angular rates of roll, yaw and sideslip respectfully. Note that the values of the coefficients m^{ω_y} and m^{β} are significantly less than that of m^{ω_x}. The corresponding values for some aircraft types are presented in Table 1.

Table 1

Aircraft	m^{ω_x}	m^{ω_y}	m^{β}
Boeing 727	-0.451	-0.100	-0.095
Boeing 747	-0.462	-0.088	-0.131
Boeing 757	-0.462	-0.094	-0.057
Boeing 777	-0.436	-0.064	-0.128

Therefore, we may neglect additional moments due to the aircraft sideslip and yaw in our preliminary analysis.

Hence, consider the equation for the roll rate provided zero values of the sideslip and the yaw rate:

$$J\frac{d\omega_x}{dt} = \frac{\rho VSl^2}{2} m^{\omega_x}\omega_x + M_1 - M_2. \qquad (1)$$

Here ω_x is the aircraft roll rate, M_1 is the vortex rolling moment (constant according to our assumption), M_2 is the maximum aileron moment (constant), ρ is the air density. Since

$$\omega_x = \frac{d\gamma}{dt},$$

Eq. (1) can be rewritten as

$$\ddot{\gamma} - a_1\dot{\gamma} - c_0 = 0 \qquad (2)$$

where $a_1 = \frac{\rho VSl^2}{2J} m^{\omega_x}$ and $c_0 = \frac{M_1}{J}$, provided ailerons are deflected, and $c_0 = \frac{M_1 - M_2}{J}$ otherwise. The dot denotes time differentiation.

Eq. (2) is an inhomogeneous linear equation with constant coefficients. Its solution is of the following form:

$$\gamma(t) = C_1 + C_2\exp(a_1 t) - \frac{c_0}{a_1}t. \qquad (3)$$

The unknown coefficients are evaluated from the initial conditions

$$\gamma(0) = \gamma_0, \dot{\gamma}(0) = \dot{\gamma}_0. \qquad (4)$$

Hence, we find from (3) and (4)

$$C_1 = \frac{a_1^2\gamma_0 - a_1\dot{\gamma}_0 - c_0}{a_1^2}, C_2 = \frac{a_1\dot{\gamma}_0 + c_0}{a_1^2}. \quad (5)$$

If the initial conditions are zero (this corresponds to the time of the vortex rolling moment generation), then

$$C_1 = -\frac{m_1}{a_1^2}, C_2 = \frac{m_1}{a_1^2} \quad (6)$$

and the dynamics of the aircraft roll is described by the relation

$$\gamma(t) = -\frac{m_1}{a_1^2} + \frac{m_1}{a_1^2}\exp(a_1 t) - \frac{m_1}{a_1} t. \quad (7)$$

Here $m_1 = \frac{M_1}{J}$.

With the aim of evaluation of the maximum angle of roll induced by the vortex disturbed motion of the aircraft, we differentiate (3) with respect to time and set the derivative equal to zero. This operation shows that the extreme point of $\gamma(t)$ is

$$t_{max} = \frac{1}{a_1}\ln\left(\frac{c_0}{a_1\dot{\gamma}_0 + c_0}\right). \quad (8)$$

The substitution of t_{max} in (3) gives us the maximum value of the aircraft angle of roll:

$$\gamma_{max} = \frac{a_1^2\gamma_0 - a_1\dot{\gamma}_0 - c_0}{a_1^2} + \frac{c_0}{a_1^2}\left[1 - \ln\left(\frac{c_0}{a_1\dot{\gamma}_0 + c_0}\right)\right]. \quad (9)$$

Let $t = 0$ corresponds to the time of the aileron deflection. Clearly, the initial conditions are determined by the values of the angle of roll and of the roll rate gained by the aircraft during its motion over the time period T corresponding to the pilot reaction time. We have from (7)

$$\gamma_0 = -\frac{m_1}{a_1^2} + \frac{m_1}{a_1^2}\exp(a_1 T) - \frac{m_1}{a_1} T, \quad (10)$$

$$\dot{\gamma}_0 = \frac{m_1}{a_1}\exp(a_1 T) - \frac{m_1}{a_1}. \quad (11)$$

Substitution of (10) and (11) in (9) and the relation

$$c_0 = m_1 - m_2$$

where $m_2 = \dfrac{M_2}{J}$, give after simple manipulations the following relation:

$$\gamma_{max} = -\frac{m_1}{a_1} T - \frac{m_2 - m_1}{a_1^2} \ln\left[1 + \frac{m_1}{m_2 - m_1}\left(1 - \exp(a_1 T)\right)\right]. \qquad (12)$$

Equating the right side of (12) to γ_{lim}, we get the following equation for the maximum admissible roll moment:

$$\gamma_{lim} = -\frac{m_1}{a_1} T - \frac{m_2 - m_1}{a_1^2} \ln\left[1 + \frac{m_1}{m_2 - m_1}\left(1 - \exp(a_1 T)\right)\right]. \qquad (13)$$

Eq. (13) is the nonlinear equation for the maximum value of the admissible vortex rolling moment coefficient, $m_1 = \dfrac{M_1}{J}$, as the function of the pilot reaction time T, of the aircraft damping coefficient $a_1 = \dfrac{\rho V S l^2}{2J} m^{\omega_x}$, and of the maximum value of the aileron moment coefficient, $m_2 = \dfrac{\rho V^2 S l}{2J} m^{\delta} \delta_{max}$, where δ_{max} is the aileron maximum angle.

Eq. (13) allows us to carry out an asymptotic analysis of the limiting cases. If

$$\left|\frac{m_1}{m_2 - m_1}\left(1 - \exp(a_1 T)\right)\right| << 1, \qquad (14)$$

then we have the following approximate relation:

$$\gamma_{lim} = -m_1\left(\frac{T}{a_1} + \frac{1 - \exp(a_1 T)}{a_1^2}\right). \qquad (15)$$

The fulfillment of (14) signifies one of the following possible situations:

1. The maximum aileron moment is of very large value, i.e. $m_1 << m_2$.
2. The aircraft inertia moment is very large, i.e. $a_1 \to 0$ or, equivalently, $J \to \infty$.
3. The pilot reaction time is very small, i.e. $T \to 0$. In this case, from (15) we have

$$m_1 = \gamma_{lim} a_1^2. \qquad (16)$$

It follows from (13) that the admissible vortex rolling moment is determined by the pilot reaction time, the aircraft inertial properties, and the maximum aileron moment.

Fig. 1 shows the calculation results for the maximum roll under different levels of vortex disturbances characterized by the coefficient k, which is determined as

$$k = \frac{M_1}{M_2}.$$

The calculation was performed for the pilot reaction time $T = 0.6$ s. It should be noted that the increase of the aircraft speed leads to the increase of the aircraft maximum angle of roll under the constant value of k.

Fig. 2 shows the calculation results for the admissible level of disturbances (the aircraft angle of roll does not exceed 10°) characterized also by the coefficient k. The results are presented for three levels of the aileron deflection angle. The case $k = 1$ signifies that such level of disturbances is compensated by the aircraft inertial properties and the larger values are impermissible, as they cannot be compensated by the aileron deflection.

3. Wake Vortex Encounter at a Nonzero Angle

Suppose that the aircraft pilot makes no efforts to compensate the disturbances while flying in wake vortices. This assumption is correct for the following reasons. The danger zone dimensions, according to our studies, do not exceed 20…30 m. After the vortex encounter at a nonzero angle, the aircraft rolling moment is decreasing. After several seconds the aircraft leaves the danger zone. The duration of the aircraft stay in the danger zone is

$$T_s = \frac{L_z}{V\cos\varphi}$$

where L_z is the danger zone dimension, V is the aircraft speed, φ is the angle between the vortex axis and the aircraft flight direction. Assuming $V = 100$ m/s, we get $T_s \approx 0.3…0.5$ s. Suppose also that the aircraft rolling moment does not change during its flight in the wake vortices and equals to the rolling moment that the aircraft experiences during its flight along the vortex axis. Then the aircraft angle of roll varies in time as follows:

$$\gamma(t) = -\frac{m_1}{a_1}T_s - \frac{m_1}{a_1^2}\left(1 - \exp(a_1 T_s)\right)\exp(a_1 t).$$

Hence, the maximum roll does not exceed the value

$$\gamma_{max} = -\frac{m_1}{a_1} T_s - \frac{m_1}{a_1^2}\left(1 - \exp(a_1 T_s)\right)$$

and the steady value of roll after the aircraft exits from the wake vortices is

$$\gamma_s = -\frac{m_1}{a_1} T_s .$$

The above results show that the coefficient k is not the invariant of the level of danger disturbances (regarding the possibility of the maximum roll angle attainment). For example, Boeing 727 (for the aileron angle of 20°) has $k \approx 1$ for its flight speed of 100 m/s and $k \approx 0.7$ for its flight speed of 150 m/s. Therefore, this coefficient is a function of the aircraft flight parameters (speed and altitude).

At the same time when evaluating the admissible value of k (or the admissible rolling moment), it is also necessary to take account of the following reasoning. The value of the admissible rolling moment is determined by the aircraft parameters (J, S, l, m^{δ}, δ_{max}), as well as by the flight parameters (the aircraft speed V and its altitude that fixes the air density). However, actually the aircraft parameters are known only up to some error and the flight parameters are maintained only in some interval.

Consider the influence of the parameters scatter on the maximum roll.

Let the admissible rolling moment is calculated for the reference aircraft parameters and given flight parameters (they are denoted by the superscript '0'):

$$M_1 = k \frac{\rho_0 V_0^2 S_0 l_0}{2} m_0^{\delta} \delta_{0max} .$$

The coefficient k is chosen so that the angle of roll that is the solution of the following equation set:

$$J_0 \frac{d\omega}{dt} = \frac{\rho_0 V_0 S_0 l_0^2}{2} m_0^{\omega_x} \omega_x + k \frac{\rho_0 V_0^2 S_0 l_0^2}{2} m_0^{\delta} \delta_{0max} - \\ - \Theta(t, T_0) \frac{\rho_0 V_0^2 S_0 l_0}{2} m_0^{\delta} \delta_{0max}, \qquad (17)$$

$$\frac{d\gamma}{dt} = \omega \qquad (18)$$

must not exceed the admissible level γ_{lim}. Here

$$\Theta(t,T)=\begin{cases}0, t<T,\\ 1, t\geq T.\end{cases}$$

However, as the actual values of the aircraft and flight parameters differ from the reference ones, the roll rate is determined not by (17) but by the equation

$$J\frac{d\omega}{dt}=\frac{\rho VSl^2}{2}m^{\omega_x}\omega_x+k\frac{\rho_0 V_0^2 S_0 l_0}{2}m_0^{\delta}\delta_{0\max}-\Theta(t,T)\frac{\rho V^2 Sl}{2}m^{\delta}\delta_{\max}.$$

To analyze the influence of the scatter of the aircraft and flight parameters on the maximum roll, consider the actual aircraft parameter value, say h, which is related to its reference value, h_0, by the relation $h=(1+f)h_0$ where $|f|<1$ is a coefficient characterizing the scatter. Table 2 shows the main reference parameters for Boeing 727 and Boeing 757. The value of f was varied in the range $-0.2\leq f\leq 0.2$ (i.e. the parameter error was ±20%). The value of T was taken as 0.6 s and $\rho = 1.225$ kg/m^3 (the low altitude flight). The aircraft speed, V_0, was in the range 50 – 250 m/s and $\delta_{\max}=20°$.

Table 2

	Boeing 727	Boeing 757
m^{δ}	-0.129	-0.143
m^{ω_x}	-0.451	-0.462
l, m	32.92	37.94
S, m	157.9	181.3
J, kg·m^2	1039000	6394000

Figs. 3 – 7 show the dependence of the maximum admissible value of k (the maximum roll does not exceed the limiting value even for deviation of one of the aircraft parameters from its reference value) on f calculated for different values of V_0. Let us note some features of the calculation results.

Fig. 3 shows that the range of admissible values of k is expanded as the reference flight speed is reduced. The reason is that the magnitude of the vortex rolling moment according to the relation

$$M_1 = kM_2 \tag{19}$$

is small for small reference flight speeds. On the other hand, small values of the vortex rolling moment are damped by the aircraft inertial properties. Fig. 3 shows also that the admissible value of k is reduced: $k(f = -0.2) < k(f = 0)$, as the deviation of the flight speed from its reference value (coefficient f) increases.

Similar tendency can be observed for the deviation of the aircraft aerodynamic parameters (Fig. 4 for m^{δ} and Fig. 5 for m^{ω_x}) and the aircraft inertial moment (Fig. 6) from their reference values. It should be noted that the admissible values of k are scarcely affected by the deviation of the aircraft inertial moment from its reference value. This fact is very important because, as opposed to the other aircraft parameters, the aircraft inertial properties are susceptible to considerable changes: they are much influenced by the aircraft load and fuel distribution.

Fig. 7 presents the effect of the pilot reaction time on the admissible values of k. One can see that the admissible values of the disturbing rolling moment are reduced as the pilot reaction time increases.

Fig. 8 demonstrates the effect of the deviation of all parameters (J, m^{δ}, m^{ω_x}, T, V) from the reference values on the maximum roll. The calculation was performed for different values of k and flight parameters (V). The value of the parameter deviations was chosen as follows:

$$f = 0.1 \text{ for } m^{\delta}, m^{\omega_x}, T; \tag{20}$$

$$f = 0.2 \text{ for } J, V. \tag{21}$$

The maximum roll increases linearly with the aircraft reference speed for a constant value of k. For larger values of k, the maximum roll attains 10° for less values of the aircraft reference speed. This is due to the fact that the maximum roll is determined by the rolling moment magnitude. The latter is proportional to the square of the aircraft speed for the fixed value of k.

Our studies show that there is no point in calculating of a single value of the admissible rolling moment for the purpose of evaluating the admissible value of the vortex rolling moment (giving rise to the aircraft roll not more than 10°). The use of a single value of the admissible rolling moment for the whole range of aircraft speed leads to the unjustified underestimating of the admissible rolling moment for large values of the aircraft speed. This fact owes to the increase of the aircraft damping properties, as well as aileron efficiency, with the aircraft speed.

On the other hand, our studies lead to the following conclusion. The use of k as a characteristic of vortex hazard would be justified in the case of its invariance with respect to the flight conditions. As it is not the case, there is good reason not to introduce any additional parameters and use directly the value of the rolling moment.

We have calculated the admissible values of the vortex rolling moment for two aircraft types on the basis of the presented approach. The calculations results are presented in Fig. 9 together with the rolling moment values corresponding to $k = 0.5$. The latter values were used by SABIGO for the danger zone evaluation. It should be noted that the approach based on $k = 0.5$ underestimates the admissible rolling moment (the curve corresponding to $k = 0.5$ is too low). Hence, the use of the presented results for the danger zone evaluation gives the zones with less dimensions, as compared to the zones evaluated by SABIGO before.

Fig. 10 presents k as a function of the aircraft speed calculated on the basis of the admissible rolling moment values presented in Fig. 9.

4. Conclusions

The presented studies show that the coefficient k does not describe hazard disturbances from wake vortices invariantly to aircraft flight parameters. In particular, this coefficient depends strongly on the aircraft speed.

Therefore, we suggest for the evaluation of danger zones, as well as of safe separations, to use the admissible rolling moment as a function of aircraft speed and altitude, $M_{x\,\mathrm{adm}}(V,H)$. Such functions for Boeing 727 and Boeing 757 are presented in Fig. 7.

Hence, the algorithm for the evaluation of danger areas and safe separations could be presented as follows:

1. Calculate the admissible rolling moment, $M_{x\,adm}(V,H)$, for the given aircraft on the basis of the simplified flight dynamics model of the aircraft under the influence of the vortex rolling moment. Account must be taken of possible errors in the aircraft aerodynamic, inertial, and flight parameters. (In the future one can use more sophisticated models to calculate $M_{x\,adm}(V,H)$. However, such models call for greater volume of information on aircraft inertial parameters. Furthermore, an enhanced model should be used to simulate pilot (or an aircraft control system) actions for compensation of disturbances in several channels: roll, longitudinal (aircraft angle of attack), and side (aircraft sideslip) channels.)
2. Calculate far wake vortices for the given aircraft-generator types and their flight parameters (altitude, speed, flap angles, ambient conditions, etc.).
3. Calculate the vortex rolling moment for the follower, $M_x(D,z,y)$, as a function of the distance, D, between the aircraft in the pair and of the follower position, (z,y), for each of the pairs 'leader – follower' and for the chosen flight conditions.
4. For the given distance D and the above-mentioned conditions, calculate the diameter and position of danger zones, Ω, which are sets of points (z,y) such that $M_x(D,z,y) \geq M_{x\,adm}(V,H)$. (Here the function $M_{x\,adm}(V,H)$ is for the follower.)
5. For the given flight conditions, calculate the separation D_{safe} which is the distance between the aircraft such that we have $M_x(D,z,y) < M_{x\,adm}(V,H)$ for any distances $D \geq D_{safe}$ and any (z,y).

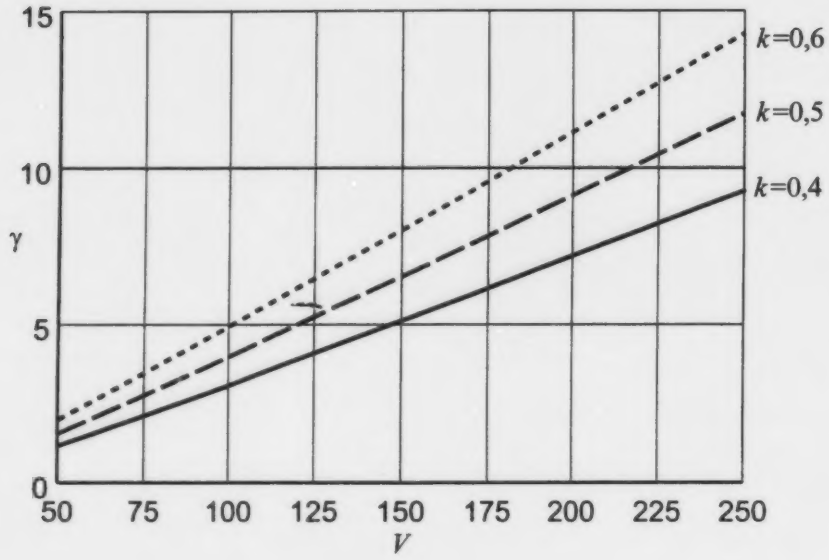

Boeing 727

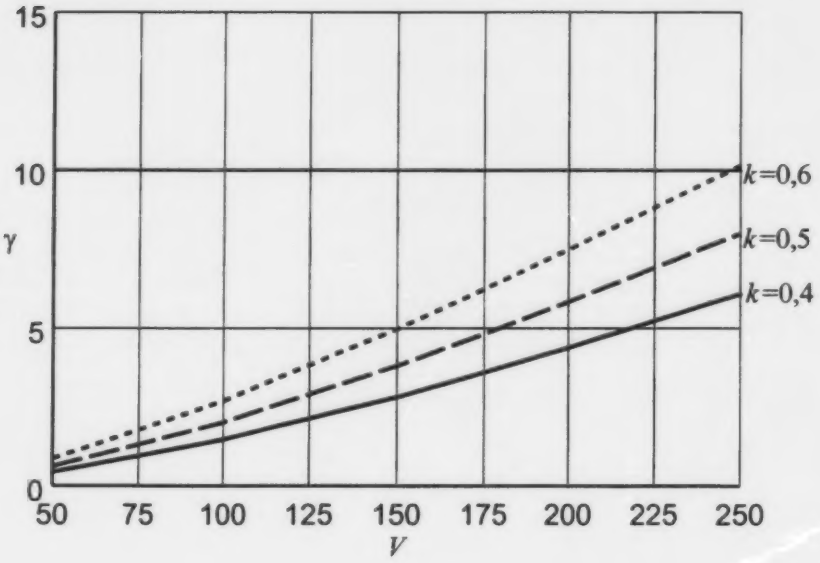

Boeing 757

Fig. 1. Maximum roll, γ, under different levels of vortex disturbances characterized by the coefficient $k = M_1 / M_2$

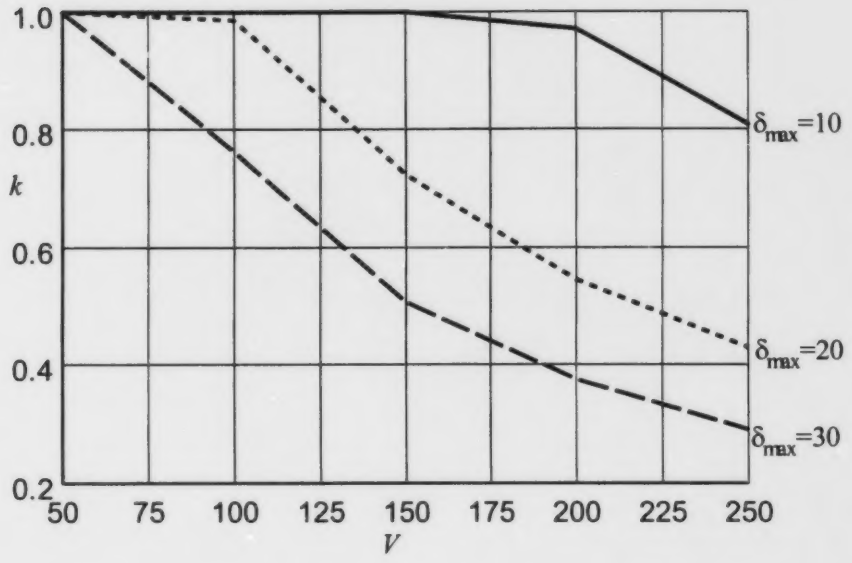

Boeing 727

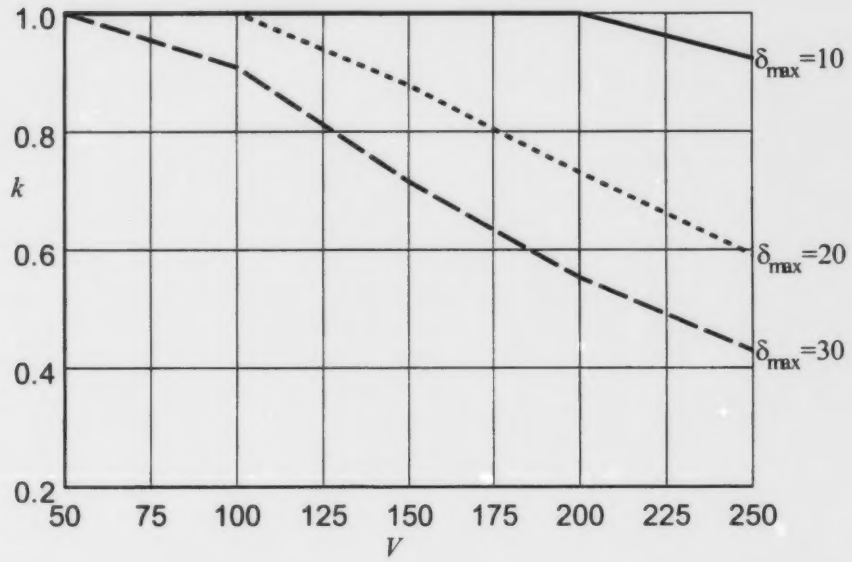

Boeing 757

Fig. 2. Admissible level of disturbances (the aircraft roll does not exceed 10°) characterized by the coefficient $k = M_1 / M_2$ for different maximum aileron deflection values, δ_{max}

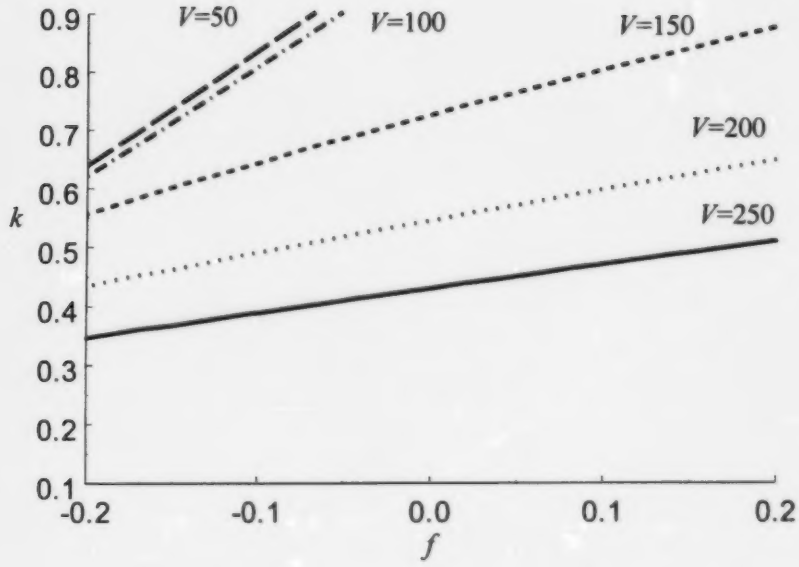

Boeing 727

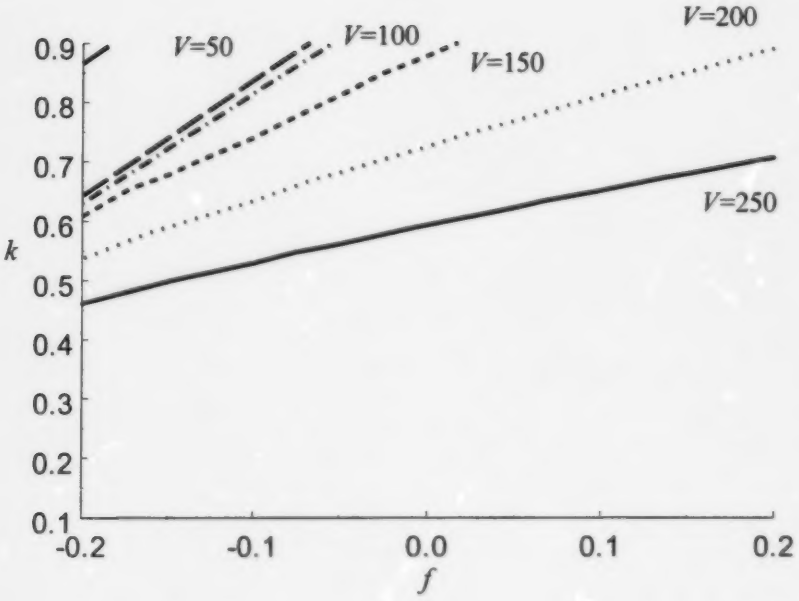

Boeing 757

Fig. 3. Effect of the aircraft speed deviation

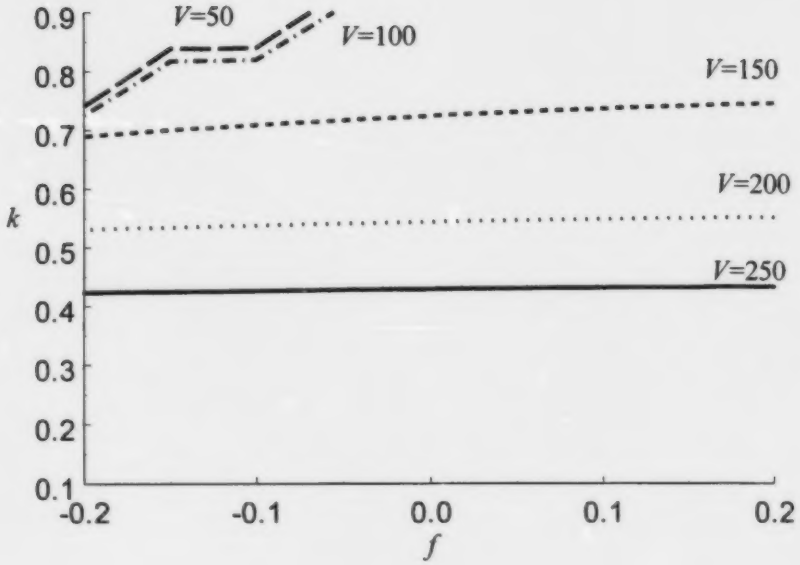

Boeing 727

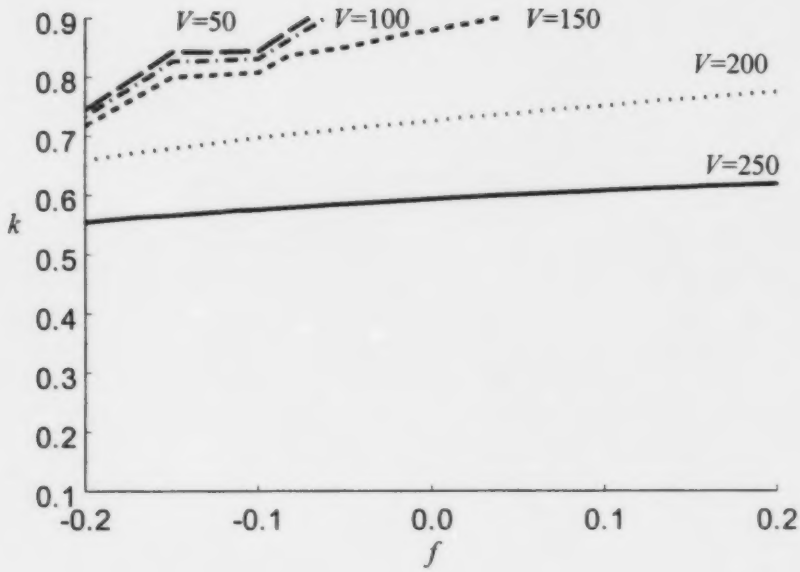

Boeing 757

Fig. 4. Effect of the m^{δ} deviation

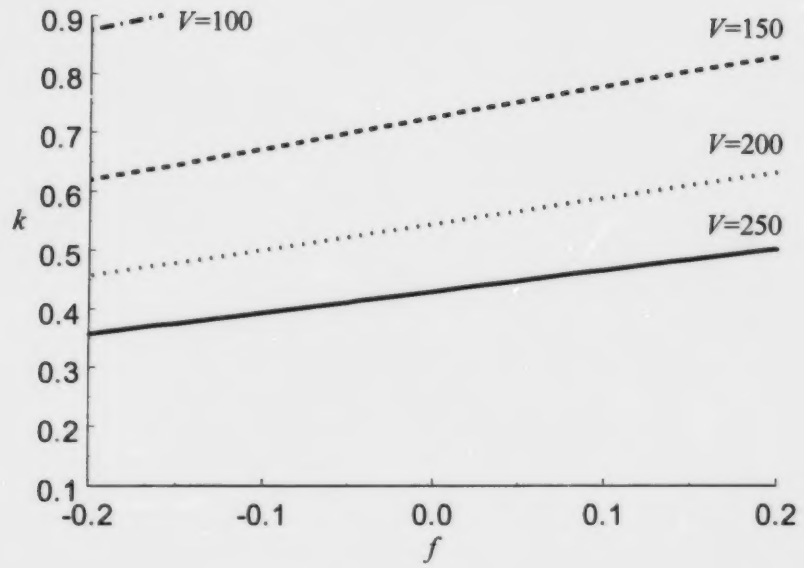

Boeing 727

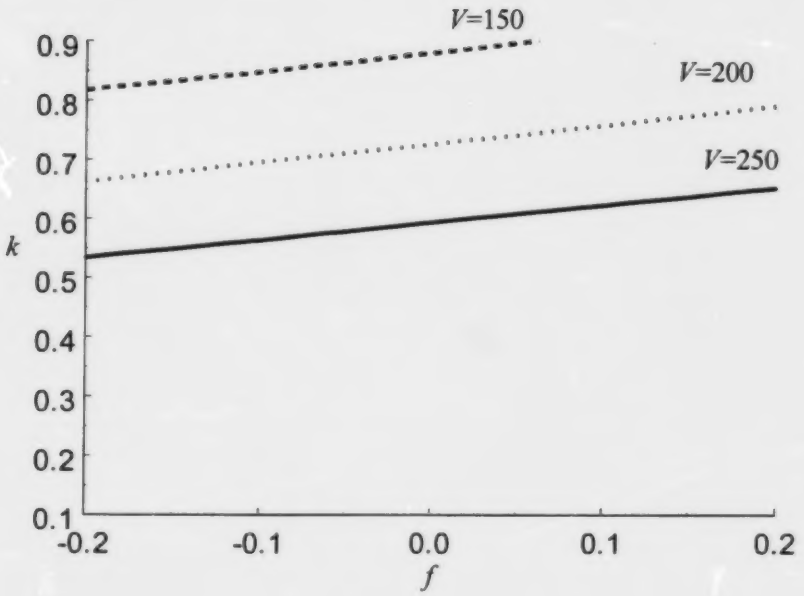

Boeing 757

Fig. 5. Effect of the m^{ω_z} deviation

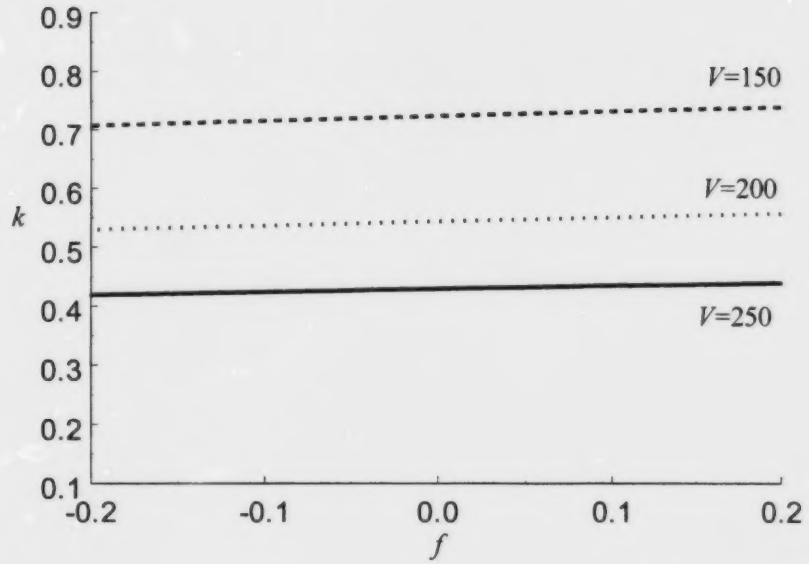

Boeing 727

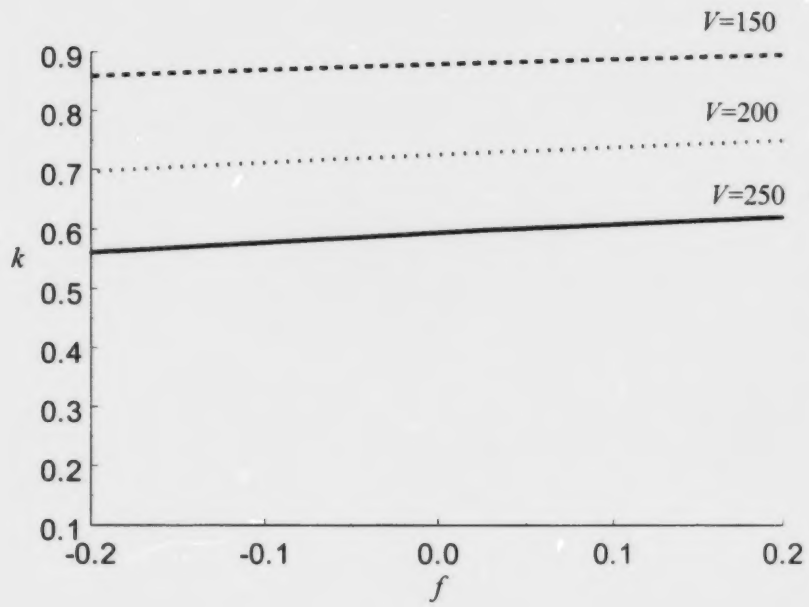

Boeing 757

Fig. 6. Effect of the J deviation

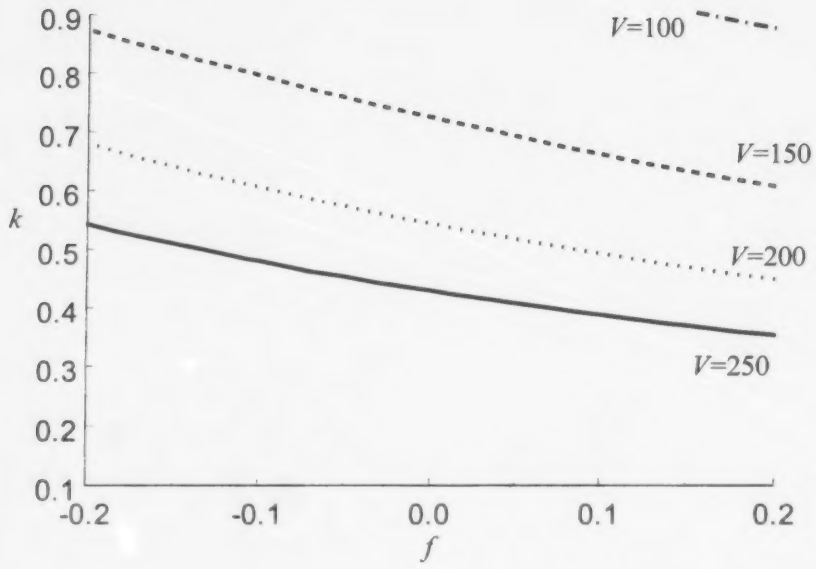

Boeing 727

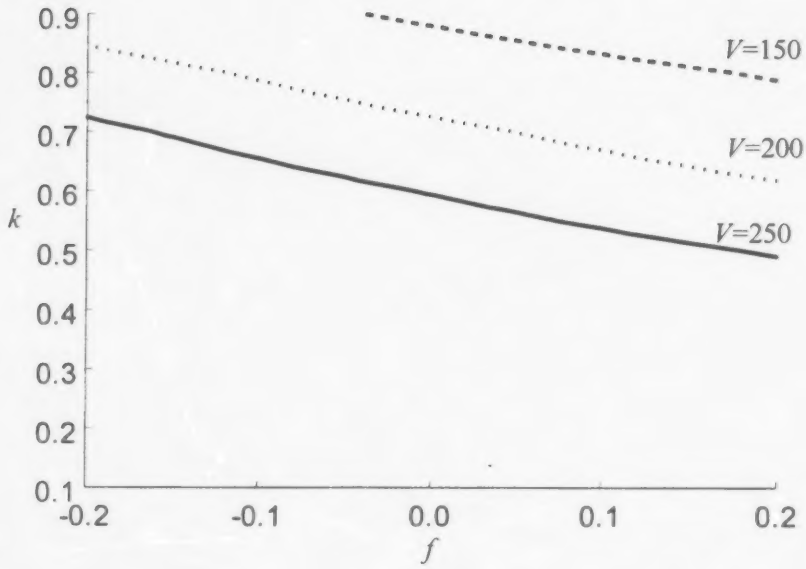

Boeing 757

Fig. 7. Effect of the pilot reaction time

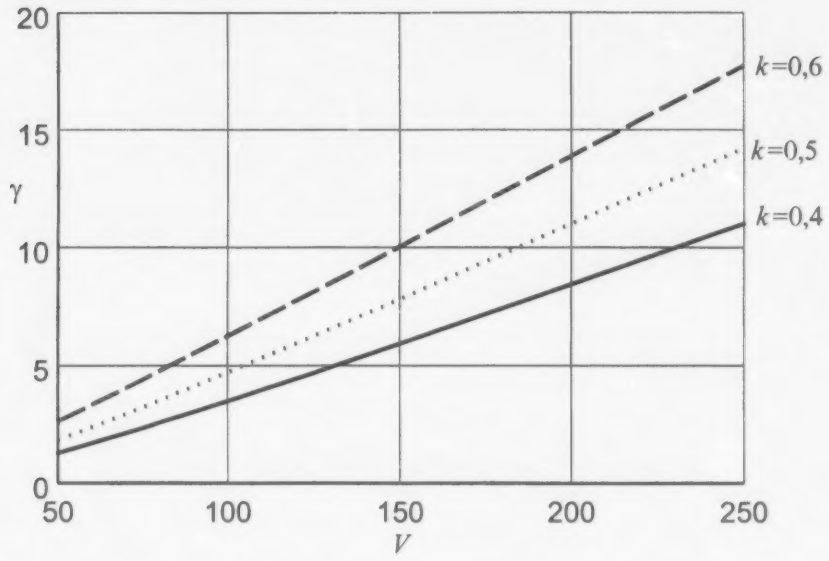

Boeing 727

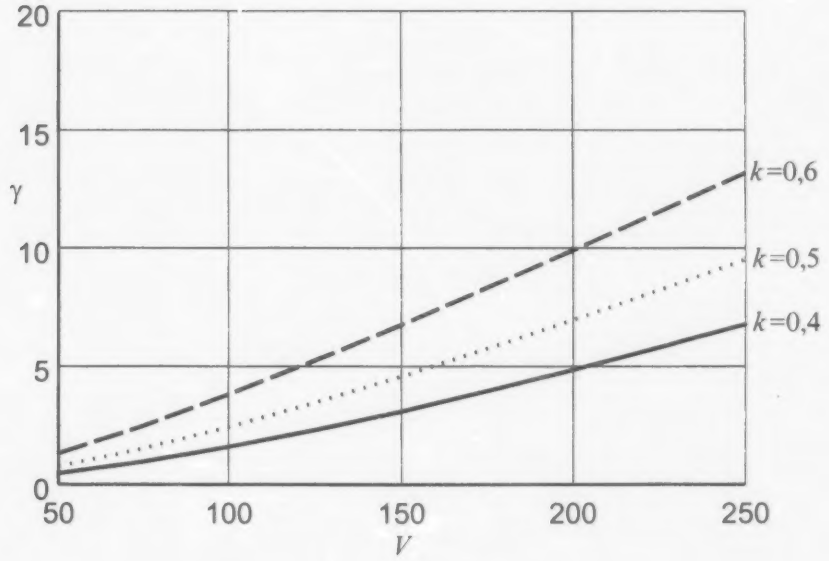

Boeing 757

Fig. 8. Maximum roll under variation of all parameters for different values of k

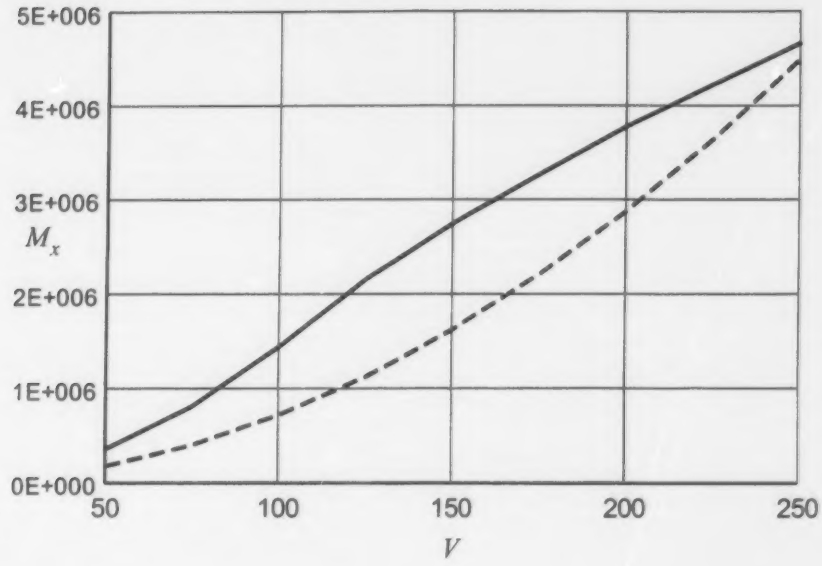

Boeing 727

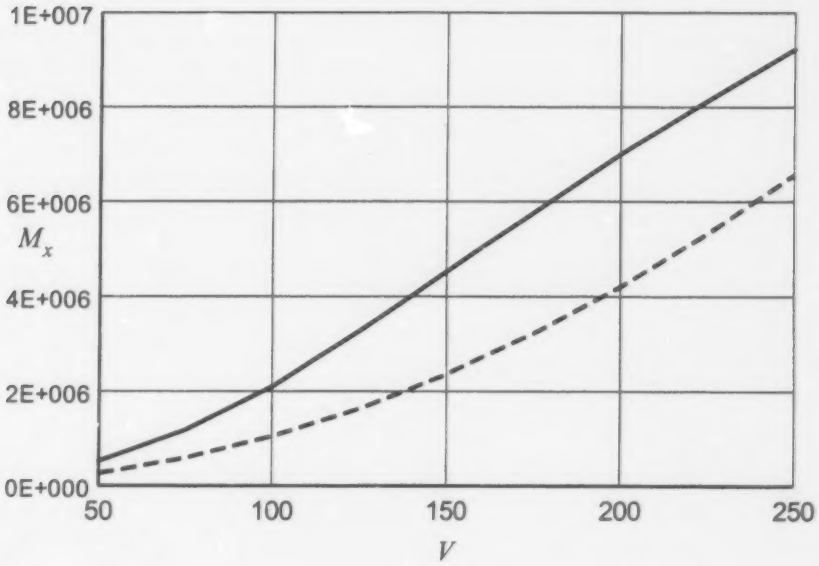

Boeing 757

- - - - - - - - - - Moment corresponding to $k = 0.5$

———————— Maximum admissible rolling moment leading to the roll not more than 10°

Fig. 9. Admissible values of the vortex rolling moment

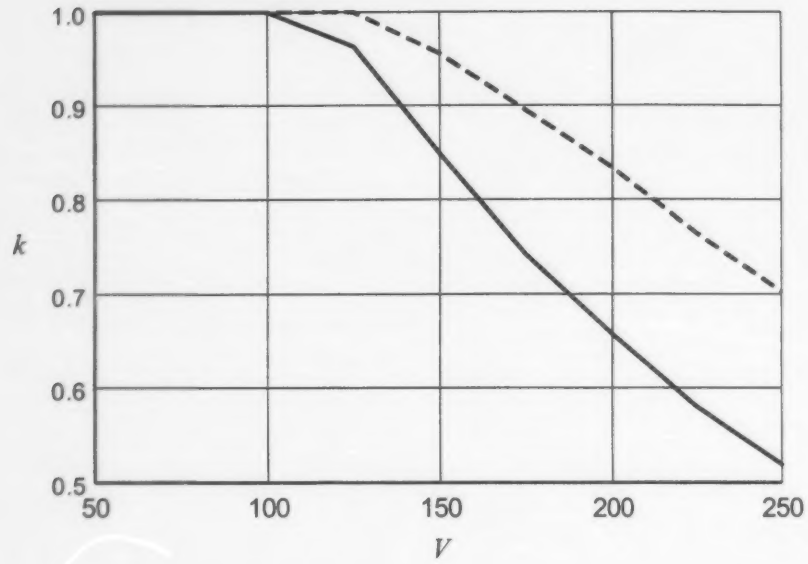

Boeing 727 ——————

Boeing 757 - - - - - - - - - -

Fig. 10. Parameter k characterizing the level of the maximum admissible rolling moment leading to the angle of roll not more than 10°

APPENDIX G

Preliminary Development of the Airborne Vortex Forecasting System

Interim Report of SABIGO for Milestone 4, Phase 6

November 2000

Scientific Advisor Andrei Belotserkovsky
Executors Nikolai Baranov, Nikita Belotserkovsky

1. Introduction

The main object of the present report is to study the possibility of development of the Airborne Vortex Forecasting System (Airborne VFS) and to outline the topics necessary for its implementation. The system is intended to put at a pilot's disposal the information on positions of danger zones related to the leader wake vortices. This information should help the pilot to avoid entering in wake vortices and thus guard against the possibility of any accidents. One of versions of the systems implementation is visualization of the above information on the cockpit windshield.

2. Necessary Input Data

The proposed system demands the following information on the aircraft board:

- the leader type;
- the time spacing between the leader and the follower;
- the flight mode: take off, landing or cruise mode;
- the wind velocity profile;
- the atmosphere turbulence condition (light, medium or strong);
- the leader and follower trajectories;
- the leader flight parameters (including its weight).

We suggest displaying the wake vortex centroid trajectories past the leader, as well as the danger zones (roughly circles).

3. Demo Version of the System

A demo version of the Airborne VFS is implemented by SABIGO as the code 'CURL' that illustrates a possibility of visualization to a pilot of the information on danger zone positions behind the leader in real time. One of the possible versions of the above information visualization on the windshield is suggested. The ergonomy problems have not been solved, as they need enlisting pilots and specialists. Besides, according to our opinion, the optimization of the danger zone visualization should be performed at the stage of the development work.

The main function of the proposed system is placing the additional information on the danger zone positions at pilot's disposal in order to increase the flight safety.

The proposed system version depicts the leader vortex centroids and danger zones. The additional data on the horizontal spacing between the leader and the follower are shown in the left part of the screen.

The proposed demo version uses Boeing 727 as the follower. The leader type could be chosen as follows:

- Boeing 727 (the wingspan is 32.9 m, the wing area is 157.9 m^2, the weight is 68 tons);
- Boeing 747 (the wingspan is 64.3 m, the wing area is 525.0 m^2, the weight is 220 tons);
- Boeing 767 (the wingspan is 47.6 m, the wing area is 283.4 m^2, the weight is 141 tons).

To choose the leader type one should use the box 'Aircraft' in the right part of the screen. Boeing 727 is used as the leader default type.

The assumptions for the leader are as follows: the leader flies along the straight line with the constant velocity 100 m/s and with the initial altitude 50 m.

The assumptions for the leader are as follows: the follower flies along the straight line with the constant velocity and with the initial altitude 50 m.

The demo version gives the possibility of changing some flight parameters for the leader and the follower. To this aim the control panel is placed in the right side of the screen.

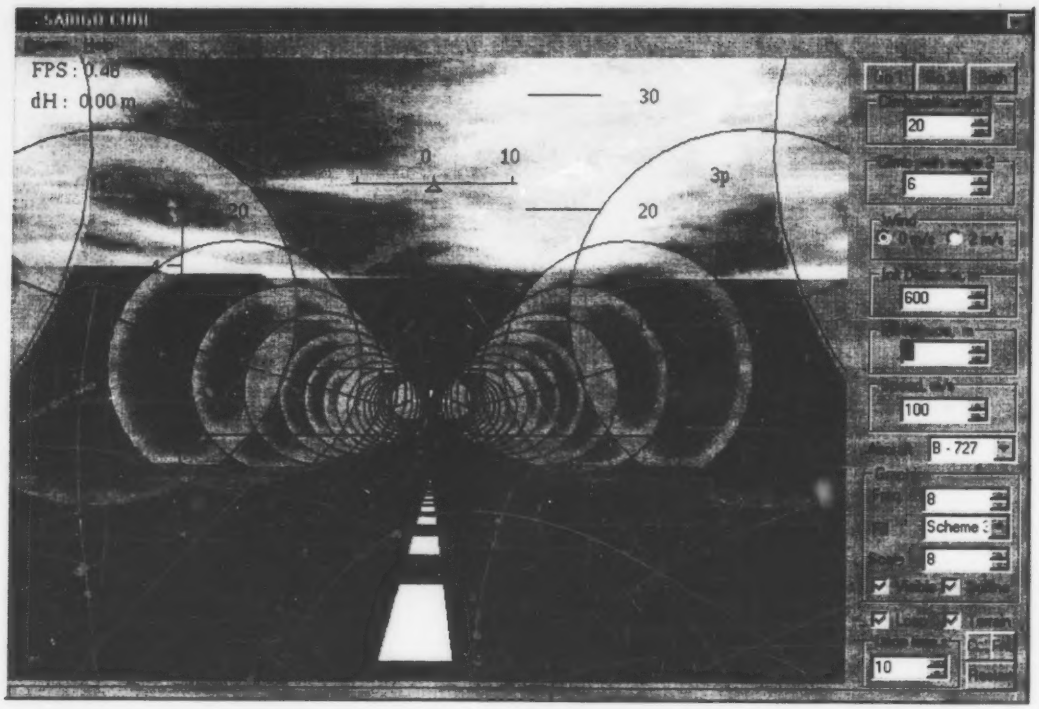

The slope can be changed for the leader (the button 'Slope 1') in the range 0…20 degrees with the step of 1 degree. The leader slope default value is 20 degrees.
The following flight parameters can be changed for the follower:

- the slope (the button 'Slope 2') in the range 0…20 degrees with the step of 1 degree. The slope default value is 20 degrees;
- the initial altitude (the button 'Init. Altitude') in the range 0…100 m with the step of 1 m. The default value is 0;
- the speed (the button 'Speed') in the range 50…150 m/s with the step of 1 m/s. The default value is 100 m/s;
- the initial horizontal spacing between the leader and the follower (the button 'Init. Spacing') in the range 30…5000 m with the nonuniform step. The default value is 300 m.

The control set 'Graphics' is used for the following purposes:

- to change the number of the vortex wake rings along the vortex wake axes (the box 'Freq.');
- to change the mode of ring filling or to cut off the ring filling at all (menu 'Fill');
- to scale the wake vortices along the vortex wake axes (the box 'Scale');
- to switch on/off the mode of vortex wake ring visualization (the box 'Visible');
- to switch on/off the mode of vortex wake ring border visualization (the box 'Outline');
- to change the colors and fonts of visualization (buttons 'Col.' and 'Fnt').

Since the proposed version is intended only for demonstrations, the aircraft dynamics is not simulated: the follower retains its flight mode.

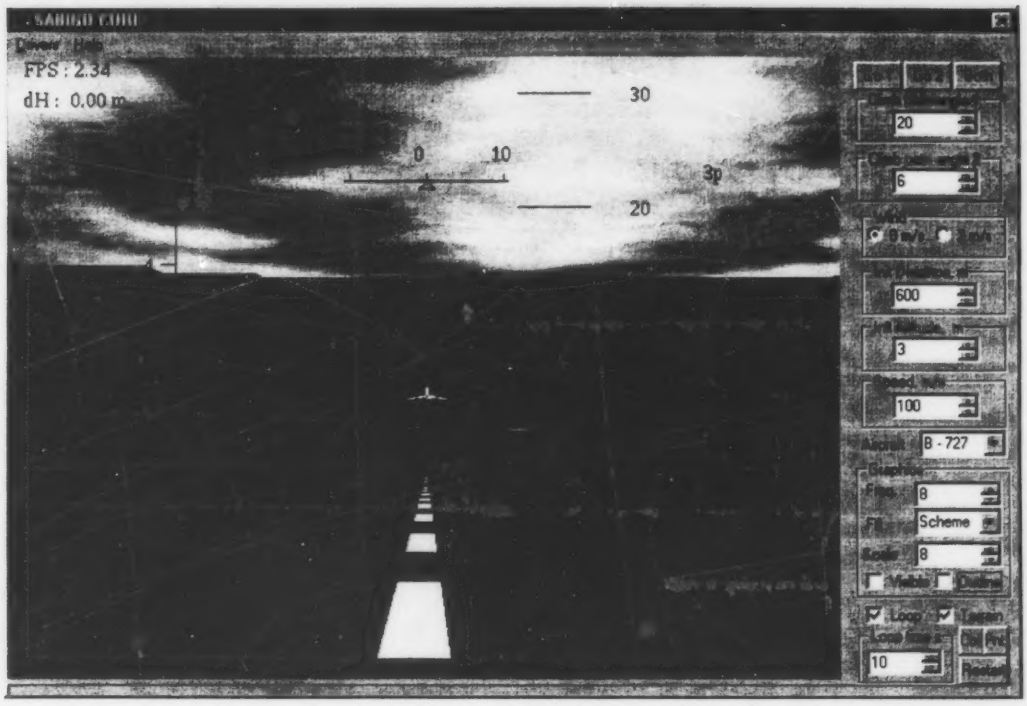

There is also the possibility to watch the danger zone position given the nonzero crosswind. To this aim there are the switches 'Wind' at the control panel. The switch '0 m/s' corresponds to the zero crosswind and the switch '2 m/s' corresponds to the crosswind of 2 м/с directed from right to left. The default value of the crosswind is zero.

The demo version allows for the time and scenario viewing control. The user can select one of two possible scenario viewing mode: cyclic or single (the switch 'Loop'). Here the scenario means the danger zone demonstration for the given set of the data. In the case of the cyclic mode (the switch is marked) the scenario is demonstrated in repetitive sequences. In the case of the single mode (the switch is not marked) the scenario is demonstrated only once. The button 'Restart' serves to repeat the demonstration or to change the data.

The user can change the scenario time in the range 10...120 s with the step of 1 s (the button 'Loop Time'). The demonstration time exactly corresponds to the real time without regard to the computer type in use. The default value is 10 s.

The bottom part of the screen contains the bar depicting the current time of demonstration.

The demonstration is restarted after the data change during the scenario viewing.

4. Example of the Code Functioning

Consider an example of the code 'CURL' functioning. The pictures show two modes of the information view (danger zones and vortex centroids).

The conditions for the example are in the Figures.

5. Main Topics for the System Development

1. To study more thoroughly the wake behavior during aircraft takeoff and landing including the wake interaction for aircraft using the other runways at an airport.

2. To develop fast algorithms for wake calculation past aircraft during their takeoff and landing on the basis of studies according 1.
3. To estimate the influence of different factors on wake evolution (position and intensity). The main factors are the aircraft type, its weight, speed, flight configuration (including the flap position), and meteorological factors (the wind velocity profile and the ambient turbulence level).
4. To choose the danger criterion for aircraft entering wake vortices.
5. To estimate inaccuracy in the initial data and its influence on the wake position and intensity.
6. To estimate the possible lack in the initial data and its influence on the wake position and intensity.
7. To develop the strategy of the danger zone database appearance (the problem is that danger zones have the spatial and time distribution dependent on different parameters: the leader and follower types, their weights, speeds, altitudes and flight directions changing in time, as well as the meteorological conditions). It is necessary to determine the optimal approximation of the danger zone distributions and optimize the distribution parametrization.
8. To study ergonomic problems on optimization of danger zone displaying.
9. To estimate the system efficiency and optimize its structure.

APPENDIX H

Cross-Comparison of the Coefficients in the EDR and TKE Decay Models

Gregoire S. Winckelmans

November 2000

Using the data from Memphis (211 MEM cases) and Dallas-Fort Worth (191 DFW cases), and that were kindly provided to us, in a reduced and useful form, by NWRA (R. E. Robins), we have been able to cross-compare the "time constant" in the two decay models (EDR and TKE). We here show the statistical comparison in two summary graphs.

It is understood that, for operational use of the EDR decay model, the EDR profile is used. Here however, a statistical cross-comparison of both decay models (EDR and TKE) is done, and we used the EDR data averaged over the altitudes seen by the wake when it proceeds downward. For TKE, we used the only data point provided: TKE at 40 m.

It appears that the altitude-averaged EDR data is better in the DFW data than in the MEM data. Indeed, in MEM, there are many averaged EDR data set to zero, even though the EDR at 40 m was small but non zero. Moreover, when comparing the EDR at 40 m to the altitude-averaged EDR, the DFW data appear statistically better than the MEM data: almost a one to one consistent comparison between EDR at 40 m and averaged EDR. This is important as the T_{demise} evaluation depends on EDR evaluation.

For uniform TKE and EDR, one can sees that both decay models behave as:

$$\frac{\Gamma(T)}{\Gamma(0)} = \exp\left(-\frac{T}{T_m}\right)$$

where T_m is the model time constant. For the EDR decay model, $T_m = T_{demise}(\eta)/C_\eta$, where T_{demise} is the non-linear function of η of Sarpkaya et al. [8]. For the TKE decay model, $T_m = T(Q)/C_Q$, where $T(Q)$ is simply $1/Q$ as in Greene et al. [1].

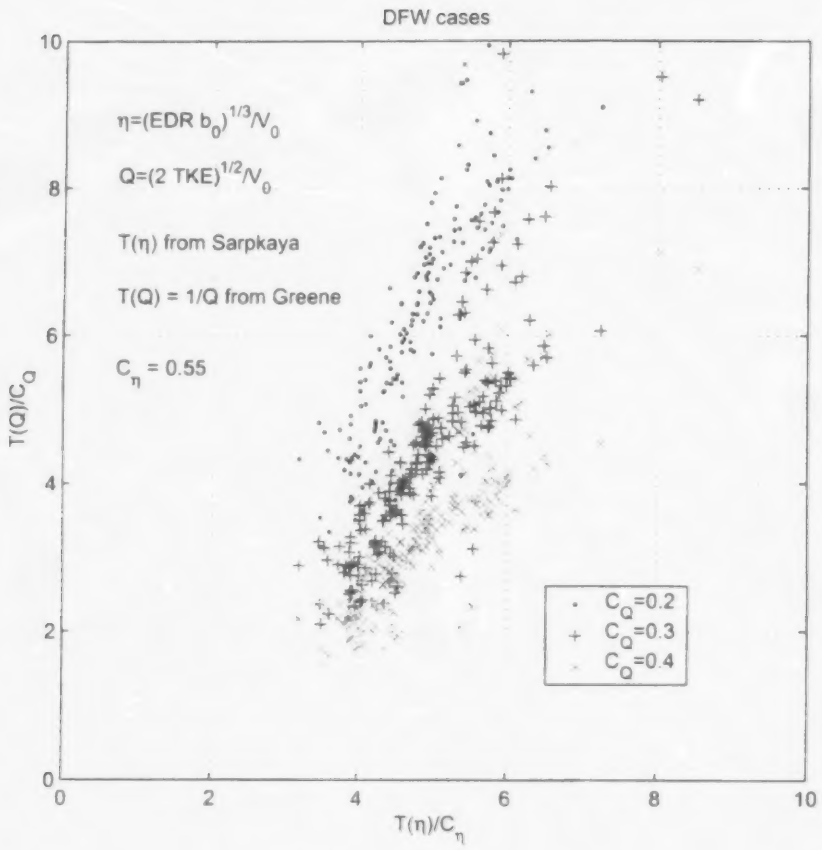

Following [8] and the practice by NWRA [7], we set C_η to 0.55 and then looked for the best C_Q, i.e., the one that provides the best cross-comparison of the time constants for the models, see graphs. The main conclusion is that $C_Q = 0.30$ is best: $C_Q = 0.20$ creates too high a time constant; $C_Q = 0.40$ is still OK, but it corresponds to slightly too low a time constant.

This, of course, is assuming that $C_\eta = 0.55$. If C_η were decreased, then C_Q should simply be decreased in the same proportion.

This study thus shows quite convincingly that the couple $(C_\eta,\ C_Q)$=(0.55, 0.3) is more "self-consistent" than the couple (0.55, 0.2) as used in the NWRA scorings of the EDR and TKE decay models [7]. Of course, EDR is a better turbulence quantity than TKE for decay: so, models should indeed use EDR-based decay when the EDR profile is available.

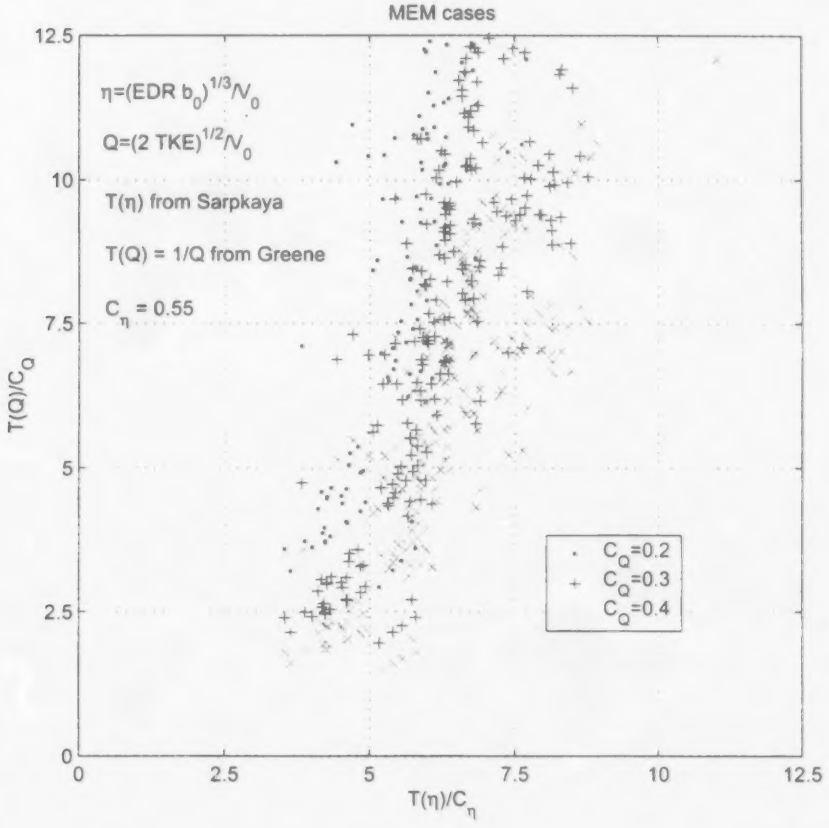

The circulation used in the VFS for operational use is the half wake circulation, $\Gamma(t)$, which is significantly different from the averaged 3-10 m circulation, $\Gamma_{3\to10}(t)$: using an estimate based on the universal near wake circulation profile, the difference, at $t=0$, is already about 15% for typical aircraft vortex wakes. The difference also increases as time

proceeds. This affects the choices of decay constants in the models. In particular (C_η, C_Q)=(0.55, 0.3) is too high when one works with $\Gamma(t)$ instead of $\Gamma_{3\to10}(t)$. The choice (C_η, C_Q)=(0.4, 0.2) is then more appropriate. This choice could be further improved, e.g., by using DFW decay data on global circulation (or, if in lack of those, on the 5 to 15 m averaged circulation, $\Gamma_{5\to15}(t)$ which is indeed a better representation of $\Gamma(t)$) and also by using more LES simulations. The model coefficients can, of course, both be changed, as they are part of the input file.

In that respect, we have recently conducted pseudo-spectral large-eddy simulations (LES) to study the evolution of a DC-10 vortex wake (with $\Gamma_0 = 489$ m^2/s and $b_0 = 39.6$ m) that is started from the improved UNW circulation profile, and that is put in a homogeneous turbulent atmosphere [4, 5]. We have studied different turbulence levels (different values of Q and η), and at different LES resolutions (up to 192 x 128 x 64 grid points), and compared them successfully with similar simulations as in [2]. Our LES simulations also confirm that the EDR decay model is better than the TKE decay model, that $\Gamma_{3\to10}(T)$ is significantly different from $\Gamma(T)$, that the absolute and relative differences both increase as the wake evolves, and that the EDR decay model coefficient for $\Gamma(T)$ is indeed significantly lower than that for $\Gamma_{3\to10}(T)$: from our LES investigations, it appears to be as low as 0.3. As to the TKE decay model, also used here for the parameterization of the $\Gamma(T)$ decay, it appears to be about 0.20.

As those LES studies are limited by the affordable computational domain (here 189 x 126 x 63 m), they all have difficulties capturing scales of the order of the atmospheric turbulence length-scale, $L_{turb} = {q_{rms}}^3 / EDR$ (in dimensionless form, $(Q/\eta)^3$), since it is quite large in the real atmosphere (of the order of 1000 m). The LES results can thus not be completely applicable. Nevertheless, the trends obtained are not that sensitive to L_{turb}

and the conclusions are qualitatively correct, at least when the ratio Q/η of the LES is fairly close to that of the atmosphere. Notice that the "quality requirement" calls for similar Q/η, not for similar $(Q/\eta)^3$: it is thus easier to satisfy. Additional LES studies are being carried out: they should help firm up the proper C_η value to use within VFS. For the time being, we use $C_\eta = 0.3 - 0.4$ (which is less than 0.55).

References cited

1. G. C. Greene, "An approximate model of vortex decay in the atmosphere", *Journal of Aircraft*, Vol. 23, July 1986, pp. 566-573.

2. J. Han, Y-L. Lin, S. Pal Arya and F. H. Proctor, *Large-eddy simulation of aircraft wake vortices in a homogeneous atmospheric turbulence: vortex decay and descent*, 37th AIAA Aerospace Sciences Meeting and Exhibit, Jan. 11-14, 1999, Reno, NV, AIAA 99-0756.

3. D. A. Hinton, J. K. Charnock and D. R. Bagwell, *Design of an aircraft vortex spacing system for airport capacity improvement*, 38th AIAA Aerospace Sciences Meeting and Exhibit, Jan. 10-13, 2000, Reno, NV, AIAA 2000-0622.

1. H. Jeanmart and G. S. Winckelmans, "Large-eddy simulations of aircraft wake vortices in a turbulent atmosphere", *Proceedings of the. 5th National Congress on Theoretical and Applied Mechanics*, Louvain-la-Neuve, Belgium, May 23-24, 2000, pp. 295-298.

2. H. Jeanmart and G. S. Winckelmans, *LES of aircraft wake vortices in a turbulent atmosphere: tensor-diffusivity mixed modelling versus classical modelling*, EUROMECH Colloquium No. 412 on LES of Complex Transitional and Turbulent Flows, Munich, Germany, Oct. 5-6, 2000.

6. F.H. Proctor, D.A. Hinton, J. Han, D.G. Schowalter and Y.-L. Lin, *Two-dimensional wake vortex simulations in the atmosphere: preliminary sensitivity studies*, 35th Aerospace Sciences Meeting & Exhibit, Jan. 6-10, 1997, Reno, NV, AIAA 97-0056.

7. R. E Robins and D. P. Delisi, *Wake vortex algorithm scoring results*, NorthWest Research Associates, Bellevue, WA, Draft report of Jan 31, 2000.

8. T. Sarpkaya, R. E. Robins and D. P. Delisi, *Wake-vortex eddy-dissipation model predictions compared with observations*, 38th AIAA Aerospace Sciences Meeting and Exhibit, Jan. 10-13, 2000, Reno, NV, AIAA 2000-0625.

9. S. Shen, F. Ding, J. Han, Y-L. Lin, S. Pal Arya and F. H. Proctor, *Numerical modeling studies of wake vortices: real case simulations*, 37th AIAA Aerospace Sciences Meeting and Exhibit, Jan. 11-14, 1999, Reno, NV, AIAA 99-0755.

10. G. S. Winckelmans and P. Ploumhans, *Modelisation of non-uniform wind shear effects onto aircraft wake dynamics for the operational VFS: testing on Memphis Case 1132 with non-uniform shear in ground proximity*, CESAME, Mechanical Engineering Department, Université catholique de Louvain, Louvain-la-Neuve, Belgium, Interim Phase 6 Report to Transport Canada, March 23, 2000.

11. G. S Winckelmans and H. Jeanmart, *Investigation of near wakes shortly after rollup*, CESAME, Mechanical Engineering Department, Université catholique de Louvain, Louvain-la-Neuve, Belgium, Interim Phase 6 Report to Transport Canada, April 13, 2000.

12. G.S. Winckelmans, F. Thirifay and P. Ploumhans, *Effect of non-uniform wind shear onto vortex wakes: parametric models for operational systems and comparison with CFD studies*, Fourth WakeNet Workshop on "Wake Vortex Encounter", October 16-17, 2000, National Aerospace Laboratory NLR, Amsterdam, The Netherlands.

APPENDIX I

Numerical Simulations of Aircraft Far-Wake Dynamics in Nonuniform Windshear and Ground Proximity

Interim Report submitted to Transport Canada

M.I. Yaras*

February 6, 2000

* Associate professor, Department of Mechanical and Aerospace Engineering, Carleton University, Ottawa, Ontario, Canada K1S 5B6.

Table of Contents

Introduction 1
Simulated Test Cases 1

Numerical Technique 5
Turbulence Model 8
Spatial and Temporal Resolution 9
Initial and Boundary Conditions 10

Simulation Results and Discussion 12
Modeling of Turbulent Diffusion 12
Sensitivity of Wake-Vortex Trajectories to Crosswind Profiles 20
Combined Effects of Non-uniform Wind Shear and Interaction with the Ground 24
Effects of Axial Motion in the Vortex Core and of Headwind Shear 25

Conclusions 29

References 30

Acknowledgments 32

Nomenclature

$a_1 \ldots a_4$ = constants used in scaling the preconditioning parameter, c
b = wake-vortex-pair initial separation distance based on elliptic lift distribution = $\pi s/4$
c = parameter used in the preconditioning of Q in the $\partial Q/\partial t_p$ term
$C_{b_1}, C_{b_2}, C_{v_1}, C_{w1}, C_{w_2}, C_{w_3}$ = constants used in the Spalart-Allmaras turbulence model
D = artificial dissipation operator
E, F, G = convective+diffusive flux vectors in the x, y and z directions, respectively
$f_{v_1} f_{v_2} f_w$ = functions used in the Spalart-Allmaras turbulence model
F_{CR} = curvature/rotation correction function used in the Spalart-Allmaras turbulence model
g = gravitational acceleration and a function used in the Spalart-Allmaras turbulence model
h = altitude
h_a = aircraft altitude at t=0 sec
N = Brunt-Väisälä frequency at wake altitude = $\left(-\frac{g}{\rho}\frac{d\rho}{dz} \right)^{1/2} \approx \left(\frac{g}{\theta}\frac{d\theta}{dz} \right)^{1/2}$
i, j, k = node indices in the ξ, η, ζ grid directions
K_c, K_d = constants used in determining the convective and diffusive pseudo-time-step limits
p = static pressure
q = atmospheric root-mean-square turbulence velocity at 40 m altitude
Q = vector of conservation variables
r = radial co-ordinate and a function used in the Spalart-Allmaras turbulence model
r_c = vortex-core radius
s = wingspan
S = surface area of control volume and scalar measure of local strain-rate tensor ($\sqrt{2S_{ij}S_{ij}}$)
S_{ij} = strain-rate tensor
Sh = shear parameter = $\frac{|\frac{dV_{hz}}{dz}|\, b}{V_0}$
t = time
t_p = pseudo time
$\vec{V}$ = velocity vector
V_a = airspeed of aircraft
V_c = crosswind, positive in the port-to-starboard direction
V_h = headwind
V_{hz} = horizontal wind
V_v = vertical wind, positive upwards
V_y = lateral rate of displacement of the wake vortices, positive port-to-starboard
V_z = vertical rate of displacement of the wake vortices, positive upwards
V_0 = ideal descent rate of the wake vortices = $\frac{\Gamma_0}{2\pi b}$
V_t = vortex-induced cross-stream (tangential) velocity
W = aircraft weight
x = longitudinal axis; positive towards the tail of the aircraft
x_c = x co-ordinate of the wake-vortex center

y = lateral axis; positive in the port-to-starboard direction
y_w = closest distance to a solid boundary
z = vertical axis; positive upwards
Γ = wake-vortex circulation
Γ_0 = initial value of the wake-vortex circulation = $\frac{W}{\rho V_a b}$
α, β = constant used in the eddy-viscosity correlations
$\varepsilon^{(2)}, \varepsilon^{(4)}$ = scaling parameters used in calculation of artificial dissipation
κ = von Karman constant (=0.41)
$\kappa^{(2)}, \kappa^{(4)}$ = constants used in calculation of artificial dissipation
K = A function used in the Spalart-Allmaras turbulence model
λ = spectral radius of the inviscid flux Jacobian
θ = virtual potential temperature at wake altitude
σ = standard deviation for trajectory-averaged quantities and a constant with a value of 2/3 used in the Spalart-Allmaras turbulence model
Ω = magnitude of vorticity
τ = viscous + Reynolds stress
ρ = density
ξ, η, ζ = co-ordinates aligned with grid directions on a structured grid
$\forall$ = size of control volume
ν = kinematic viscosity
ν_e = turbulence (eddy) viscosity
$\tilde{\nu}_e$ = eddy-viscosity variable used in the Spalart-Allmaras turbulence model

Superscripts:
* = normalized quantity; b, V_0 and b/V_0 are used as the normalizing length, velocity and time scales, respectively Γ
$\overline{}$ = parameter is averaged along the trajectory of a wake vortex

Introduction

In an effort to increase airport capacity and improve flight safety, several research programs in North America and Europe are developing systems that will allow dynamic spacing of arriving and departing aircraft at airports based on prevailing and projected weather conditions (Perry *et al*, 1997; Robins and Delisi, 1999; Konopka, 1999). The work presented herein was undertaken in support of the development of such a system named the Vortex Forecasting System (VFS) under a research program led by Transport Canada (Belotserkovsky, 1997). The requirement of real-time or near-real-time operation of such a system restricts it to relatively simple mathematical models of the dynamics of the aircraft wake under the influence of various atmospheric conditions and ground proximity. The VFS is based on the method of discrete vortices which offers a good trade off between simplicity, hence computational speed, and predictive capability. Two important simplifications associated with this system are the restriction of the simulation of wake-vortex motion to two-dimensional windows placed along the approach and departure paths of aircraft, and the use of a constant eddy viscosity in accounting for turbulent diffusion. The present work attempts to establish the impact of these approximations on the prediction of wake-vortex dynamics by considering a relatively complex test case involving interaction of the aircraft wake with nonuniform windshear in proximity of the ground. To this end, numerical simulations have been performed using a grid-based Reynolds-averaged Navier-Stokes solver. Additionally, the study identifies the accuracy and resolution of wind data that is required for reliable prediction of the wake trajectory in such ambient conditions.

Simulated Test Cases

The simulated test cases are part of the field data collected by NASA Langley Research Centre and the MIT Lincoln Laboratory at the Memphis, TN international airport in August 1995. Atmospheric and aircraft information for these cases as compiled by Yaras (1998a) are summarized in Table 1. Crosswind profiles constructed from propeller anemometer, Profiler and Sodar measurements are given in Figure 1, and the wake-vortex trajectories measured by a LIDAR are given in Figure 2. Further details on these measurement sensors are given by Campbell *et al* (1996) and Zak (1996).

a)

Case	$\bar{V}_c^*$ (σ)	$\bar{V}_h^*$ (σ)	$\bar{V}_v^*$ (σ)	$\bar{N}^*$ (σ)	$\bar{Sh}$ (σ)	q^*
1132	-0.6 (0.3)	-0.8 (0.2)	-0.1 (0.0)	0.37 (0.02)	0.56 (0.26)	0.33
1196	0.1 (0.4)	-3.5 (0.1)	-0.1 (0.0)	0.36 (0.16)	0.67 (0.26)	0.31

b)

Case	Aircraft	b (m)	V_0 (m/s)	h_a^*	$\bar{V}_y^*$ Port	$\bar{V}_y^*$ Star.	$\bar{V}_z^*$ Port	$\bar{V}_z^*$ Star.
1132	B-727 100	25.8	1.77	5.7	-1.0	-1.2	-0.9	-0.8
1196	DC10-30	39.6	1.70	4.1	-0.1	-0.1	-0.7	-0.6

Table 1. Atmospheric conditions (a) and aircraft & wake data (b) for Cases 1132 and 1196

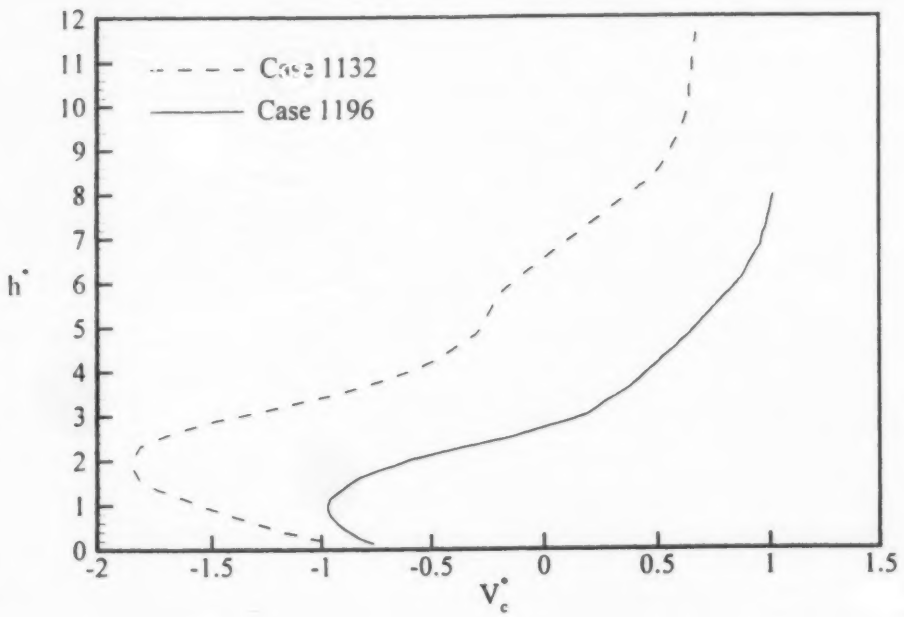

Figure 1 Crosswind profiles for Cases 1132 and 1196

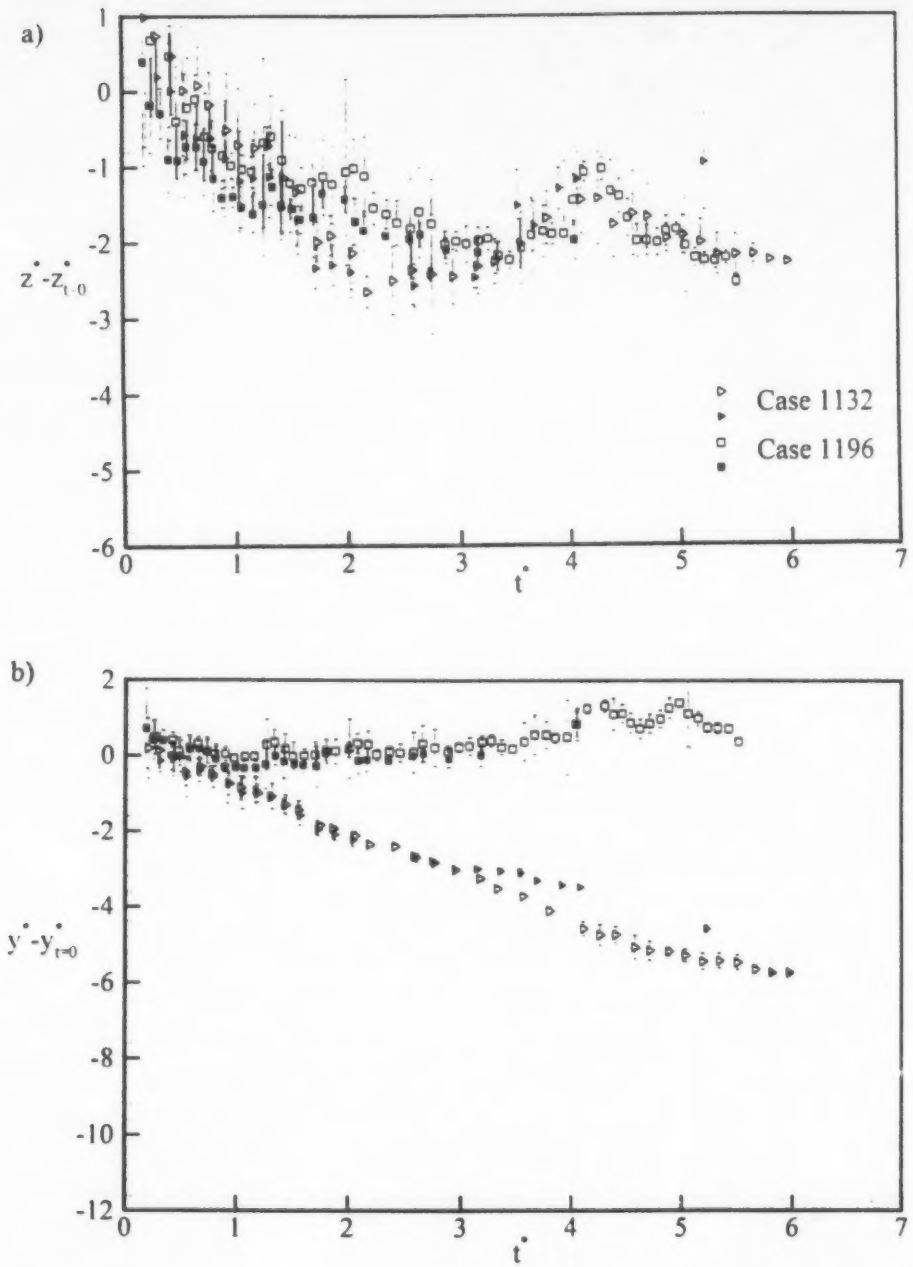

Figure 2 Vertical (a) and lateral (b) wake-vortex trajectories for Cases 1132 and 1196 (port vortex: hollow symbols; starboard vortex: filled symbols)

The bar used in the notation of the tabulated parameters denotes averaging along the wake-vortex trajectories, and the * superscript indicates a normalized quantity. Normalization is based on the initial wake-vortex spacing, b, and the ideal descent rate of the vortices, V_0. The mean values given in Table 1a are applicable to both vortices of each case. The Brunt-Vaisala frequency, $\bar{N}^*$, and the turbulence parameter, q^*, suggest a moderately stratified atmosphere with low levels of turbulence. Although the wind shear averaged along the wake trajectory, as described by the value of $\bar{Sh}$, is not very high, the standard deviation is indicative of considerable variation along the length of the wake trajectory, which is consistent with the wind profiles in Figure 1.

In Figure 2a the wake vortices are noted to follow the ideal vertical trajectory (descending at the rate of V_0) for close to three time units. In both cases the shear parameter, Sh, remains below 0.4 for the first two time units and then rapidly increases to about 0.95 by $t^*=3.0$. At this point the descent is observed to stop abruptly followed by a brief rise and eventual return to the altitude of $t^*=3.0$. This trend in the vortex vertical trajectories is similar to what one would expect in the case of interaction with the ground. However, based on the initial altitudes given in Table 1b, at $t^*=3.0$ the vortices are still about 2.5 (Case 1132) and 1.6 (Case 1196) wingspans away from the ground.

The wind profiles in Figure 1 reveal presence of a ground jet. According to these profiles, relatively small variations in ambient vorticity exists down to about $h^*=3$ (Case 1132) and $h^*=2$(Case 1196), beyond which gradients in vorticity are significantly higher with a sign reversal taking place just below these thresholds. These thresholds correspond fairly closely with the locations where the vertical motion of the wake vortices subside at $t^*=3.0$ in the respective cases (Figure 2a). These results suggest that wake-vortex induced intermixing of the nonuniform and possibly counter-sign ambient vorticity from different elevations has likely played a role in the observed development of the wake trajectory beyond $t^*=3.0$. Such influence of nonuniform crosswind shear on the wake vortex trajectories was also observed in the large-eddy simulations of Proctor (1998). The numerical simulations presented herein are aimed to shed further light onto this type of interaction, namely determining:

- the applicability of a constant eddy viscosity assumption in capturing the dynamics of this interaction;
- the added influence of ground proximity;
- the added effect of nonuniform headwind shear;
- the effect of axial motion in the vortex core;
- the required precision of wind information for reliable prediction of the wake motion in such instances.

Numerical Technique

The simulation algorithm is based on the solution of the Navier-Stokes equations expressed in integral, strong-conservation-law form:

$$\int_{\mathcal{V}} (Q_t + E_x + F_y + G_z) d\mathcal{V} = 0 \qquad (1)$$

where the subscripts indicate derivatives and,

$$Q = \begin{pmatrix} \rho \\ \rho V_x \\ \rho V_y \\ \rho V_z \end{pmatrix}, \quad E = \begin{pmatrix} \rho V_x \\ \rho V_x^2 + p - \tau_{xx} \\ \rho V_x V_y - \tau_{xy} \\ \rho V_x V_z - \tau_{xz} \end{pmatrix}, \quad F = \begin{pmatrix} \rho V_y \\ \rho V_x V_y - \tau_{yx} \\ \rho V_y^2 + p - \tau_{yy} \\ \rho V_y V_z - \tau_{yz} \end{pmatrix}, \quad G = \begin{pmatrix} \rho V_z \\ \rho V_x V_z - \tau_{zx} \\ \rho V_y V_z - \tau_{zy} \\ \rho V_z^2 + p - \tau_{zz} \end{pmatrix} \qquad (2)$$

with

$$\tau_{xx} = \frac{2}{3}\rho(\nu+\nu_e)\left(2\frac{\partial V_x}{\partial x} - \frac{\partial V_y}{\partial y} - \frac{\partial V_z}{\partial z}\right), \qquad \tau_{xy} = \rho(\nu+\nu_e)\left(\frac{\partial V_x}{\partial y} + \frac{\partial V_y}{\partial x}\right) \qquad (3)$$

and similarly for the remaining normal and shear stresses.

Although the algorithm has been developed for the prediction of both incompressible and compressible flows, the present description is given for incompressible flows in keeping with the nature of the present simulations. Discretization in space is based on a vertex-centered finite-volume scheme using a structured grid of quadrilateral (hexahedral in three-dimensional space) cells (e.g, Crumpton and Shaw, 1994). In this approach the conserved variables are stored at the vertices of the grid cells, and the faces of the control volume associated with a vertex are formed by connecting the centroids of the quadrilaterals surrounding the vertex to the midpoints of the edges passing through the vertex. Both convective and diffusive fluxes are calculated at the vertices and are interpolated to the control-volume faces. The spatial gradients appearing in the diffusive fluxes at a vertex are obtained by applying Gauss' divergence theorem to the control volume surrounding the vertex.

On a uniform grid, the interpolation of the flux terms outlined above is equivalent to centered differencing, yielding second-order accuracy. Except for very low grid-cell Reynolds numbers, such treatment of convective fluxes is well-known to cause instability and requires inclusion of an artificial dissipation term into the governing equations. This artificial dissipation term, $D(Q)$, is traditionally constructed from second- and fourth-order differences of the conservation variables in all grid directions (e.g, Jameson *et al*, 1981), i.e.:

$$\int_{\mathcal{V}} (Q_t + E_x + F_y + G_z) d\mathcal{V} - (D_\xi^{(2)} - D_\xi^{(4)} + D_\eta^{(2)} - D_\eta^{(4)} + D_\zeta^{(2)} - D_\zeta^{(4)})Q = 0 \qquad (4)$$

where subscripts ξ, η, ζ denote the three grid directions of the structured grid.

For instance considering the ξ direction,

$$D_{\xi}^{(2)}Q = \nabla_{\xi}((\lambda_{\xi})_{i-1/2,j,k}(\varepsilon_{\xi})^{(2)}_{i-1/2,j,k})\Delta_{\xi}Q_{i,j,k} \tag{5}$$

$$D_{\xi}^{(4)}Q = \nabla_{\xi}((\lambda_{\xi})_{i-1/2,j,k}(\varepsilon_{\xi})^{(4)}_{i-1/2,j,k})\Delta_{\xi}\nabla_{\xi}\Delta_{\xi}Q_{i,j,k} \tag{6}$$

where i,j,k denote indices in the ξ,η,ζ grid directions, λ is the spectral radius of the inviscid-flux Jacobian, and $\nabla_{\xi},\Delta_{\xi}$ are first-order forward and backward differencing operators in the ξ grid direction. These operators need to be modified at computational domain boundaries, and the approach recommended by Swanson and Turkel (1987) is adopted in the present algorithm.

$\varepsilon^{(2)}$ and $\varepsilon^{(4)}$ are scaling parameters for the dissipation terms. $\varepsilon^{(2)}$ is assigned values such that the $D^{(2)}$ term is activated only in regions of high pressure gradients:

$$(\varepsilon_{\xi})^{(2)}_{i-1/2,j,k} = \kappa^{(2)}\max((\varphi_{\xi})_{i-1,j,k},(\varphi_{\xi})_{i,j,k}) \tag{7}$$

$$(\varphi_{\xi})_{i,j,k} = \left|\frac{\Delta_{\xi}\nabla_{\xi}p_{i,j,k}}{(4+\Delta_{\xi}\nabla_{\xi})p_{i,j,k}}\right| , \qquad \kappa^{(2)} = 0.25. \tag{8}$$

and $\varepsilon^{(4)}$ is quantified using:

$$(\varepsilon_{\xi})^{(4)}_{i-1/2,j,k} = \max(0,\kappa^{(4)}-(\varepsilon_{\xi})^{(2)}_{i-1/2,j,k}) , \qquad \kappa^{(4)} = const. \tag{9}$$

In absence of high pressure gradients only the third-order accurate $D^{(4)}$ term is activated, allowing the second order accuracy of the spatial discretization to be retained. Due to low levels of local pressure gradients in the far-wake simulations presented herein, only the $D^{(4)}$ term influenced the solution. The minimum value of $\kappa^{(4)}$ that allowed stable convergence varied from 0.006 to 0.01 depending on the magnitude of the windshear gradients. Variation of $\kappa^{(4)}$ within this range was confirmed to have no noticeable effect on the predicted flow field.

The spectral radii of the inviscid flux Jacobian matrices are the common scaling parameters for the artificial dissipation terms (Swanson and Turkel, 1987). Matrix valued scaling (e.g., Turkel and Vatsa, 1994) results in less artificial diffusion entering into the numerical solution, albeit at the expense of reduced convergence rates (Lin and Sotiropoulos, 1997). In the present algorithm the scalar method of scaling is chosen. For example, the $(\lambda_{\xi})_{i-1/2,j,k}$ component is obtained from:

$$(\lambda_{\xi})_{i-1/2,j,k} = \left(|V_{\xi}S_{\xi}| + ((c/a_1)^2+V_{\xi}^2)^{1/2}|S_{\xi}|\right)_{i-1/2,j,k} \tag{10}$$

where S_{ξ} is the control volume surface facing the ξ grid direction, and c/a_1 is a preconditioning parameter, to be described later.

Discretization of the temporal derivative, Q_t, appearing in Eqn.1 is based on three-point backward differencing, yielding second order accuracy in time. An exception is the first time increment which is based on a two point scheme. At each real-time increment, the discretized governing equations are then solved iteratively using pseudo-time stepping for relaxation:

$$(Q_{t_p}\mathcal{V})_{i,j,k} + \int_{\mathcal{V}_{i,j,k}} (Q_t + E_x + F_y + G_z)\,d\mathcal{V} - D(Q_{i,j,k}) = 0 \tag{11}$$

The vector of conservation variables, Q, used in the pseudo-time derivative, Q_{t_p}, is preconditioned to extend the range of applicability of the algorithm to low Mach-number flows such as the far-wake flow field. The following form of preconditioning has been adopted which is similar to the one proposed by Turkel (1987):

$$\frac{\partial Q}{\partial t_p} = \begin{pmatrix} \left(\frac{a_1}{c}\right)^2 \frac{\partial p}{\partial t_p} \\ \left(\frac{a_2}{c}\right)^2 V_x \frac{\partial p}{\partial t_p} + \frac{\partial(\rho V_x)}{\partial t_p} \\ \left(\frac{a_3}{c}\right)^2 V_y \frac{\partial p}{\partial t_p} + \frac{\partial(\rho V_y)}{\partial t_p} \\ \left(\frac{a_4}{c}\right)^2 V_z \frac{\partial p}{\partial t_p} + \frac{\partial(\rho V_z)}{\partial t_p} \end{pmatrix} \tag{12}$$

where a_1, a_2, a_3, a_4 are constants and c is a parameter that is typically scaled on the local flow velocity or a fixed velocity that is representative of the overall flow motion in the computational domain. For the simulation of the far wake in windshear and close to the ground, $c = \max(10m/s, |V|)$ together with a value of about 0.7 for the coefficients $a_{i=1,4}$ was found to yield good rates of convergence.

The pseudo-time increments are adjusted locally to the maximum allowable value dictated by convective and diffusive numerical stability limitations:

$$\frac{1}{(\Delta t_p)_{i,j,k}} \le \left(\frac{1}{\Delta t_c} + \frac{1}{\Delta t_d}\right)_{i,j,k} = \left(\frac{\Sigma\lambda}{K_c \mathcal{V}} + \frac{1}{K_d \mathcal{V}^2}\Sigma(\nu+\nu_e)S^2\right)_{i,j,k} \tag{13}$$

where the summations are performed over the surfaces of the control volume. In the present study the constants K_c and K_d were set to somewhat conservative values of 2.5 and 0.25 respectively.

Marching in pseudo time is based on Runge-Kutta integration with explicit odd-numbered and implicit even-numbered stages. Such implicit treatment of alternate stages is analogous to the well-known implicit residual smoothing procedure (e.g, Jameson *et al*, 1981) and enhances the stability margin of the algorithm over the purely explicit approach. A modified version of the Strongly-Implicit Procedure of Stone (Stone, 1968; Schneider and Zedan, 1981) is used for the implicit stages.

For computational efficiency, the viscous and artificial dissipation terms are evaluated only during the odd-numbered stages. For the simulations presented herein, two-stage Runge-Kutta integration was found to be sufficient to damp-out the high frequency pseudo-transients. The coefficients of both stages were set to 1.0.

Although the Runge-Kutta time integration process efficiently removes high-frequency errors during pseudo-time stepping, it is not efficient in dealing with errors of relatively large wave lengths. A multigrid scheme is used to deal with the longer wave lengths. The scheme is based on Full-Approximation-Storage (Brandt, 1977) utilizing V cycles with conservative area-weighted interpolation during restriction and linear interpolation during prolongation. For the present simulations, two levels of grid with two coarse-grid time increments per cycle was found to provide the best trade-off between rate of reduction of residuals and increased computational effort due to the prolongation and restriction operations over each multigrid cycle. Due to reduced spatial resolution on the coarse grid, the physical and artificial diffusion terms were calculated on the fine-grid level only.

Turbulence Model

One of the primary objectives of the present study is to establish the accuracy of a constant eddy-viscosity approximation in predicting the turbulent diffusion of the wake vortices. For comparison, simulations were also performed using the one-equation model of Spalart and Allmaras (1992), excluding the transition-related terms:

$$\frac{\partial(\rho\tilde{\nu}_e)}{\partial t} + \nabla\cdot(\rho\vec{V}\tilde{\nu}_e) - \nabla\cdot\left(\frac{\rho}{\sigma}(\nu+\tilde{\nu}_e)\nabla\tilde{\nu}_e\right) = F_{CR}C_{b_1}\left(\Omega + \frac{\tilde{\nu}_e f_{\nu_2}}{K^2 y_w^2}\right)\rho\tilde{\nu}_e + \frac{C_{b_2}}{\sigma}\rho\nabla^2\tilde{\nu}_e - C_{w_1}f_w\rho\left(\frac{\tilde{\nu}_e}{y_w}\right)^2 \qquad (14)$$

where

$$K = \frac{\tilde{\nu}_e}{\nu}, \qquad f_{\nu_1} = \frac{K^3}{K^3 + C_{\nu_1}^{\ 3}}, \qquad f_{\nu_2} = 1 - \frac{K}{1 + K f_{\nu_1}}, \qquad f_w = g\left(\frac{1 + C_{w_3}^{\ 3}}{g^6 + C_{w_3}^{\ 6}}\right)^{1/6},$$

$$g = r + C_{w_2}(r^6 - r), \qquad r = \frac{\tilde{\nu}_e}{\left(\Omega + \frac{\tilde{\nu}_e f_{\nu_2}}{\kappa^2 y_w^{\ 2}}\right)\kappa^2 y_w^{\ 2}}, \qquad \nu_e = f_{\nu_1}\tilde{\nu}_e$$

C_{b_1}=0.1355 C_{b_2}=0.622 C_{ν_1}=7.1 σ=2/3 C_{w_1}=3.239 C_{w_2}=0.3 C_{w_3}=2 κ=0.41 and Ω is the magnitude of local vorticity.

The discretization of the convective and diffusive terms, and the formulation of artificial dissipation is the same as for the mass and momentum equations described earlier. The source term is linearized for enhanced stability. The resultant equation is solved with the remaining governing equations in a coupled fashion. Pre-conditioning of the pseudo-time derivative is not required for the turbulence equation, hence the constant a appearing in the pseudo-time derivative of the mass and momentum equations (see Eqn. 12) is set to zero for the turbulence equation. The curvature correction term, F_{CR} is introduced to account for the reduced levels of Reynolds stress resulting from the convex streamline pattern in the flow field of each vortex. The formulation of this term follows the recommendation of Hellsten (1998):

$$F_{CR} = \frac{1}{1 + C_{CR}\frac{\Omega}{S}\left(\frac{\Omega}{S} - 1\right)} \tag{15}$$

where Ω is the magnitude of the local vorticity vector, S is a scalar measure of the local strain rate tensor ($=\sqrt{2S_{ij}S_{ij}}$), and C_{CR} is a constant. For the results presented herein, a value of 50 was chosen for the constant C_{CR}. This choice was based on the extent of agreement of the predicted tangential velocity distribution within the vortex with field data.

Spatial and Temporal Resolution

The spatial grid was kept stationary for simulation of the wake-vortex motion, hence the lateral extent of the computational domain was chosen such that the vortices remained within the confines of the domain for the duration of interest. This resulted in lateral and vertical dimensions of (496m x 224m) for Case 1132 and (350m x 250m) for Case 1196. In some of the simulations the crosswind profile differed from the measured one. In such instances the aforementioned computational domain dimensions were adjusted accordingly. Vertical and lateral grid-node spacings were set to 1m and 0.5m for simulations involving initial vortex-core radii of $10.6\%s$ and $4.3\%s$, respectively. Grid independency of the results was confirmed with selective simulations involving higher resolution.

For three-dimensional simulations, the domain size and resolution in the axial direction were set to 48 m and 2.8 m, respectively. A sensitivity study based on 56 m domain length and 2.0 m axial-grid resolution revealed no changes in the observed wake behavior compared to the axially coarser and shorter computational domain. The present choice of axial-domain length was dictated primarily by computing times on a Pentium-III 500Mhz computer, and suppresses the development of Crow instability which has a theoretical wave length of $8.6b$ for the most amplified mode (Crow and Bate, 1976). However, the domain size is sufficient for the objectives of the present three-dimensional simulations, namely investigation of the influence of axial motion within the vortex cores and of headwind shear on the wake-vortex trajectory, prior to initiation of Crow instability.

Temporal evolution of the wake dynamics was resolved with 0.75 sec increments. This represents the largest time increment for which monotonic convergence was possible in the

simulations presented herein. Based on the ideal descent rate of the wake vortices, V_0, over a time period of 0.75 sec. the vortices in Cases 1132 and 1196 would descend by about 1.3 m which is close to the spatial resolution utilized in the simulations. Thus, a time increment of 0.75 sec is deemed sufficiently small in relation to the time-rate-of-change of the wake flow and the chosen spatial resolution.

Initial and Boundary Conditions

The velocity distribution within the computational domain was initialized by combining the atmospheric wind profiles with the velocity field induced by the wake-vortex pair. For the initialization of the wake-vortex tangential velocity field, an empirical model proposed by Proctor (1998) for the post roll-up state was used:

$$V_t = \frac{\Gamma_0}{2\pi r}\left(1 - e^{-10(r/s)^{0.75}}\right) \qquad r > r_c \qquad (16a)$$

$$V_t = \frac{\Gamma_0}{2\pi r} 1.4\left(1 - e^{-10(r_c/s)^{0.75}}\right)\left(1 - e^{-1.2527(r/r_c)^2}\right) \qquad r \le r_c \qquad (16b)$$

The far-field wake dynamics was observed to be insensitive to this initial wake-velocity distribution based on comparisons with simulation results wherein initial conditions were obtained using a Rankine vortex model. In both Cases 1132 and 1196 the initial altitude of the wake was sufficiently high to avoid consideration of any image vortices in the initialization process. The core radius of the vortices, r_c, was set to 10.6% of the wingspan of the aircraft. Although this is somewhat greater than the initial r_c values observed in field data, it allows adequate resolution of the vortex core with 1m grid-node spacing in the lateral and vertical directions. Simulations with a more realistic initial core radius of 4.3% wingspan, performed on a grid of 0.5m node spacing, indicated negligible differences in the wake-vortex trajectories. The initial vortex circulation was obtained from aircraft weight, air speed, and the initial vortex spacing, b, set equal to $\pi s/4$ based on the assumption of elliptic lift distribution. Satisfactory agreement between the simulated and measured initial descent rates of the wake vortices confirmed that such an assumption for the lift distribution is adequate for the present purposes. The initial altitude of the wake vortices corresponded to the altitude of the aircraft in Cases 1132 and 1196 as it crossed the LIDAR measurement plane. Laterally, the vortex pair was positioned such that it remained within the computational domain for the duration of interest. Finally, the initial static pressure distribution corresponding to the tangential velocity field induced by the vortices was established on the basis of radial equilibrium within the flow field of each vortex. Based on the local mass and momentum imbalances within the computational domain, any inaccuracies in these initial velocity and pressure fields are judged to influence only the first three to four time increments of the simulation.

In three-dimensional simulations, the initial cross-flow of the wake-vortex pair was assumed to be uniform in the longitudinal direction, and the wind-tunnel data of El-Ramly (1975) was adopted for initialization of the axial velocity distribution across the vortex. El-Ramly's axial velocity

distribution in the wake-vortex, normalized by the aircraft airspeed, is shown in Figure 3. These measurements correspond to a location of five wingspans downstream of the aircraft, hence can be taken to represent the post roll-up state.

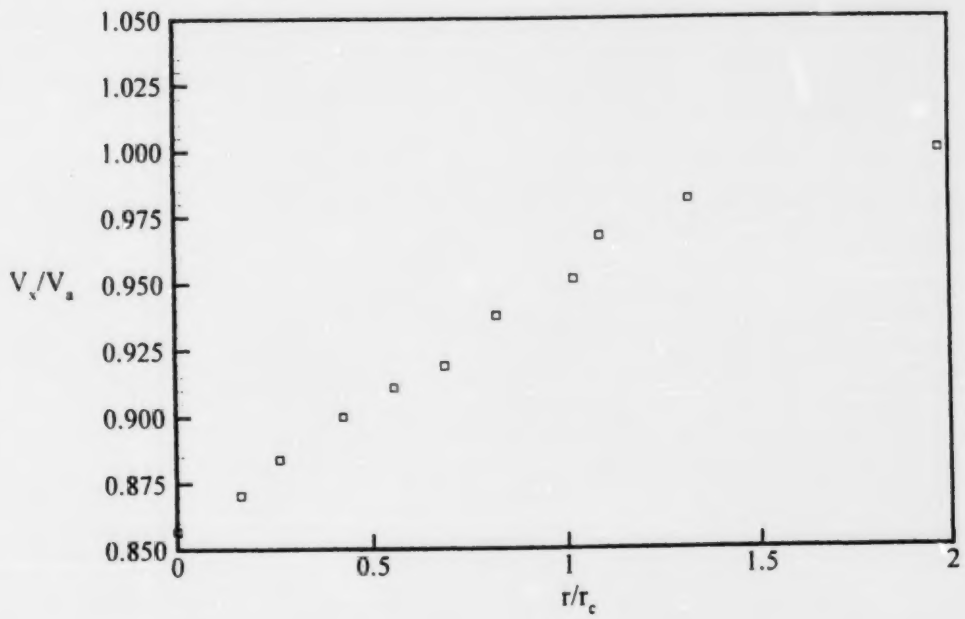

Figure 3 Axial velocity distribution across a wake-vortex measured by El-Ramly (1975)

Boundary conditions on the lower part of the computational domain consisted of no-slip condition for velocity and zero-normal-gradient for pressure. Two alternative conditions were considered for the top boundary: approximation of this boundary as a "slipwall" or imposing zero-normal-gradient conditions for all flow variables. The prediction results were found to be insensitive to these choices. Two alternative conditions were considered for the side boundaries as well. For lateral domain sizes significantly greater than the separation distance of the port and starboard vortices, such as those used in the current study, periodic treatment of the side boundaries would be reasonable, for mutual interaction of the wake vortices would be significantly larger than the induced effect of neighboring pair of vortices implied by such boundaries. An alternative treatment of the side boundaries is to impose Dirichlet conditions for the velocity field to represent the prevailing winds,

and to use Neumann conditions for pressure. This approach circumvents the issue of periodic vortex pairs, and is an accurate representation of the actual conditions for as long as the influence of the wake vortices at these boundaries remains negligible. Simulations using either type of side-boundary conditions resulted in very similar predictions, confirming applicability of both approaches. The latter approach was adopted for the simulation results discussed herein. Finally, in three-dimensional simulations periodic conditions were imposed on the bounding surfaces of the domain in the longitudinal direction.

Simulation Results and Discussion

Modeling of Turbulent Diffusion:

Currently large-eddy simulation (LES) is considered by many as the most promising approach to providing turbulence closure in the simulation of moderately high Reynolds number fluid flows. One of the main obstacles in the use of this type of closure continues to be the relatively large computational effort required. One- or two-equation eddy-viscosity type of turbulence models are computationally less expensive, however they are still not very practical for real-time or near-real-time aircraft spacing systems. Therefore zero-equation modeling of turbulence, which is based on algebraic evaluation of the turbulence diffusion coefficient, remains the most viable alternative in such real-time predictions. Although it is not reasonable to expect a large degree of generality from such simplified models, there has been some success in tailoring them for the prediction of certain flows. On this basis, it is worth exploring the possibility of using these models in the simulation of aircraft wake vortices in the far field. In the context of such flows, one can distinguish between turbulence within the aircraft wake sustained by the mean-velocity field of the wake vortices, and the ambient turbulence affected by atmospheric activity, primarily unstable stratification. The test cases selected for the present simulations involve an atmosphere of slightly stable stratification and low turbulence, and thus the dominant turbulence is that sustained by the wake-vortex flow itself. The current effort focuses on the simplest approach of accounting for the diffusive effect of this turbulence through a constant value of eddy viscosity. The simultaneous effects of the ground and nonuniform ambient shear on the wake vortices encountered in the present test cases makes them particularly challenging benchmarks.

Modeling of the turbulent diffusion in wake vortices using constant values of eddy viscosity has its roots in the work of Squire (1965) who proposed that the eddy be scaled on the vortex Reynolds number (Γ/ν). Subsequently, Owen (1970) recommended that it be scaled on $(\Gamma/\nu)^{1/2}$:

Squire (1965): $$\frac{\nu_e}{\nu} = \alpha\left(\frac{\Gamma}{\nu}\right) \tag{17a}$$

Owen (1970): $$\frac{\nu_e}{\nu} = \beta\left(\frac{\Gamma}{\nu}\right)^{1/2} \tag{17b}$$

Values of the scaling factors α and β are available from laboratory and field data and are summarized in Table 2. The experiments of Yaras and Sjolander differ from the remaining cases in that the

measured vortex was produced in a linear cascade of turbomachinery blades with tip clearance. In this respect, the case reveals the extent of changes in the diffusion rate of a vortex due to presence of a solid surface in close proximity, which is somewhat similar to what is observed in Cases 1132 and 1196. The β values listed in the table, except for that of Yaras and Sjolander, were obtained from α using the following relation:

$$\beta = 2.45\alpha\left(\frac{\Gamma}{\nu}\right)^{1/2} \tag{18}$$

	Γ/ν	$\alpha x10^3$	β
1. Dosanjh *et al*	$2x10^3$	5	0.55
2. Yaras & Sjolander	$1.0 - 1.7x10^4$	6 - 4	1.30
3. Newman	$2x10^4$	2	0.69
4. Templin	$5x10^4$	1.4	0.77
5. Mabey	$5x10^4$	1.5	0.82
6. Lezius	$4x10^4 - 2x10^5$	0.4 - 0.6	0.20-0.66
6. Rose & Dee	$\sim10^7$	0.2	1.55
7. Iverson	$2.6x10^7$	0.1	1.25

Table 2. Constants α and β used in Squire's and Owen's correlations for ν_e

which was suggested by Owen to obtain a good agreement between the predicted and experimental peak tangential velocities for cases 1, 3, 4, 5 and 7 listed in the table. The β value in the laboratory experiments of Yaras and Sjolander (1990) was calibrated to predict the correct rate of decay of peak streamwise vorticity in the vortex. α is noted to decrease fairly monotonically by a factor of 50 as the Reynolds number is increased by four orders of magnitude. β, on the other hand, remains within a much smaller range of 0.2 to 1.55, and the variations do not appear to follow a particular trend. Based on these observations one may hypothesize that ν_e/ν more closely scales on the square-root of the vortex Reynolds number rather than being directly proportional to it.

Ash and Zheng (1998) compared numerically simulated circulation decay for $\Gamma/\nu = 2.6x10^7$ with field measurements (Garodz and Clawson, 1993). Based on this comparison the authors recommended an α value of 0.00125 (β=15.6). It appears that neither α nor the implied β value is consistent with the data in Table 2. In this author's experience, the extent of random and bias errors associated with circulation information extracted from field data generally does not permit reliable evaluation of the coefficients α and β. (Yaras, 1998b). Hence, in the current study peak tangential velocities in the vortex flow field and the rate of change of the vortex core size will be used to establish proper values for β instead. It may also be argued that consideration of these quantities

rather than circulation is more relevant in the context of vortex strength as it relates to the hazard it poses to following aircraft.

Simulations were performed for Cases 1132 and 1196 covering an eddy viscosity range of $\nu_e/\nu = 5500$ to $\nu_e/\nu = 33000$. Based on the respective initial circulation values, Γ_0, this eddy viscosity range corresponds to β values from 1.3 to 7.9 in Case 1132, and 1.1 to 6.5 in Case 1196. Figures 4 and 5 compare the predicted vertical trajectories for several values of β with field data. For clarity only every fifth real-time step is shown on the simulated trajectories. The simulations are noted to reproduce the diminishing rate of descent observed in the measurements only in a qualitative sense. Uncertainty in the measured wind profiles is judged to be the source of this discrepancy which will be elaborated upon in the next section. The reduced rates of descent with increasing β is consistent with the increased rates of circulation decay observed in Figures 6 and 7. The circulations were obtained by integrating the vorticity field over a circular area of b/2 radius centered at each vortex. Sensitivity to β is seen to be more pronounced in Case 1132. As this difference between the two cases manifests itself after about $t^*=3$, which is the instant the wakes begin to interact with the ground jet, the higher levels of ambient shear in Case 1132 may be the likely source of greater sensitivity to β in this case. The smallest of the β values considered in these simulations correspond to the high end of the β values tabulated in Table 2. It is noted that doubling of this β, which is a variation similar to the range of scatter in the β values of Table 2, results in only small changes in the decay rates and trajectories in both test cases.

Having established the sensitivity of the wake trajectories to β, additional simulations were performed for Case 1132 to establish the correct value of β based on predictions of the rate of change of peak tangential velocities and vortex core size. In these simulations the initial vortex core size was reduced from $10.6\%s$ to $4.6\%s$ for more accurate representation of the field data, and the grid-node spacing was reduced from 1.0 m to 0.5m to provide adequate resolution of the smaller core. The predicted tangential velocity distribution across the vortex for a range of β values are compared to field data in Figure 8. Agreement with field data is noted to improve as β is decreased, with values less than about $\beta=1.3$ yielding fairly similar simulated cross-flows. These values are noted to be consistent with the established range of β values as tabulated in Table 2. Underprediction of the velocity peak and an overprediction of the growth rate of the vortex core is evident even with the smaller values of β, and becomes particularly evident at $t^*=4.9$. In order to establish an additional reference for these constant-eddy-viscosity simulations, the flow was predicted using the one-equation turbulence model of Spalart and Allmaras (S-A). The initial ambient eddy viscosity in these simulations was set to a low value in keeping with the low atmospheric turbulence of the test case. The initial turbulence condition within the wake field is more difficult to quantify, for it should represent the residual turbulence left behind by the aircraft. Parametric studies indicated only small sensitivity to this initial condition, with the turbulence within the wake quickly adopting a distribution consistent with the local strain field. The results of the simulations with the S-A turbulence model are compared to field data and to the results of constant-eddy-viscosity simulations in Figure 9. The S-A predictions are observed to follow very closely the results with $\beta=0.013$, and deviation from the $\beta=1.3$ results is only in the peak-velocity region. This success of the constant-eddy-viscosity approach for this type of flow is not really surprising, for the effect of eddy viscosity on the mean flow field

scales on the curvature of the velocity field when the Boussinesq approximation is employed for the Reynolds stresses. This means that in regions of flow with small gradients in shear, such as the inner core region which displays near-solid-body rotation, variations in the eddy viscosity will have relatively small effects on the resultant velocity distribution. This, in turn, allows calibration of a constant eddy viscosity with emphasis on regions of high shear gradients.

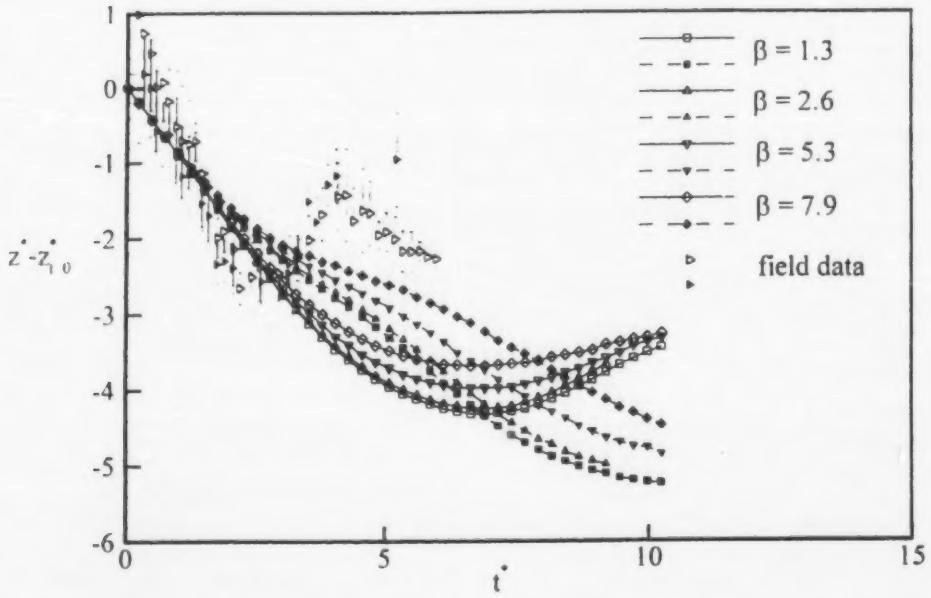

Figure 4 Case 1132 simulated wake-vortex vertical trajectories for several values of β (port: hollow symbols; starboard: filled symbols)

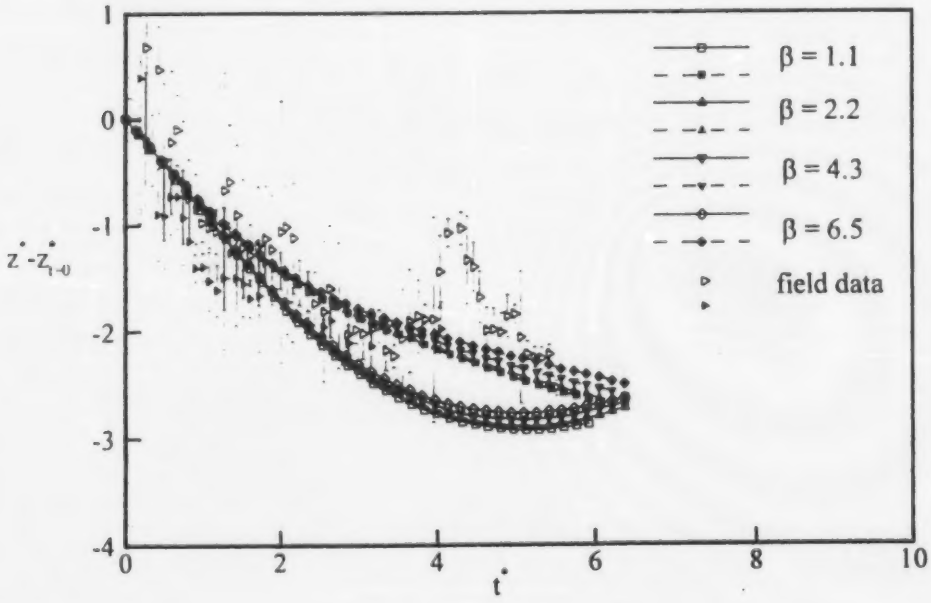

Figure 5 Case 1196 simulated wake-vortex vertical trajectories for several values of β (port: hollow symbols; starboard: filled symbols)

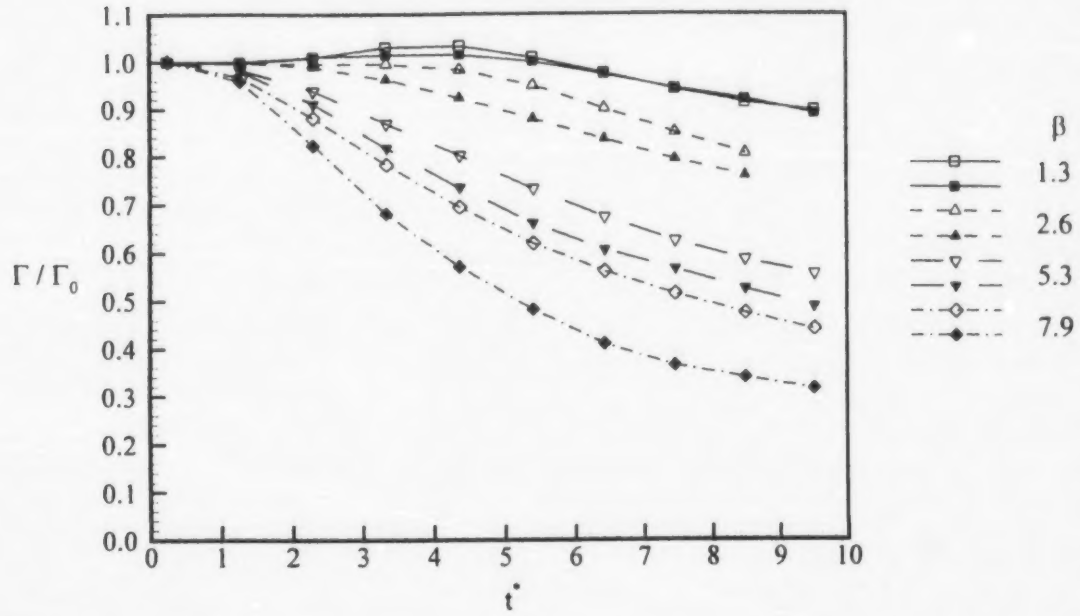

Figure 6 Case 1132 simulated wake-vortex decay rates for several values of β (port: hollow symbols; starboard: filled symbols)

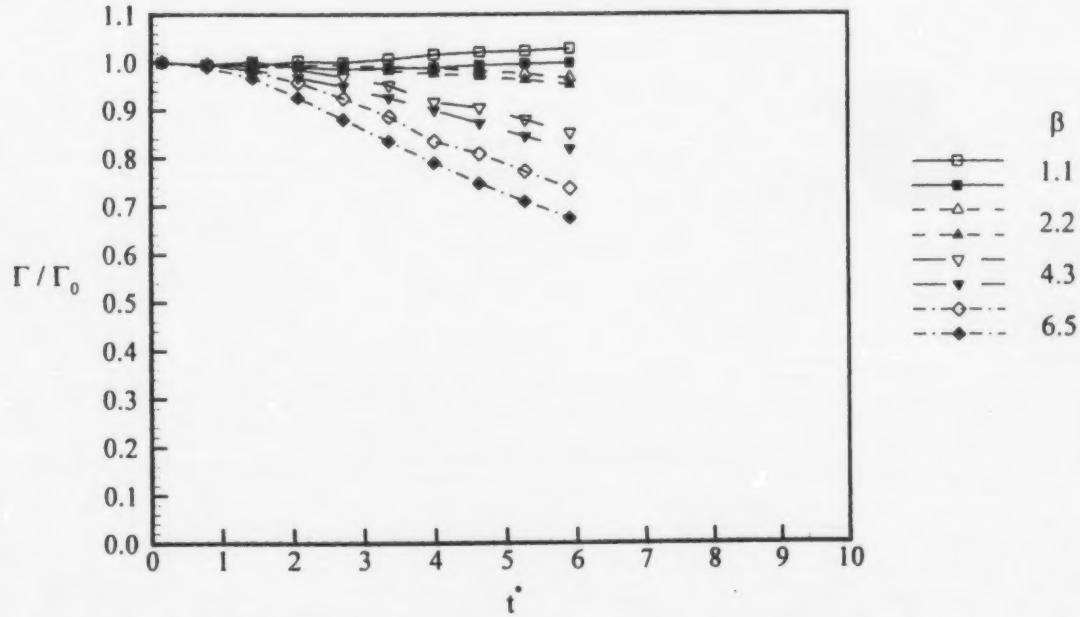

Figure 7 Case 1196 simulated wake-vortex decay rates for several values of β (port: hollow symbols; starboard: filled symbols)

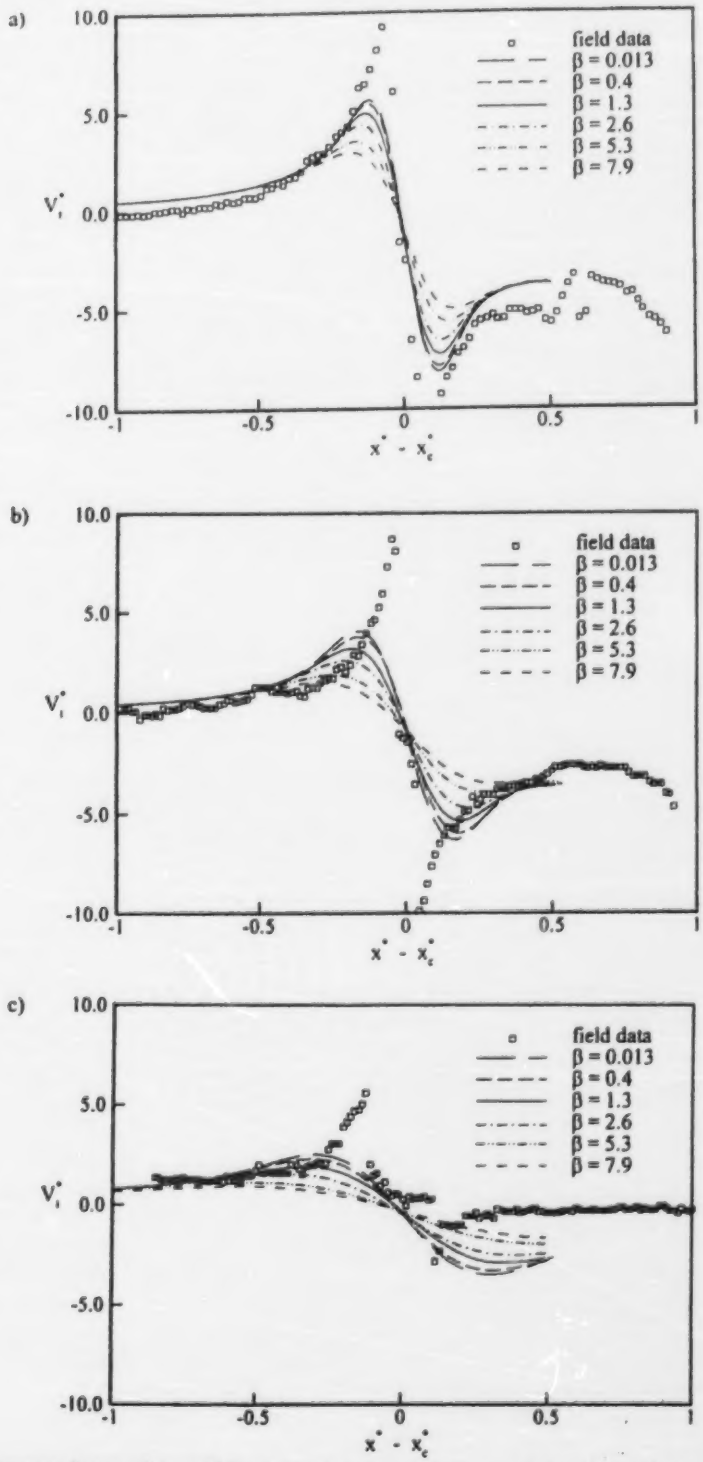

Figure 8 Comparison of predicted port-vortex tangential velocity distribution for Case 1132 with measurements a) t*=0.44 b) t*=1.45 c) t*=4.91

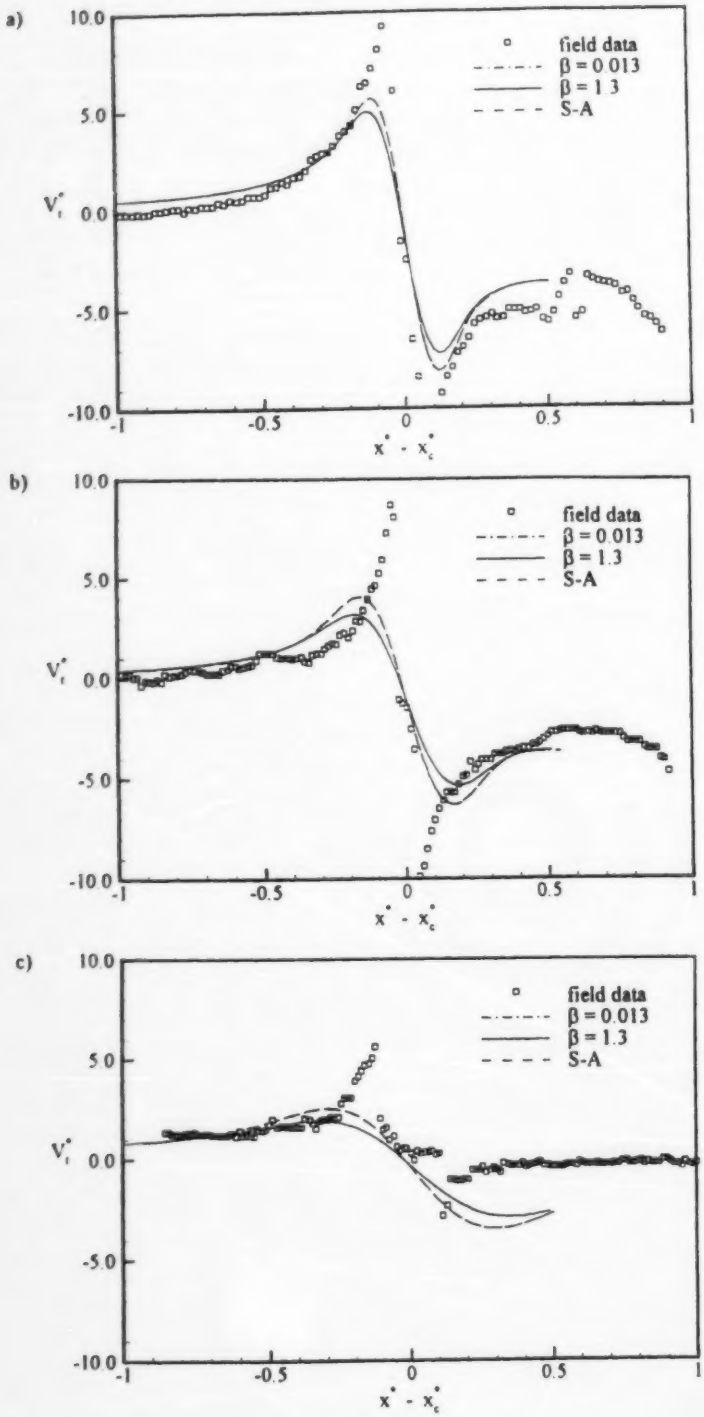

Figure 9 Comparison of constant-ν_e and S-A predictions of the tangential velocity distribution for Case 1132 with measurements a) t*=0.44 b) t*=1.45 c) t*=4.91

Sensitivity of Wake-Vortex Trajectories to Crosswind Profiles:

The atmospheric wind profiles used in the present simulations were constructed by the MIT Lincoln Laboratory using data from multiple meteorological sensors that were installed at varying locations around the airport in Memphis (Campbell *et al*, 1996). Above 40m altitude, a radar profiler was used as the primary source of wind data. The profiler provided wind information with 100m spatial resolution (i.e about $4b$ for Case 1132) and $\pm$1m/s uncertainty, and the data was averaged over 25-minute intervals. Within bounds of this uncertainty and resolution, significant variations in the wind profile, hence ambient shear levels, is feasible. In order to establish the effect of such variations in the wind profile on the wake vortex trajectories, simulations were performed with systematic alterations of the crosswind profile of Case 1132, the case for which the predicted trajectories were in lesser agreement with the field data. Four types of variations in the crosswind profile were considered as shown in Figure 10. All modifications aimed to increase the magnitude of shear between altitudes h_a^*=2.5 and h_a^*=4, i.e. the upper portion of the ground jet, and are numbered in the order of increasing shear gradients in this altitude range. Comparison of the predicted vertical trajectories with field data is given in Figure 11a. Increasing the crosswind shear is noted to have a substantial effect on the trajectory of the starboard vortex, with a clear rebound established for modified wind profiles 2,3 and 4. Such rebound of a vortex from a concentrated shear layer of opposite sign of vorticity was also observed in the LES simulations of Proctor (1998). Comparison of the simulation results with the measured starboard vertical trajectory, as well as the lateral trajectories for both vortices, suggests that in the actual wind profile the windshear gradient in the h_a^*=2.5-4 altitude range was close to that of modified profile 2. Deviation of these modified profiles from the original profile is within the bounds of uncertainty and spatial/temporal resolution of the wind sensors.

The field data for the port vortex shows that this vortex also experiences a brief rebound, after which it continues to descend. This trend is expected since the port vortex also encounters a shear layer of opposite sign of vorticity once it reaches the lower portion of the ground jet. The relative extent of reduction of the descent rate of the port vortex with the 2nd, 3rd and 4th modified crosswind profiles is mostly consistent with the relative magnitudes of the shear gradient in the lower portion of the ground jet in these instances. The exception is the 1st modified wind profile, where the lower portion of the ground jet remained unchanged from the original profile, yet the port vortex is noted to rebound at a notably lower altitude. As the port vortex goes through the upper portion of the ground jet it will tend to be amplified by the ambient vorticity which is of the same sign. This amplification is expected to be greater with the 1st modified wind profile since the shear gradient is greater in that portion of the ground jet compared to the original profile. A stronger port vortex would then be able to maintain its downward momentum for a longer duration. To highlight this interaction of the port vortex with the ground jet, the vertical trajectories with the original crosswind profile are compared to those that would prevail in a calm atmosphere (Figure 12). The earlier and stronger rebound of the port vortex in the presence of the ground jet is clear.

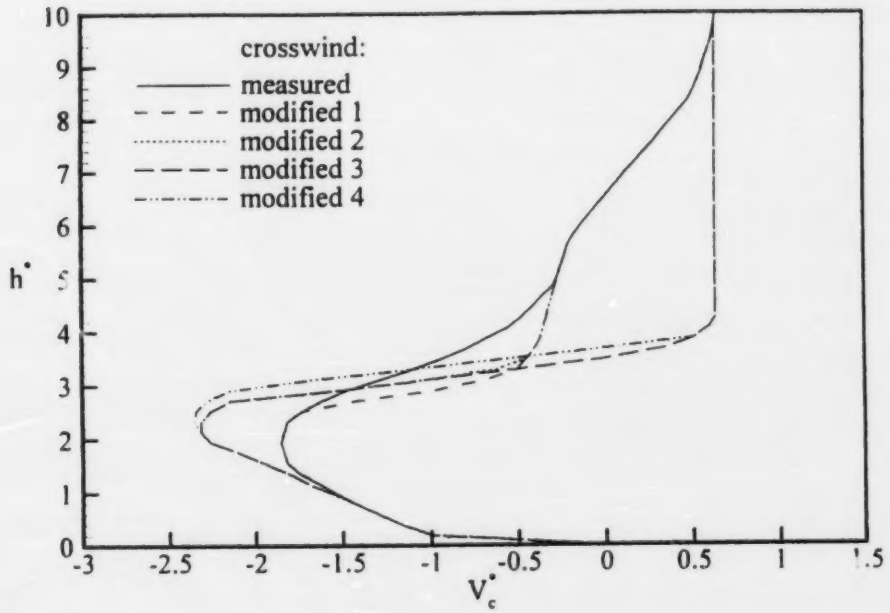

Figure 10 Case 1132 measured and modified crosswind profiles

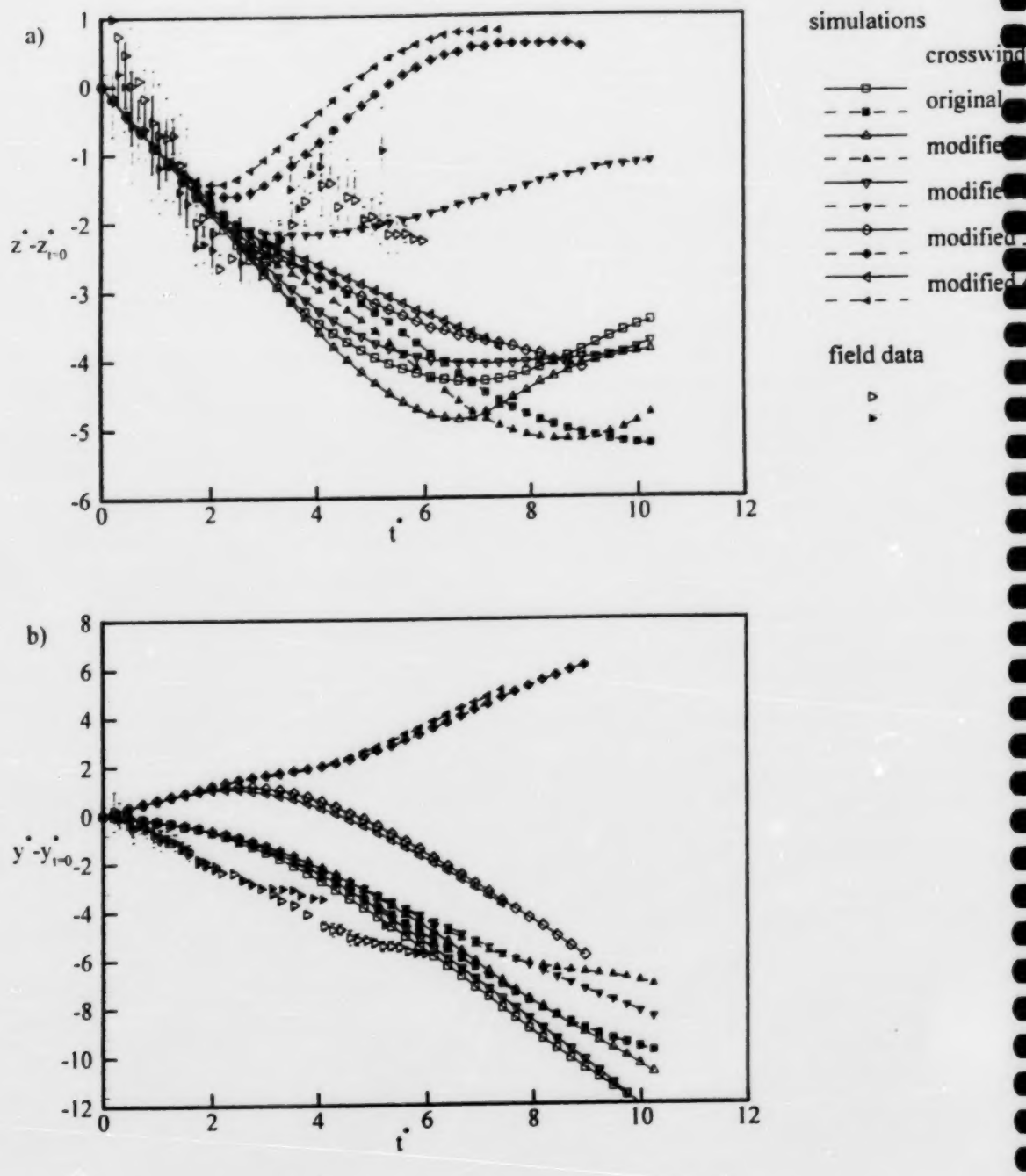

Figure 11 Case 1132 simulated wake-vortex vertical (a) and lateral (b) trajectories - sensitivity to variations in the crosswind profile (port: hollow symbols; starboard: filled symbols)

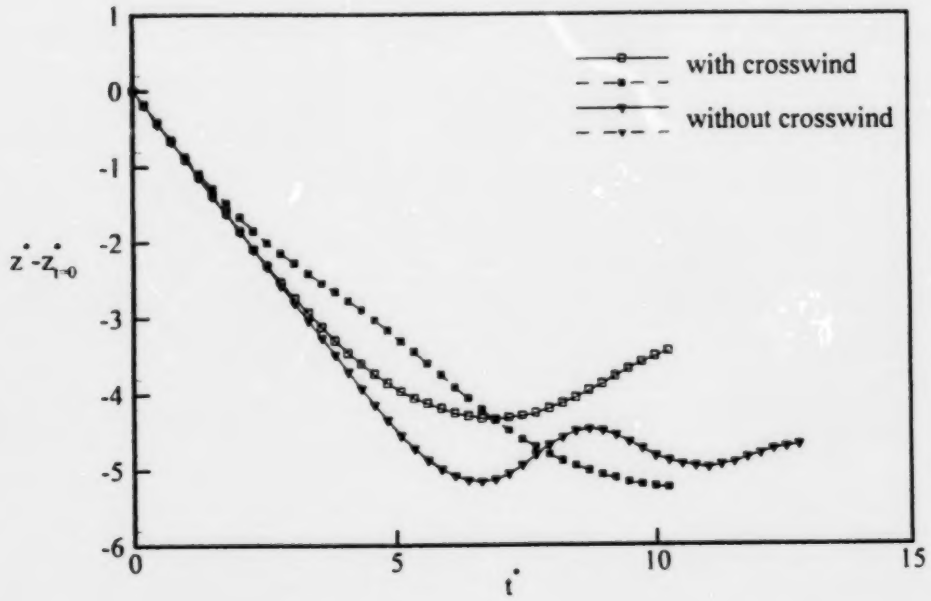

Figure 12 Case 1132 simulated wake-vortex vertical trajectories - effect of the ground jet (port: hollow symbols; starboard: filled symbols)

Combined Effects of Non-uniform Wind Shear and Interaction with the Ground:

Figure 13 compares Case 1132 wake vortex trajectories for the original crosswind profile with and without the ground present. In absence of the ground, the lower boundary of the computational domain was set to an outflow boundary, with Neumann boundary conditions for all flow variables. Comparison of the trajectories of the starboard and port vortices for the two configurations suggests that presence of the ground is *sensed* by these vortices starting at altitudes of about $2.3b$ and $1.7b$, respectively. This is in contrast with the simulation results in a calm atmosphere (Figure 12) where the vortices maintain a constant descent rate down to an altitude of about $1.2b$. This result highlights the nonlinear nature of the simultaneous interaction of the wake vortices with nonuniform windshear and the ground surface. This observation is particularly significant for aircraft-spacing algorithms which often rely on parametric representation of external effects such as ground proximity and nonuniform windshear. Proper mathematical modeling would require that the coupling between such external effects observed in the present simulations be reflected in such parametric models.

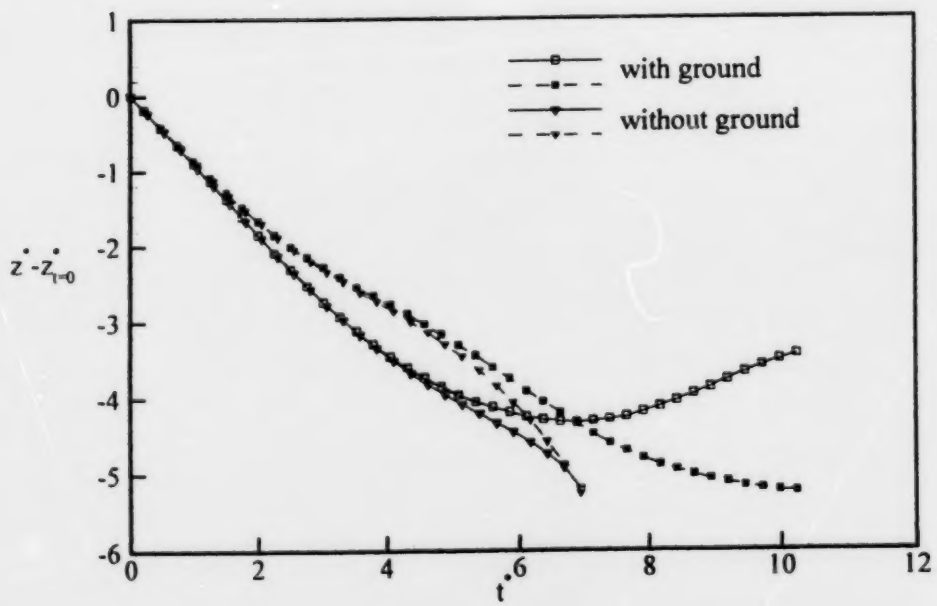

Figure 13 Case 1132 simulated wake-vortex vertical trajectories - Effect of low-level jet with and without the ground (port: hollow symbols; starboard: filled symbols)

Effects of Axial Motion in the Vortex Core and of Headwind Shear:

Existence of axial flow through vortices generated by lifting surfaces is well known (e.g., El-Ramly, 1975; Yaras and Sjolander, 1990). Although in the near wake the axial core flow may be either forward or rearward depending on the relative magnitudes of airfoil profile drag and axial pressure gradients set up by the roll-up process (Brown, 1973; Lezius, 1974), in the far field the axial motion is expected to be forward since the axial pressure gradients that result from radial diffusion of the vortex would complement the momentum deficit due to viscous effects. To the author's knowledge, published studies on mathematical modeling of the interaction of the wake-vortex pair with the surrounding atmosphere have not accounted for this flow feature. Three- dimensional simulations were thus performed to investigate the effect of such an axial flow on the wake motion observed in Case 1132. The initial distribution of axial flow through the wake vortices was matched to the measurements of El-Ramly (Fig. 3). The resultant vortex trajectories are shown in Figure 14 together with the corresponding two-dimensional simulation results. The comparison suggests only small effects of axial motion in the vortex core on the kinematics of the wake-vortex/ low-level jet interaction within the cross-stream plane. Since vorticity lines associated with cross-stream shear and with shear due to axial motion in the core are mutually perpendicular, this finding is not surprising. Once the vorticity related to the axial motion develops a cross-stream component due to, for example, deformation of the wake vortices along their axis through onset of longitudinal instability, the observed trend may be different. It should also be noted that the two-dimensional simulation results shown in Figure 14 differ slightly from the corresponding ones presented in previous figures in that the grid resolution was set to 2m in the lateral and vertical directions. The difference in the trajectories is indicative of slight grid dependency of the results, and this step was taken to maintain consistency with the spatial resolution of the three-dimensional simulations.

It is quite likely that the axial motion within the wake vortices would depend to some extent on the specifics of the roll-up process which, in turn, is dictated by details of the design of the aircraft. To establish the sensitivity of the observations in Figure 14 to such potential variations in axial motion, additional three-dimensional simulations were undertaken with significantly larger axial momentum deficiency in the wake vortices (Figure 15) than measured by El-Ramly. The results did not indicate any changes in wake-vortex trajectories from those shown in Figure 14. Increasing the axial momentum deficiency to even greater levels resulted in the vortices developing longitudinal instabilities, despite the small length of the computational domain of about $2b$. Such instabilities has been observed by others as well (e.g, Lessen and Paillet, 1974). However, such high levels of relative motion along the axes of the wake vortices is unlikely to develop naturally under the influence of streamwise pressure gradients in the roll-up phase. It should be noted that in these three-dimensional simulations the eddy-viscosity value was set to correspond with β=1.3, which was previously shown to adequately capture the cross-stream diffusion in two-dimensional simulations. Since the turbulent diffusion in the cross-stream and streamwise planes is associated with very different strain fields, the turbulent diffusion coefficient in the two planes would generally be different. Thus, the simulated rate of decay of axial motion (Figure 16) may not be representative of the actual decay process. Nonetheless, this does not prevent the present simulations from identifying any potential interaction

between the kinematics of axial and cross-stream motion in the wake flow field, since notable axial motion is noted to prevail for the full duration in these simulations.

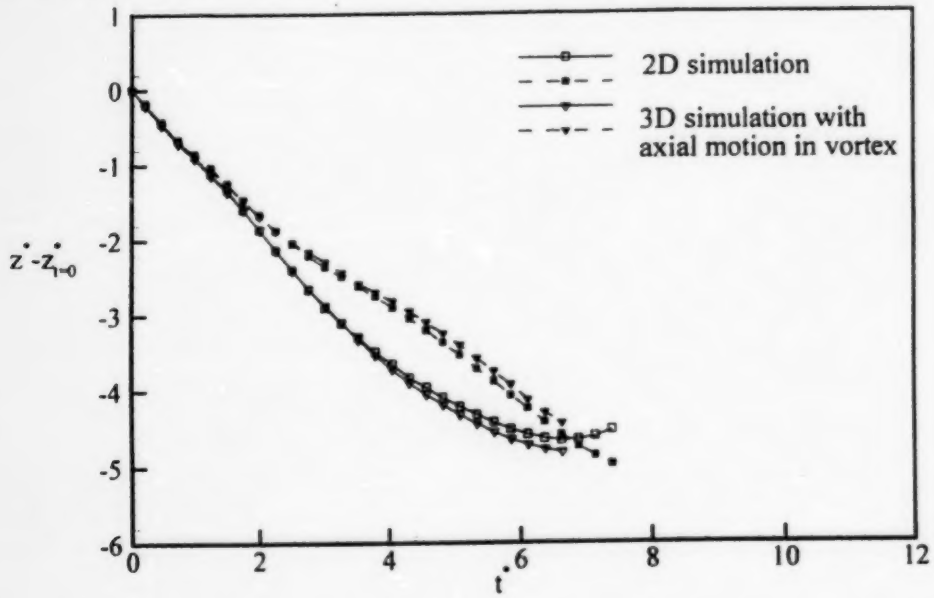

Figure 14 Case 1132 simulated wake-vortex vertical trajectories - affect of axial motion within the vortices (port: hollow symbols; starboard: filled symbols)

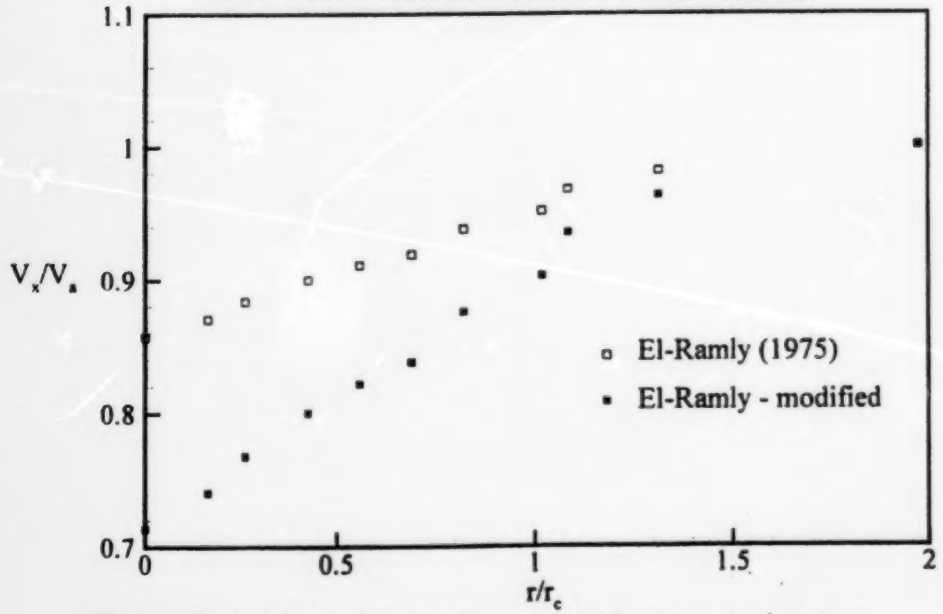

Figure 15 Axial velocity distribution within the wake vortices

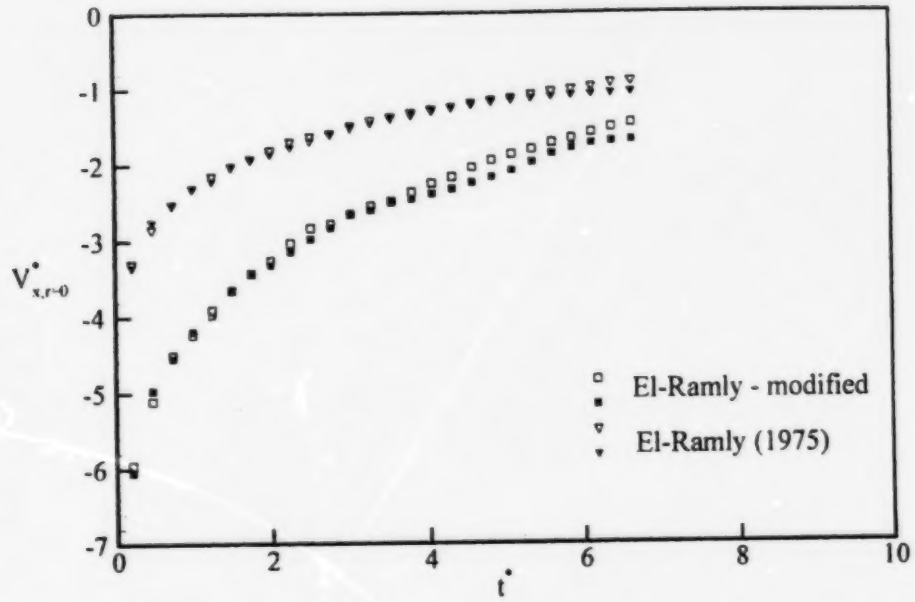

Figure 16 Rate of decay of axial velocity at the centerline of the wake vortices (port: hollow symbols; starboard: filled symbols)

The final potential influence on the wake-vortex motion that was considered in this set of simulations is headwind shear. Three dimensional simulations were performed based on the headwind profile of Case 1132 as well as a modified profile that contained significantly higher levels of shear and shear gradients (Figure 17). The vertical wake vortex trajectories shown in Figure 18 suggest a small influence on the port vortex. The reduction in the descent rate of this vortex as it descends through the crosswind shear layer is slightly enhanced by the presence of headwind shear. However, this variation is small, and very small difference is noted between the simulations with the original and enhanced headwind shear levels. These results confirm that it suffices to consider only the cross-stream component of the horizontal wind vector and associated windshear for accurate modeling the wake-vortex motion in a sheared atmosphere.

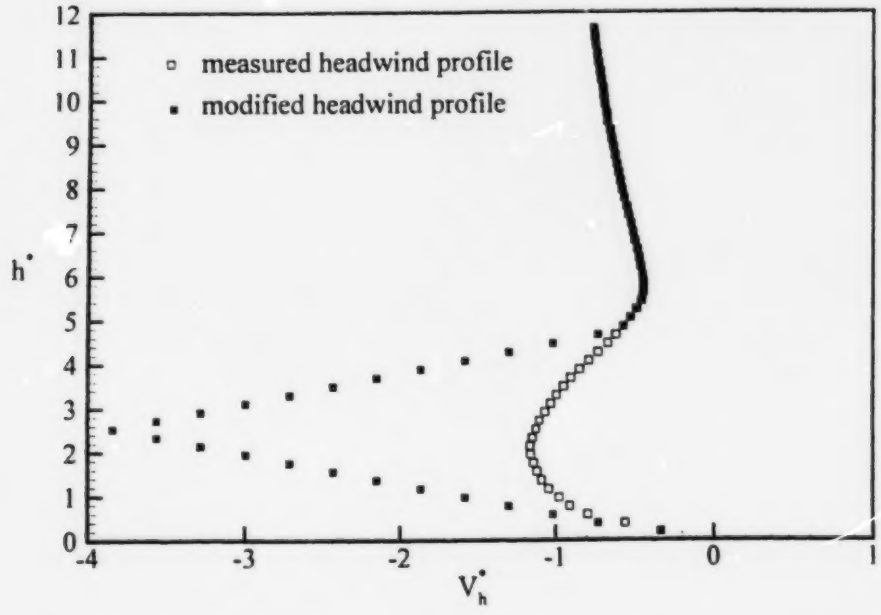

Figure 17 Case 1132 headwind profiles used in the simulations

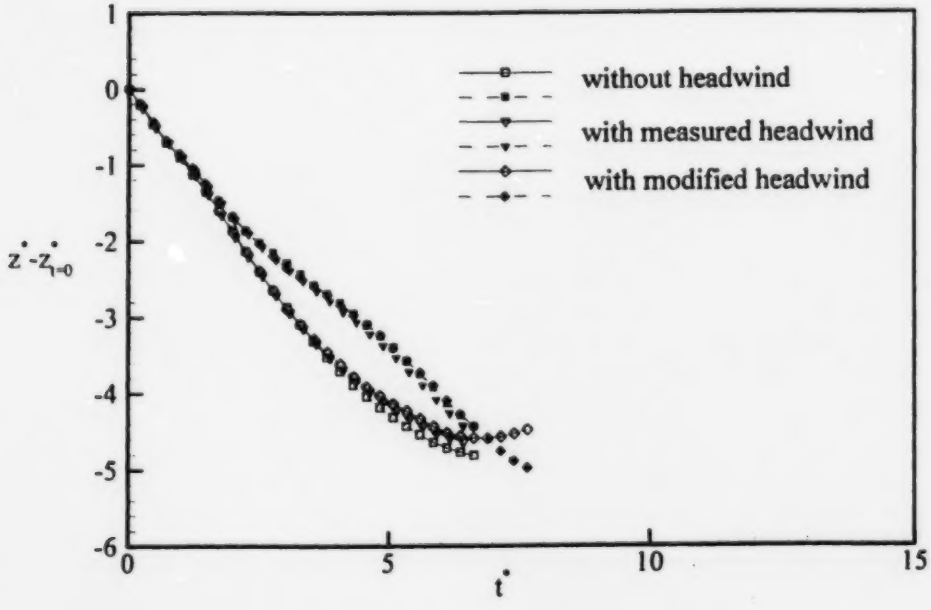

Figure 18 Case 1132 simulated wake-vortex vertical trajectories - effect of headwind shear (port: hollow symbols; starboard: filled symbols)

Conclusions

Two- and three-dimensional Reynolds-averaged Navier-Stokes simulations of the aircraft far wake development in the framework of test cases included in the Memphis field-data set have been presented. The simulations were performed to verify a number of assumptions that would benefit the computational efficiency of real-time or near-real-time aircraft spacing systems that are currently under development. Additionally, the results provide an indication of the accuracy and resolution that would be required from atmospheric sensors to successfully predict interaction of the wake vortices with nonuniform wind shear. The main conclusions of the study are as follows:

- Use of a constant eddy viscosity to represent the turbulent diffusion within the wake field is adequate for the purpose of capturing the decay rate of the vortices and their interaction with the surroundings (windshear & ground) in a low-turbulence atmosphere. The predictions are fairly insensitive to the value of the eddy viscosity within the range of variations encountered amongst the published field and laboratory data.

- Both wake vortices are observed to experience notable reduction in descent rates as they encounter a ground jet, with the vortex containing vorticity of sign opposite to that prevailing in the upper portion of the jet displaying a stronger reaction.

- The simulations have provided insight into the motion of the wake-vortex pair as it simultaneously encounters the ground and the nonuniformly sheared flow in the low-level jet This result can be used to guide "calibration" of aircraft spacing algorithms which may be based on separate parametric representation of the wake-vortex interaction with nonuniform windshear and with the ground.

- Based on the field test cases used in this study, the required accuracy and resolution of wind sensors is demonstrated for reliable prediction of the wake-vortex interaction with the type of nonuniform windshear that may be encountered in ground jets.

- Axial motion prevailing with the wake vortices as well as nonuniform head wind shear are found to have negligible influence on the wake vortex trajectories in the cross-stream plane. This helps to justify the use of two-dimensional prediction algorithms in real-time aircraft spacing systems, provided potential demise of the wake vortices through longitudinal instability is accounted for parametrically.

References

Ash, R.L. and Zheng, Z.C., 1998, "Numerical Simulations of Commercial Aircraft Wakes Subjected to Airport Surface Weather Conditions," J. of Aircraft, Vol. 35, No. 1, pp. 18-26.

Belotserkovsky, S.M., 1997, "Prediction of Aircraft Wake Vortices During Takeoff and Landing," Wake-Vortex Project Phase-3 Final Report to Transport Canada.

Brandt, A., 1977, "Multi-Level Adaptive Solutions to Boundary Value Problems," Mathematics of Computation, Vol. 31, No. 138, pp. 333-390.

Brown, C.E., 1973, "Aerodynamics of Wake Vortices," AIAA Journal, Vol. 11, No. 4, pp. 531-536.

Campbell, S.D., Dasey, T.J., Freehart, R.E., Heinrichs, R.M., Matthews, M.P., Perras, G.H. and Rowe, G.S., 1996, "Wake Vortex Field Measurement Program at Memphis, TN - Data Guide," Project Report ATC-250 prepared for NASA Langley Research Centre.

Chorin, A.J. 1967, "A Numerical Method for Solving Incompressible Viscous Flow Problems," Journal of Computational Physics, Vol. 2 pp. 12-26.

Crow, S.C. and Bate, E.R., 1976, "Lifespan of Trailing Vortices in a Turbulent Atmosphere," J. of Aircraft, Vol. 12, No. 7, pp. 476-482.

Crumpton, P.I. and Shaw, G.J., 1994, "A Vertex-Centered Finite Volume Method with Shock Detection," Int. Journal for Numerical Methods in Fluids, Vol. 18, pp. 605-625.

Dosanjh, D.S., Gasparek, E.P., Eskinazi, S., 1962, "Decay of a Viscous Trailing Vortex," Aeronautical Quarterly, Vol. 13, p. 167.

El Ramly, Z.M., 1975, "Investigation of the Development of the Trailing Vortex System Behind a Swept-Back Wing," Ph.D. Thesis, Faculty of Engineering, Carleton University, Ottawa, Canada.

Garodz, L.J. and Clawson, K.L., 1993, "Vortex Wake Characteristics of B757-200 and B767-200 Aircraft Using the Tower Fly-By Technique," National Oceanic and Atmospheric Administration, Air Resources Lab. Report 199.

Hellsten, A., 1998, "Some Improvements in Menter's k-ω SST Turbulence Model," AIAA Paper 98-2554.

Iverson, J.D., 1976, "Correlation of Turbulent Vortex Decay Data," J. of Aircraft, Vol. 13, No. 5, pp. 338-342.

Jameson, A., Schmidt, W., and Turkel, E., 1981, "Numerical Solutions of the Euler Equations by Finite Volume Methods using Runge-Kutta Time-Stepping Schemes," AIAA Paper No. 81-1259.

Konopka, J., 1999, "Predicting the Behaviour of Wake Vortices - Technological Capabilities vs. ATM Operational Requirements," Proceedings of the 2nd WakeNet Workshop, Oberpfaffenhofen, Germany.

Lessen, M. and Paillet, F., 1974, "The stability of a trailing line vortex, Part 2. Viscous theory," J. Fluid Mech., Vol. 65, No. 4, pp. 769-779.

Lezius, D.K., 1974, "Water Tank Study of the Decay of Trailing Vortices," AIAA Journal, Vol. 12, No. 8, pp. 1065-1071.

Lin, F.B. and Sotiropoulos, F., 1997, "Assessment of Artificial Dissipation Models for Three Dimensional Incompressible Flow Solutions," Journal of Fluids Engineering, Vol. 119, pp. 331-340.

Mabey, D.G., 1953, "The Formation and Decay of Vortices," DIC Thesis, Imperial College.

Newman, B.G., 1959, "Flow In a Viscous Trailing Vortex," Aeronautical Quarterly, Vol. 10, p. 149.

Owen, P.R., 1970, "The Decay of a Turbulent Trailing Vortex," Aeronautical Quarterly, pp. 69-78.

Perry, R.B., Hinton, D.A., and Stuever, R.A., 1997, "NASA Wake Vortex Research for Aircraft Spacing," AIAA Paper 97-0057.

Proctor, F.H., 1998, "The NASA-Langley Wake Vortex Modeling Effort in Support of an Operational Aircraft Spacing System," AIAA Paper No. 98-0589.

Robins, R.E. and Delisi, D.P., 1999, "Further Development of a Wake Vortex Predictor Algorithm and Comparisons to Data," AIAA Paper No. 99-0757.

Schneider, G.E. and Zedan, M., 1981, "A modified Strongly Implicit Procedure for the Numerical Solution of Field Problems," J. of Numerical Heat Transfer, Vol. 4, pp. 1-19.

Shen, S., Ding, F., Han, J., Lin, Y., Arya, S., Proctor, F., 1999, "Numerical Modeling Studies of Wake Vortices: Real Case Simulations,", AIAA Paper No. 99-0755.

Spalart, P.R. and Allmaras, S.R., 1992, "A One-Equation Turbulence Model for Aerodynamic Flows," AIAA Paper 92-0439.

Squire, H.B., 1965, "The Growth of a Vortex in Turbulent Flow," Aeronautical Quarterly, pp. 302-306.

Stone, H.L., 1968, "Iterative Solution of Implicit Approximation of Multidimensional Partial Differential Equations," SIAM J. of Numerical Analysis, Vol. 5, pp. 530-558.

Swanson, R.C. and Turkel, E., 1987, "Artificial Dissipation and Central Difference Schemes for the Euler and Navier Stokes Equations," AIAA Paper 87-1107.

Templin, R.J., 1954, "Flow Characteristics in a Plane Behind the Trailing Edge of a Low Aspect Ratio Wing as Measured by a Special Pressure Probe," NAE, Canada, LM AE-58.

Turkel, E., 1987, "Preconditioned Methods for Solving the Incompressible and Low Speed Compressible Equations," J. of Comp. Phys., Vol. 72, pp. 277-298.

Turkel, E. and Vatsa, V.N., 1994, "Effect of Artificial Viscosity on Three-Dimensional Flow Solutions," AIAA Journal, Vol. 32, No. 1, pp. 39-45.

Yaras, M.I., 1998a, "Effects of Atmospheric Conditions and Ground Proximity on the Dynamics of Aircraft Vortices," Canadian Aeronautics and Space Journal, Vol. 44, No. 2, pp. 92-101.

Yaras, M.I., 1998b, "Effects of Atmospheric Conditions and Ground Proximity on the Dynamics of Aircraft Wake Vortices: A Study of the 1994-95 Memphis Field Measurements," Final Report for Transport Canada under Contract no. T8200-7-7516/001/XSD.

Yaras, M.I. and Sjolander, S.A., 1990, "Development of the Tip-Leakage Flow Downstream of a Planar Cascade of Turbine Blades: Vorticity Field," ASME J. of Turbomachinery, Vol. 112, pp. 609-617.

Zak, J.A., 1996, "Documentation of Sensor Accuracy, Limitations, and Quality Assurance Criteria Used in the 1995 Deployment," Interim Report for NASA Contract No. NAS1-19341, Task 13.

Acknowledgments

The author gratefully acknowledges the financial support of the Transportation Development Centre (Canada) and the Civil Aviation Directorate, Safety and Security, Transport Canada for the work presented herein performed under contract no. T8200-8-8529/001/XSD.